Evaluating Metabolic Stress Response Using Ultra Performance Liquid Chromatography-High Resolution Mass Spectrometry

A Dissertation Presented for the

Doctor of Philosophy

Degree

The University of Tennessee, Knoxville

Eric David Tague

May 2019

Copyright © 2019 by Eric David Tague
All rights reserved.

DEDICATION

To all those in graduate school, just remember science is bigger than you.

ACKNOWLEDGEMENTS

I would like to thank my advisor, Dr. Shawn R. Campagna for the opportunity to research in his lab and continue to grow as a chemist. Without his motivation and constant support, I would have never reached beyond what I thought was my limit. I also want to thank my committee members, Drs. Michael Best, Christopher Baker, and Elizabeth Fozo for giving up some of their valuable time to sit on my committee.

I want to thank all my wonderful collaborators who have come into the lab with desires to answers biological questions that I did not even know existed. They have given me the opportunity to diversify my knowledge base and apply new mass spectrometry techniques. Specifically, I would like to thank Dr. Fozo and Dr. John Harp for introducing me to the world of microbiology and putting up my simple questions about how to pour plates and grow bacteria.

Over the past several years, I have become great friends with all the lab members, and I could not have survived/thrived without everyone. Stephen Dearth, my graduate student mentor, showed me how to do my first metabolomics extraction and how to clean and calibrate an Orbitrap. Allen Bourdon made all those long hours in cold room much more bearable. Josh Powers was always around and willing to listen to my crazy rants. You know what they say about 3 guys in a room? Caleb Gibson was always there to motivate me to keep working on the CRP and ORP. Brittni Woodall was always willing to pick another set of lipids for me, so I could focus on writing. Brandon Kennedy for always ready to help me with some crazy synthesis scheme. Dr. Hector Castro was an invaluable asset providing me projects and allowing me to network with new collaborators as well as being a great friend. And finally, thanks to rest of the Campagna lab (former and present) for making the laboratory a great environment to learn.

I would like to thank my parents, Vince and Kathy, for the constant support to keep doing my best and never give up. My Aunt Linda and Uncle Cliff for not letting me take a job at Gateway Packing and encouraging me to keep continuing my education.

The completion of this degree would have never even begun without my amazing wife, Jennifer. Even through her own graduate school struggles, she was there to comfort me during the dark times and celebrate with me during the successful times. I cannot thank her enough for being that beacon of motivation and inspiration that I needed.

ABSTRACT

Metabolomics measures all the small, biologically relevant molecules present within a system. An effective way to achieve high-throughput sample analysis and diverse pathway coverage in metabolomics is to use ultra performance liquid chromatography (UPLC) coupled to high-resolution mass spectrometry (HRMS). Depending on the compounds of interest, untargeted or targeted methods can be implemented. Efforts have been focused on analyzing how different forms of stress alter an organism's metabolite profile.

Genetic mutations can inhibit essential metabolic pathways of an organism, but there are often redundant or alternative routes available for continued growth. By systematically deleting single genes in *Escherichia coli* responsible for the production of individual enzymes in the tricarboxylic acid cycle, it was possible to measure alterations in metabolites and correlate them to specific mutations. With the use of untargeted UPLC-HRMS, 146 known metabolites and over 1,800 significant unknown spectral features were identified. Comparative and multivariate analysis show intense changes were observed in strains lacking Aconitase B and unique global metabolic profiles were enzymatically linked and not strictly based on pathway disruption.

Enterococcus faecalis has been shown to develop antibiotic tolerance to daptomycin by incorporation of host-produced fats. The exact biological mechanism by which this bacterium incorporates host lipids into their membranes is currently unknown. The use of a hybrid quadrupole Orbitrap mass spectrometer allowed for the development of a novel method to simultaneously quantify two-tailed phospholipids and four-tailed cardiolipins which pose analytical challenges due to low biological abundances and poor ionization efficiencies. By leveraging HILIC separation and parallel reaction monitoring (PRM), additional information with respect to identities about which specific fatty acids composition was simultaneously measured.

A sub-population of *Spodoptera frugiperda* has been identified as resistant to genetically modified corn and has been causing rampant pest related crop loss. Previous research has shown a link between resistance and a mutation to the ATP binding cassette subfamily C2 gene. Untargeted metabolomic analyses were applied to profile the gut tissue of the larvae and found potential metabolites related to this mutation. From the 126 metabolites, six were found in significantly higher amounts in resistant insects when compared of susceptible insects.

TABLE OF CONTENTS

INTRODUCTION 1
Metabolomics 2
Analytical Technique for Metabolite Analysis 3
Types of Metabolomics Analyses 5
Data Analysis for Metabolomics 6
The Future of Metabolomics 7
Outline of Dissertation 8
Chapter 1 GENETIC MUTATIONS TO THE TRICARBOXYLIC ACID CYCLE INFLUENCE METABOLOMIC AND LIPIDOMIC PROFILES 10
Preface 11
1.1 Abstract 14
1.2 Introduction 15
1.3 Experimental 17
1.3.1 Strain generation 17
1.3.2 Bacterial growth conditions 17
1.3.3 Microscopy 19
1.3.4 Metabolomics 19
1.3.5 Lipidomics 21
1.3.6 Flux analysis 22
1.3.7 Data processing 23
1.3.8 Unidentified spectral features 24
1.4 Results and Discussion 24
1.4.1 Growth changes 24
1.4.2 Global metabolites 27
1.4.3 Tricarboxylic acid cycle metabolites 29
1.4.4 Arginine biosynthesis 29
1.4.5 Chemometric analysis 32
1.4.6 Unidentified spectral features 35

1.4.7 Lipid analysis 38
1.4.8 Flux analysis 41
1.5 Conclusion 48
1.6 Appendix 49
Chapter 2 EXPANDING LIPIDOMICS COVERERAGE: EFFECTIVE ULTRA PERFROMANCE LIQUID CHROMATOGRAPHY-HIGH RESOLUTION MASS SPECTROMETER METHODS FOR THE DETECTION AND QUANTITATION OF CARDIOLIPIN PHOSPHATIDYLGLYCEROL, AND LYSYL-PHOSPHATIDYLGLYCEROL 127
Preface 128
2.1 Abstract 131
2.2 Introduction 131
2.3 Experimental Section 134
2.3.1 Untargeted standards 134
2.3.2 Targeted standards 134
2.3.3 Biological samples 135
2.3.4 Extraction of lipids from biological samples 137
2.4 Liquid Chromatography- Mass Spectrometry Parameters 137
2.4.1 Untargeted lipid analysis 138
2.4.2 Targeted phospholipid analysis 138
2.4.3 Targeted compound list 139
2.4.4 Calibration curve preparation 141
2.5 Data Analysis 141
2.5.1 Untargeted 141
2.5.2 Targeted 141
2.6 Results and Discussion 142
2.6.1 Untargeted data 142
2.6.2 Targeted data 145
2.6.3 Biological validation 147
2.7 Conclusion 150

2.8 Appendix 154
Chapter 3 MIDGUT METABOLOMIC PROFILING OF FALL ARMYWORM (*Spodoptera FRUGIPERDA*) WITH FIELD-EVOLVED RESISTANCE TO CRY1F CORN 165
Preface 166
3.1 Abstract 169
3.2 Introduction 169
3.3 Materials and Methods 171
3.3.1 Insect strains 171
3.3.2 Protoxin preparation 171
3.3.3 Bioassays 172
3.3.4 Larval treatments 173
3.3.5 Tissue sample preparation and metabolite extraction 173
3.3.6 Ultra performance liquid chromatography- high resolution mass spectrometry metabolomic analysis 174
3.4 Results 175
3.4.1 Cry1F protoxin bioassay 175
3.4.2 Metabolomics and multivariate data analysis 178
3.4.3 Comparative metabolite profiling 180
3.5 Discussion 185
3.6 Appendix 191
CONCLUSION 218
REFERENCES 221
VITA 236

LIST OF TABLES

Table 1.1: Details of gene mutations in each strain of *E.coli*.....18
Table 1.2 Growth times of 8 different *E. coli* strains.....26
Table 1.3 Number of significant *metabolites for each strain.* 30
Table 1.4 Summary of the number of knowns metabolites identified as significant in pairwise PLSDA. 36
Table 1.5 Mass/charge, identity, error and retention time of unknown features that matches to dipeptide.....39
Table 1.6 Relative pool size, relative turnover, and relative flux for five metabolites. 45
Table 1.7 Oligonucleotides used in this study.....49
Table 1.8 Ratios and p-values used for heat map of knowns 53
Table 1.9 VIP scores for pairwise PLSDA.....77
Table 1.10 Ratios and p-values used for heat map of dipeptides 91
Table 1.11 Ratios and p-values used for heat map of lipids 95
Table 1.12 Relative pool values for each strain compared to WT.....99
Table 1.13 Relative turnover values for each strain compared to WT.....112
Table 1.14 Relative flux values for each strain compared to WT 121
Table 2.1 Details for lipid standards used for the targeted analysis.....136
Table 2.2 Details for lipid standards used for the untargeted analysis.....144
Table 2.3 Quantitative lipid data for biological samples. 151
Table 2.4 Full list of compounds included in PRM. 154
Table 2.5 Averages for integrated areas used for calibration curves.....158
Table 2.6 Ratios and p-values used to create heat map for untargeted data....161
Table 2.7 Concentrations for lipids measured in each sample for the targeted method.....162
Table 3.1 Susceptibility of *S. frugiperda* lines to Cry1F protoxin in diet incorporation bioassays.....176

Table 3.2 Metabolites with VIP* score >1 that support differentiation of Ben, 456M/456F and 456LS3 samples in the PLSDA multivariate space regardless of the food source. 181
Table 3.3 Metabolites with significantly altered levels ($p < 0.05$) in Ben, 456M and 456F lines compared to larvae from the 456LS3 strain fed on meridic diet. 184
Table 3.4 Metabolites with significantly altered levels ($p < 0.05$) in Ben, 456F and 456M when compared to 456LS3 larvae fed non-Bt corn leaf tissue. 186
Table 3.5 Metabolites with significantly altered levels ($p < 0.05$) in guts from 456LS3 larvae fed leaf tissue from Cry1F-producing or the non-Bt corn isoline. 187
Table 3.6 Metabolites with Variable Importance in Projections (VIP) scores. ... 192
Table 3.7 Metabolites with Variable Importance in Projections (VIP) scores. ... 195
Table 3.8 Ratios and p-values used to make heat map for samples fed meridic diet 198
Table 3.9 Ratios and p-values used to make heat map for samples fed non-Bt corn 207

LIST OF FIGURES

Figure 1.1 Workflow for how cells were grown on isotopically labeled media. 20
Figure 1.2 Growth of *E. coli* over time....25
Figure 1.3 Heat map for known metabolites. 28
Figure 1.4 Heatmap overlaid on pathway map of TCA cycle 31
Figure 1.5 Heatmap overlaid on arginine biosynthesis pathway 33
Figure 1.6 Partial least squares discriminate analysis using known metabolites for all mutant strains and wild type....34
Figure 1.7 Partial Least Squares Discriminate Analysis using unknown features for all mutant strains and wild type....37
Figure 1.8 Heat map of unknown features annotated as dipeptides 40
Figure 1.9 Heat map for lipids detected for each strain compared to WT. 42
Figure 1.10 Flux plots showing a reduction of unlabeled material over time....44
Figure 1.11 Optical microscopy images of seven mutant and one wild type strain of *E.coli*. 51
Figure 1.12 Known metabolite pairwise PLSDA for ΔacnA....73
Figure 1.13 Known metabolite pairwise PLSDA for *ΔacnB* 73
Figure 1.14 Known metabolite pairwise PLSDA for *ΔsucAB* 74
Figure 1.15 Known metabolite pairwise PLSDA for *ΔsucCD*....74
Figure 1.16 Known metabolite pairwise PLSDA for *ΔfumA*....75
Figure 1.17 Known metabolite pairwise PLSDA for *ΔsdhAD* 75
Figure 1.18 Known metabolite pairwise PLSDA for *Δmdh*....76
Figure 1.19 Unknown feature pairwise PLSDA for *ΔacnA*....87
Figure 1.20 Unknown feature pairwise PLSDA for *ΔacnB*....87
Figure 1.21 Unknown feature pairwise PLSDA for *ΔsucAB* 88
Figure 1.22 Unknown feature pairwise PLSDA for *ΔsucCD* 88
Figure 1.23 Unknown feature pairwise PLSDA for *ΔsdhAD* 89
Figure 1.24 Unknown feature pairwise PLSDA for *ΔfumA* 89
Figure 1.25 Unknown feature pairwise PLSDA for *Δmdh*....90

Figure 2.1 Structure of fragments used to quantitate lipids cardiolipin, phosphatidylglycerol, and lysyl phosphatidylglycerol. 140
Figure 2.2 All ion fragmentation of PS (34:2) standard. 146
Figure 2.3 Heat map of lipid compounds detected using the untargeted analysis. 149
Figure 2.4 Extracted ion chromatograms of PRM data for representative compounds in targeted analysis. 156
Figure 2.5 Calibration curves for the three standards used in the targeted analysis 157
Figure 2.6 Structure of exogenous fats added to biological samples 160
Figure 2.7 Fragmentation spectra of cardiolipin compounds detected in biological samples supplemented with linoleic acid 164
Figure 3.1 Average weight of *Spodoptera frugiperda* neonates fed on diet (Diet), corn event TC1507 producing Cry1F (BtC) or the non-transgenic isoline 2T777 (NBtC) until reaching 4th instar.....177
Figure 3.2 Partial Least Squares Discriminate Analysis (PLSDA) scores plots displaying different clusters when comparing metabolite profiles of midguts from *S. frugiperda* larvae from different strains fed on meridic diet (Top) or non-Bt corn leaf tissue (Bottom). 179
Figure 3.3 Heat maps of relative levels of metabolites detected in guts of *S. frugiperda* larvae fed on meridic diet.....182
Figure 3.4 Heat maps of relative levels of metabolites detected in guts of *S. frugiperda* larvae fed on non-Bt corn leaf tissue. 183
Figure 3.5 Pathway map of all the detected metabolites (red circles). 191

INTRODUCTION

Metabolomics

Metabolomics is the most recent addition and arguably the most important level of the omics cascade with respect to biological phenotype. Unlike other, more mature and standardized omic analyses such as genomics, transcriptomics, or proteomics, metabolomics does not possess a standard approach to identification, validation, and publication of data. This presents an analytical challenge for scientists to compare and optimize experiments; however, this leaves ample opportunity to develop new approaches in attempts to find suitable metrics across the diverse metabolomics community. The field is still in its infancy, leading to a variety of constraints including lack of metabolite knowledge, instrumentation limitations, and management of immense data sets

The single, most challenging factor in metabolite detection is the sheer number of different molecule types that are included in the umbrella term “metabolomics”. In genomics, methods are optimized to detect the arrangements of four or five different nucleotides. Since these compounds are conserved across many different organisms, genomic techniques are simply transferred between unlike systems with minimal modification. A similar situation is seen in the proteomics field, but instead of detecting the nucleotides, there are a handful of amino acids that are necessary to measure. The amino acids have similar chemical properties and are common among different organisms, resulting in a small number of methods being needed. Again, this leads to measurement techniques and the data generated to be easily understood by all individuals in the field. In addition to just measuring specific amino acids, proteomics involves the probing of secondary and tertiary structures of the whole protein as well as accounting for various post translational modifications. This was the first time that the scientific community was faced with the phenomena of “big data”, where experiments were creating information faster than results and conclusions could be interpreted. This has led to large, publicly available repositories of protein data which has encouraged collaborative data analyses across the world.

Within the realm of metabolomics, the goal is to measure all metabolites present in a system. This poses a challenge unlike any other omics technique due to the large number of possible molecules that are measurable in the system of interest. Additionally, the set of metabolites present in an organism is not consistent; therefore, transferring methods across sample types can be challenging. For example, if one metabolomics experiment is optimized for plant metabolites, it is most likely not ideal for mammalian metabolite analysis. The issues are not solely based on the vast number of compounds, but the fact that the compounds have diverse structures. Metabolites typically have mass to charge ratios (*m/z)*'s up to 2,000 Da and contain a variety of functional groups. Depending on the metabolite class and its intrinsic properties, the methods required to measure these varying classes of metabolites are often very different. This further exemplifies the need to apply multiple analytical methods to measure groups of metabolites that have different structures within the same organism. The final challenge in metabolomics is being able to quickly and reproducibly halt metabolism in order to measure the metabolites present. The metabolites can be very labile, unlike proteins or DNA, therefore great care is necessary to prevent or limit the degradation throughout the sample collection, metabolite extraction, and analysis process.

Analytical Technique for Metabolite Analysis

At the onset of metabolomics, mass spectrometry was the key for detecting many compounds simultaneously. Prior to any type of mass analysis, a chromatography step is introduced to allow for the separation of compounds based on an interaction with a stationary phase. Initially, gas chromatography (GC) was chosen due to its simplicity and ability to interface with a mass spectrometer. The knowledge of GC separation was well known and produced reliable data with detectors such as flame ionization detection (FID) or thermal conductivity detection

(TCD). With the uses of a hard ionization source like electron ionization (EI) or chemical ionization (CI), it was possible to obtain mass to charge (*m/z*), and fragmentation data for compounds separated via GC. The typical mass spectrometer is coupled to a GC and uses a quadrupole or an ion trap as the mass analyzer. GC-MS provides excellent information for a variety of experiments including structure elucidation based on fragmentation, but it is limited by its low mass accuracy. GC is inherently selective for compounds that are nonpolar, have small *m/z's,* and are easily volatilized (short chain fatty acids, alkanes, alcohols, and aromatic compounds). When combining these concerns, GC-MS metabolite analyses can only cover a small portion of an organism's metabolome, especially if the organism contains a large water-soluble fraction.

In order to investigate water-soluble metabolites, liquid chromatography-mass spectrometry (LC-MS) is used. Unlike GC-MS, this technique allows for separation and detection of polar and amphiphilic molecules. Depending on the specific LC column chosen, it is possible to separate a wide variety of metabolite classes. Ionization of the LC eluent is typically achieved by electrospray ionization (ESI) or atmospheric pressure chemical ionization (APCI), creating $[M-H]^-$ or $[M+H]^+$ species. Initially, triple quadrupole mass spectrometers were the most popular choice for metabolite analysis. The detection of a metabolite is achieved by the initial selection of a parent ion, followed by a fragmentation step, then the selection of a specific fragment. This approach is ideal when looking for a limited number of specific compounds because the triple quadrupole is only capable to detecting a single *m/z* at a time. If multiple *m/z*'s are scanned during the same time window, the instrument must cycle through scan events causing a reduction in sensitivity. The mass resolution of a tripled quadrupole instrument is low, causing problems when attempting to distinguish between two *m/z's* that differ by a small amount, As the metabolomics field matures, the need to profile many compounds simultaneously, as well as perform experiments in an untargeted fashion has become apparent.

The use of high-resolution mass spectrometers (HRMS), such as Orbitraps, have attempted to resolve the limitations of the triple quadrupole. The Orbitrap uses a football shaped electrode as the mass analyzer to measure the frequency of image currents. Fast Fourier transform deconvolutes the frequencies into mass to charge ratios. This allows for the detection of all *m/z's* concurrently without the need for specific user input values. Another benefit of using HRMS, is high mass accuracy, which is five parts per million or less, providing the ability to distinguish small metabolites with very similar exact masses.

This technology advances metabolomics by providing analytical instrumentation to identify changes in biological systems based on metabolites that are both known and unknown. These "unknowns" have metabolite features in the chromatographic and mass domains but do not correspond to a known metabolite. The newest class of high-resolution mass spectrometers consists of hybrid Orbitraps, which combine the benefits of an Orbitrap with the ability to target ions using a quadrupole mass filter. This technology provides instrumentation needed to begin identifying unknown spectral features and determine what role they play in metabolism.

Types of Metabolomics Analyses

Metabolomic analyses can be divided into two broad classifications: untargeted and targeted. Each specific type of analysis has attributes that are optimized for the goals of the experiment. An untargeted experiment is used in an exploratory approach where the goal is to measure as many compounds as possible and investigate changes in metabolite trends compared to a control. Data is collected across a wide *m/z* range and metabolites are identified in a post-acquisition manner, using multiple verification factors such as retention time, exact mass, and isotopic abundance patterns. As aforementioned, this method is also able to measure changes in spectral features that are not identifiable as specific

metabolites. Data collected from this analysis tends to be in the form of relative abundances and not absolute concentrations. Metabolite comparisons are made for the same metabolite across the different sample treatments not between different metabolites within the same sample treatment.

In a targeted approach, specific compounds of interest are identified prior to analysis, allowing for the chromatographic and mass spectrometric conditions to be optimized. The only data collected are for the transitions designated by the acquisition method. These transitions are linked to the *m/z* of the parent ion and a known *m/z* fragment. Since the method is only analyzing a limited number of *m/z's*, and not scanning across a wide range, there is an increase in instrument sensitivity. This fact, combined with an external calibration curve or internal standards, allows for collection of absolute quantitative data with low detection limits. The downside to using a targeted approach is the loss of ability to search collected data for metabolites that were not originally included in the analysis. A hybrid Orbitrap, such as the Q-Exactive Orbitrap, has a quadrupole mass filter prior to the mass analyzer allowing for selection of a parent ion and a full scan of fragments, instead of being limited to a single fragment per scan event. When operating in this mode, it is possible to obtain high-resolution, quantitative data using known transitions while also gathering information about many other fragments from the same parent ion. This proves beneficial not only for quantitation from multiple fragments, but also serves as a possible way to isolate an ion which does not have a known structure. The fragmentation can then be used to attempt to identify the molecule.

Data Analysis for Metabolomics

Data analysis for metabolomics is not currently standardized which leads to processing specifics to vary based on the type of analysis, the goals of the experiment, specific metabolites detected, and the lab doing the analysis. Due to

the highly dynamic nature of metabolites, it is very important to include specific controls, blanks, and an appropriate number of replicate samples. This ensures any changes in the data are a result of the independent variable and not due to random or systematic errors propagated through the extraction and analysis steps. Chromatographic features can be classified into two classes: annotated or identified. In this dissertation, annotated features refer to features that have an exact *m/z* and retention time but cannot be correlated to a metabolite in the database. Identified refers to matching exact *m/z* and retention time to a metabolite in a database. Annotation can be performed by many freely available software packages as well as subscription-based services. Peak identification can be performed by the mass spectrometer's software, or by third party software such as XCMS. After all the peaks in the chromatogram have been annotated with *m/z's* and retention times, molecular formulas can be generated for all features that did not match to a compound in the database. This assigned formula can be used to determine potential metabolite structure and correlate molecules to compound classes or even used to discover a potential biomarker

The Future of Metabolomics

From its humble onset of detecting tens of common metabolites using a triple quadrupole, the field of metabolomics is growing at an exponential rate. As more and more sample types are being analyzed using metabolomics, there is always a need to refine metabolite protocols and extract more meaningful conclusions from the data. Currently, metabolomics is faced with challenges of complex sample matrices, such as rhizospheres. In this example, the analytical challenge comes from having many different bacterial species in a common soil, along with roots from plants. It is difficult to isolate, extract, and correlate the origin of the metabolites. To overcome this, a combination of isotopic labeling and independent extractions can be useful. Information about how different species are

symbiotically produce and consume metabolites can show how species share and utilize nutrients in a common environment. Again, this could lead to the discovery of new molecules that are responsible for metabolite transfer between organisms or to the expansion of current metabolic pathways. Additionally, in order to enhance coverage of the metabolome or analyze more complex samples, there must be continued advancement of instrumental technologies. The newest line of high-resolution mass spectrometers utilizes three different mass analyzers to achieve complex metabolite measurements simultaneously.

Outline of Dissertation

Herein, the versatility of metabolomics of and its applications within three unique environments will be discussed. The first chapter uses multiple untargeted approaches to profile hydrophilic and phospholipid compounds on a global level for seven different genetic variants of *E. coli*. In addition to relative concentrations of metabolites, a relative flux analysis was performed using the same untargeted approach, but cells were grown in the presence of an isotopically labeled substrate to measure relative rates of metabolites. The second chapter focuses on the development of a targeted method to quantitate phospholipids, currently thought to be related to antibiotic tolerance in *E. faecalis*. The same samples were used to analyze global phospholipids and free fats in the membrane of the wild type and genetically modified versions of the bacteria. The third chapter shows how metabolomics was used to probe a complex higher order organism and understand the relationship between resistance and abundant small molecules. Gut samples from toxin resistant and susceptible *Spodoptera frugiperda* larvae were analyzed using untargeted metabolomics to find indicator metabolites linked to the resistant phenotype.

CHAPTER 1 GENETIC MUTATIONS TO THE TRICARBOXYLIC ACID CYCLE INFLUENCE METABOLOMIC AND LIPIDOMIC PROFILES

Preface

Multiple metabolomic analyses were applied to an organism which lacked enzymes in a very important metabolic pathway in order to understand how it continued to grow. This not only helped quantify the changes of metabolites in this specific pathway, but also provided data to generate new hypotheses about how the distant metabolic pathways were interrelated as well as how unknown spectral features (unidentified metabolites) were changing.

Escherichia coli was genetically modified to not produce different enzymes that were critical to the tricarboxylic acid cycle (TCA). Seven different strains were made, each containing a single gene mutation, accounting for the majority of the enzymes in the cycle. It was not possible to make a viable mutant strain that lacked citrate synthase, the first enzyme in the TCA cycle, as the cells required heavy nutrient supplementation. All of the other strains were able to grow in minimal media with a single carbon source. An untargeted hydrophilic metabolite analysis was initially performed, and over 10,0000 total spectral features were detected. In addition, 146 metabolites were identified across all the strains including 8 of the 9 metabolites directly involved in the cycle. The standard metabolomics analysis provides a static view of the metabolite populations, but it was unable to show how those metabolite pools were changing over time. To achieve temporal resolution of these metabolite, an isotopically labeled flux analysis was conducted. This involved switching the bacteria's only carbon source from unlabeled glucose to one that was fully labeled with carbon-13 atoms, and sampling at different time points. The same untargeted metabolite analysis was conducted but it was now possible to identify how many carbons in the metabolite contained a heavy atom. Based on how quickly isotopologues were detected, turnover rates of the metabolite pool could be inferred, as well as if that metabolite was produced from solely glucose or from some other recycling pathway.

Knowing the metabolome consists of much more than just polar molecules, an untargeted lipidomics analysis was also performed. This technique targeted

phospholipids in five different head group classes. It was possible to detect multiple phospholipids species within a class, and distinct changes were seen among the different mutants. This showed that phospholipid levels were directly related to lack of a specific enzyme in central carbon metabolism.

This data will be part of an initial publication, which is the first to collect a global metabolite profile for these specific mutants. Future publications are planned with the intent to further investigate the unidentified features using bioinformatics tools to identify new classes of or individual molecules changing due to these mutations.

A version of this chapter is expected to be part of a future publication by:

Tague, Eric, D.; Wen, Jia; Powers, Joshua B.; Castro, Hector F.; Fozo, Elizabeth M.; Campagna, Shawn R.

Contributions:

EDT designed the experiment, conducted the metabolomics experiment, analyzed the data, and wrote the manuscript. JW made the bacterial mutants. JBP assisted in metabolite extraction and helped write the manuscript. HFC helped write the manuscript. EMF made the bacterial mutants and helped write the manuscript. SRC designed the experiment and helped write the manuscript.

1.1 Abstract

The most important process for an aerobic organism is the ability to metabolize sugars into usable energy through a series of oxidative processes. At the heart of carbon metabolism is the tricarboxylic acid cycle (TCA) which is imperative for its survival. Even in the event of a genetic mutation, a critical enzyme in this cycle could be missing but the cell does not perish. The full understanding of how an organism compensates for these enzyme deficiencies is not fully established. By measuring metabolites and how they change between mutant strains and the parental strain (or wild type strain) provides a snapshot into how the organism is compensating for this stress. Using the bacterium *Escherichia coli* as a model system, genes encoding for seven major enzymes in the TCA cycle were systematically deleted. This is the first time a comprehensive metabolic profile has been collected for these *E. coli* variants. Herein, metabolomics, lipidomics, and relative flux analyses were employed to determine how the organism adjusted its metabolite concentrations to compensate for the loss of specific enzymes. Ultra performance liquid chromatography - high resolution mass spectrometry measured 146 unique known metabolites, 28 different phospholipids, and thousands of unknown metabolite-like features. Additionally, flux analysis was used to monitor the relative rates of metabolite production and consumption over time. If the mutation exists early in the TCA cycle, the bacteria exhibits more perturbations to its metabolite pools. A strain deleted for the gene *acnB* (Aconitase B) proved to cause the most alterations in the global metabolome when compare to the other mutants. These broad analyses show that cells possess machinery to combat mutations to an essential pathway, the TCA cycle, and the effects can be measured in tangential metabolic processes, like phospholipid biosynthesis.

1.2 Introduction

Aerobic organisms utilize the tricarboxylic acid (TCA) cycle to convert a carbon source such as glucose into metabolites necessary to sustain life and replicate. The TCA cycle uses acetyl-CoA generated from the processing of pyruvate from glycolysis to produce energy carrying cofactors (NADH, and $FADH_2$) which are recycled in the electron transport chain to produce a large amount of ATP [1]. This recycling process is achieved with the aid of specific enzymes working in a cyclic fashion to generate small organic molecules necessary for the proceeding reactions. These intermediates not only provide for the continuation of the cycle but also allow for the biosynthesis of several amino acids[2]. If a single enzyme in this cycle is not functioning correctly, the cell could encounter growth inhibition, oxidative stress, and even death. To protect from these situations, cells have adopted many strategies to circumvent immediate death. It has been shown that even if a cell is missing an essential enzyme, it is still able to survive[3]. It is not fully known how such a mutant cell continues its metabolic processes and what effect it has on auxiliary pathways and those metabolite pools.

In order to understand how bacterial cells grow, three complementary metabolomic techniques will be used to correlate genetic mutations with altered metabolism. Employing an untargeted metabolomics approach captures a global snapshot of what small molecules are present. By using ultra performance liquid chromatography (UPLC) paired with high resolution mass spectrometry (HRMS), metabolites with varying size and polarity can be analyzed in a single run. This is an ideal analysis approach because it is possible to gather relative concentrations of hundreds of compounds with known *m/z*'s and retention times in addition to thousands of spectral features with unidentified biochemical functions. This technique has been applied to biological systems ranging from simple cultured bacteria[4] to the complex interactions of fungi and endobacteria[5] and shows how a unique metabolic profile is related to distinct phenotypic changes. By adjusting the extraction, and chromatographic conditions, it is possible to measure both small

(<1000 *m/z*), hydrophilic compounds and phospholipid species in under one hour. Using the same mass spectrometric technologies but substituting the carbon source with a fully isotopically labeled materials allows for temporal information regarding relative rates of metabolite flux to be collected[6]. This shows how quickly a metabolite's pool is being turned over and can elicit pathways that undergo drastic changes.

Escherichia coli (E. coli) was chosen for the study because it is easy to culture in a lab, most lab strains are nonhazardous, and the genome is fully sequenced[7]. It is considered a model organism, so the metabolomics conclusions generated from this study can be applied to more complex systems. *E.coli* does not require complex media additives to survive, making it an ideal starting place to analyze global metabolome changes as a result of non-lethal genetic mutations to the TCA cycle. Seven different enzymes in the TCA cycle of *E. coli* were systematically removed via genetic modification, and their metabolomes measured. Previously, producing these genetic mutations within this organism has been proven to be successful and selective[8]. Even though many have investigated the cellular effects of genetic mutations of *E.coli*[9-12], a large profiling of metabolites and their relative net fluxes for these specific mutants has yet to be completed. An understanding of what the cells are doing at the metabolite level in order to continue growing in the presence of genetic stress is still not known.

This work shows that it is possible to acquire and differentiate global metabolomics data for cells with a deletion of genes encoding for a single metabolic enzyme. Moreover, these data show that a single genetic mutation that affects production of a single protein will have considerable repercussions on many other pathways. Discernible effects with respect to relative amounts of specific polar molecules, and phospholipids can also be seen using this approach. Taking this into account, researchers will be keeping abreast of novel drug targets, have a clearer understanding of the linkage between cellular processes, and discover new avenues of research with respect to how an organism's global metabolite profile changes.

1.3 Experimental

1.3.1 Strain generation

The strains used in this study are listed in **Table 1.1**; all oligonucleotide sequences used in strain generation are listed in **Appendix Table1.7** Specific gene deletion strains generated were *acnA* (aconitase hydratase A), *acnB* (aconitase hydratase B) *sucAB* (alpha-ketoglutarate dehydrogenases), *sucCD* (Succinyl CoA synthase alpha and betta subunits), *shdAD* (succinate dehydrogenase subunits A,B,C, and D), *fumA* (fumarase A), and *mdh* (malate dehydrogenase). All deletion strains were generated using mini- λ Red recombination[13-16]. Primers were used to amplify the kanamycin cassette of pKD4[13], and contained approximately 40 nucleotides of homology to the chromosomal region.

1.3.2 Bacterial growth conditions

Cells were grown on M9 minimal media (42.2 mM Na_2HPO_4; 22.0 mML KH_2PO_4; 18.6 mM NH_4Cl; 0.9 mM NaCl) supplemented with micronutrients at final concentrations of 1mM $MgSO_4$, 0.1mM $CaCl_2$, 1 µg/mL thiamine, and 0.4% glucose for all experimental analysis. Agar media was prepared by adding 15 g/L agar to the previously mentioned M9 media. Strains were grown from a frozen stock and single colonies were isolated from an overnight plate before being transferred to liquid culture. Cells were kept at a constant 37°C and continuously shaken at 200 rpm. Cells were grown overnight in minimal media and diluted to an OD_{600} of 0.01 to determine generation time for biological triplicates for all strains.

For metabolomic analysis, overnight cultures were diluted 1:100 and grown to an OD_{600} of approximately 0.40. Then, 5mL of culture was filtered via vacuum onto a 0.40 µm polycarbonate filter (Whatman). Metabolism was quenched by placing the filter in cold extraction solvent (4:4:2 methanol: acetonitrile: water with 0.1% formic acid) immediately following filtration. Cells for lipidomics were grown

Table 1.1: Details of gene mutations in each strain of *E.coli*

Name	Relevant genotype or description	Source
Escherichia coli MG1655	Wildtype *E. coli*	Lab stock, Fozo
acnA::kan	MG1655 *ΔacnA::kan*	This study
acnB::kan	MG1655 *ΔacnB::kan*	This study
sucCD::kan	MG1655 *ΔsucCD::kan*	This study
sdhCADB::kan	MG1655 *ΔsdhCADB::kan*	This study
mdh::kan	MG1655 *Δmdh::kan*	This study
sucAB::kan	MG1655 *ΔsucAB::kan*	This study

similarly but were harvested via centrifugation at 16,600 x g at 4°C for 10 minutes to form a pellet.

For flux analysis, cells were initially grown in liquid media to an OD_{600} of 0.10, then 5 mL of cells were filtered and allowed to grow on the filters placed atop agar media plates (unlabeled glucose) until an OD_{600} of 0.40 (**Figure 1.1**)[17].To ascertain approximate optical densities of the cells on the filters, optical densities of an extra biological replicate were measured by washing the cells off with 5 mL of media. Media plates that contained ^{13}C glucose were prepared in the same fashion as the unlabeled plates except for the carbon source was switched to ^{13}C-6 glucose (Cambridge Isotope Laboratory, 98% purity). After the flux experiment was complete, cells were then quenched by placing filters in cold extraction solvent.

1.3.3 Microscopy

Cells were collected at an OD_{600} of ~0.40. 1 mL of cells were diluted in 4 mL of PBS and centrifuged to form a pellet. The supernatant was decanted, and 20 mL of fresh PBS was added to the tube and mixed thoroughly. An agarose mat was used to immobilize the cells prior to imaging. 20 μL of cellular solution was dropped on the mat. A bright field microscope with a 100x oil immersion lens was used to investigate any possible changes in size, shape, or growth patterns among mutants.

1.3.4 Metabolomics

The extraction protocol is adapted from a previously described method[18]. Briefly, samples were extracted using an acidic acetonitrile solution (40:40:20 ACN:MeOH:H_2O with formic acid at a final concentration of 0.1 M) . After cell collection on the filter, filters were left in extraction solvent, cell side down, for 20 minutes at -20°C. The extraction solution was then transferred to conical vials and the filter washed to ensure a complete transfer of material. The vials were then centrifuged, and supernatant moved to a clean vial. The remaining cell pellet was washed with solvent and allowed to extract for another 20 minutes, followed by

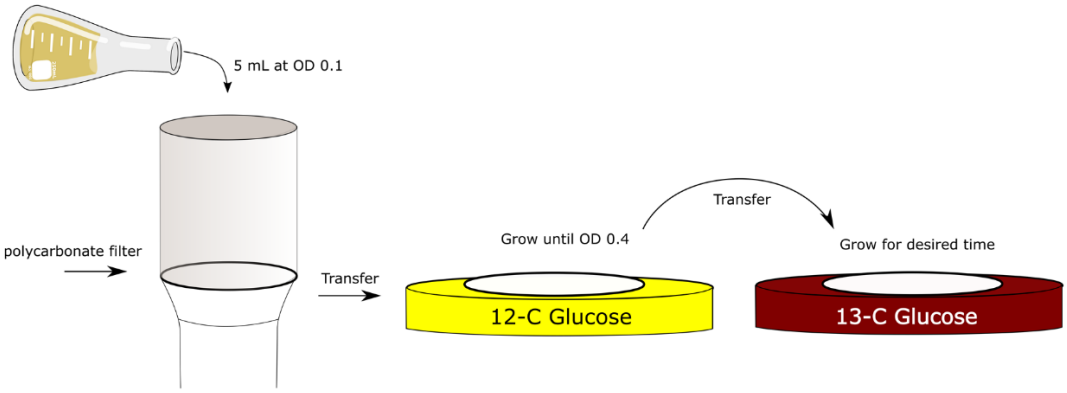

Figure 1.1 Workflow for how cells were grown on isotopically labeled media.

centrifugation and transfer of supernatant to the previous aliquot. A stream of nitrogen was used to evaporate the solvent, then 300µL of Millipore water was used to re-suspend the samples.

A Dionex UltiMate 3000 Ultra Performance Liquid Chromatography (UPLC)(Thermo Scientific, Waltham, MA) system coupled to an Exactive Plus Orbitrap Mass Spectrometer (Thermo Scientific, Waltham, MA) was used to separate and detect the metabolites found in the extracted cell cultures. The method utilized a reverse phase chromatography system with detection in the negative mode of the mass spectrometer[19]. A Synergi Hydro-RP column (100 mm x 2 mm 2.5 µm) (Phenomenex Torrance, CA, USA) was used to separate a 10 µL aliquot of sample and was maintained at 25° C. Mobile A was 15mM acetic acid, 11mM tributylamine in 97:3 (v/v) water: methanol and mobile phase B was 100% methanol. The solvent gradient was: *t*= 0 min 100% solvent A 0% solvent B; *t*=5 min 80% solvent A 20% solvent B; *t*=13 min 45% solvent A 55% solvent B; *t*=15.5 min 5% solvent A 95% solvent B; *t*= 19 min 100% solvent A 0% solvent B; *t*=25 min 100% solvent A 0% solvent B. The flow rate was kept at 0.200µL/min. An electrospray ionization source (ESI) had a sheath gas of 25, aux gas of 8, and sweep gas of 3 at a constant voltage of 3.00 kV. The capillary temperature was 300° C. The mass spectrometer collected negative ions at resolution of 140,000, with an AGC of $3x\ 10^6$ ions over the range of 72 *m/z* to 1000 *m/z*. Detection of known metabolites was based upon the exact mass of the negative ion *(m/z*), and a known retention time (RT) then compared to an in-house curated database. These two pieces of information allowed for the annotation of several hundred unique metabolites within each sample.

1.3.5 Lipidomics

The extraction of lipids from the cells used a well-established method that has been previously reported[20]. After the cell pellet was suspended in 9:1 methanol: chloroform, 10 µL of sample was injected onto the UPLC instrument with a Kinetex HILIC column (150 mm x 2.1 mm, 2.6 µm) (Phenomenex, Torrance, CA,

USA). The mobile phases consisted of 10mM ammonium formate in water, mobile phase A and 10mM ammonium formate in 93% acetonitrile and 7% water for mobile phase B, both solvents were adjusted to a pH of 3.0. The flow rate was held constant at 0.200µL per minute and the column oven was set to 25°C for the 35-minute duration. Gradient: *t*= 0 min 0% solvent A, 100% solvent B; *t* =1 min 0% solvent A 100% solvent B; *t* =15 min 19% solvent A 81% solvent B; *t* =15.1 min 52% solvent A 48% solvent B; *t* =25 min 52% solvent A 48% solvent B; *t* =25.1 min 0% solvent A 100% solvent B; *t* =35 min 0% solvent A 100% solvent B.[21]

An Exactive Plus Orbitrap mass spectrometer and Dionex UltiMate 3000 UPLC with an electrospray ionization source was used to analyze the eluent. Mass spectrometer parameters were set as follows; spray voltage set to 4 kV, heated capillary 350 °C, sheath and aux gas to 25 and 10 units respectively. Lipid analysis was performed in both positive and negative mode to detect as many phospholipids as possible. Full scan and all ion fragmentation data was gathered at maximum resolution with a mass range of 100-1,500 m/z and 30 ev normalized collision energy. Annotation of compounds was achieved by exact mass, retention time and head group fragmentation.

1.3.6 Flux analysis

After the filtered cells reached an OD_{600} of 0.40 while growing on minimal medial plates that were supplemented with unlabeled glucose, the entire filter was transferred cell side up to ^{13}C glucose supplemented minimal media plate. Cellular growth was quenched by chilled extraction solvent at 1, 2, 5, 10, 15, 30, and 60 minutes in biological triplicate for all time points[17]. Plots showing percentage incorporation over time was calculated and plotted using the FluxR package in R (publication pending). The software package averages the replicates and fits the data to a decay function $y=Ae^{-kt},+C$ allowing for the turnover rate, k, to be calculated or each metabolite across all strains. To calculate relative pool size (Rp), or relative turnover rates (Rk), a simple ratio is taken compared to the value of the wild type and the error is calculated. Relative flux (Rf) is calculated by taking

the product of the relative pool size (Rp) and the relative turnover rate (Rk) (**Equations 1 and 2**).

Equation 1:

$$Rf_x = Rp_x * Rk_x$$

Equation 2:

$$\delta Rf_x = Rf_x * \sqrt{(\frac{\delta Rp_x}{Rp_x})^2 + (\frac{\delta Rk_x}{Rk_x})^2}$$

Rf_x= relative flux of metabolite x

Rp_x= relative pool size of metabolite x

Rk_x= relative turnover rate of metabolite x

δRf_x= error of relative flux of metabolite x

δRk_x= standard deviation of turnover rate of metabolite x

δRp_x= standard deviation of pool size for metabolite x

1.3.7 Data processing

Data files were converted to mzML using MsConvert[22] a tool within Proteowizard[23] and processed using MAVEN software[24]. Annotation parameters consisted of exact masses within a ±5 ppm window and known retention times of standards. All integrated areas were normalized to optical density. Heatmaps were generated using an in-house created R Script with all fold changes being log_2 transformed prior to plotting. Significance was determined by a Student's T-test. Comparisons were made with respect to the wild type strain and fold changes are based on a log_2 scale. The DiscriMiner package in R was utilized for multivariate analysis such as partial least squares discriminate analysis (PLSDA)[25] with a leave one out cross validation. Data were log transformed, three components were used, and leave one out cross validation was applied. The calculation of relative flux for each metabolite is the product of the relative metabolite pool and the relative turnover rate.

1.3.8 Unidentified spectral features

XCMS, an open source script developed to analyze chromatographic peaks generated by high resolution mass spectrometry data[26] was used to annotate *m/z*-retention time pairs. CAMERA[27] was then used to identify *m/z*-RT pairs as possible adducts and/or isotopes. These features were removed prior to any further processing to avoid potential metabolite bias from these features. To further reduce the quantity of features and reduce the noise, the signal intensity had to be 3 times the signal intensity of the extraction and media controls. Values were normalized to OD_{600} measurements, prior to any analysis. Multivariate analysis was performed on the data set to determine features with significant change. Theoretical molecular formulas were generated by using Seven Golden Rules[28], with a 5 ppm error window, and restrictions to the following elements: C, N,H, O, P, and S.

1.4 Results and Discussion

1.4.1 Growth changes

Though the cells were all grown in the same media with glucose as the only source of carbon, distinct changes in their generation time was observed **(Figure 1.2**). The WT (MG1655) strain reached stationary phase the fastest with a doubling time of 1.68 hours, which is consistent with literature values[29, 30]. All seven mutant strains had a significantly longer doubling time than the wild type, most likely because the pathway for energy production, the tricarboxylic acid cycle, lacked critical enzymes. Doubling times ranged from over 2.75 hours for *ΔacnB* strain to 1.90 hours for *ΔfumA* strain (**Table 1.2**). The *ΔacnB*, *ΔsucAB* and*, ΔsucCD* strains all had doubling times that were significantly different from the other 4 mutant stains, but not significantly different from one another. The *ΔacnA, ΔsdhAD, ΔfumA,* and *Δmdh* mutant strains also had doubling times that were similar to one another but significantly different from the previously mentioned mutant strains. The difference in doubling times demonstrates that if a gene is deleted that codes

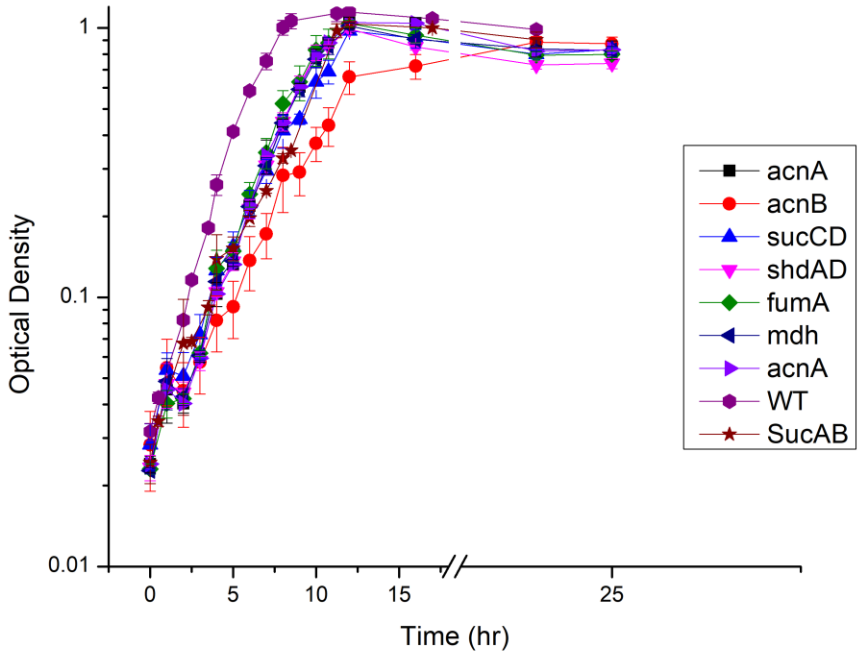

Figure 1.2 Growth of *E. coli* over time

Table 1.2 Growth times of 8 different *E. coli* strains

Error is calculated by standard deviation of the replicates, and significance is calculated by an unpaired Student's T-test. Values in bold represent comparisons of doubling time that is <0.05.

Strain	Td (hr)	p-values							
		ΔacnB	***ΔsucAB***	***ΔsucCD***	***Δmdh***	***ΔsdhAD***	***ΔacnA***	***ΔfumA***	**WT**
ΔacnB	2.79±0.29	1	*0.163*	0.099	**0.035**	**0.029**	**0.032**	**0.031**	**0.022**
ΔsucAB	2.44±0.12	0.163	*1*	0.216	**0.011**	**0.009**	**0.008**	**0.008**	**0.007**
ΔsucCD	2.31±0.07	0.099	*0.216*	1	**0.014**	**0.015**	**0.003**	**0.002**	**0.002**
Δmdh	2.01±0.09	**0.035**	***0.011***	**0.014**	1	0.657	0.315	0.148	**0.020**
ΔsdhAD	1.98±.010	**0.029**	***0.009***	**0.015**	0.657	1	0.633	0.336	**0.036**
ΔacnA	1.94±0.06	**0.032**	***0.008***	**0.003**	0.315	0.633	1	0.464	**0.014**
ΔfumA	1.90±0.05	**0.031**	**0.008**	**0.002**	0.148	0.336	0.464	1	**0.012**
WT	1.68±0.02	**0.022**	**0.007**	**0.002**	**0.020**	**0.036**	**0.014**	**0.012**	1

for an enzyme in the beginning of the TCA cycle, their growth will be similar to the other mutant strains which lack enzymes in this half of the cycle. The opposite is also true for mutant stains lacking enzymes in the second half of TCA cycle. The only exception to this trend appears to be the *ΔacnA* strain. Although not possessing an enzyme that is located at the beginning of the cycle, its growth pattern resembles mutant strains with enzyme deficiencies later in the cycle. Upon optical inspection of the wildtype and mutant stains, all cells appeared to be rod-shaped with no observable anomalies and relatively consistent sizes (**Appendix Figure 1.11).**

1.4.2 Global metabolites

Using an in-house curated list of standards, 146 metabolites were identified based on exact mass (± 5 ppm) and retention time. The heat map shows all identified metabolites in which each strain is compared to the WT (**Figure 1.3, Appendix Table 1.8**). Metabolites that had significant changes are noted with the following: p-value <0.01-***, <0.05-**,<0.1-*. The color of the box indicates the direction of the change, orange representing the metabolite was detected in higher amounts in the mutant strains when compared to the wild type strain. The first column, representing *ΔacnA* strain, shows that 50% of the metabolites measured, had fold changes greater than 2, and only 1 metabolite had a fold change less than 0.5. The opposite trend can be seen the *ΔacnB* strain where 42.5% of the metabolites showed a fold change of less than 0.5, as represented by the blue color in the heatmap. The *Δmdh* strain had the fewest number (8%) of fold changes greater than 2 and less than 0.5. This is visually interpreted by the muted colored cells in the last column of the **Figure 1.3**. This is not overly surprising because malate dehydrogenase is the final enzyme in the TCA cycle so many of the critical intermediate metabolites necessary for biosynthesis have already been produced earlier in the cycle.

A similar trend in fold changes is seen when comparing *ΔacnB* and *ΔsucCD* strains. In addition to observing large wholistic fold changes, some of the smaller

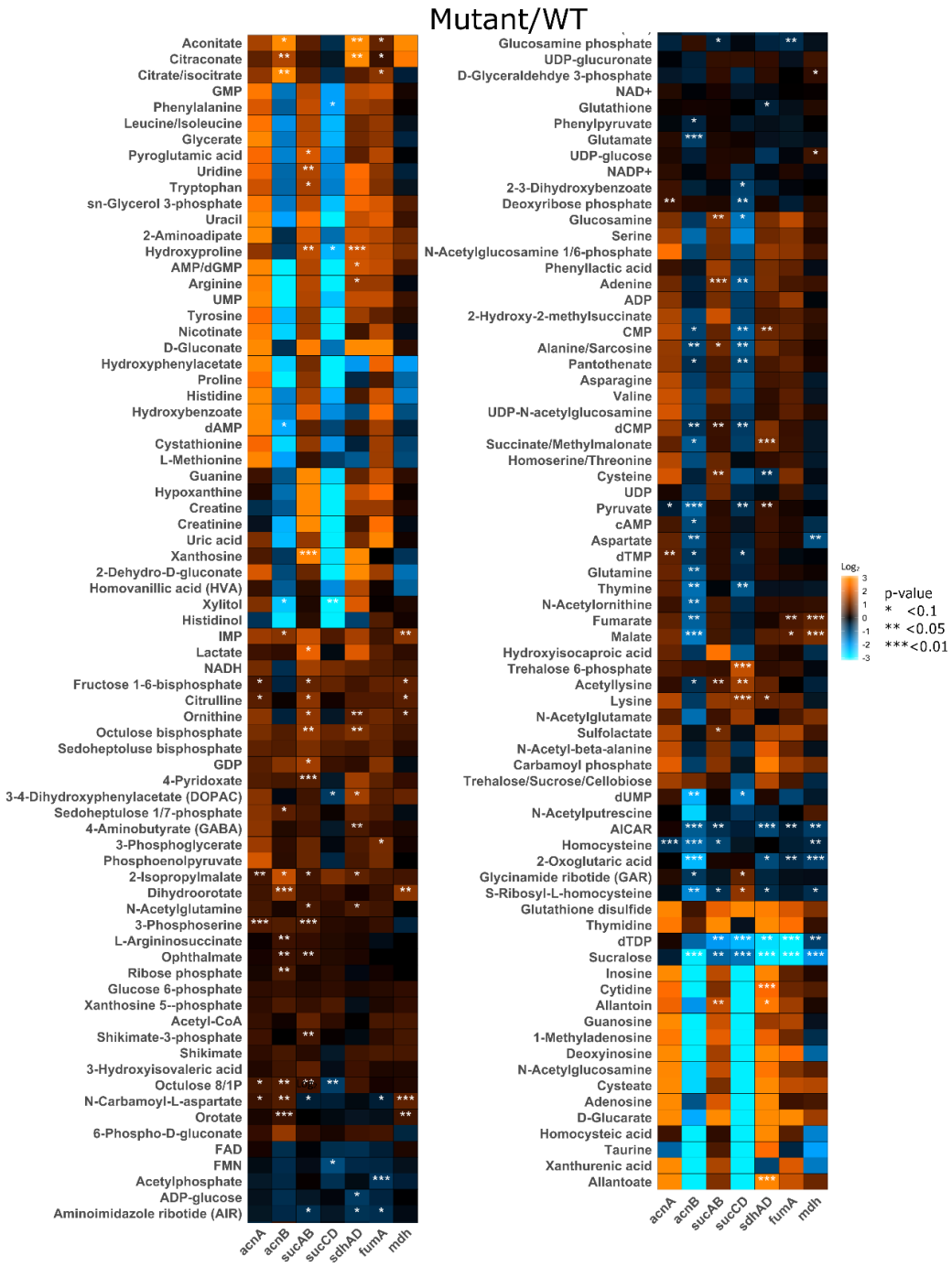

Figure 1.3 Heat map for known metabolites.

Each column represents a $\log_2$ fold change of the average intensity for each metabolite compared to the average intensity of the WT. p-values are represented by asterisks

fold changes are still significant can aid in explaining how the mutation is affecting metabolism. Again, we see *ΔacnB* mutants have the greatest number of significant fold changes (p-value <0.1) with 39 metabolites (**Table 1.3**). While *ΔacnA* had the least number of significant fold changes, and the intensity of these fold changes were very large, suggesting large variation within this mutant strain.

1.4.3 Tricarboxylic acid cycle metabolites

Changes in the relative amounts of TCA metabolites were anticipated to be observed and this analysis was able to detect 6 of 9 of those metabolites. The TCA pathway with overlaid heat map slices was created to allow for the direct comparisons to be made (**Figure 1.4**). Once again, deletion of Δ*acnB* perturbed many metabolites throughout the pathway. Pyruvate was 2.4 times lower in the *ΔacnB* strain indicating that the amount of substrate entering the cycle is lower compared to the wild type strain. Next, the levels of citrate and aconitate were over ten times higher in this strain, presumably due to the lack of biosynthesis of isocitrate. It is important to note that citrate and isocitrate were detected as the same feature because they have identical *m/z* and are not separable in the chromatographic space used. All metabolites in the TCA cycle after the aconitase B deleted enzyme (2-oxoglutraric acid, succinate, fumarate, and malate) showed significant decreases, leading to the assumption that there is slow down of cycle. This was confirmed by the above-mentioned increase in doubling time. These changes are not mirrored by the homologous enzyme AcnA, but this is consistent with previous data suggesting these enzymes operate under unique conditions[31] We see a significant accumulation of succinate and decrease in fumarate in the *ΔshdAD* strain, confirming that the dehydrogenation reaction is reduced.

1.4.4 Arginine biosynthesis

In addition to being able to look at molecules directly related to the cycle where the mutation has occurred, an untargeted metabolomics approach can produce information about a wide variety of other pathways. The arginine biosynthesis pathway had near complete coverage with the detection of 12

Table 1.3 Number of significant metabolites for each strain.

Significance is based on Student's T-test (p≤0.1)

Strain	Significant Metabolites	Metabolites with a fold change >2	Metabolites with a fold change <0.5
ΔacnA	10	73	1
ΔacnB	39	9	62
ΔsucAB	34	64	2
ΔsucCD	25	8	61
ΔsdhAD	27	55	4
ΔfumA	14	49	2
Δmdh	18	11	12

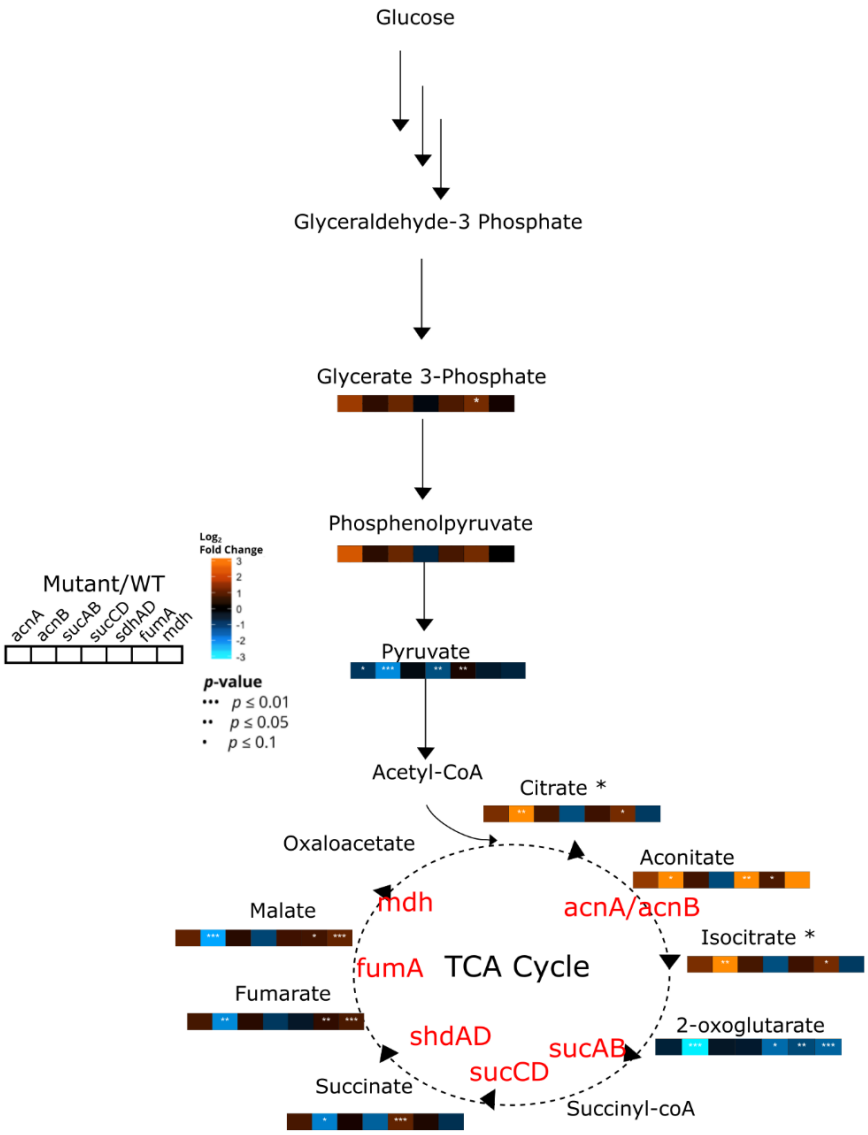

Figure 1.4 Heatmap overlaid on pathway map of TCA cycle

metabolites. Arginine is an essential amino acid for the continuation of cell growth, and accounts for 5% of all amino acids in the proteins within in *E.coli*[32]. Since these cells were grown in minimal media, they must produce these compounds *de novo* which starts with the conversion of glutamate, followed by a variety of intermediates which serve as branching off points for other metabolic pathways, before finally producing arginine[33]. With the ability to measure many of the intermediates, it is possible to explain how the cells' metabolite pools are changing (**Figure 1.5**). A decrease in all identified metabolites, except for aginosuccinate are observed for the *ΔacnB* strain. The overall decrease can be traced back to the low levels for 2-oxoglutaric acid, a precursor to glutamate, which was produced as a direct effect of the genetic mutation. None of the other strains demonstrate this total decrease in metabolite levels throughout arginine synthesis, presumably because there is an adequate supply of glutamate being produced

1.4.5 Chemometric analysis

Multivariate tools like PLSDA were used to separate mutants based on which metabolites showed the greatest change[34, 35] among groups. These plots attempt to calculate how much of the explained variance is being contributed from each variable, or metabolite[36]. The PLSDA (**Figure 1.6**) shows the separation of all seven mutant strains and the wild type using the 146 identified metabolites. The distance between the ellipses denotes the degree of uniqueness of the mutation's metabolite profile. Using this analysis *ΔacnB* strain is completely isolated in component space, indictive of its metabolome being vastly different from the WT strain and the other strains. The other mutant strains have metabolite profiles similar to the WT strain when compared to the *ΔacnB* strain. To determine which specific metabolites were driving the separations, variable importance in projection values (VIP) were extracted and analyzed. These values represent which metabolites contribute most to the separation seen within the PLSDA plot. A score greater than 1 was used as the minimum to be considered a significant metabolite in the separation[36-38]. A total of 43 metabolites were reported as having a

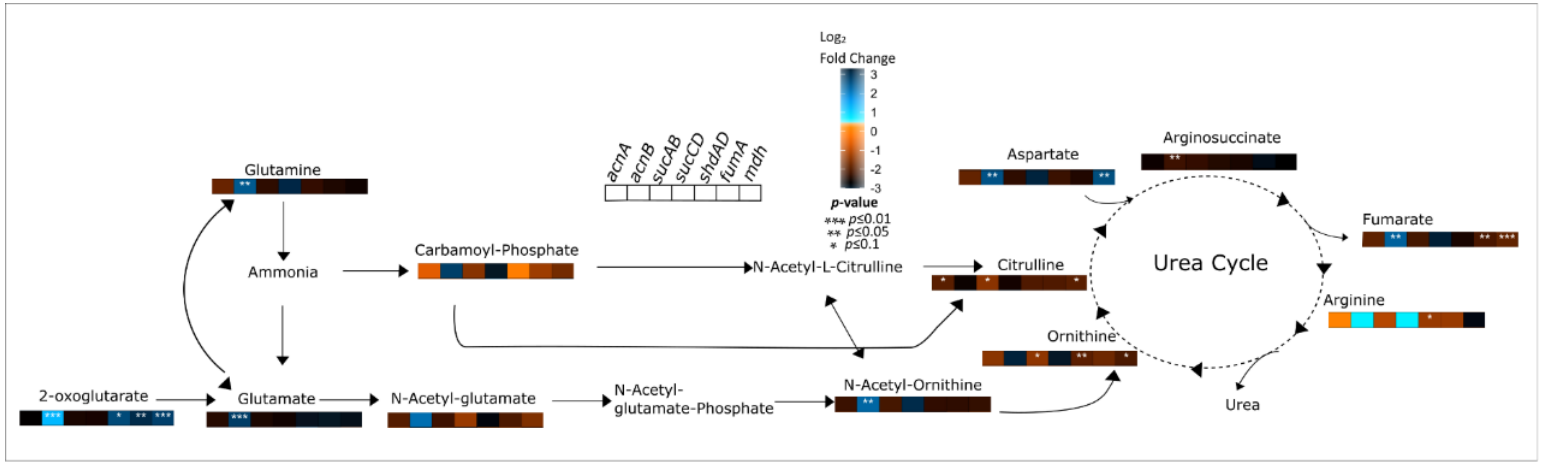

Figure 1.5 Heatmap overlaid on arginine biosynthesis pathway

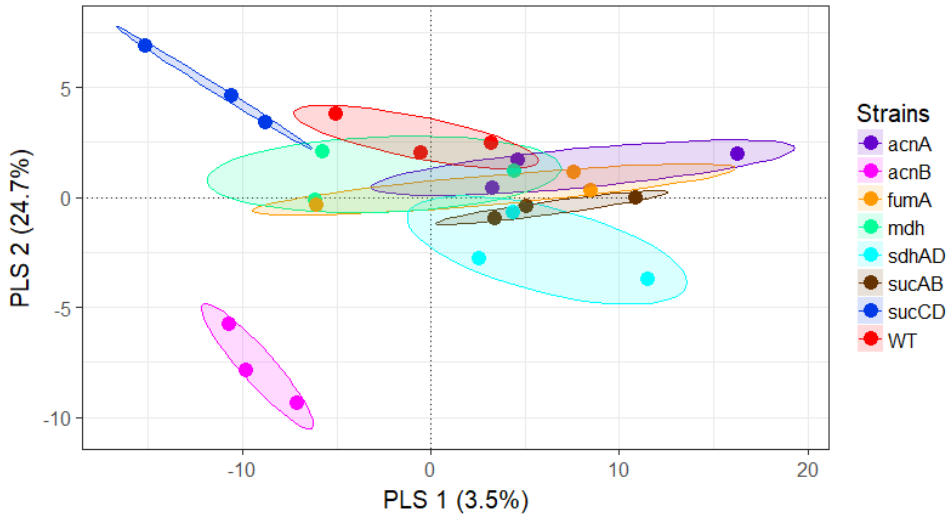

Figure 1.6 Partial least squares discriminate analysis using known metabolites for all mutant strains and wild type

significant weight for driving the separation, and almost all of them were directly related to the production of amino acids or nucleotide base synthesis (data not shown). This further solidifies the argument that deletion of this single gene has detrimental effects on the cell's ability for cellular reproduction and protein substrate formation. Pairwise PLSDA comparisons (**Appendix Figures 1.12-1.18**) and VIP scores (**Appendix Table 1.9**) between each mutant and wild type strain show each group is separable by multivariate analysis; however the metabolites that drive the separation are different. Mutations *ΔacnB* and *ΔsucCD* had the most metabolites with VIP scores greater than 1, while *ΔacnA* had the fewest (**Table 1.4)**. Only one metabolite, glucosamine, was identified as contributing to separation between each mutant and the wild type strains.

1.4.6 Unidentified spectral features

One benefit of using a high-resolution mass spectrometer in full scan modes is the collection of chromatographic peaks across a large *m/z* range. This means it is possible to identify a m/z-retention time peak as a "known" metabolite it if matches a previously analyzed standard. In addition to the metabolites that have been identified, there were thousands of other *m/z*-RT pairs (spectral features) that did not match any compound in the selected database. After postprocessing the unknown spectral features generated by XCMS and CAMERA, 1869 features remained. These features exhibited metabolite like characteristics, but the exact structures are not known. After meticulous data reduction, it is possible to use this data gathered for multivariate analyses to determine what unknown features were changing across the strains. The PLSDA for the unknowns (**Figure 1.7**) look very similar to the PLSDA of the known metabolites (**Figure 1.6**). This plot shows the profiles of unknown metabolites are unique for the *ΔacnB* strain when compared to the WT and the other genetically modified strains. Again, pairwise PLSDA was performed (**Appendix Figures 1.19-1.25**) showing each individual strain has an unknown metabolite profile that separable in multivariate space compared to the wild type. When VIP scores were calculated of this set of unknows, 822 features

Table 1.4 Summary of the number of knowns metabolites identified as significant in pairwise PLSDA.

Strain	VIP >1
ΔacnB	78
ΔacnA	47
ΔsucAB	68
ΔsucCD	74
ΔsdhAD	70
ΔfumA	54
Δmdh	54

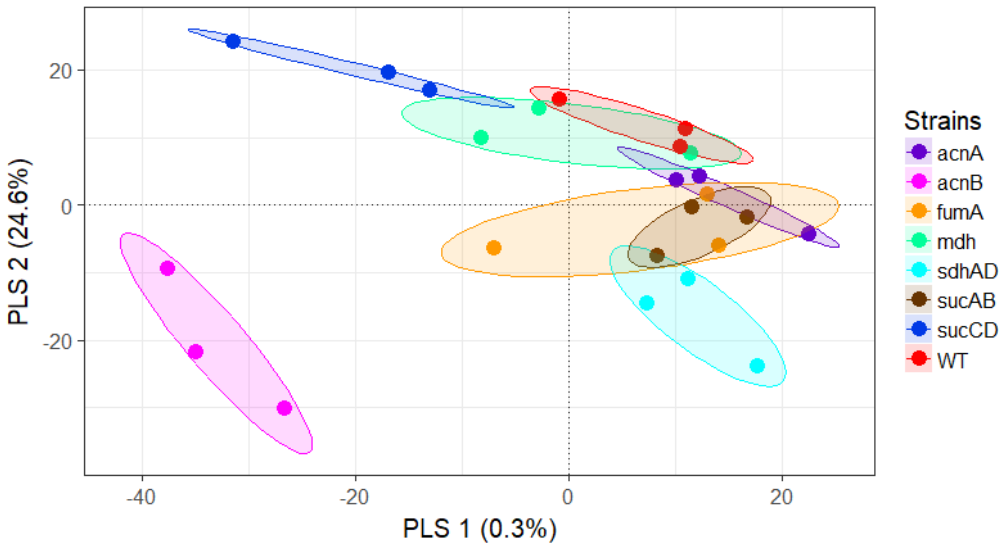

Figure 1.7 Partial Least Squares Discriminate Analysis using unknown features for all mutant strains and wild type

had values ≥1. Eleven of these significant VIPs features corresponded the exact *m/z* for different dipeptides.

Aside from looking at the unknown features collectively, it is also possible to further probe the data for individual compounds that may not have any direct relation to the pathways of interests or have a specific function. Within these data, 22 features were tentatively annotated as dipeptides, based on an exact mass with an error less than 5 ppm (**Table 1.5**), and a molecular formula match using the Seven Golden Rules. Since the UPLC-HRMS method did not perform any fragmentation scans, and standards for each dipeptide were not in the reference library used, it was not possible to confirm the exact identity of any isomeric amino acid residues. The heat map (**Figure 1.8, Appendix Table 1.10**) shows how these dipeptides are changing in relative abundance when compared to the wild type. There were relatively few significant changes, but the bulk of the changes are seen in the *ΔacnB* and *ΔsucAB* strains with 6 and 7 significant changes respectively. This corresponds with the earlier known metabolomics data that shows these two strains result in the most varied metabolome. With the *ΔacnB* strain, the majority of the dipeptides are in lower abundance, and most notability are Gly-Asp, Met-Glu, Met-Asp, and Glu-Pro. The individual free amino acids, glutamate, methionine, and aspartic acid are all lower in abundance as well (**Figure 1.8**). Conversely, the *ΔsucAB* strain have the majority of the dipeptides in greater abundance than the wild type, as seen by glycine-cystine, and glutamine-alanine. The detection of these short peptides has only been reported in a handful of bacterial samples, notability when the organism is facing some sort of stress

1.4.7 Lipid analysis

Previous literature reports phosphatidylethanolamine (PE), phosphatidylglycerol (PG), and cardiolipin (CL) are the major lipid species present in *E.coli*, membranes[39] while others show that PA and PS make up much smaller percentages.[40-42] Although many studies have focused on investigating how lipid composition changes during different growth phases in response to temperature

Table 1.5 Mass/charge, identity, error and retention time of unknown features that matches to dipeptide

m/z detected	Exact *m/z* of Dipeptide	Dipeptide ID	Error (ppm)	RT (min)
159.0774	159.0775	Ala-Ala	0.629	1.18
173.0930	173.0931	Val-Gly	0.578	1.69
177.0339	177.0338	Gly-Cys	0.565	1.47
189.0517	189.0516	Gly-Asp	0.529	8.23
191.0672	191.0673	Ser-Ser	0.523	1.16
201.0881	201.0880	Ser-Pro	0.497	8.33
202.0833	202.0832	Asn-Ala	0.495	6.71
215.1035	215.1036	Thr-Pro	0.465	1.24
216.0991	216.0989	Gln-Ala	0.926	7.37
217.0828	217.0830	Glu-Ala	0.921	4.51
233.0778	233.0779	Glu-Ser	0.429	6.43
243.0986	243.0986	Glu-Pro	0.000	4.88
251.0515	251.0528	Cys-Met	5.178	11.18
259.1299	259.1299	Leu-Glu	0.000	8.89
260.0888	260.0888	Asn-Glu	0.000	4.98
261.0730	261.0728	Asp-Glu	0.766	11.25
263.0707	263.0706	Met-Asp	0.380	8.65
275.0889	275.0885	Glu-Glu	1.454	11.17
277.0864	277.0863	Met-Glu	0.361	7.40
279.0834	279.0841	Met-Met	2.508	4.63
309.1096	309.1092	Glu-Tyr	1.294	9.96
336.1669	336.1677	Arg-Tyr	2.380	9.27

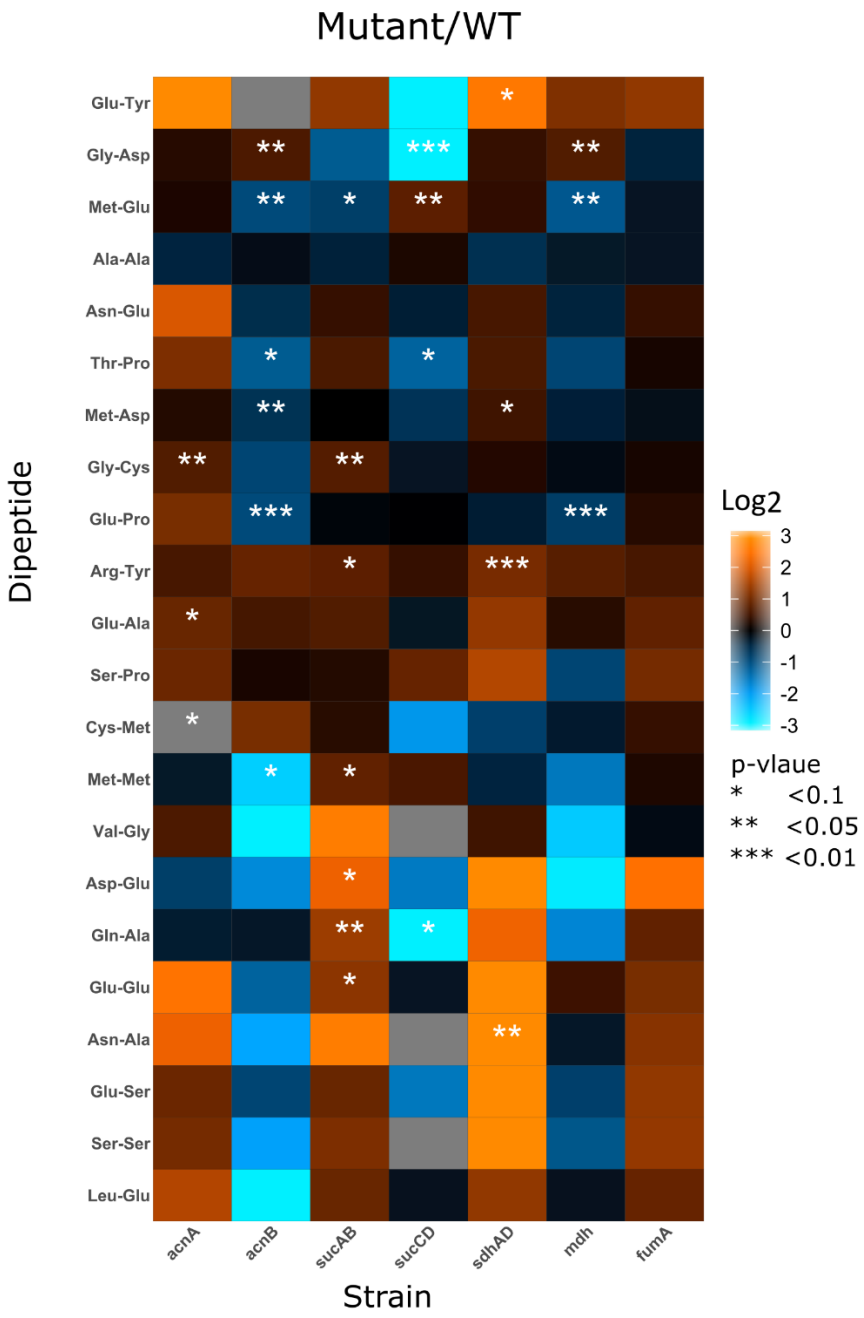

Figure 1.8 Heat map of unknown features annotated as dipeptides

Ratios are mutant compared to the wild type. Significance is dented by the asterisks

or by the elimination of a protein responsible for lipid synthesis[39], lipidomic analysis is able to capture lipid changes based on genetic mutations in a cycle not directly related to the biosynthesis of phospholipids. Primary acyl chain lengths in *E.coli* are hexadecanoic acid (C16:0), tetradecanoic (C14:0), cis-9-hexadecanoic (C16:1), and cis-11-octadecenoic (C18:1).[43] The untargeted lipid analysis detected five different phospholipid classes; phosphatidylethanolamine (PE), phosphatidylglycerol (PG), phosphatidic acid (PA), phosphatidylserine (PS), and cardiolipin (CL). Unique compounds were identified by exact mass (±5 ppm) and known head group retention time. Since this analysis is not capable of determining the exact fatty acid tails attached to the glycerol backbone, unique species are listed by head group abbreviation, the sum of carbons, and double bonds in all fatty acid tails. Four CL, five PA, nine, PE, six PG, and four PS compounds were identified across all samples. A heat map shows all detected phospholipids compared to the wild type (**Figure 1.9, Appendix Table 1.11**). The continued trend that a deletion of the *ΔacnB* gene causes large changes is also reflected in the lipidomics data. All the significant lipids show a decrease for the *ΔacnB* mutant, whereas many of the other mutants have very small and nonsignificant fold changes. When investigating the nine PE compounds detected, eight of the lipids were significantly decreased in the *ΔacnB* strain. Although *E.coli* possesses a mechanism to maintain the ratio of PE to PG/CL[44],drastic changes can be seen for PE(30:2) and PE(28:1) in *ΔacnA* and *ΔfumA* mutants. It is known that PE makes up 70% of the cell's membrane, and the inability to produce such compounds can lead to complications within cellular division[45, 46]. It is surprising to see such negligible changes in all mutants other than *ΔacnB*. These data support the idea that the phospholipid composition is highly dependent on the site of mutation.

1.4.8 Flux analysis

The flux analysis was able to measure isotopic labeling of carbons in 87 of the 146 metabolites detected, including six metabolites used as substrates in the TCA cycle. Not all metabolites measured showed appreciable labeling due to slow

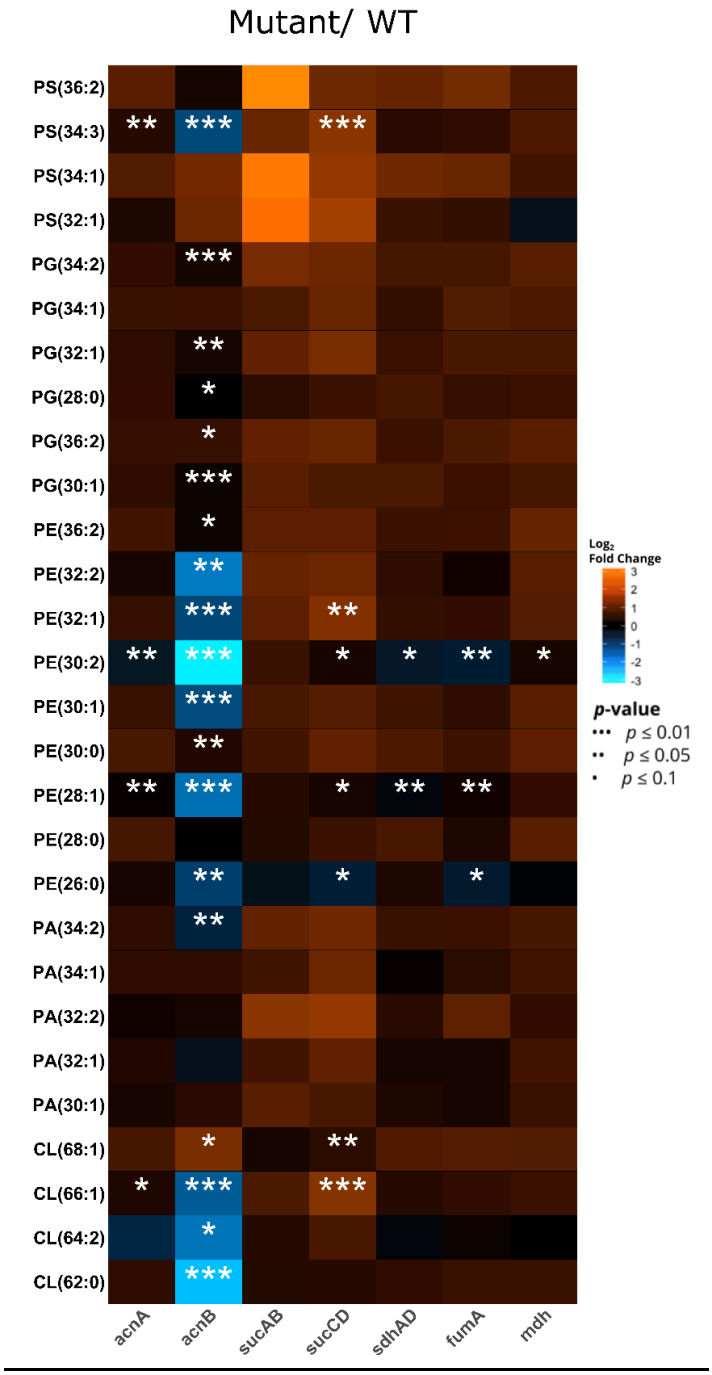

Figure 1.9 Heat map for lipids detected for each strain compared to WT.

Significance depicted by asterisks

de novo biosynthesis. Six metabolites that had different rates of incorporation for specific mutants are shown (**Figure 1.10**). 2-oxoglutrate shows very rapid labeling in the WT and all mutant strains except for *ΔacnA* and *ΔsucAB*. These mutants showed a slight decrease in how quickly these metabolites were labeled with ^{13}C. Succinate showed quick labeling in the wild type strain which indicates that the first half of the TCA cycle was working rapidly, but the *ΔsdhAD* strain, which is responsible for the dehydrogenation of succinate to form fumarate, only became partially labeled after 60 minutes. This suggests that only half of the succinate molecule is being produced from the labeled glucose and taken through the TCA cycle. Strangely, all other deletion strains show no labeling suggesting that succinate in not being produced from glucose, but from some salvage pathway. Once again, *ΔacnB* mutants show unique behavior for fumarate, malate, and glutamate with decreased labeling. Phenylalanine has an opposite trend where the WT, *ΔacnA*, and *ΔacnB* strains show no labeling but the remaining mutant strains show a similar trend of rapid incorporation.

It is also possible to compare the relative flux of the metabolite pools, which considers the metabolite concentration and the turnover rate of the metabolite[47]. The relative flux calculation is based on the ratio of mutant flux compared to wild type for both the metabolite pool and the turnover rate. The metabolite pool is collected from the untargeted metabolomics data, and the turnover rate is collected from the isotope flux data. If the flux is large, it could be a result of a very large fold change in a metabolite, a very quick turnover, or some combination of both. Relative flux was only calculated for eighty-one metabolites, **(Appendix Tables 1.12-1.14**) since a metabolite must be detected in both the untargeted metabolomics data and the flux experiment. A subset of relative flux data shows drastic changes across the different strains (**Table 1.6**). This phenomenon is best observed when comparing glutamate, glutamine, 2-oxoglutaric acid glutathione, and glutathione disulfide.

As noted in the arginine section above, *ΔacnB* strains show a significant decrease in pool size of these intermediate metabolites, which include glutamine,

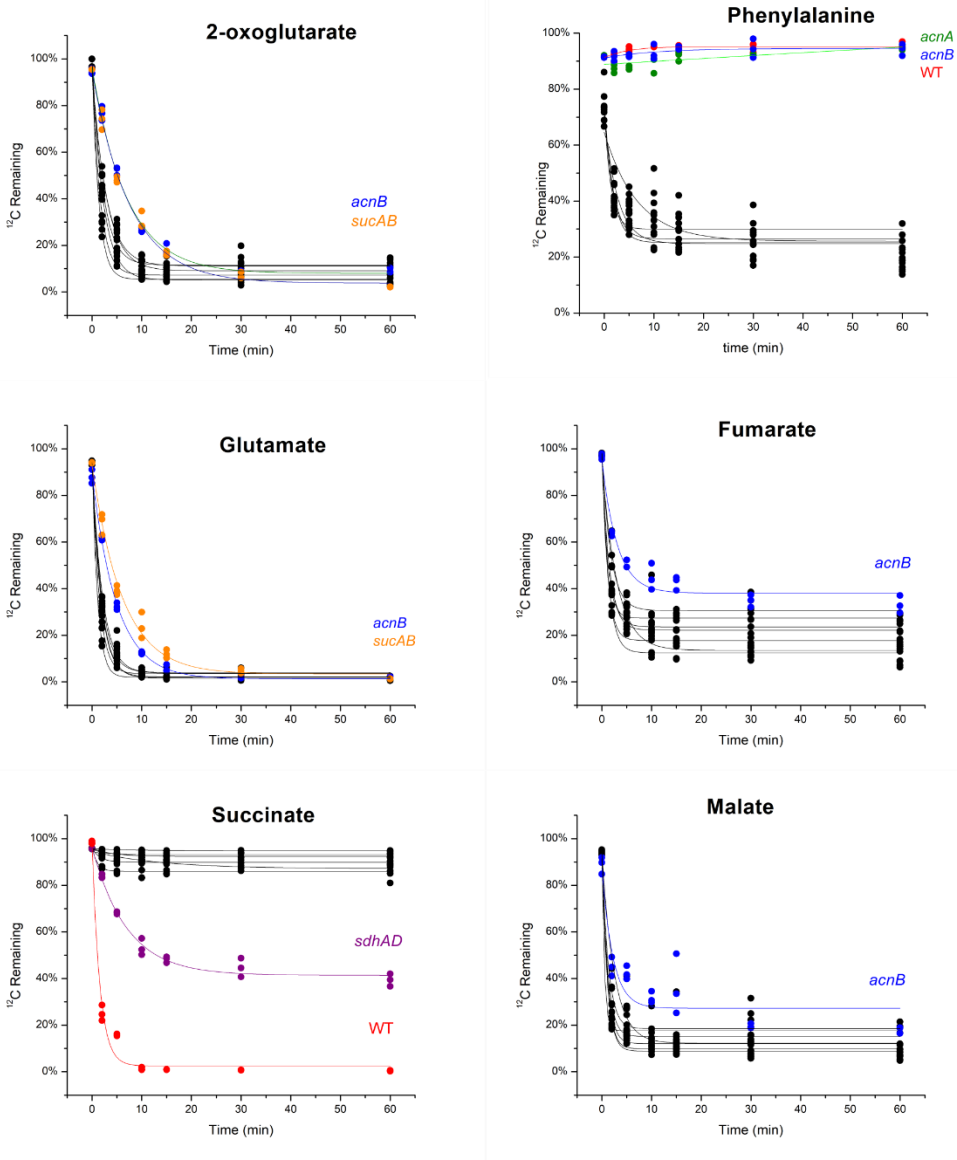

Figure 1.10 Flux plots showing a reduction of unlabeled material over time

Table 1.6 Relative pool size, relative turnover, and relative flux for five metabolites.

All comparisons are made with reference to the wild type strain.

Metabolite	Relative Pool Size						
	ΔacnA	*ΔacnB*	*ΔsucAB*	*ΔsucCD*	*ΔsdhAD*	*Δmdh*	*ΔfumA*
Glutathione	1.03±0.18	1.06±0.14	1.05±0.16	1.00±0.34	0.78±0.1	1.16±0.18	0.91±0.15
Glutathione disulfide	7.41±10.39	1.41±1.53	4.54±5.37	7.58±12.57	6.98±9.17	2.24±1.57	4.02±4.3
2-oxoglutaric acid	1.01±0.24	0.19±0.04	1.09±0.13	1.07±0.48	0.52±0.29	0.56±0.06	0.70±0.14
glutamate	1.17±0.27	0.58±0.07	1.1±0.17	1.05±0.13	0.89±0.21	0.91±0.09	0.87±0.12
glutamine	1.90±0.96	0.44±0.09	1.22±0.59	0.73±0.27	1.27±0.42	1.04±0.42	1.13±0.33

Metabolite	Relative Trunover						
	ΔacnA	*ΔacnB*	*ΔsucAB*	*ΔsucCD*	*ΔsdhAD*	*Δmdh*	*ΔfumA*
Glutathione	1.07±0.02	1.12±0.03	0.88±0.04	1.11±0.05	1.00±0.04	1.03±0.02	0.93±0.02
Glutathione disulfide	1.54±0.17	1.39±0.17	0.99±0.12	1.51±0.18	1.21±0.15	1.15±0.13	0.73±0.14
2-oxoglutaric acid	2.4±0.31	0.45±0.05	0.46±0.05	1.46±0.17	1.23±0.19	0.94±0.14	1.83±0.25
glutamate	1.84±0.16	0.42±0.03	0.32±0.02	1.13±0.09	1.15±0.09	0.91±0.08	1.36±0.13
glutamine	1.87±0.25	0.47±0.05	0.29±0.03	1.14±0.14	1.17±0.15	0.93±0.13	1.39±0.19

Table 1.6 continued

Metabolite	Relative Flux						
	ΔacnA	*ΔacnB*	*ΔsucAB*	*ΔsucCD*	*ΔsdhAD*	*Δmdh*	*ΔfumA*
Glutathione	1.07±0.02	1.12±0.03	0.88±0.04	1.11±0.05	1.00±0.04	1.03±0.02	0.93±0.02
Glutathione disulfide	11.46±16.07	1.96±2.13	4.5±5.34	11.51±19.11	8.46±11.13	2.58±1.81	2.94±3.19
2-oxoglutaric acid	2.42±0.61	0.08±0.02	0.5±0.06	1.57±0.71	0.64±0.37	0.53±0.08	1.28±0.29
glutamate	2.16±0.51	0.24±0.03	0.35±0.05	1.19±0.16	1.03±0.25	0.83±0.1	1.18±0.19
glutamine	3.56±1.81	0.21±0.04	0.36±0.17	0.83±0.31	1.48±0.5	0.97±0.39	1.57±0.47

glutamate, and 2-oxoglutaric acid. This information combined with the lower relative turnover rates (~0.43) resulted in drastically diminished flux of material through this cycle. Flux rates were 8% of the wild type for 2-oxoglutaric acid, and 21% and 22% of the wild type for glutamate and glutamine. This further shows that the arginine cycle is not only subjected to low amounts of material entering the cycle, but also slowed conversion of metabolites within this cycle. Interestingly, the opposite trend was seen with the *ΔacnA* strain in which metabolite concentrations were not significantly different than the wild type. However, flux rates were between 200%-350% of the wild type. This shows that even though these two strains act on the same substrate in the TCA cycle they have drastically distinct effects on the arginine biosynthetic pathway.

The Δ*sucAB* strain does not produce the oxoglutarate dehydrogenase complex, limiting the conversion of 2-oxoglutate to succinyl-CoA through the TCA cycle, but this mutation would not directly interfere with the conversion of 2-oxoglutarate into glutamate which happens at the beginning of the arginine biosynthetic pathway. Measuring the pool size or turnover rate independently would not provide enough information to understand if the alterations observed were related to amount of metabolite available (pool size) or if the metabolite's conversion rate (turnover) was slowed. No change was seen in the pool size of 2-oxglutarate or glutamate, but there was a steep decrease in the relative flux of these metabolites due to the low turnover rates (**Table 1.6**). These data further suggest that the inability to produce a single enzyme effects metabolism is adjacent pathways, leading to unique metabolite profiles.

In an ancillary pathway centered around glutathione metabolism, changes to glutathione (GSH) and glutathione disulfide (GSSH) levels are indicative of the oxidative stress of the cell. Investigating the flux of these two metabolites reveled a stark discrepancy between strains, with flux ratios hovering around 1 for glutathione and values ranging from 2 to over 11 for glutathione across all mutants. These values are a result of differences in total metabolite pool size and not the turnover rate of the metabolites (**Table 1.6**). Since the metabolomics experiment

does not provide absolute quantities and ionization efficiencies of each metabolite are varied, it is not possible to generate meaningful ratios between these two metabolites. Presence of large amounts of the oxidized glutathione has been shown to directly relate to stress conditions in cells due to interactions with reactive oxygen species [48, 49]. Generalities relating to increased oxidative stress can be seen across all of the strains with genetic mutations compared to the wild type.

1.5 Conclusion

Using an untargeted UPLC-HRMS approach on a systematic set of central carbon metabolism mutants in *Escherichia coli* allowed for the identification of 146 metabolites to be profiled and their relative changes applied to specific pathways. Effects were not only seen on the direct metabolites of the TCA cycle, but also measured on auxiliary pathways like arginine biosynthesis. The Aconitase B deletion strain was the only strain that had a depressed growth rate as well as a unique metabolite profile as determined by PLSDA. Over 1,700 unidentified features were detected and by applying multivariate analyses as well as Van Krevelen diagrams, information about how the small molecules were changing collectively were elucidated. Twenty-two unknowns were putatively assigned as dipeptides, which have cellular functions yet to be determined. Lipid analysis showed *ΔacnB* strain had reduced levels of several phosphatidylethanolamine and cardiolipin species, where as other strains had few significant changes. The flux analysis probed the conversion specific metabolites within the TCA and arginine pathways showing changes in a metabolite can be due to total metabolite levels or due to changes in metabolite turnover. It been shown by combining three different metabolomic analyses a clearer understanding of how small molecules are changing across global metabolic pathways in response to a genetic mutation.

1.6 Appendix

Table 1.7 Oligonucleotides used in this study

Name	5'-3' Sequence (Nucleotides that correspond to *E. coli* MG1655 genome in italics; capital letters for pKD4 template)	Use
EF1352	*caccctgaagagaatcagggcttcgcaaccctgtcattaag*GTGTAGGCTGGAGCTGCTTC	deletion of *acnA*
EF1353	*ccgtcgcgccgggttgtaggttttgcagatcgccaatatc*CATGGGAATTAGCCATGGTCC	deletion of *acnA*
EF1356	*gcgtgaagagaatcgcctgccgcactatgacaatgagagcgagg*GTGTAGGCTGGAGCTGCTTC	deletion of *acnB*
EF1357	*gtgtactgagaaagctggttgaagttcagataacggtaagtatc*CATGGGAATTAGCCATGGTCC	deletion of *acnB*
EF1360	*Gcacgcacatcactgtgcgtggtagtatccacggcgaagtaag*TCAAGAGACAGGATGAGGATCGTTT-CGCAT	deletion of *sucAB*
EF1361	*aatgccttatccggtctacagtgcaggtgaaacttaaacta*TCAGAAGAACTCGTCAAGAAGGCGA	deletion of *sucAB*

Table 1.7 continued

Name	5'-3' Sequence (Nucleotides that correspond to *E. coli* MG1655 genome in italics; capital letters for pKD4 template)	Use
EF1364	*cccggaagcgatacgaaatattcggtctacggtttaaaag*TCAAGAGACAGGATGAGGATCGTTTC-GCAT	deletion of *sucCD*
EF1365	*gtagagggaagcggcgagggctatttcttattacagatattta*TCAGAAGAACTCGTCAAGAAGGCGA	deletion of *sucCD*
EF1368	*ctccaggtaacagaaagttaacctctgtgcccgtagtccccag*GTGTAGGCTGGAGCTGCTTC	deletion of *sdhCADB*
EF1369	*ggtttacgcattacgttgcaacaacatcgacttgatatggcc*CATGGGAATTAGCCATGGTCC	deletion of *sdhCADB*
EF1376	*cagcggagcaacatatcttagtttatcaatataataaggag*GTGTAGGCTGGAGCTGCTTC	deletion of *mdh*
EF1377	cgtatccagcataccttccagcgcgttctgttcaaatgcgctcagCATGGGAATTAGCCATGGTCC	deletion of *mdh*
EF1394	*caacggaacacccgcccagagcataaccaaaccaggcagtaag*GTGTAGGCTGGAGCTGCTTC	deletion of *fumA*
EF1395	*cttccctgcgccaatacagcggccggaccaccgatactgc* CATGGGAATTAGCCATGGTCC	deletion of *fumA*

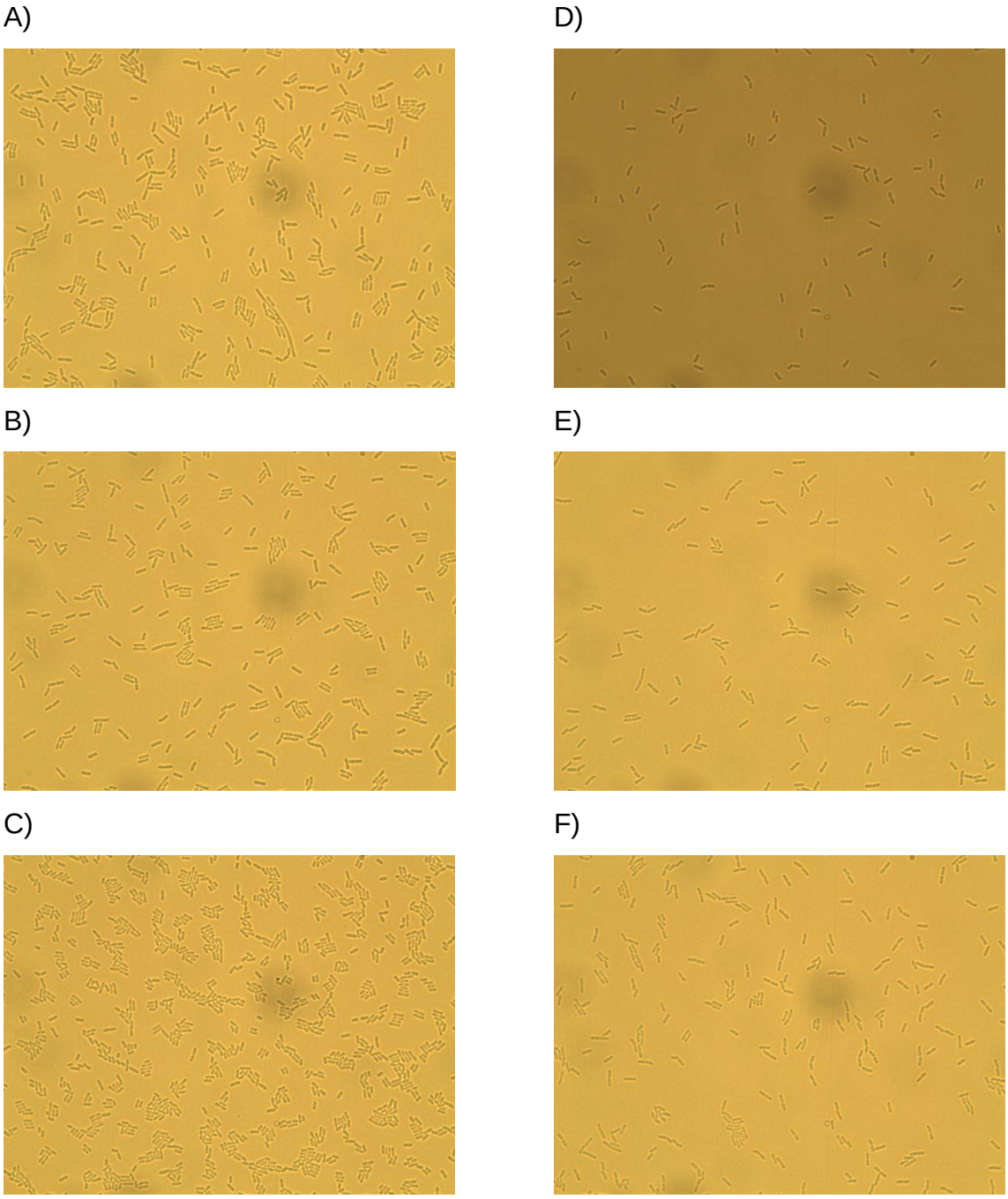

Figure 1.11 Optical microscopy images of seven mutant and one wild type strain of *E.coli*.

A) *ΔacnA* cells; B) *ΔacnB* cells; C) *ΔsucAB* cells; D) *ΔsucCD* cells; E) *ΔshdAD* cells; F) *ΔfumA* cells; G) *Δmdh* cells; H) Wild type cells

G)

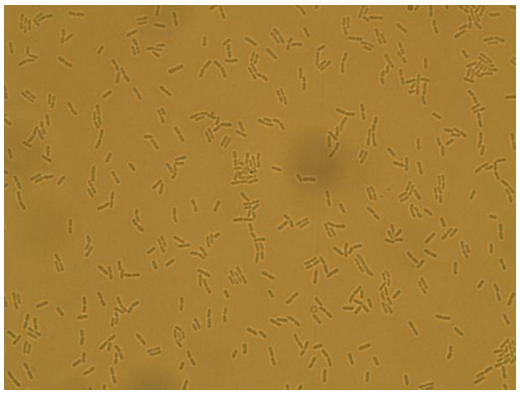

H)

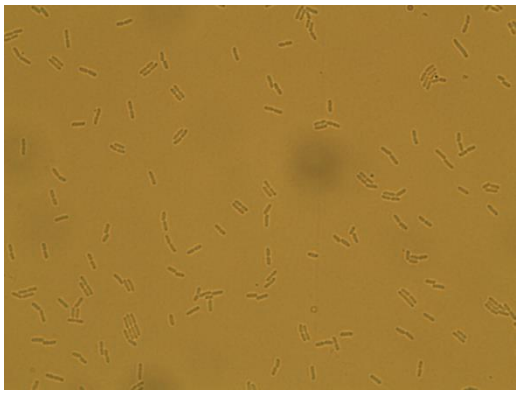

Figure 1.11 continued

Table 1.8 Ratios and p-values used for heat map of knowns

Compound	Ratio compared to WT						
	ΔacnA	*ΔacnB*	*ΔsucAB*	*ΔsucCD*	*ΔsdhAD*	*ΔfumA*	*Δmdh*
Pyruvate	0.817559	0.408834	1.192752	0.662213	1.356302	1.079559	0.979796
Alanine/Sarcosine	2.599924	0.543318	1.99279	0.462391	2.122322	1.558015	1.050535
Lactate	1.383265	1.260585	4.586125	0.94888	4.182785	1.715196	1.243399
4-Aminobutyrate (GABA)	2.443333	1.154082	1.397196	0.852195	1.538444	1.276367	1.129969
Serine	2.81257	0.379781	2.160891	0.288083	2.008892	2.312769	1.136157
Glycerate	7.538137	0.333212	3.208331	0.201578	2.018131	2.447011	0.747273
Uracil	9.563469	0.232203	5.87937	0.110987	3.557714	4.333116	1.348408
Creatinine	0.899143	0.20559	9.469383	0.061896	1.503947	5.378761	0.940182
Proline	5.591032	0.061975	2.430255	0.107863	0.708409	1.555911	0.387508
Fumarate	1.779682	0.412344	1.459412	0.802468	1.08632	1.528558	1.828354
Valine	3.648324	0.499727	2.031192	0.480008	1.231319	1.729553	0.880606
Succinate/Methylmalonate	1.795821	0.445029	1.328169	0.566887	2.138568	1.375372	0.861365
3-Hydroxyisovaleric acid	1.142933	1.410548	1.729162	0.926189	1.379613	1.130431	1.130838
Homoserine/Threonine	3.214791	0.507339	1.927303	0.945646	1.256575	1.433747	0.848805

Table 1.8 continued

Compound	Ratio compared to WT						
	ΔacnA	*ΔacnB*	*ΔsucAB*	*ΔsucCD*	*ΔsdhAD*	*ΔfumA*	*Δmdh*
Cysteine	3.871757	0.781341	2.018452	0.46256	0.647504	2.212705	0.942082
Nicotinate	6.63197	0.153298	2.575137	0.08917	1.427931	3.320796	0.923592
Taurine	0.402968	0.100164	1.566734	0.026815	5.330869	0.733307	0.234901
Thymine	1.753228	0.36707	0.972456	0.461619	0.892933	0.897483	0.866856
Pyroglutamic acid	5.11582	0.305763	3.956248	0.261902	1.751922	3.206496	0.983102
Citraconate	1.788604	3.052834	1.367968	0.871908	8.895901	1.352892	6.498326
N-Acetylputrescine	0.997376	0.15651	0.845436	0.620806	0.741228	1.00056	1.568425
N-Acetyl-beta-alanine	3.486717	0.765327	2.145103	0.642692	4.356841	1.881201	0.901909
Hydroxyproline	2.502303	0.583862	3.369341	0.198118	3.7062	3.261463	2.159947
Creatine	0.688364	0.450644	7.580578	0.054622	2.683826	2.691387	1.148442
Leucine/Isoleucine	5.73384	0.269982	3.049796	0.194697	1.986458	2.552818	0.906318
Asparagine	3.244821	0.564972	1.594903	0.460796	1.436331	1.558249	0.84441
Hydroxyisocaproic acid	1.864028	0.626585	5.739818	0.440571	1.228531	1.097088	0.692171
Ornithine	2.430611	0.774572	2.491186	0.861141	1.742193	1.997608	1.564771
Aspartate	1.836341	0.481845	1.24309	0.761951	1.374369	1.140794	0.492444

Table 1.8 continued

Compound	Ratio compared to WT						
	ΔacnA	*ΔacnB*	*ΔsucAB*	*ΔsucCD*	*ΔsdhAD*	*ΔfumA*	*Δmdh*
Homocysteine	0.631608	0.377504	0.541333	0.870647	1.008292	0.815081	0.743085
Adenine	2.001719	0.749836	2.244176	0.45282	2.176883	1.499465	1.357539
Hypoxanthine	1.143556	0.371931	9.294552	0.092317	3.534935	5.348831	1.037236
Hydroxybenzoate	9.359499	0.301932	4.539554	0.28089	0.506388	5.631176	0.489996
Acetylphosphate	0.85148	0.723526	1.023923	0.668612	0.936944	0.624193	0.79658
Carbamoyl phosphate	4.254655	0.567499	2.35573	0.873407	6.645534	2.762511	2.080337
Histidinol	0.640886	0.136758	1.199794	0.123238	0.558329	1.614433	1.067868
2-Oxoglutaric acid	1.011598	0.195506	1.097869	1.070703	0.522836	0.701251	0.56353
Glutamine	1.904689	0.447973	1.22787	0.730874	1.271724	1.131239	1.043497
Lysine	3.204039	0.601794	2.548965	2.4315	1.871548	1.905474	0.868669
Glutamate	1.171228	0.58048	1.109454	1.054979	0.897603	0.870723	0.914434
2-Hydroxy-2-methylsuccinate	3.015156	0.5383	3.697426	0.568479	1.50545	1.676633	1.292648
L-Methionine	7.332898	0.234882	1.374438	0.571223	0.448249	2.722408	0.518033
Guanine	1.394658	0.460679	7.995589	0.148	1.840911	3.648315	1.227919
Hydroxyphenylacetate	9.251212	0.160269	2.075246	0.123668	0.2548	4.786232	0.247012

Table 1.8 continued

Compound	Ratio compared to WT						
	ΔacnA	*ΔacnB*	*ΔsucAB*	*ΔsucCD*	*ΔsdhAD*	*ΔfumA*	*Δmdh*
Xylitol	2.256215	0.172082	1.121968	0.090117	4.102346	1.023754	1.128361
2-3-Dihydroxybenzoate	1.38224	0.771676	0.95845	0.550185	0.767852	0.964008	1.005449
Histidine	11.40544	0.302309	2.955617	0.211636	1.539817	3.854994	0.312439
Orotate	1.096382	1.356069	1.00348	0.949207	0.881372	0.910768	1.414926
Dihydroorotate	1.420312	2.361942	1.362844	1.400315	1.075346	1.326142	2.403442
Allantoin	4.716015	0.261038	3.487318	0.01386	6.342719	2.759211	1.108042
2-Aminoadipate	9.371814	0.683427	3.922114	0.372044	3.72092	3.215391	1.988742
Phenylpyruvate	0.96189	0.756318	1.046036	0.847224	0.919344	0.874964	1.011164
Phenylalanine	4.048332	0.421759	3.452762	0.23434	2.816218	2.491669	1.019163
Phenyllactic acid	1.372359	0.881605	2.778919	0.57037	2.141397	1.798984	0.925527
Phosphoenolpyruvate	3.923624	1.21529	1.924871	0.740034	1.500343	2.07519	1.002911
Uric acid	2.204427	0.19315	2.56087	0.023116	2.096855	7.433322	1.051663
3-4-Dihydroxyphenylacetate (DOPAC)	2.361691	0.951139	1.406228	0.601898	2.813496	1.649975	1.861731
Cysteate	11.5133	0.151236	2.133426	0.055773	11.72645	3.422364	3.155136

Table 1.8 continued

Compound	Ratio compared to WT						
	ΔacnA	*ΔacnB*	*ΔsucAB*	*ΔsucCD*	*ΔsdhAD*	*ΔfumA*	*Δmdh*
Sulfolactate	3.167741	0.908813	2.075801	0.912203	3.017429	3.064962	1.44379
D-Glyceraldehdye 3-phosphate	0.852538	0.773496	1.246961	0.726963	1.245555	1.00339	1.262345
sn-Glycerol 3-phosphate	6.218536	0.327668	3.34111	0.182198	4.96311	3.980677	1.66124
Aconitate	2.930559	10.15992	1.734409	0.689959	13.29157	1.848187	9.178361
Shikimate	1.231818	1.460672	1.194573	0.852308	1.414955	1.536265	1.492225
N-Acetylornithine	1.352175	0.397064	1.474562	0.698786	1.252374	1.243904	1.296039
Arginine	7.102184	0.11298	3.218138	0.095762	2.650289	2.688913	0.953388
Citrulline	1.719241	1.038782	2.388313	1.062527	1.586526	1.589883	1.710965
N-Carbamoyl-L-aspartate	1.354358	1.638516	0.810493	0.812686	0.946863	0.812921	1.788641
Allantoate	9.854608	0.004105	2.243668	0.002558	7.487993	3.62477	1.961358
2-Isopropylmalate	1.441357	3.555884	1.435344	2.199517	1.777269	1.494843	1.448003
Glucosamine	2.221652	0.606628	2.381403	0.346521	2.167028	3.350744	1.364071
Tyrosine	5.268642	0.187487	2.511975	0.126022	2.740414	1.803791	1.197748
Homovanillic acid (HVA)	1.298503	0.432882	1.198988	0.279216	3.173546	1.044708	0.420466

Table 1.8 continued

Compound	Ratio compared to WT						
	ΔacnA	*ΔacnB*	*ΔsucAB*	*ΔsucCD*	*ΔsdhAD*	*ΔfumA*	*Δmdh*
Homocysteic acid	1.400728	0.095233	1.23194	0.016431	9.650709	1.681537	0.304546
4-Pyridoxate	1.613595	1.473651	1.695174	0.850279	2.773981	1.761852	1.27167
3-Phosphoserine	1.605564	1.640136	1.495041	1.192422	1.132869	1.296696	0.763316
3-Phosphoglycerate	2.715271	1.229201	1.918035	0.956163	1.575748	2.099121	1.062949
N-Acetylglutamine	1.485194	1.089171	1.488591	1.234549	1.53487	1.422357	0.987455
Acetyllysine	1.250287	0.665801	1.609792	2.723738	1.866086	1.011614	0.786242
N-Acetylglutamate	1.650854	0.370694	1.394935	2.666892	0.968358	1.567312	2.271437
Citrate/isocitrate	2.493952	17.25215	1.756963	0.660992	1.668573	2.432668	0.790152
2-Dehydro-D-gluconate	3.980524	0.522708	1.938809	0.066004	10.82273	2.732236	0.363228
D-Gluconate	7.945641	0.65773	6.578516	0.357373	9.982397	8.042475	1.236061
Tryptophan	3.734099	0.393015	2.909213	0.311004	4.986518	2.24324	0.889259
Xanthurenic acid	11.90371	0.006628	3.014224	0.005151	0.543634	4.114538	0.329907
D-Glucarate	33.00513	0.220341	7.789856	0.039015	13.77967	19.56253	2.773641
Deoxyribose phosphate	1.396047	1.136123	1.130736	0.529849	1.098417	0.798009	1.160815
Pantothenate	2.543105	0.671166	1.558541	0.53127	1.50719	1.810509	1.104043

Table 1.8 continued

Compound	Ratio compared to WT						
	ΔacnA	*ΔacnB*	*ΔsucAB*	*ΔsucCD*	*ΔsdhAD*	*ΔfumA*	*Δmdh*
N-Acetylglucosamine	7.539576	0.151323	3.506879	0.041498	6.023714	2.290944	1.726523
Cystathionine	5.020598	0.149044	2.544757	0.271944	0.780783	2.747714	0.552731
Ribose phosphate	1.082406	1.539087	1.095683	1.220328	0.950142	1.066856	1.00538
Thymidine	6.288857	1.802158	11.66445	0.889888	71.52812	5.401197	1.310555
Cytidine	5.334848	0.058048	2.198278	0.007294	5.226988	1.962057	1.623158
Uridine	4.917963	0.385754	3.08733	0.293487	5.337861	2.399608	0.776382
Shikimate-3-phosphate	1.382471	1.000213	1.444664	1.020679	0.947174	1.240452	1.470273
Deoxyinosine	14.26959	0.047914	2.873008	0.010961	13.20736	5.294777	0.399697
Glucosamine phosphate	0.759313	1.288793	0.767206	0.958057	0.757546	0.6792	0.904602
Glucose 6-phosphate	1.22936	1.305655	1.182584	1.239902	1.115238	1.17743	1.263294
S-Ribosyl-L-homocysteine	0.937026	0.294905	0.663814	2.499252	0.688943	0.843503	0.679761
Adenosine	11.29933	0.470685	4.001915	0.051083	19.91322	1.393327	1.499717
Inosine	12.45544	0.097312	3.319042	0.011562	7.486919	1.776252	1.149079
6-Phospho-D-gluconate	1.28075	2.566063	1.25326	1.090835	1.390978	1.450253	0.746247
1-Methyladenosine	6.301512	0.08015	4.390298	0.032655	4.646201	1.989057	0.68354

Table 1.8 continued

Compound	Ratio compared to WT						
	ΔacnA	*ΔacnB*	*ΔsucAB*	*ΔsucCD*	*ΔsdhAD*	*ΔfumA*	*Δmdh*
Guanosine	11.78554	0.034277	3.635347	0.021395	2.706876	3.097138	0.895944
Xanthosine	1.566921	0.607456	7.219069	0.137127	17.6873	1.002636	0.645449
Glycinamide ribotide (GAR)	1.165352	0.615558	0.871689	1.825291	0.744214	0.918876	0.926487
Ophthalmate	1.074735	1.398286	1.304632	1.167689	1.10377	0.997524	1.004373
Sedoheptulose 1/7-phosphate	2.368293	1.745418	1.489786	1.039251	1.801168	1.55371	0.939441
L-Argininosuccinate	1.033199	1.399447	1.2863	1.163563	1.08611	0.934547	0.998164
Aminoimidazole ribotide (AIR)	0.872952	0.713945	0.668699	0.865067	0.651038	0.678655	0.941627
N-Acetylglucosamine1/6-phosphate	5.685138	0.542695	2.061399	0.469715	2.591054	2.458341	1.433114
dCMP	2.633051	0.64221	1.37099	0.591884	2.246449	1.331868	0.864121
Glutathione	1.038381	1.066427	1.051167	1.003517	0.781016	0.914961	1.164645
dUMP	1.360428	0.205407	1.034724	0.33133	1.137782	0.539705	0.843618
Octulose 8/1P	1.482358	1.631491	1.400373	0.581056	1.445783	1.075167	1.146374
dTMP	1.815937	0.609651	1.221246	0.66859	1.263741	0.943098	0.980325
CMP	3.338158	0.554875	1.833774	0.424429	1.952661	1.844476	1.203728

Table 1.8 continued

Compound	Ratio compared to WT						
	ΔacnA	*ΔacnB*	*ΔsucAB*	*ΔsucCD*	*ΔsdhAD*	*ΔfumA*	*Δmdh*
UMP	8.016368	0.089128	3.107172	0.182362	3.457899	3.475042	1.351323
cAMP	1.472813	0.522246	1.234339	0.882613	1.390511	1.137886	0.688245
dAMP	7.644848	0.219817	1.769097	0.528377	1.462176	2.866802	0.780611
AICAR	1.076166	0.439659	0.662515	0.789972	0.527173	0.772698	0.585088
Fructose 1-6-bisphosphate	1.510135	0.752697	1.848661	1.845592	1.442023	1.813032	1.793679
Trehalose/Sucrose/Cellobiose	2.816096	2.086252	1.307267	0.489209	3.225713	1.5062	0.723092
AMP/dGMP	7.718746	0.106969	3.121977	0.097167	3.800375	3.467976	1.516861
IMP	2.702533	2.355208	3.584845	1.595023	2.887482	1.429597	2.422436
GMP	6.196369	0.346137	3.221855	0.238211	3.286996	3.679078	1.081144
Xanthosine 5--phosphate	1.240618	1.562197	1.301846	1.57425	0.920716	1.130003	1.258852
Sedoheptoluse bisphosphate	1.790522	1.623576	2.158161	1.622842	1.488936	1.771769	1.196282
Octulose bisphosphate	2.128861	1.639425	2.582704	1.876357	2.217216	1.836527	1.427445
Sucralose	0.811571	0.128594	0.399461	0.348711	0.128819	0.110828	0.272512
dTDP	1.095808	0.394028	0.250553	0.193797	0.142857	0.106998	0.56189
UDP	1.091648	0.606564	1.942985	0.774482	0.937755	1.410943	0.799198

Table 1.8 continued

Compound	Ratio compared to WT						
	ΔacnA	*ΔacnB*	*ΔsucAB*	*ΔsucCD*	*ΔsdhAD*	*ΔfumA*	*Δmdh*
Trehalose 6-phosphate	1.594984	1.383391	1.312339	3.514777	1.237247	1.353936	0.959988
ADP	2.417404	0.830957	2.147184	0.584052	1.730543	2.55483	0.970592
GDP	1.691171	2.311809	2.790494	1.364149	1.235829	2.348203	0.938009
FMN	0.938344	0.693389	0.93031	0.506128	0.715199	0.738716	0.901063
UDP-glucose	1.131803	0.797451	1.144863	1.131207	0.618039	0.965063	1.421822
UDP-glucuronate	0.974791	0.797922	1.290523	1.293456	1.272567	0.899373	1.419145
ADP-glucose	0.905388	0.67405	0.862655	0.967736	0.603296	0.758243	0.98903
UDP-N-acetylglucosamine	3.869191	0.500877	1.449668	0.577016	1.215771	1.732194	1.169687
Glutathione disulfide	7.417341	1.410187	4.544838	7.581481	6.982106	4.028293	2.249509
NAD+	1.156482	0.978494	1.073981	0.875703	0.942093	1.011531	1.019715
NADH	2.065357	0.679624	2.831388	2.093241	1.821029	1.639478	1.453124
NADP+	1.213001	0.968979	1.148822	0.646595	0.964138	1.141682	0.949886
FAD	1.070981	0.688994	0.976141	0.683638	0.665256	0.80389	1.123639
Acetyl-CoA	1.321138	1.056979	1.814033	1.234619	1.006229	1.507803	1.502358
Malate	2.110262	0.335274	1.454708	0.720285	1.693052	1.730418	2.150864

Table 1.8 continued

Compound	p-value						
	ΔacnA	*ΔacnB*	*ΔsucAB*	*ΔsucCD*	*ΔsdhAD*	*ΔfumA*	*Δmdh*
Pyruvate	0.051	0.001	0.261	0.044	0.010	0.399	0.876
Alanine/Sarcosine	0.285	0.044	0.051	0.026	0.180	0.190	0.867
Lactate	0.568	0.690	0.077	0.934	0.163	0.323	0.692
4-Aminobutyrate (GABA)	0.259	0.269	0.393	0.324	0.044	0.331	0.597
Serine	0.326	0.315	0.211	0.266	0.151	0.366	0.894
Glycerate	0.368	0.362	0.384	0.296	0.276	0.361	0.752
Uracil	0.354	0.243	0.107	0.199	0.102	0.251	0.742
Creatinine	0.828	0.156	0.227	0.126	0.713	0.353	0.932
Proline	0.354	0.291	0.561	0.309	0.702	0.676	0.460
Fumarate	0.207	0.024	0.229	0.361	0.780	0.021	0.005
Valine	0.384	0.177	0.262	0.167	0.493	0.388	0.753
Succinate/Methylmalonate	0.334	0.072	0.190	0.134	0.007	0.146	0.749
3-Hydroxyisovaleric acid	0.421	0.126	0.284	0.710	0.110	0.557	0.475
Homoserine/Threonine	0.336	0.224	0.279	0.882	0.470	0.511	0.716
Cysteine	0.362	0.628	0.041	0.182	0.035	0.433	0.852

Table 1.8 continued

Compound	p-value						
	ΔacnA	*ΔacnB*	*ΔsucAB*	*ΔsucCD*	*ΔsdhAD*	*ΔfumA*	*Δmdh*
Nicotinate	0.320	0.240	0.421	0.217	0.514	0.293	0.932
Taurine	0.426	0.267	0.564	0.241	0.415	0.735	0.324
Thymine	0.435	0.030	0.953	0.040	0.499	0.723	0.686
Pyroglutamic acid	0.228	0.271	0.053	0.250	0.249	0.277	0.978
Citraconate	0.148	0.044	0.232	0.456	0.031	0.091	0.421
N-Acetylputrescine	0.996	0.110	0.729	0.352	0.555	0.999	0.235
N-Acetyl-beta-alanine	0.322	0.453	0.134	0.294	0.300	0.165	0.773
Hydroxyproline	0.159	0.295	0.039	0.075	0.002	0.325	0.158
Creatine	0.550	0.349	0.197	0.161	0.214	0.409	0.809
Leucine/Isoleucine	0.388	0.256	0.122	0.224	0.324	0.328	0.903
Asparagine	0.303	0.163	0.375	0.105	0.151	0.369	0.771
Hydroxyisocaproic acid	0.531	0.509	0.437	0.354	0.676	0.872	0.579
Ornithine	0.226	0.268	0.064	0.493	0.029	0.187	0.062
Aspartate	0.334	0.043	0.326	0.211	0.609	0.533	0.046
Homocysteine	0.006	0.001	0.092	0.453	0.969	0.299	0.034

Table 1.8 continued

Compound	p-value						
	ΔacnA	*ΔacnB*	*ΔsucAB*	*ΔsucCD*	*ΔsdhAD*	*ΔfumA*	*Δmdh*
Adenine	0.233	0.197	0.000	0.017	0.283	0.407	0.116
Hypoxanthine	0.794	0.270	0.133	0.153	0.504	0.338	0.960
Hydroxybenzoate	0.395	0.293	0.417	0.283	0.423	0.234	0.413
Acetylphosphate	0.559	0.262	0.917	0.113	0.448	0.010	0.238
Carbamoyl phosphate	0.203	0.479	0.100	0.844	0.295	0.101	0.347
Histidinol	0.547	0.180	0.780	0.175	0.412	0.541	0.943
2-Oxoglutaric acid	0.940	0.001	0.248	0.823	0.098	0.037	0.004
Glutamine	0.218	0.036	0.552	0.208	0.318	0.515	0.868
Lysine	0.317	0.168	0.161	0.005	0.069	0.311	0.760
Glutamate	0.371	0.002	0.338	0.525	0.487	0.180	0.228
2-Hydroxy-2-methylsuccinate	0.354	0.281	0.408	0.330	0.247	0.242	0.546
L-Methionine	0.422	0.122	0.680	0.282	0.199	0.495	0.240
Guanine	0.545	0.416	0.164	0.215	0.631	0.333	0.808
Hydroxyphenylacetate	0.440	0.202	0.585	0.190	0.236	0.325	0.232
Xylitol	0.170	0.050	0.705	0.045	0.298	0.967	0.906

Table 1.8 continued

Compound	p-value						
	ΔacnA	*ΔacnB*	*ΔsucAB*	*ΔsucCD*	*ΔsdhAD*	*ΔfumA*	*Δmdh*
2-3-Dihydroxybenzoate	0.452	0.203	0.848	0.066	0.200	0.841	0.980
Histidine	0.421	0.256	0.410	0.215	0.604	0.336	0.260
Orotate	0.225	0.006	0.984	0.797	0.154	0.503	0.038
Dihydroorotate	0.106	0.003	0.438	0.247	0.806	0.498	0.022
Allantoin	0.177	0.196	0.035	0.131	0.053	0.338	0.933
2-Aminoadipate	0.351	0.620	0.367	0.367	0.303	0.330	0.634
Phenylpyruvate	0.744	0.058	0.759	0.398	0.489	0.317	0.938
Phenylalanine	0.358	0.107	0.114	0.065	0.222	0.357	0.972
Phenyllactic acid	0.393	0.629	0.247	0.168	0.386	0.265	0.759
Phosphoenolpyruvate	0.309	0.482	0.382	0.418	0.104	0.264	0.993
Uric acid	0.553	0.271	0.153	0.212	0.457	0.438	0.966
3-4-Dihydroxyphenylacetate (DOPAC)	0.183	0.780	0.256	0.099	0.056	0.376	0.405
Cysteate	0.292	0.149	0.182	0.131	0.139	0.274	0.559

Table 1.8 continued

Compound	p-value						
	ΔacnA	*ΔacnB*	*ΔsucAB*	*ΔsucCD*	*ΔsdhAD*	*ΔfumA*	*Δmdh*
Sulfolactate	0.232	0.652	0.081	0.744	0.293	0.193	0.203
D-Glyceraldehdye 3-phosphate	0.619	0.285	0.128	0.406	0.133	0.984	0.060
sn-Glycerol 3-phosphate	0.323	0.213	0.343	0.161	0.249	0.240	0.678
Aconitate	0.308	0.066	0.334	0.397	0.037	0.083	0.456
Shikimate	0.458	0.210	0.488	0.661	0.280	0.244	0.141
N-Acetylornithine	0.395	0.050	0.279	0.177	0.215	0.224	0.267
Arginine	0.268	0.203	0.292	0.197	0.053	0.331	0.965
Citrulline	0.065	0.804	0.063	0.765	0.167	0.124	0.065
N-Carbamoyl-L-aspartate	0.051	0.040	0.092	0.314	0.676	0.072	0.006
Allantoate	0.217	0.131	0.504	0.130	0.001	0.341	0.675
2-Isopropylmalate	0.036	0.078	0.059	0.257	0.061	0.206	0.106
Glucosamine	0.137	0.166	0.013	0.053	0.120	0.345	0.306
Tyrosine	0.363	0.303	0.247	0.277	0.143	0.478	0.875
Homovanillic acid (HVA)	0.547	0.283	0.685	0.206	0.436	0.939	0.274

Table 1.8 continued

Compound	p-value						
	ΔacnA	*ΔacnB*	*ΔsucAB*	*ΔsucCD*	*ΔsdhAD*	*ΔfumA*	*Δmdh*
Homocysteic acid	0.551	0.210	0.737	0.188	0.373	0.608	0.312
4-Pyridoxate	0.275	0.143	0.007	0.324	0.168	0.122	0.184
3-Phosphoserine	0.003	0.204	0.004	0.724	0.491	0.348	0.185
3-Phosphoglycerate	0.354	0.459	0.109	0.912	0.144	0.082	0.673
N-Acetylglutamine	0.221	0.649	0.071	0.334	0.078	0.230	0.945
Acetyllysine	0.331	0.099	0.034	0.029	0.272	0.955	0.366
N-Acetylglutamate	0.124	0.140	0.366	0.140	0.935	0.169	0.114
Citrate/isocitrate	0.408	0.041	0.296	0.369	0.205	0.058	0.521
2-Dehydro-D-gluconate	0.412	0.428	0.155	0.167	0.400	0.336	0.317
D-Gluconate	0.385	0.540	0.196	0.252	0.346	0.280	0.841
Tryptophan	0.423	0.256	0.095	0.217	0.326	0.345	0.860
Xanthurenic acid	0.437	0.387	0.546	0.387	0.666	0.322	0.544
D-Glucarate	0.387	0.177	0.432	0.135	0.328	0.315	0.572
Deoxyribose phosphate	0.049	0.425	0.289	0.034	0.536	0.266	0.189
Pantothenate	0.339	0.051	0.443	0.012	0.197	0.248	0.588

Table 1.8 continued

Compound	p-value						
	ΔacnA	*ΔacnB*	*ΔsucAB*	*ΔsucCD*	*ΔsdhAD*	*ΔfumA*	*Δmdh*
N-Acetylglucosamine	0.214	0.279	0.387	0.240	0.365	0.384	0.712
Cystathionine	0.414	0.143	0.566	0.181	0.632	0.490	0.360
Ribose phosphate	0.738	0.031	0.517	0.379	0.676	0.767	0.973
Thymidine	0.200	0.634	0.307	0.886	0.376	0.280	0.806
Cytidine	0.249	0.197	0.460	0.183	0.004	0.538	0.742
Uridine	0.366	0.208	0.017	0.171	0.290	0.322	0.651
Shikimate-3-phosphate	0.394	0.999	0.018	0.952	0.777	0.361	0.135
Deoxyinosine	0.359	0.286	0.423	0.272	0.429	0.333	0.488
Glucosamine phosphate	0.298	0.150	0.073	0.681	0.124	0.049	0.461
Glucose 6-phosphate	0.380	0.107	0.246	0.159	0.644	0.254	0.262
S-Ribosyl-L-homocysteine	0.744	0.022	0.083	0.052	0.098	0.394	0.092
Adenosine	0.210	0.630	0.228	0.391	0.313	0.795	0.788
Inosine	0.357	0.173	0.276	0.153	0.372	0.579	0.911
6-Phospho-D-gluconate	0.139	0.170	0.163	0.864	0.278	0.133	0.246
1-Methyladenosine	0.361	0.305	0.282	0.287	0.338	0.505	0.751

Table 1.8 continued

Compound	p-value						
	ΔacnA	*ΔacnB*	*ΔsucAB*	*ΔsucCD*	*ΔsdhAD*	*ΔfumA*	*Δmdh*
Guanosine	0.372	0.235	0.182	0.231	0.150	0.367	0.924
Xanthosine	0.690	0.621	0.002	0.237	0.368	0.997	0.663
Glycinamide ribotide (GAR)	0.574	0.098	0.191	0.065	0.343	0.608	0.769
Ophthalmate	0.504	0.014	0.030	0.344	0.254	0.984	0.970
Sedoheptulose 1/7-phosphate	0.209	0.066	0.358	0.886	0.327	0.256	0.823
L-Argininosuccinate	0.680	0.033	0.158	0.474	0.209	0.542	0.985
Aminoimidazole ribotide (AIR)	0.376	0.164	0.085	0.355	0.078	0.086	0.791
N-Acetylglucosamine 1/6-phosphate	0.301	0.220	0.436	0.176	0.130	0.268	0.626
dCMP	0.203	0.033	0.028	0.041	0.376	0.342	0.270
Glutathione	0.739	0.465	0.605	0.987	0.077	0.410	0.163
dUMP	0.168	0.042	0.867	0.059	0.520	0.105	0.504
Octulose 8/1P	0.053	0.043	0.040	0.030	0.115	0.719	0.500
dTMP	0.027	0.067	0.211	0.097	0.518	0.699	0.888
CMP	0.286	0.087	0.418	0.050	0.035	0.300	0.765

Table 1.8 continued

Compound	p-value						
	ΔacnA	*ΔacnB*	*ΔsucAB*	*ΔsucCD*	*ΔsdhAD*	*ΔfumA*	*Δmdh*
UMP	0.347	0.189	0.456	0.219	0.173	0.289	0.804
cAMP	0.311	0.094	0.466	0.640	0.574	0.630	0.373
dAMP	0.238	0.100	0.537	0.222	0.406	0.347	0.662
AICAR	0.654	0.001	0.034	0.342	0.009	0.048	0.033
Fructose 1-6-bisphosphate	0.069	0.298	0.083	0.410	0.122	0.129	0.076
Trehalose/Sucrose/Cellobiose	0.414	0.527	0.483	0.222	0.336	0.476	0.477
AMP/dGMP	0.311	0.233	0.473	0.230	0.059	0.276	0.755
IMP	0.237	0.051	0.279	0.138	0.261	0.391	0.026
GMP	0.364	0.273	0.416	0.222	0.229	0.279	0.933
Xanthosine 5--phosphate	0.250	0.269	0.131	0.349	0.629	0.522	0.160
Sedoheptoluse bisphosphate	0.169	0.207	0.146	0.548	0.102	0.108	0.528
Octulose bisphosphate	0.132	0.291	0.034	0.481	0.042	0.171	0.312
Sucralose	0.420	0.009	0.019	0.001	0.000	0.001	0.000
dTDP	0.832	0.176	0.020	0.006	0.014	0.005	0.039
UDP	0.802	0.107	0.123	0.623	0.880	0.263	0.314

Table 1.8 continued

Compound	p-value						
	ΔacnA	*ΔacnB*	*ΔsucAB*	*ΔsucCD*	*ΔsdhAD*	*ΔfumA*	*Δmdh*
Trehalose 6-phosphate	0.566	0.353	0.560	0.009	0.635	0.505	0.924
ADP	0.374	0.723	0.214	0.353	0.256	0.147	0.927
GDP	0.370	0.396	0.061	0.671	0.579	0.258	0.860
FMN	0.723	0.187	0.681	0.056	0.177	0.210	0.573
UDP-glucose	0.524	0.294	0.502	0.596	0.105	0.860	0.097
UDP-glucuronate	0.913	0.410	0.439	0.634	0.662	0.744	0.272
ADP-glucose	0.664	0.105	0.394	0.880	0.067	0.184	0.950
UDP-N-acetylglucosamine	0.362	0.121	0.566	0.151	0.389	0.310	0.745
Glutathione disulfide	0.374	0.667	0.339	0.445	0.350	0.308	0.197
NAD+	0.257	0.810	0.523	0.237	0.684	0.906	0.828
NADH	0.103	0.572	0.263	0.232	0.376	0.214	0.393
NADP+	0.427	0.896	0.510	0.304	0.922	0.571	0.771
FAD	0.765	0.136	0.905	0.213	0.116	0.280	0.528
Acetyl-CoA	0.286	0.904	0.143	0.749	0.981	0.244	0.180
Malate	0.233	0.010	0.264	0.358	0.256	0.071	0.001

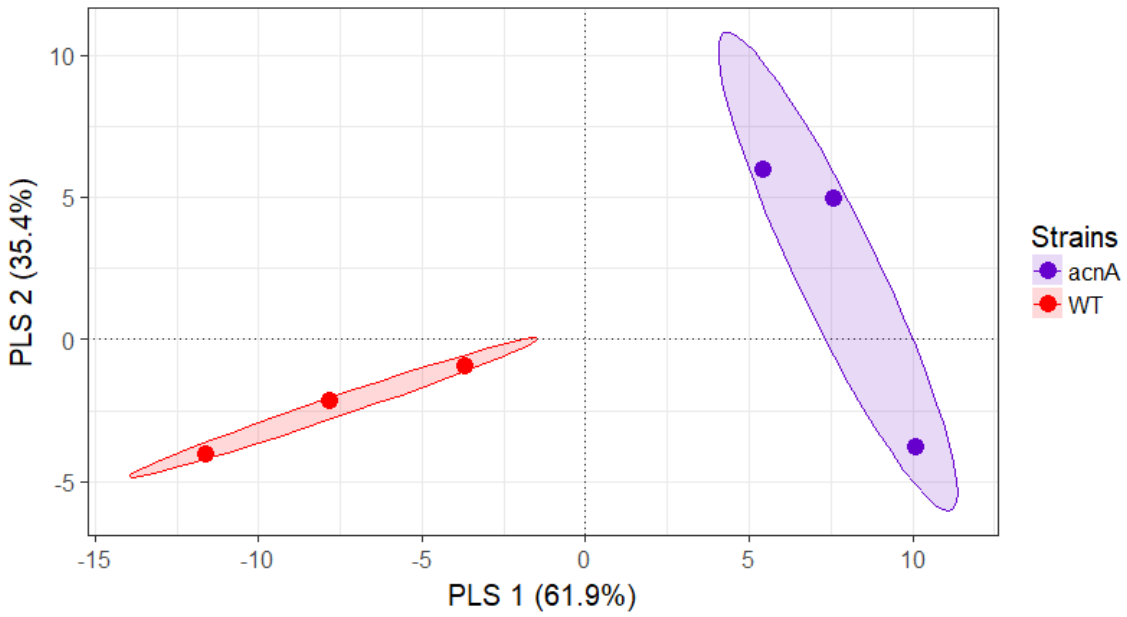

Figure 1.12 Known metabolite pairwise PLSDA for ΔacnA

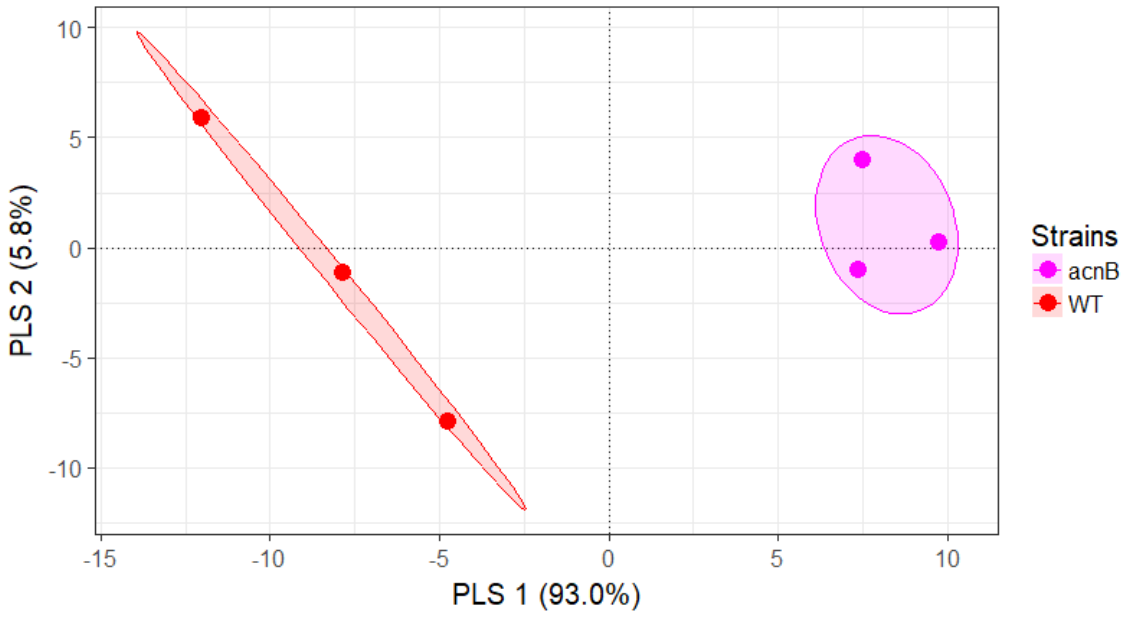

Figure 1.13 Known metabolite pairwise PLSDA for *ΔacnB*

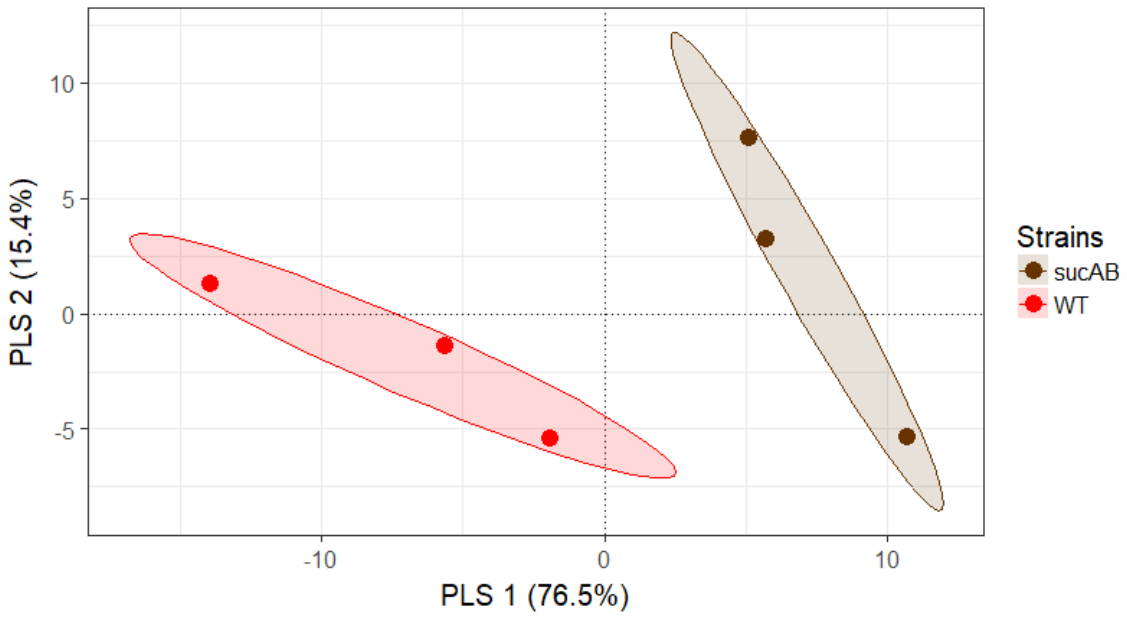

Figure 1.14 Known metabolite pairwise PLSDA for *ΔsucAB*

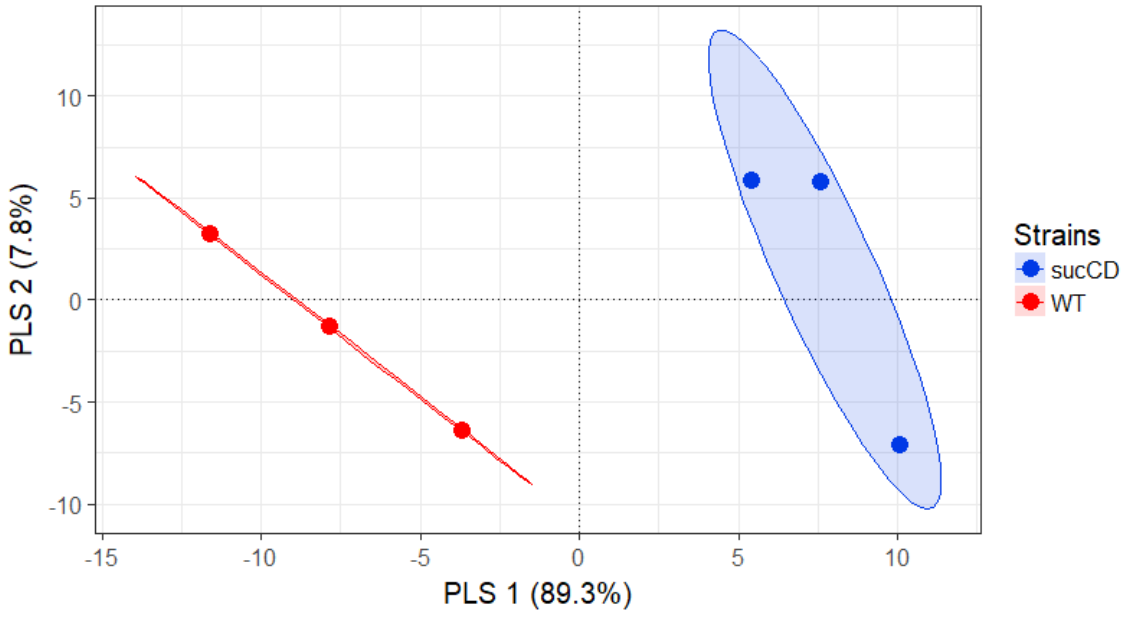

Figure 1.15 Known metabolite pairwise PLSDA for *ΔsucCD*

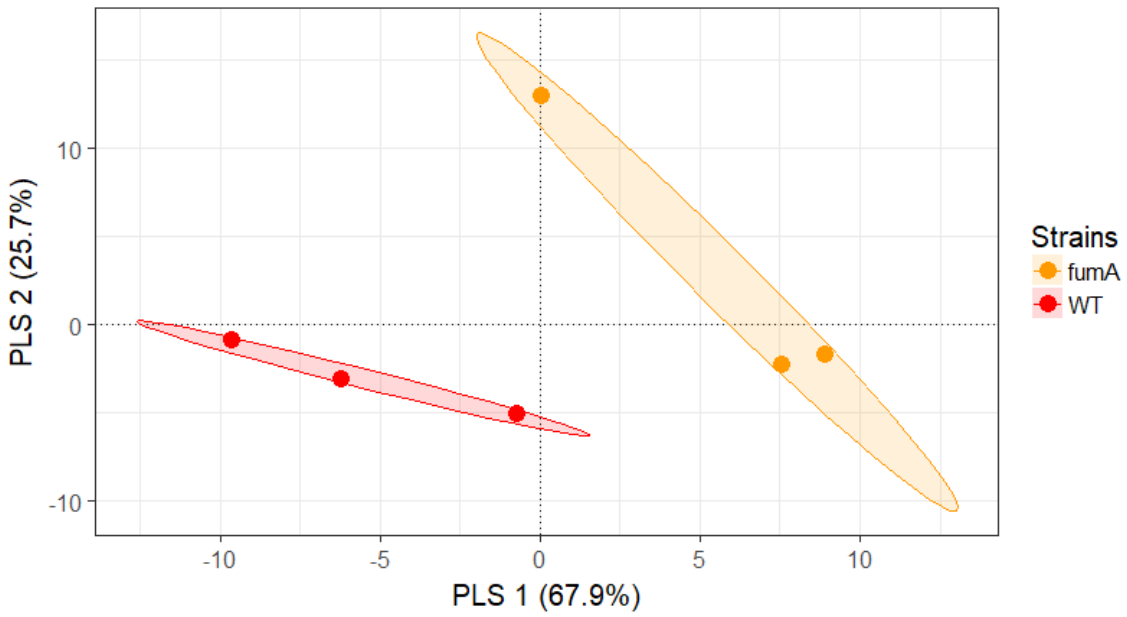

Figure 1.16 Known metabolite pairwise PLSDA for *ΔfumA*

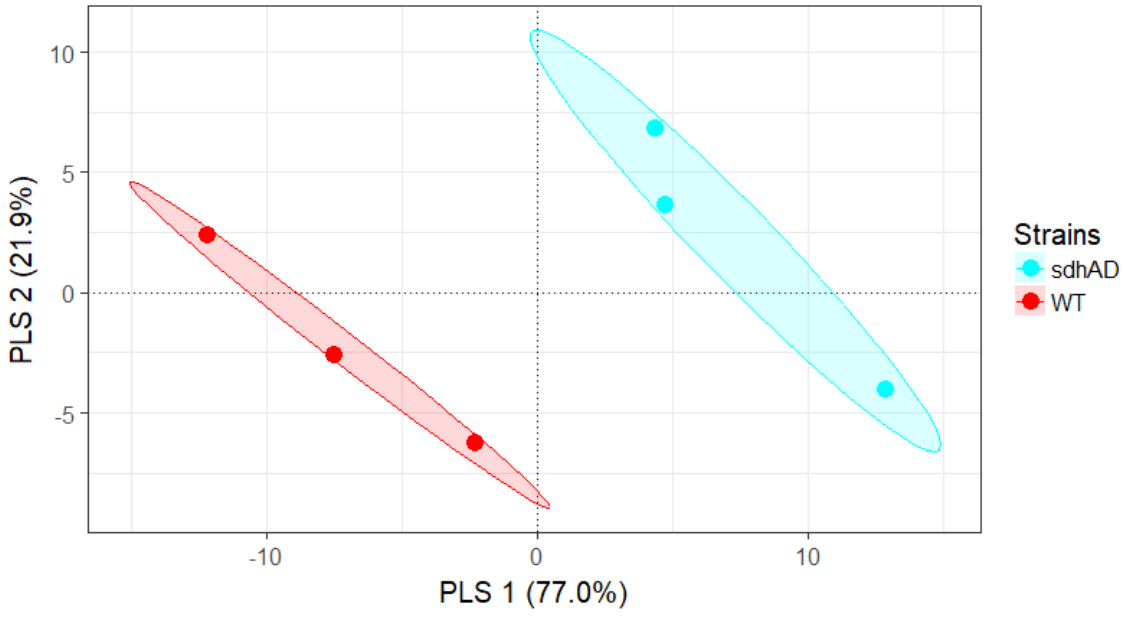

Figure 1.17 Known metabolite pairwise PLSDA for *ΔsdhAD*

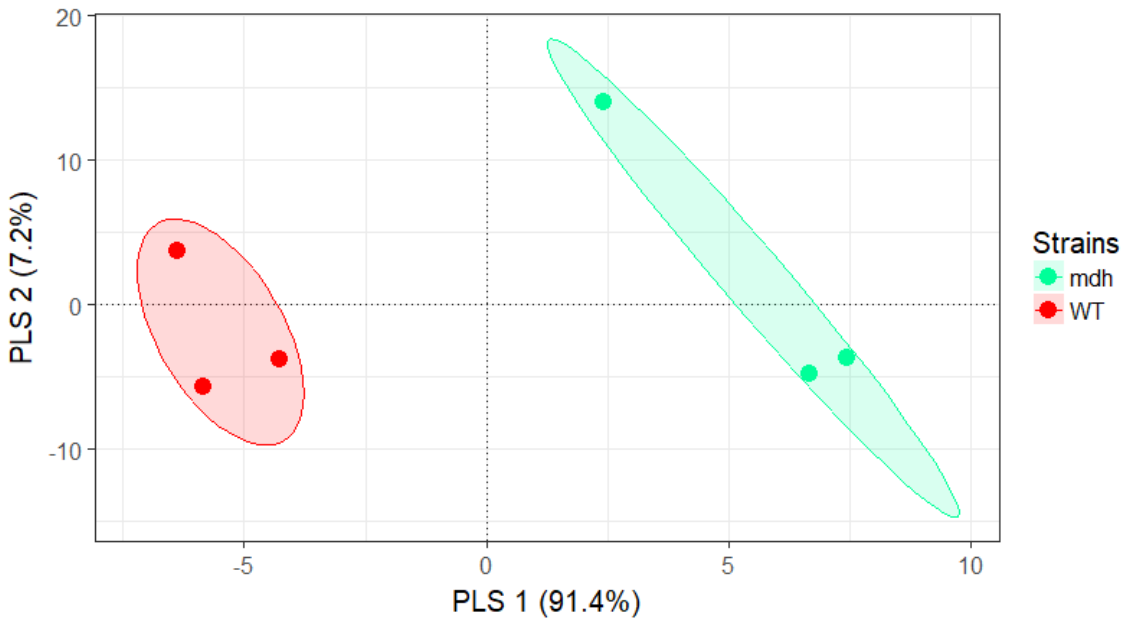

Figure 1.18 Known metabolite pairwise PLSDA for *Δmdh*

Table 1.9 VIP scores for pairwise PLSDA

Metabolite	VIP scores for pairwise comparisons						
	ΔacnB	*ΔacnA*	*ΔsucAB*	*ΔsucCD*	*ΔsdhAD*	*ΔfumA*	*Δmdh*
Glucosamine	1.019	1.032	1.311	1.145	1.055	1.098	1.080
Allantoate	1.333	1.076	0.708	1.392	1.298	1.012	1.212
X2.Isopropylmalate	1.252	1.400	1.134	0.928	1.206	1.213	1.560
IMP	1.247	1.024	1.136	1.142	1.048	0.871	1.886
UDP	1.004	1.281	1.077	0.655	1.006	1.050	1.079
X2.Oxoglutaric.acid	1.346	1.362	0.862	0.438	1.431	1.754	1.959
Homocysteine	1.316	1.879	1.203	0.709	0.189	1.156	1.891
Citraconate	1.282	1.001	0.908	0.601	1.430	1.413	1.012
N.Carbamoyl.L.aspartate	1.250	1.555	1.280	0.826	0.609	1.677	1.938
Octulose.8.1P	1.196	1.232	1.208	1.249	1.069	0.539	0.714
N.Acetylglutamate	1.184	1.232	0.697	1.145	0.811	1.178	1.528
dCMP	1.155	1.014	1.258	1.180	0.839	0.912	1.120
ADP.glucose	1.064	1.547	1.204	0.463	1.237	1.346	0.318
Cysteate	1.055	1.009	1.003	1.282	1.227	0.767	0.574

Table 1.9 continued

Metabolite	VIP scores for pairwise comparisons						
	ΔacnB	*ΔacnA*	*ΔsucAB*	*ΔsucCD*	*ΔsdhAD*	*ΔfumA*	*Δmdh*
Pyruvate	1.327	1.800	0.955	1.179	1.354	0.904	0.417
dUMP	1.307	1.279	0.243	1.368	0.784	1.388	0.694
Orotate	1.296	1.093	0.166	0.479	1.121	0.808	1.821
L.Argininosuccinate	1.239	1.133	1.088	0.618	1.027	0.655	0.433
Arginine	1.237	1.082	0.915	1.301	1.103	0.764	0.869
AMP.dGMP	1.198	1.010	0.710	1.264	1.133	0.782	0.626
Glycinamide.ribotide..GAR.	1.037	1.522	1.012	1.289	0.810	0.789	0.512
Pyroglutamic.acid	1.013	1.055	1.172	1.093	0.911	0.860	0.346
Dihydroorotate	1.287	1.140	0.779	0.894	0.276	0.907	1.833
Ophthalmate	1.224	1.090	1.328	0.759	0.870	0.291	0.420
dTMP	1.131	1.345	0.951	1.110	0.700	0.520	0.273
N.Acetylglucosamine	1.010	1.038	0.914	1.307	0.989	0.807	0.680
dAMP	1.236	1.027	0.705	0.995	0.844	0.772	0.799
dTDP	0.762	1.085	1.177	1.367	1.419	1.460	1.808
S.Ribosyl.L.homocysteine	1.343	0.864	1.201	1.315	1.091	0.858	1.635

Table 1.9 continued

Metabolite	VIP scores for pairwise comparisons						
	ΔacnB	*ΔacnA*	*ΔsucAB*	*ΔsucCD*	*ΔsdhAD*	*ΔfumA*	*Δmdh*
AICAR	1.324	0.846	1.361	0.835	1.387	1.621	1.740
Alanine.Sarcosine	1.201	0.947	1.246	1.225	1.094	1.146	0.337
X4.Pyridoxate	1.045	0.884	1.308	0.776	1.164	1.426	1.286
Ornithine	0.906	1.019	1.329	0.653	1.242	1.211	1.606
Sulfolactate	0.497	1.016	1.188	0.554	1.005	1.345	1.289
Citrulline	0.469	1.158	1.354	0.532	1.133	1.281	1.636
Pantothenate	1.248	0.898	0.774	1.281	1.003	1.092	0.686
Succinate.Methylmalonate	1.213	0.883	1.008	0.938	1.249	1.224	0.691
Phenylalanine	1.168	0.911	1.261	1.326	1.014	0.759	0.426
Inosine	1.154	0.997	0.983	1.280	0.969	1.010	1.019
Uracil	1.109	0.978	1.237	1.286	1.125	0.787	0.423
Lysine	1.097	0.935	1.024	1.388	1.132	0.869	0.692
Acetyllysine	1.079	0.732	1.174	1.381	0.959	0.787	1.002
Glucose.6.phosphate	1.063	0.799	0.969	1.181	0.808	1.113	1.102
Uridine	1.039	0.923	1.231	1.190	1.071	0.833	0.599
Aminoimidazole.ribotide..AIR.	1.036	0.649	1.170	0.935	1.081	1.462	0.356

Table 1.9 continued

Metabolite	VIP scores for pairwise comparisons						
	ΔacnB	*ΔacnA*	*ΔsucAB*	*ΔsucCD*	*ΔsdhAD*	*ΔfumA*	*Δmdh*
X6.Phospho.D.gluconate	1.015	0.931	1.021	0.473	0.878	1.233	1.114
FMN	0.852	1.027	0.978	1.130	1.021	1.387	0.628
Shikimate	0.824	1.418	0.940	0.450	1.144	1.235	1.337
Octulose.bisphosphate	0.739	1.056	1.307	0.570	1.196	1.227	0.961
Fructose.1_6.bisphosphate	0.695	1.065	1.156	0.473	0.957	1.421	1.564
Thymidine	0.424	1.268	1.133	0.648	1.007	1.026	0.427
Citrate.isocitrate	1.349	0.902	0.941	0.723	1.013	1.586	0.887
Glutamate	1.334	0.778	0.822	0.558	0.706	1.312	1.185
Fumarate	1.323	0.976	0.973	0.735	0.822	1.610	1.885
Thymine	1.314	0.932	0.870	1.342	0.965	1.026	0.741
Aconitate	1.310	0.804	0.850	0.687	1.401	1.313	0.452
N.Acetylornithine	1.293	0.763	0.922	0.926	0.838	1.136	1.092
Xylitol	1.279	0.999	0.910	1.391	1.024	0.964	0.779
Guanosine	1.260	0.946	0.986	1.266	1.013	0.832	0.923
UMP	1.252	0.971	0.713	1.189	1.083	0.752	0.637

Table 1.9 continued

Metabolite	VIP scores for pairwise comparisons						
	ΔacnB	*ΔacnA*	*ΔsucAB*	*ΔsucCD*	*ΔsdhAD*	*ΔfumA*	*Δmdh*
L.Methionine	1.251	0.814	0.664	0.925	1.399	0.630	1.375
CMP	1.212	0.980	0.792	1.322	1.208	0.903	0.413
Cytidine	1.099	0.792	0.883	1.327	1.109	0.879	0.906
Leucine.Isoleucine	1.095	0.899	1.094	1.220	0.931	0.794	0.517
X1.Methyladenosine	1.085	0.928	1.031	1.280	0.961	0.860	0.943
sn.Glycerol.3.phosphate	1.085	0.983	0.886	1.286	1.090	0.896	0.445
FAD	1.069	0.899	0.499	0.844	1.219	1.041	0.699
Histidine	1.058	0.884	0.849	1.177	0.884	0.814	1.493
Hydroxyphenylacetate	1.018	0.777	0.638	1.137	0.965	0.712	1.272
N.Acetylglucosamine.1.6.phosphate	0.997	1.003	0.780	1.123	1.124	0.915	0.539
D.Glucarate	0.987	1.009	0.776	1.103	1.120	0.772	0.526
X3.Phosphoserine	0.963	1.449	1.386	0.392	0.587	0.904	1.257
Uric.acid	0.865	1.067	1.056	1.241	0.879	0.707	0.669
Deoxyribose.phosphate	0.607	1.806	0.918	1.146	0.512	0.951	1.302
Glutathione	0.572	1.008	0.538	0.289	1.222	0.747	1.329

Table 1.9 continued

Metabolite	VIP scores for pairwise comparisons						
	ΔacnB	*ΔacnA*	*ΔsucAB*	*ΔsucCD*	*ΔsdhAD*	*ΔfumA*	*Δmdh*
Shikimate.3.phosphate	0.410	1.541	1.527	0.424	0.445	0.884	1.590
N.Acetylputrescine	1.244	0.090	0.437	0.643	0.486	0.365	1.137
Aspartate	1.230	0.835	0.709	0.975	0.679	0.592	1.810
Ribose.phosphate	1.222	0.788	0.789	0.832	1.100	0.575	0.349
Cystathionine	1.219	0.740	0.639	1.139	0.482	0.636	0.998
Proline	1.178	0.868	0.679	1.136	0.491	0.808	0.964
Sedoheptulose.1.7.phosphate	1.175	0.993	0.845	0.691	0.916	1.076	0.235
UDP.N.acetylglucosamine	1.161	0.906	0.727	1.017	0.824	0.906	0.427
Nicotinate	1.153	0.990	0.797	1.288	0.848	0.762	0.580
Xanthurenic.acid	1.123	0.916	0.769	1.192	0.794	0.869	0.886
Asparagine	1.109	0.951	0.856	1.201	0.952	0.878	0.768
Valine	1.104	0.879	0.977	1.170	0.842	0.845	0.545
Tyrosine	1.060	0.909	0.978	1.193	1.000	0.816	0.500
X3.Hydroxyisovaleric.acid	1.021	0.709	0.960	0.603	1.082	0.810	0.837
Histidinol	1.009	0.717	1.012	0.948	0.626	0.811	0.480

Table 1.9 continued

Metabolite	VIP scores for pairwise comparisons						
	ΔacnB	*ΔacnA*	*ΔsucAB*	*ΔsucCD*	*ΔsdhAD*	*ΔfumA*	*Δmdh*
Trehalose.6.phosphate	0.974	1.041	0.766	1.373	0.668	0.873	0.252
UDP.glucuronate	0.574	1.005	0.624	0.423	0.756	0.571	1.087
Xanthosine	0.543	1.103	1.142	0.842	0.913	0.823	0.501
Glutamine	1.294	0.967	0.712	0.873	0.794	0.848	0.328
cAMP	1.121	0.929	0.729	0.650	0.871	0.837	0.935
Phenylpyruvate	1.105	0.793	0.550	0.695	0.846	0.889	0.277
Homoserine.Threonine	1.045	0.911	0.939	0.458	0.741	0.841	0.545
Hydroxyisocaproic.acid	0.639	1.010	0.782	0.891	0.779	0.888	0.423
Sucralose	0.939	0.752	1.381	1.428	1.530	1.475	1.986
Allantoin	0.894	0.938	1.130	1.333	1.197	0.854	1.022
Hydroxyproline	0.790	0.978	1.298	1.303	1.306	0.767	1.403
Glutathione.disulfide	0.346	0.883	1.013	0.467	1.001	1.148	1.304
Tryptophan	0.999	0.929	1.129	1.147	1.020	0.814	0.469
Sedoheptoluse.bisphosphate	0.885	0.980	1.147	0.427	1.018	1.375	0.643
Adenine	0.857	0.999	1.473	1.205	0.979	0.798	1.558

Table 1.9 continued

Metabolite	VIP scores for pairwise comparisons						
	ΔacnB	*ΔacnA*	*ΔsucAB*	*ΔsucCD*	*ΔsdhAD*	*ΔfumA*	*Δmdh*
Acetylphosphate	0.851	0.641	0.359	1.015	0.531	1.711	1.254
Homocysteic.acid	0.811	0.744	1.034	1.075	0.897	0.769	1.024
D.Glyceraldehdye.3.phosphate	0.806	0.862	1.138	0.735	1.005	0.556	1.643
Lactate	0.777	0.727	1.178	0.789	1.075	1.101	0.868
N.Acetyl.beta.alanine	0.710	0.941	1.068	0.775	1.030	1.187	0.334
N.Acetylglutamine	0.685	0.921	1.107	0.839	1.068	1.081	0.272
X2.Dehydro.D.gluconate	0.587	0.892	1.031	1.120	0.920	0.773	1.102
D.Gluconate	0.584	0.923	1.156	0.982	1.054	1.026	0.531
Phenyllactic.acid	0.542	0.935	1.027	1.047	0.891	1.006	0.253
X3.Phosphoglycerate	0.539	0.895	1.177	0.511	1.050	1.475	0.591
X3_4.Dihydroxyphenylacetate..DOPAC.	0.528	0.917	0.942	1.110	1.253	0.887	1.039
Carbamoyl.phosphate	0.427	0.932	1.029	0.506	1.019	1.150	0.989
Acetyl.CoA	0.290	0.791	1.030	0.635	0.511	1.084	1.237
Creatinine	0.998	0.813	1.291	1.317	0.841	0.701	0.742
Deoxyinosine	0.996	0.913	0.744	1.194	0.765	0.678	1.229

Table 1.9 continued

Metabolite	VIP scores for pairwise comparisons						
	ΔacnB	*ΔacnA*	*ΔsucAB*	*ΔsucCD*	*ΔsdhAD*	*ΔfumA*	*Δmdh*
Glucosamine.phosphate	0.993	0.832	1.159	0.529	0.983	1.445	0.934
X2_3.Dihydroxybenzoate	0.991	0.976	0.765	1.068	1.428	0.785	0.230
GMP	0.974	0.916	0.816	1.130	1.035	0.821	0.546
Hypoxanthine	0.845	0.818	1.308	1.164	0.783	0.749	0.418
Guanine	0.762	0.599	1.321	1.162	0.679	0.717	0.508
Xanthosine.5..phosphate	0.757	0.785	1.013	0.724	0.748	0.660	1.342
Adenosine	0.748	0.994	1.039	0.923	1.104	0.900	0.654
UDP.glucose	0.736	0.718	0.560	0.536	1.295	0.384	1.467
Creatine	0.722	0.741	1.206	1.020	0.951	0.674	0.512
Cysteine	0.581	0.879	1.327	0.756	1.518	0.755	0.470
NADH	0.529	0.961	0.732	1.027	0.708	1.179	0.933
ADP	0.488	0.886	1.014	0.733	0.972	1.304	0.300
GDP	0.391	0.861	1.135	0.466	0.830	1.103	0.290
Hydroxybenzoate	0.972	0.819	0.717	1.035	0.969	0.889	0.924
Serine	0.947	0.904	0.956	1.086	0.985	0.839	0.458

Table 1.9 continued

Metabolite	VIP scores for pairwise comparisons						
	ΔacnB	*ΔacnA*	*ΔsucAB*	*ΔsucCD*	*ΔsdhAD*	*ΔfumA*	*Δmdh*
Glycerate	0.868	0.892	0.885	1.106	0.927	0.848	0.594
X4.Aminobutyrate..GABA.	0.805	0.987	0.830	0.802	1.239	0.965	0.666
X2.Hydroxy.2.methylsuccinate	0.784	0.920	0.811	0.793	0.873	1.058	0.768
Taurine	0.764	0.753	0.955	1.052	0.846	0.830	0.607
Homovanillic.acid..HVA.	0.705	0.657	0.997	0.990	0.841	0.725	1.001
Phosphoenolpyruvate	0.540	0.975	0.827	0.703	1.070	0.995	0.421
Trehalose.Sucrose.Cellobiose	0.355	0.875	0.957	1.016	0.784	0.829	0.696
X2.Aminoadipate	0.498	0.953	0.876	0.870	0.977	0.862	0.436
NADP.	0.259	0.834	0.706	0.759	0.947	0.569	0.365
NAD.	0.246	0.791	0.661	0.855	0.923	0.370	0.476

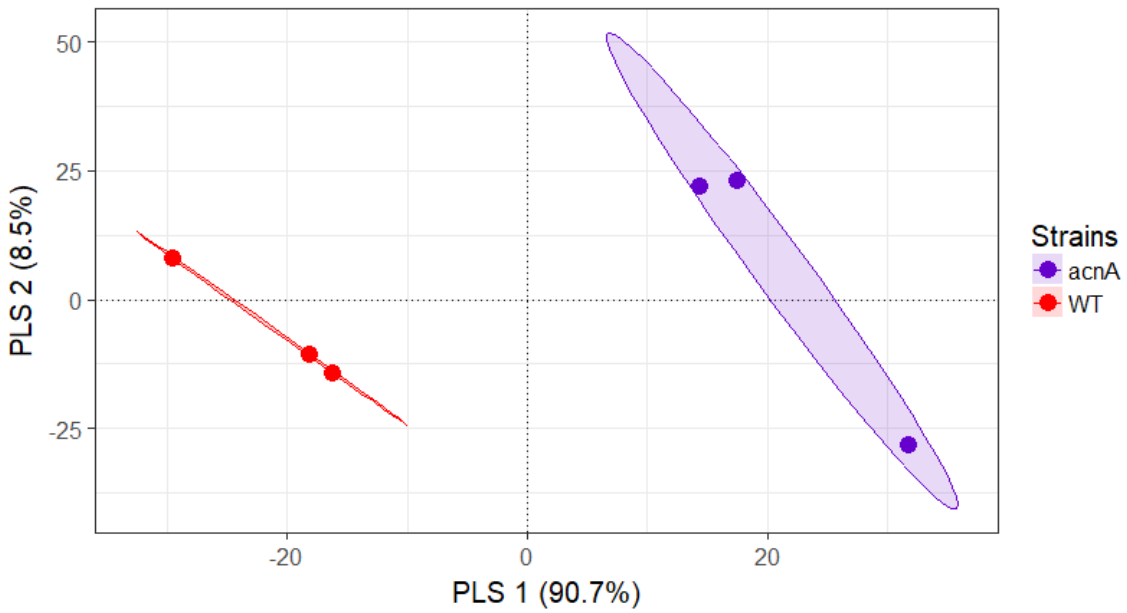

Figure 1.19 Unknown feature pairwise PLSDA for *ΔacnA*

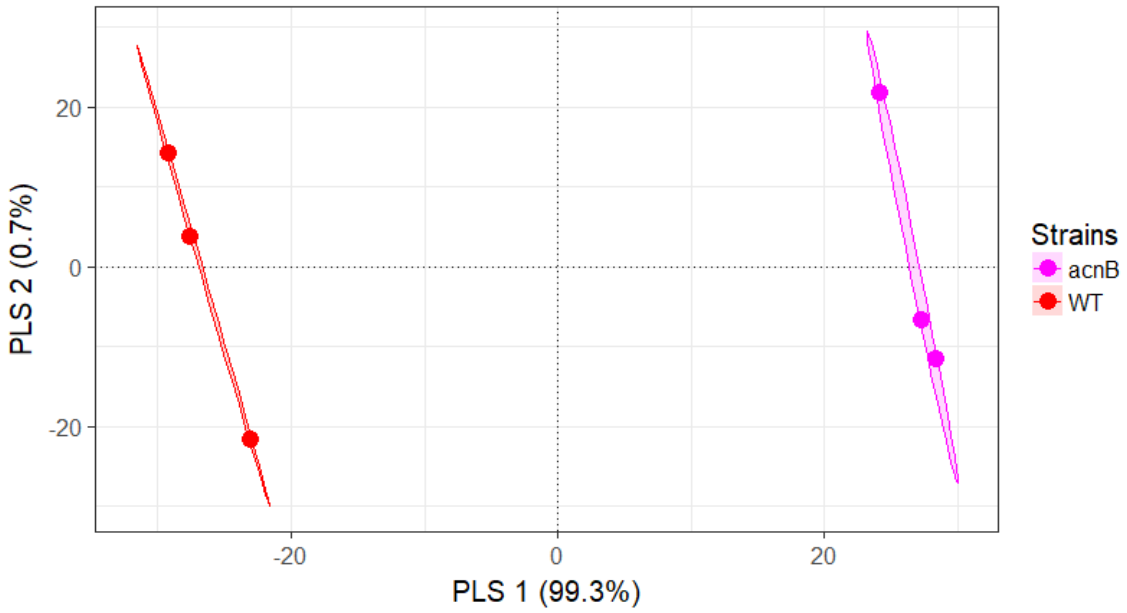

Figure 1.20 Unknown feature pairwise PLSDA for *ΔacnB*

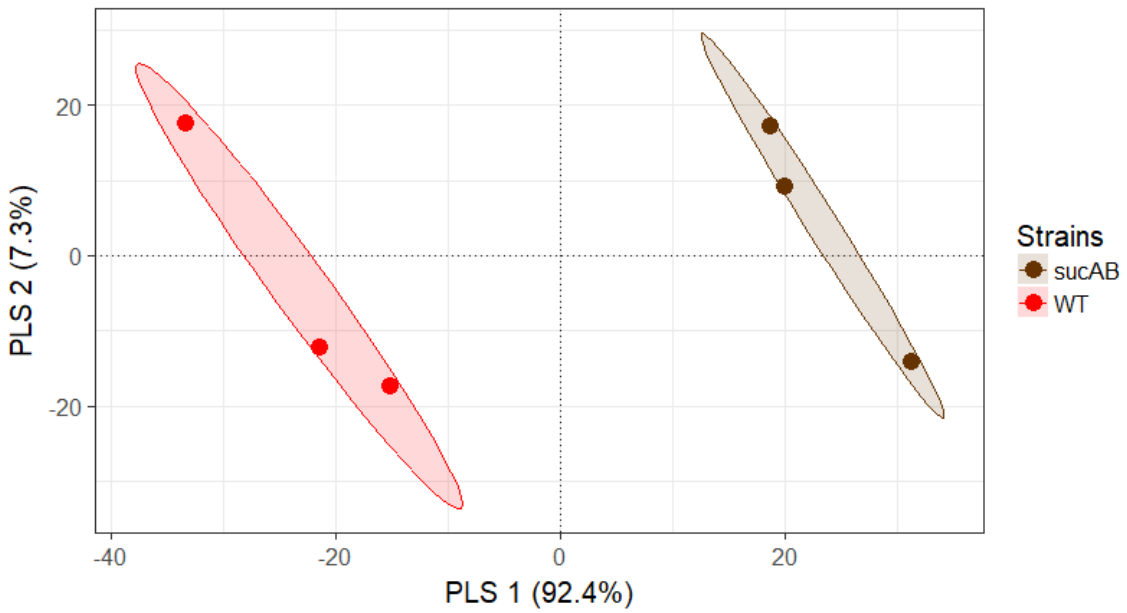

Figure 1.21 Unknown feature pairwise PLSDA for *ΔsucAB*

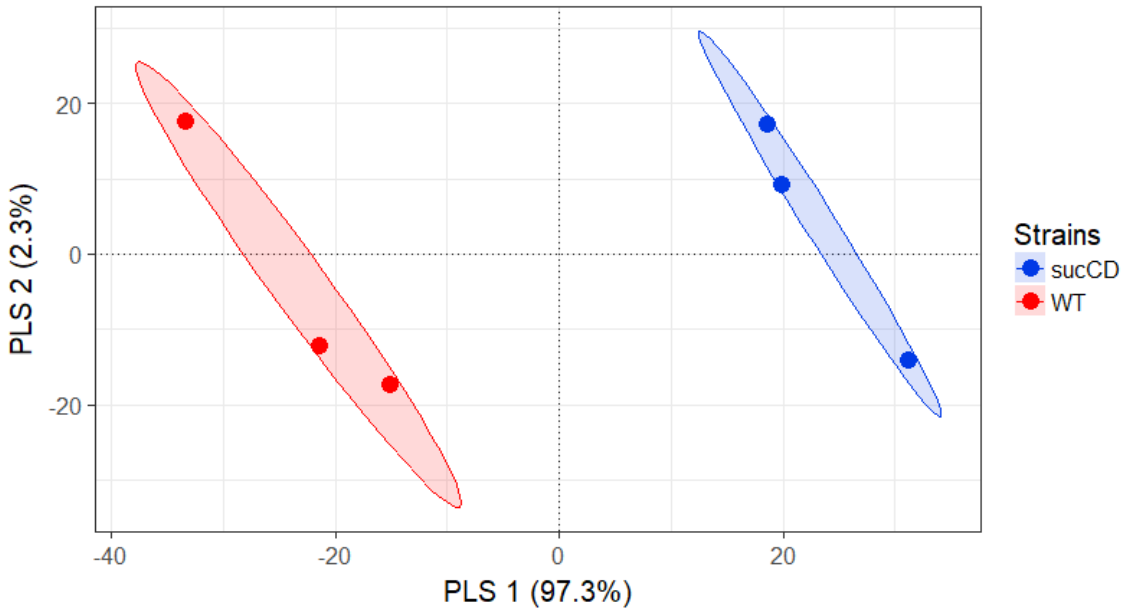

Figure 1.22 Unknown feature pairwise PLSDA for *ΔsucCD*

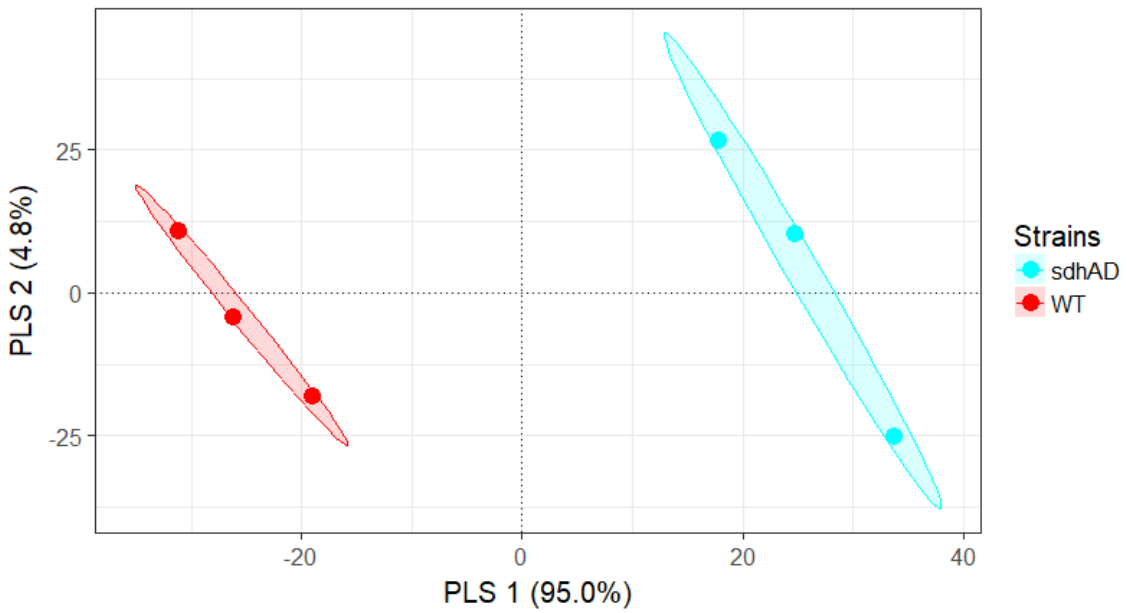

Figure 1.23 Unknown feature pairwise PLSDA for *ΔsdhAD*

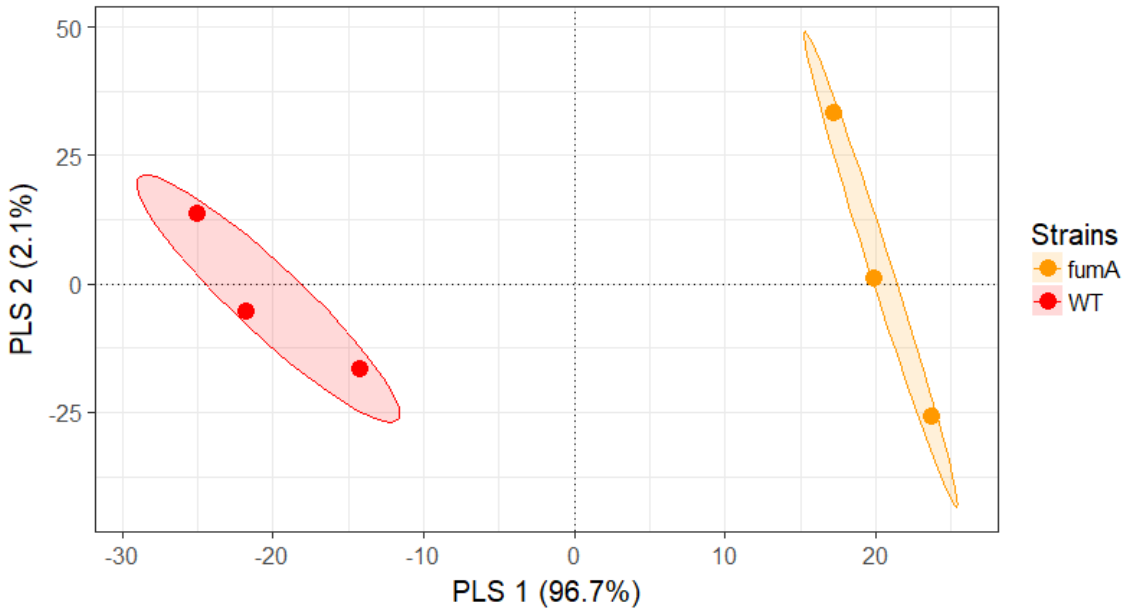

Figure 1.24 Unknown feature pairwise PLSDA for *ΔfumA*

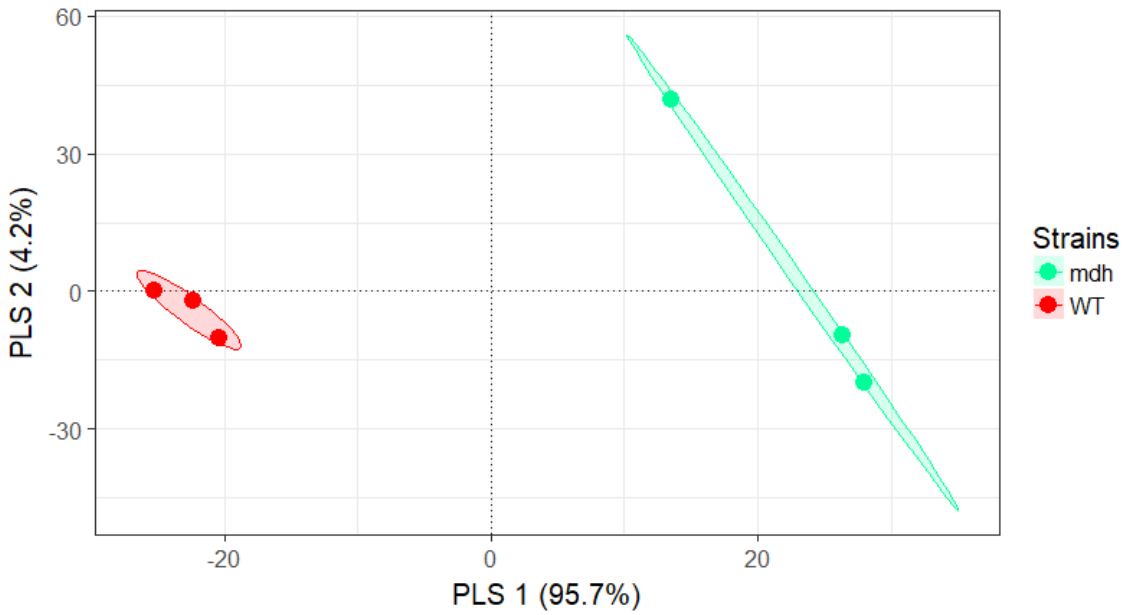

Figure 1.25 Unknown feature pairwise PLSDA for *Δmdh*

Table 1.10 Ratios and p-values used for heat map of dipeptides

compound	Ratio compared to WT						
	ΔacnA	*ΔacnB*	*ΔsucAB*	*ΔsucCD*	*ΔsdhAD*	*Δmdh*	*ΔfumA*
Ala-Ala	0.75	0.93	0.78	1.11	0.67	0.85	0.88
Val-Gly	1.57	0.1	6.76	0	1.41	0.17	0.94
Gly-Cys	1.63	0.54	1.66	0.88	1.15	0.94	1.08
Gly-Asp	1.17	1.58	0.44	0.02	1.31	1.63	0.76
Ser-Ser	2.1	0.24	2.19	0	14.22	0.46	2.57
Ser-Pro	1.96	1.09	1.16	1.87	3.18	0.54	2.09
Asn-Ala	4.63	0.23	6.7	0	9.86	0.86	2.37
Thr-Pro	2.21	0.44	1.54	0.41	1.53	0.54	1.08
Gln-Ala	0.83	0.86	2.72	0.11	4.74	0.3	1.81
Glu-Ala	1.91	1.47	1.64	0.87	2.57	1.2	1.81
Glu-Ser	1.95	0.54	1.91	0.34	13.49	0.56	2.52
Glu-Pro	2.14	0.51	0.97	0.99	0.82	0.58	1.18
Cys-Met	0	2.13	1.2	0.26	0.56	0.84	1.32
Leu-Glu	3.14	0.09	1.93	0.89	2.54	0.89	1.87

Table 1.10 continued

compound	Ratio compared to WT						
	ΔacnA	*ΔacnB*	*ΔsucAB*	*ΔsucCD*	*ΔsdhAD*	*Δmdh*	*ΔfumA*
Asn-Glu	4.02	0.69	1.32	0.81	1.51	0.76	1.3
Asp-Glu	0.57	0.29	4.62	0.33	12.62	0.13	5.59
Met-Asp	1.16	0.65	1	0.64	1.43	0.79	0.91
Glu-Glu	5.92	0.41	2.46	0.88	8.23	1.4	2.15
Met-Glu	1.1	0.51	0.57	1.75	1.25	0.45	0.88
Met-Met	0.85	0.16	1.81	1.52	0.75	0.34	1.13
Glu-Tyr	13.62	0	2.53	0.04	6.24	2.24	2.53
Arg-Tyr	1.51	1.88	1.73	1.32	2.11	1.69	1.49

Table 1.10 continued

compound	p-value						
	ΔacnA	*ΔacnB*	*ΔsucAB*	*ΔsucCD*	*ΔsdhAD*	*Δmdh*	*ΔfumA*
Ala-Ala	0.28	0.66	0.26	0.61	0.13	0.46	0.54
Val-Gly	0.73	0.35	0.41	0.31	0.7	0.38	0.95
Gly-Cys	0.04	0.28	0.04	0.87	0.7	0.89	0.84
Gly-Asp	0.48	0.05	0.11	0.01	0.19	0.02	0.2
Ser-Ser	0.45	0.28	0.41	0.2	0.41	0.49	0.49
Ser-Pro	0.23	0.88	0.85	0.23	0.41	0.49	0.17
Asn-Ala	0.26	0.28	0.11	0.2	0.05	0.89	0.39
Thr-Pro	0.47	0.08	0.24	0.06	0.59	0.11	0.84
Gln-Ala	0.86	0.8	0.02	0.1	0.2	0.15	0.34
Glu-Ala	0.09	0.27	0.18	0.74	0.48	0.59	0.12
Glu-Ser	0.46	0.36	0.35	0.21	0.4	0.4	0.17
Glu-Pro	0.48	0	0.83	0.96	0.67	0.01	0.29
Cys-Met	0.1	0.45	0.8	0.16	0.42	0.69	0.71
Leu-Glu	0.32	0.24	0.24	0.87	0.49	0.87	0.29

Table 1.10 continued

compound	p-value						
	ΔacnA	*ΔacnB*	*ΔsucAB*	*ΔsucCD*	*ΔsdhAD*	*Δmdh*	*ΔfumA*
Asn-Glu	0.39	0.19	0.19	0.38	0.39	0.29	0.53
Asp-Glu	0.58	0.25	0.09	0.26	0.4	0.17	0.34
Met-Asp	0.26	0.03	0.98	0.17	0.06	0.19	0.69
Glu-Glu	0.24	0.13	0.09	0.73	0.3	0.69	0.3
Met-Glu	0.6	0.05	0.06	0.04	0.19	0.04	0.56
Met-Met	0.78	0.08	0.1	0.2	0.7	0.14	0.85
Glu-Tyr	0.3	0.17	0.43	0.17	0.06	0.64	0.36
Arg-Tyr	0.15	0.19	0.06	0.53	0.01	0.23	0.6

Table 1.11 Ratios and p-values used for heat map of lipids

compound	Ratio compared to WT						
	ΔacnA	*ΔacnB*	*ΔsucAB*	*ΔsucCD*	*ΔsdhAD*	*ΔfumA*	*Δmdh*
CL(62:0)	0.83	0.20	0.79	0.80	0.84	0.88	0.88
CL(64:2)	0.56	0.32	0.80	0.97	0.69	0.73	0.71
CL(66:1)	0.77	0.38	0.98	1.33	0.80	0.85	0.90
CL(68:1)	0.95	1.26	0.75	0.82	1.01	1.03	1.02
PA(30:1)	0.76	0.81	1.04	0.96	0.77	0.76	0.88
PA(32:1)	0.78	0.65	0.93	1.10	0.75	0.75	0.93
PA(32:2)	0.74	0.76	1.36	1.43	0.81	1.09	0.85
PA(34:1)	0.83	0.83	0.92	1.17	0.72	0.82	0.93
PA(34:2)	0.83	0.58	1.12	1.20	0.88	0.90	0.95
PE(26:0)	0.76	0.46	0.66	0.60	0.77	0.62	0.70
PE(28:0)	0.94	0.71	0.79	0.90	0.96	0.77	1.05
PE(28:1)	0.72	0.33	0.80	0.76	0.69	0.74	0.85
PE(30:0)	0.96	0.78	0.93	1.10	1.00	0.91	1.08
PE(30:1)	0.88	0.42	0.96	1.03	0.92	0.83	1.04

Table 1.11 contined

compound	Ratio compared to WT						
	ΔacnA	*ΔacnB*	*ΔsucAB*	*ΔsucCD*	*ΔsdhAD*	*ΔfumA*	*Δmdh*
PE(30:2)	0.64	0.15	0.88	0.76	0.63	0.61	0.75
PE(32:1)	0.87	0.44	1.07	1.31	0.86	0.85	1.03
PE(32:2)	0.76	0.31	1.13	1.17	0.83	0.74	1.04
PE(36:2)	0.93	0.73	1.07	1.07	0.90	0.91	1.13
PG(30:1)	0.84	0.73	1.04	0.98	0.98	0.90	0.95
PG(36:2)	0.87	0.87	1.10	1.16	0.89	0.98	1.06
PG(28:0)	0.85	0.71	0.82	0.90	0.95	0.87	0.89
PG(32:1)	0.83	0.75	1.10	1.26	0.89	0.97	0.96
PG(34:1)	0.88	0.89	0.98	1.16	0.86	1.02	0.99
PG(34:2)	0.85	0.75	1.24	1.17	0.94	0.94	1.04
PS(32:1)	0.77	1.17	2.55	1.56	0.88	0.86	0.65
PS(34:1)	1.02	1.21	2.80	1.44	1.20	1.15	0.93
PS(34:3)	0.80	0.43	1.16	1.37	0.81	0.84	1.00
PS(36:2)	1.06	0.75	3.35	1.19	1.13	1.22	0.99

Table 1.11 continued

compound	p-value						
	ΔacnA	*ΔacnB*	*ΔsucAB*	*ΔsucCD*	*ΔsdhAD*	*ΔfumA*	*Δmdh*
CL(62:0)	0.34	0.00	0.41	0.20	0.37	0.49	0.49
CL(64:2)	0.18	0.05	0.51	0.93	0.33	0.37	0.33
CL(66:1)	0.06	0.00	0.89	0.00	0.25	0.18	0.39
CL(68:1)	0.30	0.08	0.15	0.01	0.87	0.53	0.72
PA(30:1)	0.24	0.58	0.82	0.90	0.27	0.25	0.52
PA(32:1)	0.39	0.22	0.80	0.78	0.41	0.37	0.81
PA(32:2)	0.18	0.34	0.18	0.11	0.60	0.85	0.59
PA(34:1)	0.50	0.54	0.76	0.70	0.34	0.50	0.83
PA(34:2)	0.25	0.03	0.59	0.28	0.72	0.75	0.85
PE(26:0)	0.33	0.03	0.32	0.08	0.28	0.09	0.24
PE(28:0)	0.67	0.10	0.31	0.48	0.78	0.16	0.78
PE(28:1)	0.04	0.00	0.38	0.06	0.03	0.05	0.24
PE(30:0)	0.68	0.04	0.61	0.26	0.98	0.30	0.42
PE(30:1)	0.31	0.00	0.81	0.81	0.60	0.17	0.79

Table 1.11 continued

compound	p-value						
	ΔacnA	*ΔacnB*	*ΔsucAB*	*ΔsucCD*	*ΔsdhAD*	*ΔfumA*	*Δmdh*
PE(30:2)	0.04	0.00	0.66	0.10	0.09	0.02	0.08
PE(32:1)	0.26	0.00	0.60	0.02	0.42	0.17	0.83
PE(32:2)	0.18	0.01	0.53	0.34	0.49	0.18	0.85
PE(36:2)	0.52	0.06	0.75	0.62	0.50	0.40	0.46
PG(30:1)	0.20	0.01	0.73	0.87	0.88	0.34	0.61
PG(36:2)	0.35	0.10	0.50	0.33	0.45	0.78	0.61
PG(28:0)	0.30	0.06	0.36	0.46	0.68	0.32	0.52
PG(32:1)	0.24	0.02	0.32	0.16	0.44	0.82	0.79
PG(34:1)	0.29	0.20	0.88	0.35	0.20	0.88	0.89
PG(34:2)	0.31	0.01	0.11	0.27	0.73	0.64	0.79
PS(32:1)	0.45	0.64	0.22	0.49	0.71	0.66	0.30
PS(34:1)	0.91	0.34	0.25	0.47	0.37	0.56	0.63
PS(34:3)	0.04	0.00	0.11	0.00	0.32	0.22	0.98
PS(36:2)	0.85	0.36	0.27	0.76	0.66	0.60	0.97

Table 1.12 Relative pool values for each strain compared to WT

Metabolite	*Relative Pool ± standard Dev.*						
	ΔacnA	*ΔacnB*	*ΔsucAB*	*ΔsucCD*	*ΔsdhAD*	*Δmdh*	*ΔfumA*
1-Methyladenosine	6.3±10.72	0.08±0.13	4.39±6.52	0.03±0.03	4.64±7.4	0.68±1.37	1.98±3.04
2_3-Dihydroxybenzoate	1.38±0.76	0.77±0.17	0.95±0.34	0.55±0.25	0.76±0.2	1±0.35	0.96±0.28
2-Aminoadipate	9.37±14.91	0.68±0.65	3.92±5.72	0.37±0.36	3.72±4.9	1.98±3.54	3.21±4.26
2-Dehydro-D-gluconate	3.98±5.86	0.52±0.65	1.93±1.52	0.06±0.08	10.82±18.03	0.36±0.63	2.73±3.17
2-Hydroxy-2-methylsuccinate	3.01±3.34	0.53±0.41	3.69±4.91	0.56±0.49	1.5±0.86	1.29±0.88	1.67±1.11
2-Isopropylmalate	1.44±0.27	3.55±1.48	1.43±0.33	2.19±1.38	1.77±0.51	1.44±0.39	1.49±0.54
2-Oxoglutaric acid	1.01±0.24	0.19±0.04	1.09±0.13	1.07±0.48	0.52±0.29	0.56±0.06	0.7±0.14
3_4-Dihydroxyphenylacetate (DOPAC)	2.36±1.34	0.95±0.25	1.4±0.57	0.6±0.22	2.81±1.12	1.86±1.5	1.64±1.08

Table 1.12 continued

Metabolite	*Relative Pool ± standard Dev.*						
	ΔacnA	*ΔacnB*	*ΔsucAB*	*ΔsucCD*	*ΔsdhAD*	*Δmdh*	*ΔfumA*
3-Hydroxyisovaleric acid	1.14±0.28	1.41±0.44	1.72±0.97	0.92±0.3	1.37±0.34	1.13±0.3	1.13±0.37
3-Phosphoglycerate	2.71±2.55	1.22±0.49	1.91±0.73	0.95±0.62	1.57±0.56	1.06±0.24	2.09±0.77
3-Phosphoserine	1.6±0.2	1.64±0.62	1.49±0.18	1.19±0.82	1.13±0.29	0.76±0.22	1.29±0.44
4-Aminobutyrate (GABA)	2.44±1.62	1.15±0.21	1.39±0.65	0.85±0.21	1.53±0.28	1.12±0.37	1.27±0.39
4-Pyridoxate	1.61±0.76	1.47±0.44	1.69±0.32	0.85±0.21	2.77±1.52	1.27±0.31	1.76±0.61
6-Phospho-D-gluconate	1.28±0.3	2.56±1.41	1.25±0.28	1.09±0.82	1.39±0.54	0.74±0.28	1.45±0.45
Acetyl-CoA	1.32±0.53	1.05±0.76	1.81±0.94	1.23±1.17	1±0.41	1.5±0.69	1.5±0.77
Acetyllysine	1.25±0.41	0.66±0.17	1.6±0.42	2.72±0.85	1.86±1.08	0.78±0.33	1.01±0.33
Acetylphosphate	0.85±0.37	0.72±0.32	1.02±0.35	0.66±0.23	0.93±0.12	0.79±0.22	0.62±0.09
Aconitate	2.93±2.71	10.15±5.83	1.73±1.2	0.68±0.49	13.29±6.67	9.17±15.82	1.84±0.86
Adenine	2±1.04	0.74±0.24	2.24±0.23	0.45±0.18	2.17±1.41	1.35±0.28	1.49±0.84

Table 1.12 continued

Metabolite	*Relative Pool ± standard Dev.*						
	ΔacnA	*ΔacnB*	*ΔsucAB*	*ΔsucCD*	*ΔsdhAD*	*Δmdh*	*ΔfumA*
Adenosine	11.29±19.75	0.47±1.08	4±6.79	0.05±0.09	19.91±38.89	1.49±3.41	1.39±2.85
ADP	2.41±2.4	0.83±0.72	2.14±1.46	0.58±0.58	1.73±1.1	0.97±0.5	2.55±1.65
ADP-glucose	0.9±0.33	0.67±0.17	0.86±0.2	0.96±0.34	0.6±0.19	0.98±0.28	0.75±0.18
AICAR	1.07±0.25	0.43±0.08	0.66±0.13	0.78±0.29	0.52±0.11	0.58±0.16	0.77±0.11
Alanine/Sarcosine	2.59±1.98	0.54±0.14	1.99±0.62	0.46±0.19	2.12±1.06	1.05±0.48	1.55±0.6
Allantoate	9.85±11.01	0±0	2.24±3.06	0±0	7.48±5.26	1.96±3.65	3.62±4.44
Allantoin	4.71±4.55	0.26±0.37	3.48±2.62	0.01±0.01	6.34±4.98	1.1±2.03	2.75±3.09
Aminoimidazole ribotide (AIR)	0.87±0.17	0.71±0.25	0.66±0.14	0.86±0.17	0.65±0.2	0.94±0.34	0.67±0.16
AMP/dGMP	7.71±11.18	0.1±0.1	3.12±5.05	0.09±0.09	3.8±3.77	1.51±2.78	3.46±4.3
Arginine	7.1±9.1	0.11±0.09	3.21±3.8	0.09±0.08	2.65±2.23	0.95±1.67	2.68±3.18
Asparagine	3.24±3.05	0.56±0.19	1.59±1.05	0.46±0.19	1.43±0.53	0.84±0.82	1.55±0.99
Aspartate	1.83±1.22	0.48±0.15	1.24±0.41	0.76±0.18	1.37±1.11	0.49±0.15	1.14±0.37

Table 1.12 continued

Metabolite	*Relative Pool ± standard Dev.*						
	ΔacnA	*ΔacnB*	*ΔsucAB*	*ΔsucCD*	*ΔsdhAD*	*Δmdh*	*ΔfumA*
cAMP	1.47±0.74	0.52±0.2	1.23±0.54	0.88±0.37	1.39±1.08	0.68±0.48	1.13±0.48
Carbamoyl phosphate	4.25±4.67	0.56±0.62	2.35±1.95	0.87±0.95	6.64±8.86	2.08±2.26	2.76±2.54
Citraconate	1.78±0.72	3.05±1.05	1.36±0.47	0.87±0.24	8.89±3.11	6.49±9.58	1.35±0.29
Citrate/isocitrate	2.49±2.56	17.25±7.26	1.75±1.03	0.66±0.52	1.66±0.76	0.79±0.48	2.43±0.92
Citrulline	1.71±0.56	1.03±0.24	2.38±0.89	1.06±0.34	1.58±0.62	1.71±0.56	1.58±0.56
CMP	3.33±2.92	0.55±0.13	1.83±1.49	0.42±0.11	1.95±0.62	1.2±1.05	1.84±1.15
Creatine	0.68±0.53	0.45±0.54	7.58±8.29	0.05±0.07	2.68±2.61	1.14±1.08	2.69±3.46
Creatinine	0.89±0.68	0.2±0.25	9.46±10.47	0.06±0.06	1.5±2.23	0.94±1.11	5.37±7.2
Cystathionine	5.02±7.5	0.14±0.1	2.54±4.22	0.27±0.19	0.78±0.6	0.55±0.5	2.74±3.98
Cysteate	11.51±14.92	0.15±0.19	2.13±1.71	0.05±0.04	11.72±10.99	3.15±5.74	3.42±3.62
Cysteine	3.87±4.28	0.78±0.67	2.01±0.52	0.46±0.48	0.64±0.13	0.94±0.48	2.21±2.18
Cytidine	5.33±6.56	0.05±0.09	2.19±2.92	0±0	5.22±4.57	1.62±3.12	1.96±2.76

Table 1.12 continued

Metabolite	*Relative Pool ± standard Dev.*						
	ΔacnA	*ΔacnB*	*ΔsucAB*	*ΔsucCD*	*ΔsdhAD*	*Δmdh*	*ΔfumA*
dAMP	7.64±7.82	0.21±0.14	1.76±1.97	0.52±0.3	1.46±0.98	0.78±0.74	2.86±2.98
dCMP	2.63±1.57	0.64±0.15	1.37±0.21	0.59±0.2	2.24±1.94	0.86±0.16	1.33±0.5
Deoxyinosine	14.26±25.4	0.04±0.06	2.87±4.58	0.01±0.02	13.2±26.26	0.39±0.82	5.29±8.44
Deoxyribose phosphate	1.39±0.27	1.13±0.27	1.13±0.19	0.52±0.21	1.09±0.25	1.16±0.18	0.79±0.24
D-Glucarate	33±55.27	0.22±0.36	7.78±13.16	0.03±0.04	13.77±19.65	2.77±4.94	19.56±27.61
D-Gluconate	7.94±12.27	0.65±0.69	6.57±6.89	0.35±0.33	9.98±14.56	1.23±1.92	8.04±10.08
D-Glyceraldehdye 3-phosphate	0.85±0.44	0.77±0.28	1.24±0.24	0.72±0.46	1.24±0.24	1.26±0.18	1±0.27
Dihydroorotate	1.42±0.39	2.36±0.68	1.36±0.73	1.4±0.56	1.07±0.5	2.4±0.82	1.32±0.76
dTDP	1.09±0.7	0.39±0.53	0.25±0.27	0.19±0.12	0.14±0.04	0.56±0.14	0.1±0.1
dTMP	1.81±0.5	0.6±0.16	1.22±0.26	0.66±0.19	1.26±0.63	0.98±0.2	0.94±0.21
dUMP	1.36±0.44	0.2±0.08	1.03±0.33	0.33±0.11	1.13±0.35	0.84±0.32	0.53±0.22
FAD	1.07±0.39	0.68±0.17	0.97±0.32	0.68±0.32	0.66±0.17	1.12±0.33	0.8±0.21

Table 1.12 continued

Metabolite	*Relative Pool ± standard Dev.*						
	ΔacnA	*ΔacnB*	*ΔsucAB*	*ΔsucCD*	*ΔsdhAD*	*Δmdh*	*ΔfumA*
FMN	0.93±0.25	0.69±0.28	0.93±0.24	0.5±0.22	0.71±0.21	0.9±0.24	0.73±0.18
Fructose 1_6-bisphosphate	1.51±0.44	0.75±0.3	1.84±0.72	1.84±1.5	1.44±0.48	1.79±0.68	1.81±0.78
Fumarate	1.77±0.79	0.41±0.06	1.45±0.53	0.8±0.3	1.08±0.48	1.82±0.35	1.52±0.25
GDP	1.69±1.32	2.31±2.41	2.79±1.69	1.36±1.4	1.23±0.77	0.93±0.52	2.34±1.91
Glucosamine	2.22±1.16	0.6±0.2	2.38±0.88	0.34±0.26	2.16±1.08	1.36±0.61	3.35±3.49
Glucosamine phosphate	0.75±0.3	1.28±0.25	0.76±0.14	0.95±0.15	0.75±0.18	0.9±0.19	0.67±0.16
Glucose 6-phosphate	1.22±0.41	1.3±0.3	1.18±0.25	1.23±0.26	1.11±0.4	1.26±0.37	1.17±0.24
Glutamate	1.17±0.27	0.58±0.07	1.1±0.17	1.05±0.13	0.89±0.21	0.91±0.09	0.87±0.12
Glutamine	1.9±0.96	0.44±0.09	1.22±0.59	0.73±0.27	1.27±0.42	1.04±0.42	1.13±0.33
Glutathione	1.03±0.18	1.06±0.14	1.05±0.16	1±0.34	0.78±0.1	1.16±0.18	0.91±0.15
Glutathione disulfide	7.41±10.39	1.41±1.53	4.54±5.37	7.58±12.57	6.98±9.17	2.24±1.57	4.02±4.3

Table 1.12 continued

Metabolite	*Relative Pool ± standard Dev.*						
	ΔacnA	*ΔacnB*	*ΔsucAB*	*ΔsucCD*	*ΔsdhAD*	*Δmdh*	*ΔfumA*
Glycerate	7.53±12.3	0.33±0.33	3.2±4.68	0.2±0.2	2.01±2.22	0.74±1.11	2.44±3.18
Glycinamide ribotide (GAR)	1.16±0.44	0.61±0.25	0.87±0.13	1.82±0.45	0.74±0.36	0.92±0.38	0.91±0.24
GMP	6.19±9.04	0.34±0.28	3.22±4.49	0.23±0.23	3.28±3.43	1.08±1.58	3.67±4.23
Guanine	1.39±1.3	0.46±0.7	7.99±8.74	0.14±0.21	1.84±2.96	1.22±1.61	3.64±4.73
Guanosine	11.78±20.14	0.03±0.03	3.63±4.31	0.02±0.03	2.7±2.99	0.89±1.7	3.09±4.39
Histidine	11.4±19.95	0.3±0.23	2.95±3.98	0.21±0.19	1.53±1.85	0.31±0.26	3.85±4.93
Histidinol	0.64±0.75	0.13±0.12	1.19±1.25	0.12±0.14	0.55±0.44	1.06±1.53	1.61±1.81
Homocysteic acid	1.4±1.35	0.09±0.15	1.23±1.27	0.01±0.02	9.65±15.58	0.3±0.58	1.68±2.36
Homocysteine	0.63±0.08	0.37±0.08	0.54±0.28	0.87±0.25	1±0.33	0.74±0.06	0.81±0.24
Homoserine/ Threonine	3.21±3.44	0.5±0.25	1.92±1.44	0.94±0.56	1.25±0.64	0.84±0.61	1.43±1.13

Table 1.12 continued

Metabolite	*Relative Pool ± standard Dev.*						
	ΔacnA	*ΔacnB*	*ΔsucAB*	*ΔsucCD*	*ΔsdhAD*	*Δmdh*	*ΔfumA*
Homovanillic acid (HVA)	1.29±0.94	0.43±0.29	1.19±0.89	0.27±0.18	3.17±4.44	0.42±0.31	1.04±0.97
Hydroxybenzoate	9.35±15.65	0.3±0.25	4.53±7.17	0.28±0.24	0.5±0.45	0.48±0.49	5.63±6.79
Hydroxyisocaproic acid	1.86±2.44	0.62±0.51	5.73±9.69	0.44±0.36	1.22±1	0.69±0.57	1.09±1.03
Hydroxyphenylacetate	9.25±16.58	0.16±0.12	2.07±3.27	0.12±0.09	0.25±0.24	0.24±0.24	4.78±6.28
Hydroxyproline	2.5±1.61	0.58±0.49	3.36±1.72	0.19±0.11	3.7±1.62	2.15±1.31	3.26±3.32
Hypoxanthine	1.14±0.96	0.37±0.49	9.29±8.81	0.09±0.13	3.53±5.97	1.03±1.22	5.34±7.11
IMP	2.7±1.86	2.35±0.78	3.58±3.13	1.59±0.56	2.88±2.19	2.42±0.7	1.42±0.74
Inosine	12.45±19.2	0.09±0.14	3.31±3.71	0.01±0.01	7.48±11.37	1.14±2.13	1.77±2.4
Lactate	1.38±1.36	1.26±1.24	4.58±4.67	0.94±0.91	4.18±4.66	1.24±1.14	1.71±1.66

Table 1.12 continued

Metabolite	*Relative Pool ± standard Dev.*						
	ΔacnA	*ΔacnB*	*ΔsucAB*	*ΔsucCD*	*ΔsdhAD*	*Δmdh*	*ΔfumA*
L-Argininosuccinate	1.03±0.12	1.39±0.18	1.28±0.24	1.16±0.33	1.08±0.1	0.99±0.15	0.93±0.16
Leucine/Isoleucine	5.73±8.79	0.26±0.21	3.04±2.85	0.19±0.15	1.98±2.02	0.9±1.2	2.55±2.92
L-Methionine	7.33±11.56	0.23±0.12	1.37±1.48	0.57±0.29	0.44±0.24	0.51±0.29	2.72±3.85
Lysine	3.2±3.07	0.6±0.19	2.54±1.51	2.43±0.82	1.87±0.77	0.86±0.66	1.9±1.32
Malate	2.11±1.17	0.33±0.19	1.45±0.55	0.72±0.41	1.69±0.8	2.15±0.33	1.73±0.46
N-Acetyl-beta-alanine	3.48±3.63	0.76±0.36	2.14±1.26	0.64±0.35	4.35±4.6	0.9±0.51	1.88±1.09
N-Acetylglucosamine	7.53±9.87	0.15±0.21	3.5±5.28	0.04±0.04	6.02±9.62	1.72±3.35	2.29±3.01
N-Acetylglucosamine 1/6-phosphate	5.68±6.41	0.54±0.26	2.06±2.11	0.46±0.23	2.59±1.66	1.43±1.43	2.45±2.01
N-Acetylglutamate	1.65±0.82	0.37±0.17	1.39±0.8	2.66±1.76	0.96±0.62	2.27±1.36	1.56±0.79
N-Acetylglutamine	1.48±0.62	1.08±0.32	1.48±0.44	1.23±0.41	1.53±0.5	0.98±0.28	1.42±0.57
N-Acetylornithine	1.35±0.64	0.39±0.09	1.47±0.66	0.69±0.26	1.25±0.34	1.29±0.44	1.24±0.3
N-Acetylputrescine	0.99±0.87	0.15±0.08	0.84±0.66	0.62±0.42	0.74±0.59	1.56±0.95	1±0.56
NAD+	1.15±0.21	0.97±0.13	1.07±0.19	0.87±0.13	0.94±0.22	1.01±0.14	1.01±0.15
NADH	2.06±1.41	0.67±0.78	2.83±2.71	2.09±1.7	1.82±1.65	1.45±1.04	1.63±1.01

Table 1.12 continued

Metabolite	*Relative Pool ± standard Dev.*						
	ΔacnA	*ΔacnB*	*ΔsucAB*	*ΔsucCD*	*ΔsdhAD*	*Δmdh*	*ΔfumA*
NADP+	1.21±0.45	0.96±0.38	1.14±0.38	0.64±0.46	0.96±0.57	0.94±0.25	1.14±0.42
N-Carbamoyl-L-aspartate	1.35±0.21	1.63±0.3	0.81±0.13	0.81±0.25	0.94±0.19	1.78±0.24	0.81±0.08
Nicotinate	6.63±9.49	0.15±0.15	2.57±3.52	0.08±0.08	1.42±1.35	0.92±1.4	3.32±4.1
Octulose 8/1P	1.48±0.34	1.63±0.4	1.4±0.24	0.58±0.14	1.44±0.39	1.14±0.34	1.07±0.33
Octulose bisphosphate	2.12±1.04	1.63±0.92	2.58±1	1.87±1.84	2.21±0.86	1.42±0.68	1.83±0.9
Ophthalmate	1.07±0.18	1.39±0.2	1.3±0.18	1.16±0.26	1.1±0.13	1±0.18	0.99±0.2
Ornithine	2.43±1.57	0.77±0.2	2.49±0.99	0.86±0.28	1.74±0.53	1.56±0.49	1.99±1.03
Orotate	1.09±0.11	1.35±0.12	1±0.27	0.94±0.3	0.88±0.1	1.41±0.19	0.91±0.19
Pantothenate	2.54±2.17	0.67±0.09	1.55±1.04	0.53±0.14	1.5±0.51	1.1±0.3	1.81±0.91
Phenylalanine	4.04±4.69	0.42±0.16	3.45±2.05	0.23±0.09	2.81±2.08	1.01±0.87	2.49±2.35
Phenyllactic acid	1.37±0.74	0.88±0.32	2.77±2.16	0.57±0.22	2.14±1.95	0.92±0.34	1.79±1.11
Phenylpyruvate	0.96±0.18	0.75±0.14	1.04±0.24	0.84±0.25	0.91±0.17	1.01±0.23	0.87±0.17
Phosphoenolpyruvate	3.92±3.85	1.21±0.49	1.92±1.5	0.74±0.45	1.5±0.47	1±0.55	2.07±1.31

Table 1.12 continued

Metabolite	*Relative Pool ± standard Dev.*						
	ΔacnA	*ΔacnB*	*ΔsucAB*	*ΔsucCD*	*ΔsdhAD*	*Δmdh*	*ΔfumA*
Proline	5.59±9.21	0.06±0.07	2.43±4.47	0.1±0.12	0.7±0.81	0.38±0.63	1.55±2.51
Pyroglutamic acid	5.11±5.85	0.3±0.25	3.95±3.49	0.26±0.22	1.75±1.47	0.98±1	3.2±3.65
Pyruvate	0.81±0.09	0.4±0.06	1.19±0.24	0.66±0.16	1.35±0.12	0.97±0.2	1.07±0.14
Ribose phosphate	1.08±0.39	1.53±0.34	1.09±0.24	1.22±0.38	0.95±0.17	1±0.25	1.06±0.36
Sedoheptoluse bisphosphate	1.79±0.86	1.62±0.77	2.15±1.11	1.62±1.57	1.48±0.51	1.19±0.52	1.77±0.74
Sedoheptulose 1/7-phosphate	2.36±1.63	1.74±0.75	1.48±0.91	1.03±0.44	1.8±1.3	0.93±0.39	1.55±0.85
Serine	2.81±3.32	0.37±0.3	2.16±2.04	0.28±0.24	2±1.65	1.13±1.68	2.31±2.68
Shikimate	1.23±0.55	1.46±0.66	1.19±0.49	0.85±0.5	1.41±0.68	1.49±0.6	1.53±0.79
Shikimate-3-phosphate	1.38±0.61	1±0.48	1.44±0.11	1.02±0.53	0.94±0.28	1.47±0.33	1.24±0.35
sn-Glycerol 3-phosphate	6.21±8.05	0.32±0.24	3.34±3.94	0.18±0.12	4.96±5.37	1.66±2.57	3.98±4.07

Table 1.12 continued

Metabolite	*Relative Pool ± standard Dev.*						
	ΔacnA	*ΔacnB*	*ΔsucAB*	*ΔsucCD*	*ΔsdhAD*	*Δmdh*	*ΔfumA*
S-Ribosyl-L-homocysteine	0.93±0.3	0.29±0.07	0.66±0.18	2.49±0.84	0.68±0.17	0.67±0.16	0.84±0.26
Succinate/ Methylmalonate	1.79±1.2	0.44±0.13	1.32±0.43	0.56±0.32	2.13±0.66	0.86±0.66	1.37±0.39
Sucralose	0.81±0.32	0.12±0.17	0.39±0.17	0.34±0.02	0.12±0.03	0.27±0.04	0.11±0.09
Sulfolactate	3.16±2.38	0.9±0.29	2.07±0.84	0.91±0.41	3.01±2.6	1.44±0.56	3.06±2.04
Taurine	0.4±0.58	0.1±0.12	1.56±1.98	0.02±0.03	5.33±9.14	0.23±0.31	0.73±1.05
Thymidine	6.28±6.84	1.8±2.8	11.66± 16.21	0.88±1.19	71.52± 121.12	1.31±2.08	5.4±6.63
Thymine	1.75±1.39	0.36±0.07	0.97±0.72	0.46±0.09	0.89±0.22	0.86±0.5	0.89±0.44
Trehalose 6-phosphate	1.59±1.71	1.38±0.78	1.31±0.96	3.51±2.04	1.23±0.89	0.95±0.66	1.35±0.97
Trehalose/Sucrose/ Cellobiose	2.81±3.38	2.08±2.67	1.3±0.81	0.48±0.25	3.22±3.48	0.72±0.48	1.5±1.22
Tryptophan	3.73±5.35	0.39±0.28	2.9±2.29	0.31±0.21	4.98±6.31	0.88±0.96	2.24±2.3
Tyrosine	5.26±8.31	0.18±0.19	2.51±3.01	0.12±0.13	2.74±3.08	1.19±2.11	1.8±2.33

Table 1.12 continued

Metabolite	*Relative Pool ± standard Dev.*						
	ΔacnA	*ΔacnB*	*ΔsucAB*	*ΔsucCD*	*ΔsdhAD*	*Δmdh*	*ΔfumA*
UDP	1.09±0.59	0.6±0.23	1.94±0.84	0.77±0.68	0.93±0.64	0.79±0.21	1.41±0.58
UDP-glucose	1.13±0.35	0.79±0.23	1.14±0.36	1.13±0.41	0.61±0.16	1.42±0.41	0.96±0.31
UDP-glucuronate	0.97±0.36	0.79±0.32	1.29±0.63	1.29±0.97	1.27±0.98	1.41±0.64	0.89±0.47
UDP-N-acetylglucosamine	3.86±4.43	0.5±0.18	1.44±1.22	0.57±0.27	1.21±0.43	1.16±0.84	1.73±1.11
UMP	8.01±11.86	0.08±0.07	3.1±4.68	0.18±0.17	3.45±3.49	1.35±2.33	3.47±4.11
Uracil	9.56±14.63	0.23±0.2	5.87±5.72	0.11±0.09	3.55±3.34	1.34±1.83	4.33±5.06
Uric acid	2.2±3.55	0.19±0.32	2.56±2.67	0.02±0.02	2.09±2.8	1.05±1.97	7.43±13.53
Uridine	4.91±6.51	0.38±0.25	3.08±1.81	0.29±0.18	5.33±6.13	0.77±0.7	2.39±2.33
Valine	3.64±4.43	0.49±0.22	2.03±1.45	0.48±0.21	1.23±0.61	0.88±0.58	1.72±1.35
Xanthine	1.56±2.46	0.6±1.05	7.21±6.57	0.13±0.14	17.68±29.66	0.64±1.11	1±1.3
Xanthosine	1.24±0.34	1.56±0.73	1.3±0.32	1.57±0.88	0.92±0.24	1.25±0.28	1.13±0.34
Xanthosine 5--phosphate	11.9±27.06	0±0.01	3.01±6.7	0±0.01	0.54±0.89	0.32±0.74	4.11±7.66
Xanthurenic acid	2.25±1.32	0.17±0.08	1.12±0.54	0.09±0.03	4.1±4.11	1.12±1.69	1.02±0.91

Table 1.13 Relative turnover values for each strain compared to WT

Metabolite	*Relative Turnover ± standard Dev.*						
	ΔacnA	*ΔacnB*	*ΔsucAB*	*ΔsucCD*	*ΔsdhAD*	*Δmdh*	*ΔfumA*
2_3-Dihydroxybenzoate	6.4±2.51	8.07±3	0.13±0.05	4.7±1.74	4.64±1.75	9.23±3.36	5.12±1.97
2-Hydroxy-2-methylsuccinate	2.26±0.36	0.56±0.08	0.41±0.07	1.56±0.22	1.69±0.26	1.34±0.22	1.87±0.3
2-Isopropylmalate	1.22±0.33	1.07±0.26	0.32±0.08	1.07±0.26	0.97±0.24	1.02±0.28	1.23±0.32
2-Oxoglutaric acid	2.4±0.31	0.45±0.05	0.46±0.05	1.46±0.17	1.23±0.19	0.94±0.14	1.83±0.25
2-Oxoisovalerate	1.27±0.4	0.7±0.24	0.11±0.03	0.89±0.29	1.08±0.33	0.49±0.16	1.2±0.39
6-Phospho-D-gluconate	1.26±0.92	0.81±0.42	1.12±0.63	1.22±0.66	0.96±0.5	1.17±0.63	1.08±0.57
6-Phospho-D-gluconolactone	0.96±0.45	0.8±0.34	0.29±0.05	1.18±0.13	1.39±0.15	1.16±0.26	1.19±0.75
Acetylphosphate	1.34±0.16	0.97±0.11	0.91±0.11	1.03±0.11	1.05±0.12	1.11±0.11	1.25±0.14
Aconitate	2.8±2.37	57.41±35.03	105.26± 67.04	1.79±1.41	1.39±1.06	1.71±1.23	1.51±1.53
AICAR	1.37±0.22	1.06±0.18	0.79±0.12	0.89±0.13	1.3±0.18	1.11±0.17	1.16±0.19

Table 1.13 continued

Metabolite	*Relative Turnover ± standard Dev.*						
	ΔacnA	*ΔacnB*	*ΔsucAB*	*ΔsucCD*	*ΔsdhAD*	*Δmdh*	*ΔfumA*
Alanine/Sarcosine	12.94±6.89	8.07±4.38	10.68±5.76	8.27±4.41	19.53± 10.78	17.26± 9.76	19.2±10.18
Aminoimidazole ribotide (AIR)	1.01±0.07	0.93±0.13	0±0	0.91±0.07	#DIV/0!	#DIV/0!	1.56±0.21
AMP/dGMP	3.72±0.95	2.35±0.59	0.68±0.17	4.03±1.01	3.7±0.99	2.25±0.66	#DIV/0!
Arginine	6.03±2.34	2.07±0.77	0.74±0.27	4.47±1.65	4.56±1.92	2.37±1.06	4.21±1.61
Asparagine	2.51±1.01	1.47±0.61	0.66±0.27	2.13±0.85	2.91±1.37	2.25±1.12	2.63±1.07
Aspartate	27.29±16.71	3.35±2.13	35.66± 23.89	30.69± 20.13	38.14± 26.37	30.79± 21.73	27.22± 18.42
cAMP	4.37±2.29	0.22±0.36	1.49±0.67	5.58±2.44	4.83±2.17	3.25±1.45	-0.27±0.42
Citraconate	3.24±1.03	1.13±0.31	0.34±0.11	2.52±0.78	2±0.68	1.78±0.55	2.79±0.9
Citrate/isocitrate	0.89±2.76	269.43± 307.12	19.26± 25.81	2.78±3.93	2.5±3.29	3.27±4.19	3.57±5.22
Citrulline	2.02±0.28	0.61±0.07	0.37±0.04	1.29±0.2	1.51±0.19	1.34±0.18	1.91±0.29

Table 1.13 continued

Metabolite	*Relative Turnover ± standard Dev.*						
	ΔacnA	*ΔacnB*	*ΔsucAB*	*ΔsucCD*	*ΔsdhAD*	*Δmdh*	*ΔfumA*
CMP	1.18±0.1	0.89±0.09	0.35±0.04	1.31±0.14	1.23±0.14	1.04±0.1	1.05±0.09
Creatine	0.6±0.33	0.01±0	0.01±0	0.16±0.13	0.01±0.01	0.68±0.33	0.42±0.21
Cystathionine	1.36±0.85	#DIV/0!	0.58±0.38	#DIV/0!	#DIV/0!	1.25±0.78	#DIV/0!
Cysteine	0.84±0.24	0.8±0.25	0.04±0.02	1.28±0.42	58.78±1.03	0.7±0.19	1.05±0.3
Deoxyribose phosphate	1.52±0.1	1.28±0.07	1.08±0.14	1.03±0.05	1.05±0.05	1.17±0.07	1.72±0.13
D-Gluconate	11.61±11.76	8.91±8.9	4.75±5.62	9.14±9.77	2.9±3.7	4.85±5.12	8.83±8.92
Dihydroorotate	2.08±0.23	1.25±0.12	2.66±0.35	1.4±0.13	1.74±0.17	1.61±0.18	2.21±0.23
dTMP	4.91±2.81	2.73±1.32	0.45±0.23	8.5±4.3	4.38±2.41	2.68±1.47	1.72±1.4
Fumarate	1.98±0.68	0.13±0.04	0.14±0.06	1.08±0.37	#DIV/0!	1±0.28	2.51±0.75
Glucosamine phosphate	1.27±0.28	1.02±0.21	1.12±0.24	1±0.2	1±0.2	1.08±0.24	1.22±0.26
Glucose 1-phosphate	1.14±0.33	0.98±0.28	0.93±0.26	1.07±0.3	1.04±0.29	1.06±0.31	1.17±0.34
Glutamate	1.84±0.16	0.42±0.03	0.32±0.02	1.13±0.09	1.15±0.09	0.91±0.08	1.36±0.13

Table 1.13 continued

Metabolite	*Relative Turnover ± standard Dev.*						
	ΔacnA	*ΔacnB*	*ΔsucAB*	*ΔsucCD*	*ΔsdhAD*	*Δmdh*	*ΔfumA*
Glutamine	1.87±0.25	0.47±0.05	0.29±0.03	1.14±0.14	1.17±0.15	0.93±0.13	1.39±0.19
Glutathione	1.07±0.02	1.12±0.03	0.88±0.04	1.11±0.05	1±0.04	1.03±0.02	0.93±0.02
Glutathione disulfide	1.54±0.17	1.39±0.17	0.99±0.12	1.51±0.18	1.21±0.15	1.15±0.13	0.73±0.14
Glycerate	3.33±1.63	3.02±1.46	1.66±0.96	3.61±1.78	1.88±1.27	1.96±1.11	3.25±1.76
Glycerone phosphate	1.12±0.08	0.88±0.06	0.65±0.05	0.99±0.07	0.97±0.06	1.02±0.07	1.17±0.09
Glycinamide ribotide (GAR)	1.28±0.1	#DIV/0!	0.94±0.05	#DIV/0!	#DIV/0!	1.18±0.14	0.89±0.09
Guanidoacetic acid	0.96±0.57	0.62±0.46	0.21±0.29	0.69±0.47	0.71±0.44	0.76±0.45	0.79±0.51
Guanine	3.68±1.05	2.42±0.76	1.22±0.31	3.62±0.94	4.32±1.26	1.02±0.41	1.13±0.49
Histidine	1.46±0.77	2.12±1.12	1.61±0.86	1.68±0.95	1.84±1.01	2.13±1.08	2±1.07
Homocysteine	1.35±0.16	1.08±0.11	1.2±0.12	0.5±0.05	1.23±0.09	1.14±0.12	0.9±0.15

Table 1.13 continued

Metabolite	*Relative Turnover ± standard Dev.*						
	ΔacnA	*ΔacnB*	*ΔsucAB*	*ΔsucCD*	*ΔsdhAD*	*Δmdh*	*ΔfumA*
Homoserine/ Threonine	1.95±0.23	1.44±0.18	0.45±0.05	1.5±0.16	0.97±0.09	1.24±0.14	1.66±0.19
Hypoxanthine	1104.22±6159.85	120.63±679.54	236.12±1320.8	1571.45±8760.88	692.07±3869.6	166.82±954.07	34.79±193.66
IMP	0.84±0.23	1.12±0.28	0.01±0	0.93±0.23	1±0.25	1.25±0.33	0.94±0.25
Lactate	4.3±6.9	0.2±4.86	87.78±134.32	6.7±10.22	3.16±5.43	5.78±8.98	3.58±5.73
Leucine/ Isoleucine	26.08±19.82	22.92±17.85	5.77±4.46	32.33±25.33	35.11±28.97	35.37±29.77	32.96±25.18
L-Methionine	1.24±0.84	1.13±0.84	0.55±0.38	1.17±0.8	1.18±1	1.39±1.48	1.44±0.98
Lysine	2.34±0.45	3.48±0.71	2.92±0.54	2.08±0.4	1.6±0.3	1.51±0.31	1.01±0.29
Malate	2.3±0.66	0.18±0.06	1.65±0.55	1.98±0.59	2.44±0.82	0.82±0.23	2.25±0.64
N-Acetyl-beta alanine	2.05±0.56	1.75±0.34	0.98±0.18	1.29±0.32	1.41±0.36	2.04±0.4	1.76±0.48

Table 1.13 continued

Metabolite	*Relative Turnover ± standard Dev.*						
	ΔacnA	*ΔacnB*	*ΔsucAB*	*ΔsucCD*	*ΔsdhAD*	*Δmdh*	*ΔfumA*
N-Acetylglucosamine1/ 6-phosphate	1.44±0.54	12.14±4.2	10.76±4.14	7.25±2.62	4.36±1.45	5.88±2.24	5.78±2.12
N-Acetylglutamate	1.54±0.22	0.76±0.12	0.46±0.07	1.07±0.15	1.21±0.18	1.2±0.22	1.53±0.22
N-Acetylglutamine	2.5±0.6	1.94±0.46	1.13±0.29	1.92±0.45	1.96±0.46	1.82±0.43	2.37±0.57
N-Acetylornithine	1.63±0.39	0.75±0.19	0.65±0.16	1.31±0.3	1.42±0.33	1.33±0.35	1.57±0.4
NAD+	1±0.03	0.97±0.03	0.85±0.03	1.06±0.05	1.02±0.04	0.9±0.03	0.9±0.03
N-Carbamoyl-L-aspartate	1.84±0.13	1.1±0.06	2.27±0.19	1.28±0.06	1.63±0.09	1.54±0.09	1.94±0.14
Nicotinate	0.31±0.23	0.24±0.23	-0.09±0.26	0.28±0.29	0.11±0.22	0.28±0.23	0.36±0.23
Ophthalmate	1.24±0.05	1.03±0.05	1.05±0.1	1.2±0.07	0.81±0.04	0.95±0.04	1.13±0.05
Ornithine	1.85±0.17	0.57±0.05	0.33±0.03	1.2±0.12	1.31±0.09	1.11±0.09	1.41±0.14
Orotate	2.01±0.38	1.39±0.25	2.87±0.88	1.47±0.23	1.85±0.31	1.44±0.31	2.38±0.45
Phenylalanine	1.01±0.58	2.25±1.13	43.89±21.89	48.17± 25.56	34.95± 23.01	28.73± 20.71	64.12± 36.34
Phenylpyruvate	1.15±0.33	0±0	0±0	0.91±0.22	0.88±0.22	1.13±0.48	1.14±0.4

Table 1.13 continued

Metabolite	*Relative Turnover ± standard Dev.*						
	ΔacnA	*ΔacnB*	*ΔsucAB*	*ΔsucCD*	*ΔsdhAD*	*Δmdh*	*ΔfumA*
Phosphoenolpyruvate	-1214.93± 9523.88	-576.12± 1735.18	-10.85± 35.51	-296.55± 886.93	-275.81± 824.15	-511.73±]1564.45	-767.87± 2489.58
Proline	2.68±1.15	3.31±1.21	3.49±1.25	3.8±1.6	1.51±0.84	2.24±1.01	1.99±0.95
Pyroglutamic acid	2.33±0.93	2.45±0.89	2.75±1.03	1.66±0.67	0.84±0.47	2.21±0.93	1.54±0.67
Pyruvate	#DIV/0!	16.08± 7.75	6±3.07	#DIV/0!	15.23± 7.43	4.42±2.23	17.22± 8.82
Ribose phosphate	1.06±0.09	1.06±0.12	0.9±0.11	0.93±0.11	1.12±0.12	1±0.13	0.94±0.11
Sedoheptulose 1/7-phosphate	0.79±1.04	0.84±1.11	1±1.32	0.92±1.2	0.85±1.12	1.09±1.54	0.95±1.25
Serine	5.7±5.19	2.48±2.29	1.35±1.27	1.94±1.93	2.68±2.62	2.07±2.17	#DIV/0!
Shikimate	1.5±0.2	0.84±0.11	0.16±0.03	1.75±0.24	1.17±0.18	1.16±0.18	1.41±0.2
Shikimate-3-phosphate	3.72±9197.15	1.48±2.13	0±0	1.41±0.33	1.53±0.47	1.67±0.97	1.53±0.97
sn-Glycerol 3-phosphate	34.98± 32.02	36.66± 34.09	4.41±4.39	43.81± 40.12	41.27± 38.85	57.74± 57.61	47.26± 43.39

Table 1.13 continued

Metabolite	*Relative Turnover ± standard Dev.*						
	ΔacnA	*ΔacnB*	*ΔsucAB*	*ΔsucCD*	*ΔsdhAD*	*Δmdh*	*ΔfumA*
S-Ribosyl-L-homocysteine	1.51±0.22	0.7±0.14	0.31±0.04	1.04±0.14	0.99±0.14	1.27±0.26	1.17±0.16
Thymine	2.23±0.59	0.72±0.2	0.45±0.12	#DIV/0!	1.89±0.57	1.16±0.34	1.66±0.45
Trehalose 6-phosphate	1.8±1.95	1.05±0.36	1.03±0.43	#DIV/0!	0.75±0.24	1.11±0.51	1.23±0.49
Trehalose/Sucrose/ Cellobiose	38.4±33.25	6.04±5.34	4.59±3.91	1.73±1.85	5.14±4.55	2.5±2.46	#DIV/0!
Tryptophan	34±31.58	15.27± 14.56	8.02±7.45	#DIV/0!	47.24±45. 79	62.52±61. 84	54.45± 50.87
Tyrosine	27.95±19.3 8	21.65± 15.39	4.9±3.49	32.23± 22.86	33.96± 24.7	36.42± 27.8	35.11± 25.03
UDP	0±0	0±0	0±0	0±0	0±0	0±0	0±0
UDP-glucose	1.35±0.11	1.14±0.09	0.79±0.07	0.99±0.07	1.17±0.09	1.13±0.1	1.24±0.11
UDP-glucuronate	0±0	0±0	0±0	0±0	0±0	0±0	0±0
UDP-N-acetylglucosamine	1.83±0.19	1.03±0.1	0.57±0.06	1.28±0.13	1.3±0.13	1.38±0.14	1.85±0.2

Table 1.13 continued

Metabolite	*Relative Turnover ± standard Dev.*						
	ΔacnA	*ΔacnB*	*ΔsucAB*	*ΔsucCD*	*ΔsdhAD*	*Δmdh*	*ΔfumA*
UMP	4.15±1.44	3.13±1.05	0.5±0.16	4.63±1.5	4.17±1.43	2.51±0.96	2.45±0.94
Uracil	-6.86±38.25	82.02±450.35	9.36±51.7	37.73±207.29	-16.17±89.1	49.83±273.68	78.34±430.33
Uric acid	0.87±2.72	-3.35±7.65	-1.25±3.44	-0.22±1.73	-0.39±2.12	-0.43±2.17	-0.36±1.91
Uridine	0±0	0±0	0±0	0±0	0±0	0±0	0±0
Valine	4.32±1.63	3.75±1.49	1.04±0.46	4.62±1.73	4.48±1.88	2.29±1	4.14±1.61
Xanthine	3.16±1.46	1.83±0.84	1±0.54	-0.42±0.3	7.55±3.52	4.5±2.6	2.77±1.35

Table 1.14 Relative flux values for each strain compared to WT

Metabolite	*Relative Flux ± standard Dev.*						
	ΔacnA	*ΔacnB*	*ΔsucAB*	*ΔsucCD*	*ΔsdhAD*	*Δmdh*	*ΔfumA*
2_3-Dihydroxybenzoate	8.85±5.33	6.23±1.88	0.12±0.06	2.58±1.28	3.56±1.21	9.28±3.67	4.94±1.81
2-Hydroxy-2-methylsuccinate	6.83±7.6	0.3±0.23	1.52±2.03	0.89±0.78	2.54±1.47	1.73±1.2	3.13±2.1
2-Isopropylmalate	1.76±0.43	3.81±1.62	0.46±0.11	2.35±1.49	1.73±0.53	1.48±0.47	1.84±0.72
2-Oxoglutaric acid	2.42±0.61	0.08±0.02	0.5±0.06	1.57±0.71	0.64±0.37	0.53±0.08	1.28±0.29
6-Phospho-D-gluconate	1.61±0.94	2.09±1.18	1.41±0.47	1.33±1.04	1.34±0.54	0.87±0.37	1.57±0.54
Acetylphosphate	1.14±0.51	0.7±0.31	0.93±0.33	0.69±0.25	0.99±0.14	0.88±0.25	0.78±0.12
Aconitate	8.21±9.05	583.28± 338.62	182.56± 132.07	1.23±1.08	18.55±12.71	15.76± 27.86	2.79±2.62
AICAR	1.47±0.39	0.46±0.1	0.52±0.12	0.71±0.27	0.68±0.16	0.65±0.19	0.9±0.17
Alanine/ Sarcosine	33.64±26.66	4.38±1.55	21.28±8.2	3.82±1.78	41.45±23.36	18.13±9.78	29.92±13.02

Table 1.14 continued

Metabolite	*Relative Flux ± standard Dev.*						
	ΔacnA	*ΔacnB*	*ΔsucAB*	*ΔsucCD*	*ΔsdhAD*	*Δmdh*	*ΔfumA*
Aminoimidazole ribotide (AIR)	0.88±0.17	0.66±0.25	0±0	0.79±0.17	#DIV/0!	#DIV/0!	1.06±0.28
AMP/dGMP	28.75±41.73	0.25±0.24	2.14±3.47	0.39±0.38	14.07±14.09	3.41±6.29	#DIV/0!
Arginine	42.88± 55.36	0.23±0.19	2.4±2.84	0.42±0.37	12.09±10.55	2.26±4.03	11.33± 13.51
Asparagine	8.17±7.75	0.83±0.31	1.06±0.72	0.98±0.42	4.18±1.94	1.9±1.94	4.1±2.67
Aspartate	50.12± 34.85	1.61±0.66	44.33±20. 8	23.38±9.1 4	52.42±46.92	15.16±7.6 4	31.05± 14.91
cAMP	6.44±4.08	0.11±0.18	1.84±0.96	4.93±2.43	6.72±5.53	2.23±1.68	-0.3±0.48
Citraconate	5.8±2.57	3.46±1.24	0.47±0.18	2.2±0.71	17.83±7.37	11.56± 17.17	3.78±1.07
Citrate/isocitrate	2.24±6.81	4648.37± 2025.55	33.84±31. 32	1.84±2.12	4.17±3.39	2.58±2.2	8.7±8.65
Citrulline	3.47±1.17	0.63±0.15	0.88±0.33	1.37±0.47	2.41±0.95	2.3±0.77	3.03±1.13
CMP	3.94±3.46	0.49±0.12	0.65±0.53	0.55±0.15	2.41±0.79	1.25±1.1	1.94±1.21
Creatine	0.41±0.39	0±0	0.07±0.1	0±0.01	0.05±0.05	0.78±0.82	1.13±1.56
Cystathionine	6.83±10.25	#DIV/0!	1.49±2.51	#DIV/0!	#DIV/0!	0.69±0.63	#DIV/0!
Cysteine	3.26±3.63	0.62±0.55	0.08±0.04	0.59±0.63	38.06±6.70	0.66±0.34	2.33±2.32
Deoxyribose phosphate	2.12±0.43	1.45±0.35	1.22±0.26	0.54±0.22	1.16±0.27	1.36±0.22	1.37±0.43
D-Gluconate	92.27±145.1 9	5.86±6.4	31.26± 39.12	3.26±3.39	28.99±48.66	6±9.69	71.04± 91.44
Dihydroorotate	2.96±0.85	2.96±0.86	3.62±1.99	1.96±0.79	1.87±0.88	3.89±1.36	2.94±1.69

Table 1.14 continued

Metabolite	*Relative Flux ± standard Dev.*						
	ΔacnA	*ΔacnB*	*ΔsucAB*	*ΔsucCD*	*ΔsdhAD*	*Δmdh*	*ΔfumA*
dTMP	8.91±3.96	1.67±0.54	0.55±0.18	5.68±2.09	5.53±3.27	2.63±0.99	1.62±1.16
Fumarate	3.53±1.78	0.05±0.01	0.2±0.1	0.86±0.39	#DIV/0!	1.83±0.42	3.84±0.88
Glucosamine phosphate	0.97±0.41	1.32±0.31	0.86±0.2	0.96±0.2	0.76±0.21	0.98±0.25	0.82±0.23
Glucose 6-phosphate	1.41±0.49	1.28±0.31	1.1±0.24	1.33±0.29	1.16±0.42	1.34±0.42	1.38±0.32
Glutamate	2.16±0.51	0.24±0.03	0.35±0.05	1.19±0.16	1.03±0.25	0.83±0.1	1.18±0.19
Glutamine	3.56±1.81	0.21±0.04	0.36±0.17	0.83±0.31	1.48±0.5	0.97±0.39	1.57±0.47
Glutathione	1.12±0.2	1.2±0.16	0.92±0.15	1.11±0.39	0.78±0.11	1.2±0.18	0.85±0.14
Glutathione disulfide	11.46±16.07	1.96±2.13	4.5±5.34	11.51±19.11	8.46±11.13	2.58±1.81	2.94±3.19
Glycerate	25.17±41.28	1±1.02	5.35±8.02	0.72±0.73	3.8±4.59	1.46±2.24	7.95±10.6
Glycinamide ribotide (GAR)	1.49±0.58	#DIV/0!	0.82±0.12	#DIV/0!	#DIV/0!	1.1±0.47	0.82±0.23
Guanine	5.14±4.92	1.11±1.72	9.8±10.82	0.53±0.76	7.95±12.9	1.26±1.71	4.13±5.6
Histidine	16.67±29.59	0.64±0.54	4.78±6.59	0.35±0.34	2.84±3.54	0.66±0.58	7.72±10.15
Homocysteine	0.85±0.14	0.41±0.09	0.65±0.34	0.44±0.13	1.24±0.41	0.85±0.1	0.73±0.25
Homoserine/Threonine	6.28±6.74	0.73±0.37	0.87±0.66	1.42±0.85	1.22±0.63	1.05±0.77	2.38±1.88
Hypoxanthine	1262.73±1204.97	44.86±71.88	2194.67±2468.86	145.07±214.33	2446.44±4369.99	173.04±307.98	186.08±251.89
IMP	2.27±1.6	2.64±0.9	0.07±0.06	1.49±0.54	2.91±2.23	3.04±0.96	1.35±0.72

Table 1.14 continued

Metabolite	*Relative Flux ± standard Dev.*						
	ΔacnA	*ΔacnB*	*ΔsucAB*	*ΔsucCD*	*ΔsdhAD*	*Δmdh*	*ΔfumA*
Lactate	5.95±6.71	0.25±6.12	402.58± 425.31	6.36±6.34	13.24±18.34	7.19±7.18	6.15±6.81
Leucine/Isoleucine	149.59± 230.88	6.18±5.21	17.61± 16.95	6.29±5.31	69.75±75.54	32.06± 44.44	84.14± 97.77
L-Methionine	9.14±14.43	0.26±0.15	0.75±0.83	0.67±0.35	0.52±0.39	0.72±0.72	3.93±5.57
Lysine	7.52±7.24	2.1±0.73	7.45±4.47	5.06±1.77	3±1.28	1.31±1.01	1.93±1.41
Malate	4.87±2.8	0.06±0.03	2.41±1.06	1.42±0.86	4.14±2.17	1.77±0.36	3.89±1.18
N-Acetyl-beta-alanine	7.17±7.64	1.34±0.65	2.12±1.27	0.83±0.49	6.17±6.64	1.84±1.07	3.32±2.08
N-Acetylglucosamine 1/6-phosphate	8.23±9.46	6.58±3.4	22.18± 23.3	3.4±1.82	11.31±7.39	8.43±8.66	14.21± 11.98
N-Acetylglutamate	2.55±1.28	0.28±0.13	0.64±0.37	2.86±1.9	1.18±0.76	2.72±1.67	2.4±1.23
N-Acetylglutamine	3.72±1.59	2.11±0.64	1.69±0.54	2.37±0.81	3.01±1	1.79±0.52	3.38±1.37
N-Acetylornithine	2.21±1.07	0.29±0.08	0.96±0.44	0.92±0.35	1.78±0.49	1.73±0.63	1.95±0.54
NAD+	1.15±0.21	0.95±0.13	0.91±0.16	0.93±0.14	0.96±0.23	0.92±0.13	0.91±0.14
N-Carbamoyl-L-aspartate	2.5±0.42	1.81±0.34	1.84±0.33	1.04±0.32	1.55±0.32	2.76±0.39	1.58±0.17
Nicotinate	2.06±3.28	0.03±0.05	-0.23± 0.74	0.02±0.03	0.16±0.34	0.26±0.45	1.22±1.67
Ophthalmate	1.34±0.22	1.45±0.21	1.38±0.23	1.41±0.32	0.9±0.11	0.95±0.18	1.13±0.23
Ornithine	4.49±2.93	0.44±0.11	0.82±0.33	1.03±0.35	2.29±0.7	1.74±0.55	2.82±1.47

Table 1.14 continued

Metabolite	*Relative Flux ± standard Dev.*						
	ΔacnA	*ΔacnB*	*ΔsucAB*	*ΔsucCD*	*ΔsdhAD*	*Δmdh*	*ΔfumA*
Orotate	2.21±0.34	1.89±0.25	2.88±1.09	1.4±0.45	1.63±0.22	2.04±0.41	2.17±0.52
Phenylalanine	4.09±4.96	0.95±0.42	151.56± 95.37	11.29±5.6 4	98.43±86.6	29.28±30. 1	159.78± 160.65
Phenylpyruvate	1.1±0.28	0±0	0±0	0.77±0.24	0.81±0.17	1.15±0.48	0.99±0.33
Phosphoenol-pyruvate	-4766.93± 34878.75	-700.16± 419.07	-20.9± 32.58	-219.45± 146.79	-413.81± 160.64	-513.22± 451.64	-1593.48± 2271.39
Proline	15.01±25.02	0.2±0.23	8.5±15.67	0.41±0.48	1.07±1.31	0.87±1.45	3.1±5.12
Pyroglutamic acid	11.94±13.86	0.74±0.61	10.9±9.74	0.43±0.38	1.48±1.41	2.17±2.28	4.95±5.79
Ribose phosphate	1.15±0.41	1.63±0.38	0.99±0.23	1.14±0.37	1.06±0.2	1.01±0.27	1±0.35
Sedoheptulose 1/7-phosphate	1.88±1.31	1.47±0.65	1.5±0.94	0.95±0.41	1.54±1.12	1.03±0.68	1.47±0.83
Serine	16.04±19.86	0.94±0.85	2.93±3.05	0.55±0.55	5.39±5.23	2.35±3.8	#DIV/0!
Shikimate	1.84±0.84	1.24±0.57	0.19±0.08	1.49±0.88	1.66±0.82	1.74±0.72	2.17±1.14
Shikimate-3-phosphate	5.15±12714. 78	1.48±2.24	0±0	1.44±0.8	1.45±0.59	2.45±1.49	1.9±1.29
sn-Glycerol 3-phosphate	217.57±2 84.76	12.01±9.3 2	14.74± 18.57	7.98±5.67	204.84± 229.5	95.93± 154.58	188.15± 196.45
S-Ribosyl-L-homocysteine	1.41±0.47	0.2±0.06	0.21±0.06	2.6±0.88	0.68±0.17	0.86±0.25	0.98±0.31
Thymine	3.91±3.11	0.26±0.06	0.44±0.33	#DIV/0!	1.69±0.5	1±0.6	1.49±0.75
Trehalose 6-phosphate	2.88±4.29	1.46±0.85	1.35±1.07	#DIV/0!	0.93±0.67	1.06±0.82	1.66±1.26

Table 1.14 continued

Metabolite	*Relative Flux ± standard Dev.*						
	ΔacnA	*ΔacnB*	*ΔsucAB*	*ΔsucCD*	*ΔsdhAD*	*Δmdh*	*ΔfumA*
Trehalose/Sucrose /Cellobiose	108.14± 131.74	12.61± 16.53	6±3.8	0.84±0.71	16.6±18.49	1.81±1.52	#DIV/0!
Tryptophan	126.98± 183.74	6±4.67	23.35±19. 02	#DIV/0!	235.56± 309.08	55.59± 64.39	122.15± 128.39
Tyrosine	147.28±234. 09	4.05±4.33	12.32±15. 1	4.06±4.34	93.09± 108.12	43.62± 78.88	63.34± 83.66
UDP-glucose	1.53±0.48	0.91±0.27	0.9±0.29	1.12±0.41	0.72±0.19	1.61±0.48	1.2±0.39
UDP-N-acetylglucosamine	7.11±8.16	0.51±0.18	0.83±0.7	0.73±0.34	1.58±0.56	1.62±1.17	3.2±2.05
UMP	33.27±49.57	0.27±0.25	1.58±2.39	0.84±0.82	14.44±14.79	3.4±5.93	8.53±10.3
Uracil	-65.65± 118.6	19.04±16. 98	55.03± 63.73	4.18±3.7	-57.54± 60.69	67.2± 92.08	339.47± 404.43
Uric acid	1.91±5.23	-0.64± 1.15	-3.2±6.17	0±0.03	-0.81±4.2	-0.46± 2.21	-2.7± 13.83
Valine	15.77±19.3	1.87±0.91	2.12±1.62	2.22±1.03	5.51±3.02	2.02±1.43	7.16±5.76
Xanthine	4.95±7.87	1.11±1.94	7.24±7.08	-0.05± 0.07	133.62±226. 17	2.9±5.15	2.78±3.69

CHAPTER 2 EXPANDING LIPIDOMICS COVERERAGE: EFFECTIVE ULTRA PERFROMANCE LIQUID CHROMATOGRAPHY-HIGH RESOLUTION MASS SPECTROMETER METHODS FOR THE DETECTION AND QUANTITATION OF CARDIOLIPIN PHOSPHATIDYLGLYCEROL, AND LYSYL-PHOSPHATIDYLGLYCEROL

Preface

This chapter includes details regarding the development and implementation of a targeted metabolomics method which was initially used as a means for quantitation for a defined set of lipids within *Enterococcus faecalis (E. faecalis)*. This method can be easily applied to many other systems with minimal adjustments to the chromatograph or mass spectrometer and a new set of lipid compounds could be quantified. It can be seen in this chapter that metabolomics is a powerful tool even when only looking at a relatively small number of metabolites. A thirty-minute chromatographic method was able to identify and quantitate three different classes of lipids which corresponded to 45 individual compounds.

This project was performed in collaboration with Dr. Elizabeth Fozo and her graduate students in the Department of Microbiology at the University of Tennessee. The Fozo laboratory is focused on the ability of *E. faecalis* to become tolerant to antibiotics, like daptomycin, when exposed to mammalian fluids like serum or bile. This tolerance was thought to be caused by the uptake of unsaturated fatty acids from the extracellular matrix, and their incorporation into the bacteria's membrane as modified phospholipids. Historically, this was performed by thin layer chromatography (TLC) which is simple to perform but is limited by only being able to elucidate bulk changes in compound class with no information about specific lipids. Fatty acid methyl esterification (FAME) using gas chromatography-mass spectrometry (GC-MS) is another technique employed to probe lipid membrane composition but relies on a derivatization step. Since this is an indirect method of quantitation, information is lost about which lipid head group the esterified fat was attached. Another problem with GC-MS is the esterification of membrane harbored free fats that are not attached to a phospholipid. Depending on the derivatization method, the products detected will be a summation of the tails from phospholipids and any free fats present.

After several attempts with the above-mentioned techniques by my collaborators, I was approached by Dr. Fozo, and offered my expertise. This is where a high-resolution mass spectrometric technique can be very useful and overcome many of the limitations of TLC and FAME analyses. The Fozo laboratory was interested in measuring only specific phospholipids including a low abundant four tailed lipid, cardiolipin. To measure these phospholipids, a targeted metabolomics approach on a hybrid quadruple Orbitrap instrument was chosen in conjunction with a HILIC column. Since cardiolipin is not a “standard” phospholipid in many bacterial systems, separation conditions had to be optimized in order to reliably detect cardiolipin without losing detection of the more common two tailed phospholipids. Over the course of several months, various column conditions were tried until a 5.8 pH buffered ammonium acetate mobile phase was chosen.

When using the mass spectrometer, parallel reaction monitoring (PRM) was selected to only focus on the handful of metabolites that were of biological interest in the study. This created full scan data of the fragments based on the isolation of a parent ion. Post analysis allowed for quantitation from multiple fragments and the opportunity to identify what types of specific fatty acids were bound to a specific cardiolipin. Finally, an untargeted lipidomics method was also used to collect a global lipidome from the same bacteria, and interestingly free fats were detected in the membrane (in large amounts) of samples supplemented with the same fatty acid. This accumulation was not originally thought to occur.

This targeted and corresponding untargeted lipidomics analyses are being published as a standalone method, which uses a small portion of the biological data as a proof of concept. Currently, this method is being used heavily to measure phospholipid changes for a multitude of different genetic variants responsible for phospholipid synthesis and will result in several other publications.

A version of this chapter was originally published by in *Metabolomics* and was reproduced with permission of the journal containing the following citation.

Citation:

Tague, E. D.; Woodall, B. M.; Harp, J. R.; Farmer, A. T.; Fozo, E. M.; Campagna, S. R., Expanding lipidomics coverage: effective ultra performance liquid chromatography-high resolution mass spectrometer methods for detection and quantitation of cardiolipin, phosphatidylglycerol, and lysyl-phosphatidylglycerol. *Metabolomics* **2019**, 15 (4), 53.

Contributions:

EDT, EMF, JRH, ATF, and SRC designed the experiment. EDT, ATF and BMW, created the method and ran standards. EDT, and BMW analyzed the data. EMF, and JRH grew the bacteria. SRC, EDT, BMW, EMF, JRH, wrote and edited the manuscript.

2.1 Abstract

Lipidomics is capable of revealing global alterations in a broad class of molecules whose functions are innately linked to physiology. Monitoring changes in the phospholipid composition of biological membranes in response to stressors can aid the development of targeted therapies. However, exact quantitation of cardiolipins is not a straightforward task due to low ionization efficiencies and poor chromatographic separation. Herein, a method is reported to quantitate phospholipids using internal phospholipid standards. An extraction using chloroform and methanol paired with a Q Exactive orbitrap mass spectrometer allows for quantifying 23 cardiolipins, 10 phosphatidylglycerols and 10 lysyl-phosphatidylglycerols with detection limits as low as 50 nM in addition to measuring changes in free fatty acids. Biological validation with *Enterococcus faecalis*, a Gram-positive bacterium, demonstrates that this analysis is sensitive enough to monitor the incorporation of oleic and linoleic acids into the tails of membrane lipids as well as discovering free fats in the membrane. When supplemented with oleic acid, the amounts of free oleic acid detected is 100 times higher and the concentration of polyunsaturated cardiolipin increase to over 3.5 μM.

2.2 Introduction

Lipids play an essential role for multiple cellular functions including energy acquisition, maintenance of cellular physiology, cellular mobility, and cellular transport[50]. Biological membranes contain several types of phospholipids, and the phospholipid composition can vary drastically depending on genetics or environmental factors[51]. Membrane phospholipids consist of polar head groups and multiple non-polar tails which form an amphipathic lipid bilayer, creating a barrier between internal cellular components and the extracellular environment.

The head groups of membrane phospholipids are highly variable and tend to combine with tails of varying length and degrees of unsaturation, creating a large number of possible combinations. Although the numbers of possible lipids are vast, bacteria have limited their membranes to use only three or four different head groups[52, 53]. Bacterial membranes are primarily composed of various combinations of cardiolipin (CL), phosphatidylglycerol (PG), phosphatidylethanolamine (PE), phosphatidylinositol (PI), phosphatidic acid (PA), or phosphatidylserine (PS). Depending on the bacterium, lipids with lyso or amino acid modifications may also be present[54]. Membrane fluidity can be altered by adjusting the fatty acid tails (adding degrees of unsaturation) or changing ratios of lipid classes, providing a quick way to respond to external stressors[55]. The ability to alter membrane composition has been used to preserve viability when bacteria are challenged by antibiotics[56] or extreme temperatures[57].

To date, most research has used glycerol phospholipids, which have two positions containing fatty acids varying in lengths from 14-18 carbons with the possibility of zero, one, or two degrees of unsaturation. The low number of biologically relevant tails, combined with their high abundance in biological samples, allows this set of lipids being easily measured[53]. Over 90% of the bacterial membranes studied consist of two-tailed lipids such as PG or PE[58], which come from PA. Cardiolipins (CL) are essentially two PG molecules connected by a shared glycerol molecule resulting in a four tailed lipid[59]. These four-tailed lipids are not as abundant in biological specimens as two-tailed lipids[50, 58]. Doubling the number of tails, doubles the number of possible biologically relevant combinations. Thus, combining their low abundance in biological membranes with the high number of possible CL tail combinations leads to difficulty in measurement.

Current lipidomics analysis includes various mass spectrometric techniques such as direct injection of extracted lipid sample, separation of lipid sample components based on chromatography followed by tandem mass-spectrometry, and analysis of lipids and imaging of tissues utilizing MALDI[60-62]. Separation of lipids can be done by using reverse phase chromatography, which differentiates

based on the aliphatic tails[63], or with hydrophilic interaction liquid chromatography (HILIC) which differentiates based on the polar head group[64-66]. Compounds are typically ionized using electrospray ionization in both positive and negative mode, and the parent ion or a fragment from a MS/MS experiment is detected. Although there are many mass spectrometry experiments that allow the detection of common phospholipids,[64] there are only a handful of methods that explicitly measure cardiolipins[67-69]. An even smaller number of methods quantify cardiolipin[70, 71].Specifically, Minkler and coworkers used a reverse phase column with triethylamine coupled to triple quadrupole ion trap mass spectrometer to measure relative amounts 8 different cardiolipin species[67], and Rashid and coworkers profiled the lipidome of *Enterococcus faecalis* by the quantitation of PG and LPG using a triple quadruple, thus the latter was not able to fully quantitate any cardiolipins[68]. Six different lipid classes including CL were analyzed in mitochondrial membranes using a C_{18} column and an Orbitrap, but no exact quantities for CL were measured[69]. Cardiolipins were quantified with an internal standard using a triple quadrupole, but the method only focused on cardiolipins, neglecting the other phospholipids[70]. A HILIC MS/MS method that was able to quantitate CL, PG, PA, BMP, and PG has been reported[71]. However, this analysis used a triple quadrupole not allowing for a high-resolution quantitation of multiple fragments. The method reported here eliminates the need for an ion-paring agent, allows the detection of lipids in an untargeted fashion based on head group similarity, and quantitates of over 30 individual compounds using a high-resolution mass analyzer.

Often there is a tradeoff between coverage and the ability to measure specific compounds in UPLC analyses. However, this method demonstrates the practicality of using a single extraction method for both targeted and untargeted lipid analysis. The untargeted analysis uses an orbitrap mass spectrometer operating in full scan mode to provide relative quantitation of the six most common phospholipid head groups, the lysyl- derivatives, and four free fatty acids that make up the tails of bacterial phospholipids. Each of these compound classes have the

potential to detect over 30 unique *m/z* resulting in hundreds of possible known lipids detected along with the opportunity to mine the data for unknown lipid-like compounds. The targeted approach uses a hybrid quadrupole mass spectrometer, allowing for the quantification of specific cardiolipin, phosphatidylglycerol, and lysyl-phosphatidylglycerol compounds within a sample. The method was validated by analyzing relative lipidome changes as well as measuring exact quantities of three lipid classes in *Enterococcus faecalis* (*E.faecalis*) samples that were supplemented with two unsaturated exogenous fatty acids.

2.3 Experimental Section

2.3.1 Untargeted standards

Phospholipid standards were used to verify retention time and head group ionization. The standards assessed were as follows: phosphatidylinositol with two 16:0 tails (PI 32:0), phosphatidic acid with one 18:0 and one 18:1 tail (PA 36:1), phosphatidylglycerol with two 18:0 tails (PG 36:0), phosphatidylcholine with two 18:0 tails (PC 36:0), phosphatidylserine with one 16:0 tail and one 18:2 tail (PS 34:2), phosphatidylethanolamine with two 16:0 tails (PE 32:0), and lysyl-phosphatidylglycerol with two 18:1 tails (LPG 36:2). All standards were purchased from Avanti Lipids, Inc. and one representative compound was chosen from each head group class. The fatty acid standards: cis-9-ocatdecanoic acid (oleic acid), cis 9,12 octadecadienoic acid (linoleic acid), octadecanoic acid (stearic acid), and hexadecenoic acid (palmitic acid) were purchased from Sigma Aldrich.

2.3.2 Targeted standards

Representative standards from three head group classes; cardiolipin (CL), phosphatidylglycerol (PL), and lysyl-phosphatidylglycerol (LPG) were purchased from Avanti Polar Lipids Inc. Even though this method was targeted, exact

matched compounds were not available for all species of interest, therefore one compound from each of the three classes was used to make external calibrations. Cardiolipin, (CL 72:4) with four 18:1 tails, phosphatidylglycerol, (PG 36:0) with two 18:0 tails, and lysyl-phosphatidylglycerol, (LPG 36:2) with two 18:1 tails were chosen as external standards. Since HILIC chromatography was used, it was hypothesized that there would be minimal retention time variation between molecules within the same head group regardless of tail configurations. Internal standards were chosen based on lipids that were not present or had very limited presence in the biological samples. Cardiolipin with four 14:0 tails (CL 56:0) and phosphatidylglycerol with two 18:0 tails (PG 36:0) were chosen as the internal standards. It should be noted that based on gas chromatography fatty acid methyl ester analyses, a small portion (<5%) of fatty acid tails in *E. faecalis* membranes are tetradecanoic acid (C14:0)[72, 73]. There were no non-naturally abundant LPG standards available for purchase, therefore external calibration curves were used to quantify LPGs. Data for the targeted standards is presented in **Table 2.1**. Calibration and test samples were spiked with an internal standard to account for any loss of signal due to ionization efficiency or suppression.

2.3.3 Biological samples

Enterococcus faecalis cultures were grown in brain heart infusion (BHI) medium at 37°C. Overnight cultures were diluted into fresh BHI to an optical density (OD_{600}) of 0.01 and supplemented with either 10μg/mL of linoleic acid or 20μg/mL oleic acid and allowed to grow until an OD_{600} of 0.3. 0.1%. Ethanol was used as the solvent control.

Table 2.1 Details for lipid standards used for the targeted analysis

Compound Class	Formula	Tails	RT (min)	Abbr.	Species	Transition	Standard Type	IS Variation
Cardiolipin	$C_{81}H_{150}O_{17}P_2$	18:1	4.50	CL (72:4)	$[M-2H]^{2-}$	619.4162-> 152.9958	External	1.92%
Cardiolipin	$C_{65}H_{126}O_{17}P_2$	14:0	4.50	CL (54:0)	$[M-2H]^{2-}$	727.5101-> 152.9958	Internal	
phosphatidylglycerol	$C_{42}H_{83}O_{10}P$	18:0	2.00	PG (36:0)	$[M-H]^-$	777.5651-> 152.9958	External	2.20%
phosphatidylglycerol	$C_{22}H_{43}O_{10}P$	8:0	2.00	PG (16:0)	$[M-H]^-$	497.2521-> 152.9958	Internal	
lysyl phosphatidylglycerol	$C_{48}H_{91}N_2O_{11}P$	18:1	10.20	LPG (36:2)	$[M-H]^-$	901.6288-> 145.0948	External	N/A

2.3.4 Extraction of lipids from biological samples

Enterococcus faecalis supplemented with the previously mentioned fatty acids were harvested in 15 mL aliquots at mid log phase (OD_{600} ~ 0.3). The cells were washed twice with 1X PBS via centrifugation, resuspended in 1mL of 1X PBS, and treated with 100μg/mL of lysozyme. After 20 minutes of incubation at 37°C, the lysozyme treated cells were transferred to plastic screw top microfuge tubes containing 0.5 g of glass beads (≤106 um). The cells were then homogenized using a mini bead-beater (Biospec Products, Bartlesville, OK) for two, 1-minute intervals. The homogenized cells were then transferred to a 15 mL polypropylene conical vial containing a mixture of chloroform: methanol 2:1 (v/v)[74, 75]. Samples were briefly vortexed and then centrifuged for 5 minutes at 3500 rpm. Layers formed containing the glass beads at the bottom and the cell debris in the middle. The two phases were carefully transferred to a clean 15mL polypropylene conical vial containing 1.5mL of 0.9% NaCl, leaving behind the cell debris and glass beads. After briefly vortexing, samples were centrifuged, and the lower lipid containing organic phase was transferred to a glass screw top vial. Lipid extracts were dried under nitrogen gas and suspended in 260 µL of 1:1 methanol: chloroform and 40 µL of internal standard before being transferred to autosampler vials with PTFE septa.

2.4 Liquid Chromatography- Mass Spectrometry Parameters

Samples and standards were stored at -20 °C until they could be analyzed and kept at 4 °C in the autosampler during the analysis. A Dionex ultra performance chromatograph (UPLC)(Sunnyvale, CA) was used in conjunction with a Kinetex HILIC column 100 Å 2.6µm 150 mm x 2.1 mm (Phenomenex, Torrance, CA) to separate lipid compounds for both the targeted and untargeted analysis.

2.4.1 Untargeted lipid analysis

The untargeted method used 10 mM ammonium formate adjusted to a pH of 3.0 for mobile phase A, and 97:3 acetonitrile: water adjusted to a pH of 3.0 with 10 mM ammonium formate for mobile phase B. Gradient: *t*=0 min 0% solvent A, 100% solvent B; *t*=1 min 0% solvent A, 100% solvent B; *t*=15 min 19% solvent A, 81% solvent B; *t*=15.1 min 52% solvent A, 48% solvent B ; *t*=25 min 52% solvent A, 48% solvent B; *t*=25.1 min 0% solvent A, 100% solvent B; *t*=35 0% solvent A, 100% solvent B. The flow rate was set to 0.200 mL/min. An Exactive Plus Orbitrap mass spectrometer (Thermo Scientific, Waltham, MA) was used to detect the different phospholipids and fatty acids. Electrospray ionization (ESI) was utilized under the following settings: sheath gas-25 (arbitrary units); auxiliary gas-10 (arbitrary units); spray voltage-4 kV; capillary temperature-350 °C; resolution-140,000. Ions between 100-1500 *m/z* were recorded in both positive and negative mode in separate scan events. In addition to full scan data, the all ion fragmentation (AIF) was collected throughout the run using a normalized collisional energy of 30 eV with a stepped energy of 50%. Calibration was performed every 24 hours in positive and negative mode using calibration solutions from Thermo Scientific.

2.4.2 Targeted phospholipid analysis

The targeted analysis used 5 mM ammonium acetate adjusted to a pH of 5.8 for mobile phase A, and 97:3 acetonitrile: water adjusted to a pH of 5.8 with a final concentration of 5 mM ammonium acetate. Gradient: *t*=0 min 3% solvent A, 97% solvent B; *t*=1 min 3% solvent A, 97% solvent B; *t*=1.2 min 5% solvent A, 95% solvent B; *t*=4 min 5% solvent A, 95% solvent B; *t*=4.2 min 10% solvent A, 90% solvent B; *t*=7.6 min 10% solvent A, 90% solvent B; *t*=8.1 min 30% solvent A, 70% solvent B; *t*=10.9 min 30% solvent A, 70% solvent B; *t*=11 min 50% solvent A, 50% solvent B; *t*=18 min 50% solvent A, 50% solvent B. The flow rate for separation was 0.200 mL/min. Following the 18 min separation, the gradient was set to 3%

solvent A, 97% solvent B at a flow rate of 0.500 mL/min for 12 minutes to re-equilibrate the column.

Eluent was ionized using an electrospray ionization (ESI) source operated under the following settings: sheath gas 30 (arbitrary units); aux gas 8 (arbitrary units); sweep gas 3 (arbitrary units); spray voltage 3kV; capillary temperature 300 °C. A Q-Exactive Plus Orbitrap mass spectrometer (Thermo Scientific, Waltham, MA) was used to collected data for all targeted data. All ions were detected in negative mode using parallel reaction monitoring (PRM), which requires a list of parent *m/z*'s to isolate and subsequently collects a full scan of the fragments produced. Parameters for the mass spectrometer were as follows: resolution-140,000; automatic gain control (AGC)-$3x10^6$ ions; maximum IT time-100 ms; isolation window-0.4 *m/z*; normalized collision energy 35 eV. Calibration was performed on the instrument every 24 hours using a negative mode calibration solution from Thermo Scientific.

2.4.3 Targeted compound list

Phosphatidylglycerol (PG) and lysyl-phosphatidylglycerol (LPG) compounds were detected as the $[M-H]^-$ ion and the cardiolipin (CL) compounds were detected as $[M-2H]^{2-}$ ions. In total, 23 unique CL, 10 PG, and 10 LPG masses were targeted for quantitation. This list only included the most abundant fatty acids bound to each head group, C16:0, C16:1, C18:0, C18:1, and C18:2, based on bacterial profiles[56, 72, 73]. A complete list of all the lipids included in the analysis is provided in **Appendix Table 2.4.** The *m/z* listed in the table corresponds to the parent mass isolated and eventually fragmented. However, quantitation was performed by selecting a specific fragment that is common to the head group not the specific lipid. A dehydrated glycerol phosphate (GP) fragment with a *m/z (-)* of 152.9958 was used for all PG and CL compounds, and a lysine fragment with a *m/z* of145.0948 was used for LPG, as shown in **Figure 2.1**. In addition, the PRM

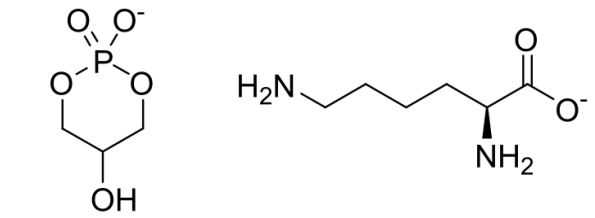

GP Fragment
m/z 152.9958

Lysine Fragment
m/z 145.0948

Figure 2.1 Structure of fragments used to quantitate lipids cardiolipin, phosphatidylglycerol, and lysyl phosphatidylglycerol.

analysis method has the advantage of determining the relative concentrations of specific fatty acid tails attached to the parent ion.

2.4.4 Calibration curve preparation

Standards for calibration curves were dissolved in 1:1 methanol: chloroform using masses of purchased solid standards. A mixed stock of CL 72:4, PG 36:0, and LPG 36:2 was prepared at 75µM and stored at -20 °C. Serial dilutions from the stock were made at the following concentrations; 50, 10, 5, 1, 0.5, 0.1, 0.05, 0.01, 0.005, and 0.001 µM. Internal standards of CL 56:0 and PG 16:0 were made by dissolving the solid standard in solvent to make a mixed working stock of 50 µM and added to each calibration standard at a final concentration of 8.3 µM.

2.5 Data Analysis

2.5.1 Untargeted

Data generated from the Xcalibur software was converted from the *.raw* file extension to the *.mzML* using msconvert, a tool in ProteoWizard[76, 77]. All peak area integration was performed within MAVEN[78], using a 5 ppm mass window and exact *m/z* based on chemical formula and preferred ionization mode. Phospholipids with the head groups of PA, PE, PI, PS, PG, LPG, and fatty acids were detected a $[M-H]^-$, and PC were detected as $[M+H]^+$.

2.5.2 Targeted

Xcalibur's Quan Browser (Thermo Scientific, Waltham, MA) was used to integrate areas under the curve for fragment masses that corresponded to exact *m/z* of the specific ion of interest and were also matched to retention time range of phospholipid classes. Cardiolipin molecules elute at 4.5 minutes, phosphatidylglycerol elutes at 2 minutes, and lysyl-phosphatidylglycerol elutes at 10 minutes. Calibration plots were made by plotting the log of the ratios of the

area of the analyte to the area of the internal standard "log(A_a/A_{is})" vs. the log of the ratios of concentration of the analyte to the concentration of the internal standard "log([C_a]/[C_{is}])". Biological data was analyzed using the same protocol, and the exact concentration of the lipid was interpolated using the regression line for the corresponding standard. Each calibration level was analyzed in replicates of six and standard error was calculated.

2.6 Results and Discussion

2.6.1 Untargeted data

Operating the instrument in dual polarity full scan mode, along with all ion fragmentation (AIF) allowed for the collection of information about the parent ion and the fragments produced. Although the hydrophobic extraction preferentially selects for compounds with lipid-like moieties, the mass spectrometer is only constrained by its *m/z* range. This allows for analysis of experiments that are exploratory in nature or of unknown sample composition. The analysis leads to an initial understanding of the lipid profiles in samples, which has not been previously studied. Additionally, global lipidome changes can be measured between a treatment group and a control. The HILIC chromatography is concentrated on hydrophobicity therefore, any phospholipid with the same polar head group (PE, PC, PG, etc.) will have the same retention time (RT) without regard to the composition of aliphatic tails. A typical experiment requires a standard to be analyzed using the exact chromatographic and mass spectrometric conditions for each compound that is to be identified, but this is not the case for this untargeted method. Identification for exact lipid species can be made by matching two factors: exact mass and retention time of the head group. Each phospholipid head group only needs to have one representative standard analyzed, saving instrument time and cost. This makes it possible to identify any possible tail combination for all

head groups, without having multiple standards. This can be very advantageous if the compounds desired are not easily purchased or synthesized.

As a proof of concept, six phospholipid standards, one from each of the most abundant head groups, were analyzed by the untargeted lipidomics methods and were detected in either positive or negative mode. There was complete temporal resolution between groups except for phosphatidylinositol (5.08 min) and phosphatidic acid (4.99 min), but because a high-resolution mass analyzer was used, there was a low possibility of lipid misidentification. The lysine conjugated PG was also detected at 12.3 minutes. Even though no additional amino acid (AA) modified phospholipid standards were analyzed, it is indicative that this HILIC-MS method is capable of detecting many other AA modified lipids. It has been shown that these compounds serve an important role in creating surface membrane charge sites, thus providing some form of antibiotic tolerance[79, 80] and reduces attraction of host generated antimicrobial peptides[81]

Since free fatty acids (FFA) are the building blocks of phospholipids it would be beneficial to detect those as well[82, 83]. These compounds were not retained by the column, which was expected, but four biologically relevant FFA were detected. A summary of this information is provided in **Table 2.2**.

This method has shown its ability to discriminate seven different phospholipids and four fatty acids; it is reasonable to assume that other lipids that do not contain phosphorus or have a sugar moiety as a head group will be detected in this approach (unpublished data). Photosynthetic organisms have sulfolipids such as sulfoquinovosyl diacylglycerols (SQDG) and can replace phospholipids with sulfur containing lipids under phosphorus limited conditions[84, 85]. Monogalactosyldiacylglycerol (MGDG) and digalactosyldiacylglycerol (DGDG) are the major lipid classes present in plants and have roles in photosynthesis[86, 87].

Being able to precisely measure a large set of compounds within and across a lipid class in a 30-minute analysis is very valuable. However, it is possible to accurately

Table 2.2 Details for lipid standards used for the untargeted analysis

Lipid class	Abbr.	Formula	Species Detected	RT (min)	Exact *m/z*	Detected *m/z*	Error (ppm)
Phosphatidylinositol	PI (32:0)	$C_{41}H_{79}O_{13}P$	$[M-H]^-$	5.08	809.5180	809.5209	3.58
Phosphatidic acid	PA (36:1)	$C_{39}H_{75}O_8P$	$[M-H]^-$	4.99	701.5121	701.5146	3.56
Phosphatidylcholine	PC (36:0)	$C_{44}H_{88}NO_8P$	$[M+H]^+$	11.91	790.6326	790.6315	1.39
Phosphatidylserine	PS (34:2)	$C_{40}H_{74}NO_{10}P$	$[M-H]^-$	10.79	758.4972	758.4992	2.64
Phosphatidylethanolamine	PE (32:0)	$C_{37}H_{74}NO_8P$	$[M-H]^-$	9.17	690.5074	690.5093	2.75
Phosphatidylglycerol	PG (36:0)	$C_{42}H_{83}O_{10}P$	$[M-H]^-$	3.43	777.5665	777.5659	0.77
Lysyl-phosphatidylglycerol	LPG (36:2)	$C_{48}H_{91}N_2O_{11}P$	$[M-H]^-$	12.3	901.6282	901.6307	2.77
Oleic acid	OA	$C_{18}H_{34}O_2$	$[M-H]^-$	1.59	281.2481	281.2491	3.56
Linoleic acid	LA	$C_{18}H_{32}O_2$	$[M-H]^-$	1.66	279.2324	279.2334	3.58
Palmitic acid	P	$C_{16}H_{32}O_2$	$[M-H]^-$	1.74	255.2324	255.2334	3.92
Stearic acid	S	$C_{18}H_{36}O_2$	$[M-H]^-$	1.53	283.2637	283.2648	3.88

detect thousands of *m/z* that may not match any known lipid. Matching the *m/z's* retention time can help identify the head group, and AIF can be used to identify fragments that are present, aiding in piecing the molecule back together. An example can be seen in **Figure 2.2**. The standard for PS (34:2) elutes at 10.7 minutes, and several fragments that match the structure can be identified. Based upon theoretical fragmentation data from LipidMaps[88, 89], it is possible to identify at least 5 fragments of the parent ion, including the 16:0 (255.2333 *m/z*) and 18:2 (279.2334 *m/z*) fatty acid tail fragments. This added feature can be useful for structure elucidation in the case of an unidentified ion.

2.6.2 Targeted data

In efforts to compliment the untargeted approach, the design and optimization of a targeted approach was used to quantify a reduced number of lipids. Although this exact method only focuses on three lipid classes (CL, PG, and LPG) present in a specific bacterium[68, 90], the fundamentals can be applied to any set of lipids that desire a more precise measurement.

Herein, we have created a method to quantify CL without the use ion paring agents, while still being able to quantify two other lipid classes, PG and LPG. The above-mentioned untargeted method uses 10 mM ammonium formate at pH 3, which provides excellent detection of all six common phospholipid classes and several other lipid species; however, CL do not ionize well with these conditions. It was determined that rising the pH to 5.8 and changing the buffer's concentration to 5 mM ammonium acetate resulted in reliable detection in cardiolipin standards. This is supported by experimentation showing pK_{a1} and pK_{a2} have values of 2.15 and 3.15 respectively[91], thus shifting equilibrium towards the doubly deprotonated form at a pH of 5.8. Again, due to the HILIC nature of the chromatography, separation can be achieved based on headgroup regardless of tail composition. There are discrete regions in the chromatogram where PG, CL and LPG's elute (**Appendix Figure 2.4**). In contrast to the AIF that is used in the untargeted method, parallel

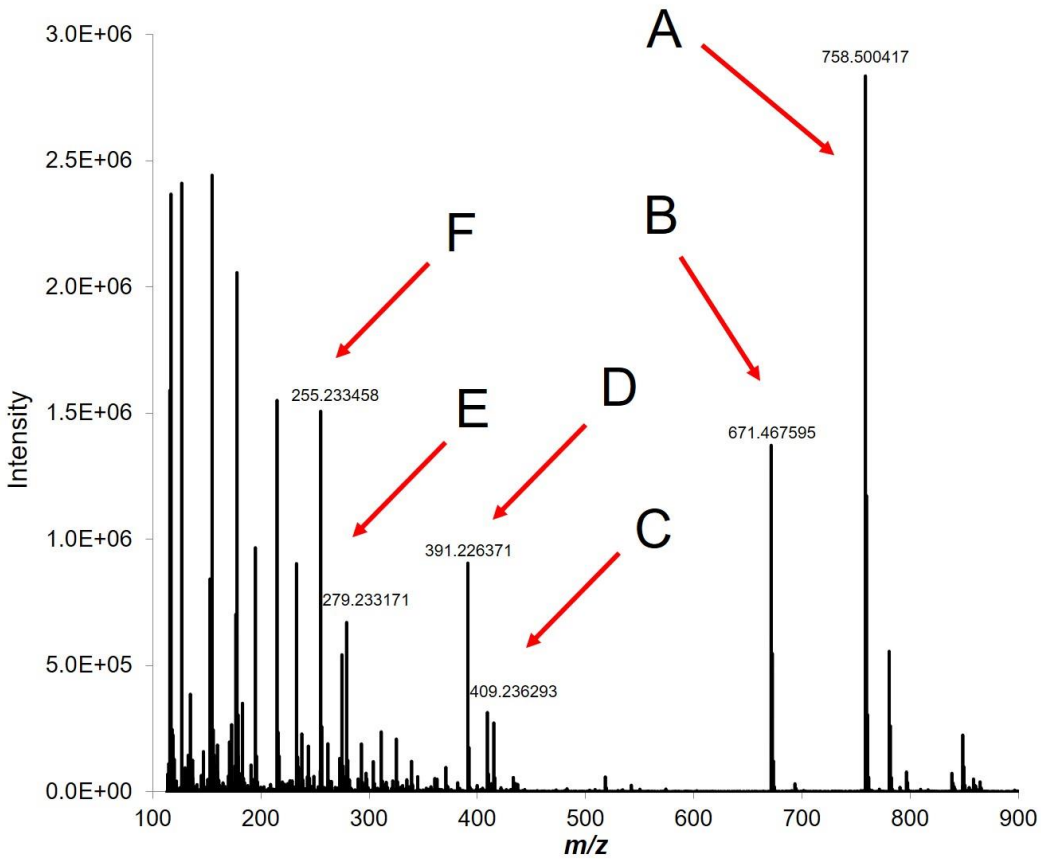

Figure 2.2 All ion fragmentation of PS (34:2) standard.

A: $[M-H]^-$, B: loss of serine, C: loss of serine and C18:2 fatty acid as ketene D: loss of serine and C18:2 fatty acid as neutral specie, E: C18:2 fatty acid, F: C16:0 fatty acid.

reaction monitoring (PRM) is used to isolate and fragment individual lipid *m/z*. High resolution data of the all the fragments originating from the parent mass is obtained. This provides an extra level to confirm to the exact structural moieties present in a mixed FA lipid while reducing noise thus lowering the detection limit.

To make the targeted method as quantitative as possible, a calibration curve was made by using a single external standard each for lipid class and adding an internal standard that is not naturally found in biological samples. Since standards for each specific lipid of interest are not available, this methodology for quantitation accounts for any changes in ionization efficiency between the chosen external standard and the detected lipid. When calibration curves were plotted, a high correlation of determination value (R^2) was achieved for all lipid classes (**Appendix Figure 2.5 and Appendix Table 2.5)**. Less than 2% variation was seen in the internal standard across all points in the calibration curve **(Table 2.1**). Cardiolipin and PG were analyzed with a detection limit of 416 nM and 41.6 nM for LPG. Linear range for CL and PG spanned three orders of magnitude, and LPG was linear over four orders of magnitude. Signal for the standards below these concentrations was either not detected or not above the noise.

2.6.3 Biological validation

To show the application of this lipidomics approach, *Enterococcus faecalis* (*E. faecalis*) cells were supplemented with exogenous fatty acids, and their lipids were profiled using both the untargeted and targeted approaches. Treated and control samples were grown, and lipids were extracted as mentioned in the earlier section. It has been shown that when *E.faecalis* cells are grown in the presence of host unsaturated fatty acids (oleic acid or linoleic acid), **Appendix Figure 2.6**, a tolerance to daptomycin is observed along with alterations in membrane fatty acid profiles as measured through GC-FAME[56]. Applying our approach on this bacterial system shows the advantages of performing both analyses on a single sample. Several studies have been published measuring lipid changes in *E.faecalis* using thin layer chromatography (TLC)[90, 92, 93], and GC-FAME[56, 72, 73]. TLC methods

suffer from the ability to only identify different classes of lipids and has limited use for quantitation. GC-FAME allows for quantitation of individual fatty acids but is hindered by the non-specific esterification of phospholipids resulting in loss of information about head groups. One group explicitly measured individual phospholipids (LPG and PG) in these bacterium[68]. Table S3 compares what lipids were detected by Rashid and coworkers to what was measured in this study.

The untargeted analysis also facilitated the detection of two free fatty acids (FFA), 9 lysyl-phosphatidylglycerols (LPG), and 12 phosphatidylglycerols (PG). The heat map in **Figure 2.3** shows the $\log_2$ fold change in the normalized areas for each lipid detected (exact ratios shown in **Appendix Table 2.6**). Each column represents the ratio of the samples supplemented with exogenous fatty acids compared to the control samples. As expected, a significant difference is seen in the relative amounts of FFAs detected in the corresponding supplemented samples (e.g. oleic acid is more abundant in the samples when supplemented with oleic acid, and likewise for linoleic acid). Smaller, positive, significant fold changes are seen in the oleic acid samples for LPG 34:2, LPG 36:2, and LPG 36:4, showing that some amount of oleic acid is being incorporated into membrane as LPG. An opposite trend is seen when looking at the linoleic acid samples; a decrease is seen in monosaturated LPGs such as 36:1, 32:1 34:1. These compounds have one degree of unsaturation in either of the two fatty acid tails, but this method is lacking the ability to determine exactly which fatty acid tail harbors the double bond. Regardless of the fatty acid that is supplemented, there is a global decrease in all of the PGs detected when compared to the controls. The one thing this analysis cannot provide is the ability to compare the fold change of one lipid to the fold change to another lipid (e.g. the fold change for LPG 36:4 vs the fold change for PG 36:1). While the untargeted method provides the ability to quickly examine how multiple lipids species (within and across head groups) are changing compared to others, information about exact concentrations is lacking. This

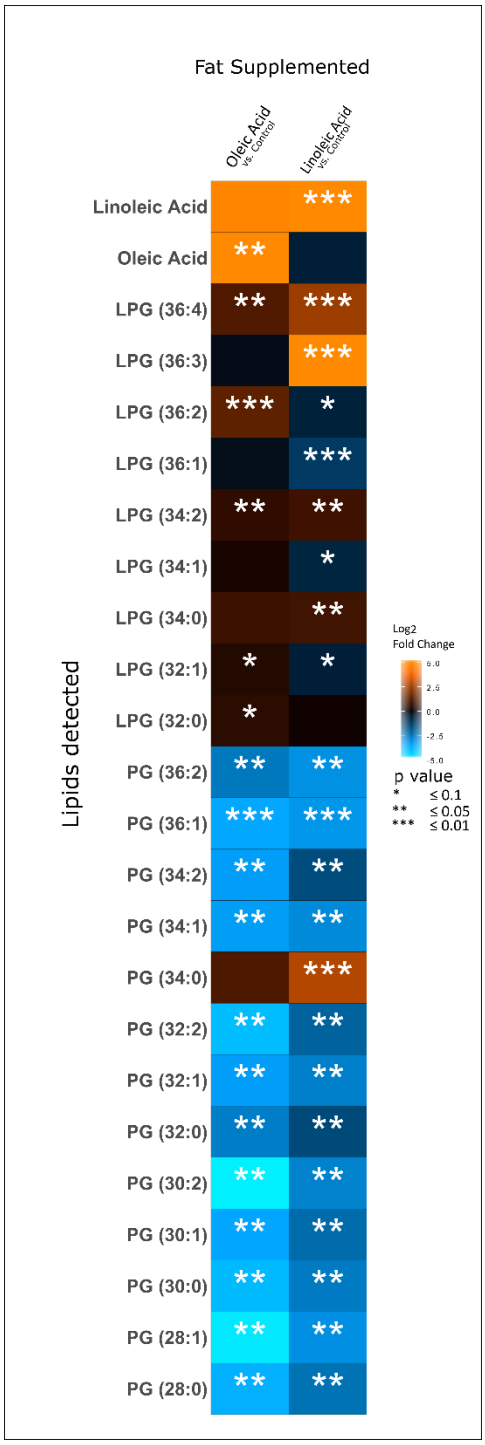

Figure 2.3 Heat map of lipid compounds detected using the untargeted analysis.

All fold changes are compared to control samples and then log_2 transformed. An orange color represents a fold change >1, and a blue color represents a fold change <1. Asterisks depict the level of confidence based on a Student's T-test.

limitation can be overcome by using the targeted method, thus gaining more information about lipid species identified as significant from the untargeted method. The targeted analysis (n= 6 per group) was able to quantify 9 phosphatidylglycerols (PG), 8 cardiolipins (CL) and 10 lysyl-phosphatidylglycerols (LPG), (**Table 2.3 and Appendix Table 2.7).** If a value is listed at <LOQ, a peak was identified but its concentration was lower than the limit of quantitation, and if a ND is listed, no peak was below the limit of detection. This method was capable of quantifying cardiolipins which has been difficult to do with previous methods. When the cells were provided linoleic acid, the polyunsaturated CL (72:7 and 72:8) were at 1.46 and 2.69 µM respectively and were not detected in in the oleic acid and control samples. Within the PRM data, it can be verified that the CL72:7 compound's major tail fragment is a C18:2 (*m/z* 279.2231), and a minor component of C18:1 (*m/z* 281.2486). As expected, the CL72:8 fragmentation data showed only C18:2 tail fragments **(Appendix Figure 2.7**). It is clear that the quantity of PG lipids with C16 tails (saturated or unsaturated) was very low when given either of the fats, which was also seen in the untargeted data. The targeted approach showed the most abundant PG in the control samples is PG 34:1 and has a concentration of 11.21 µM, which is two times higher than the next most abundant PG. This information is not obtainable from the untargeted method alone. This increases the understanding of how the membrane composition is changing within a head group, but not necessarily across treatments.

2.7 Conclusion

The intent of these methods was to highlight the importance of analyzing lipids from an untargeted and targeted standpoint. It has shown that using a high-resolution mass spectrometer in full scan mode allows for the detection of many different lipid classes with the ability to discriminate within each class, and a more holistic understanding of how lipid profiles change. It was possible to detect 6 major

Table 2.3 Quantitative lipid data for biological samples.

The first column represents the lipid species detected, and the second, third, and fourth columns represent the three different exogenous fats that were added. The data is an average of six replicates and the standard error

Lipid	Concentration (μM)		
	Control	Oleic Acid	Linoleic Acid
PG (32:0)	1.79 ±0.23	<LOD	<LOD
PG (32:1)	4.98 ±0.92	<LOD	<LOD
PG (34:0)	1.28 ±0.12	<LOD	<LOD
PG (34:1)	11.21 ±1.76	<LOD	<LOD
PG (34:2)	0.97 ±0.12	<LOD	1.25 ±0.18
PG (36:1)	<LOD	1.21 ±0.25	<LOD
PG (36:2)	1.87 ±0.44	18.34 ±2.2	<LOD
PG (36:3)	ND	<LOD	0.79 ±0.15
PG (36:4)	<LOD	<LOD	8.14 ±1.57
CL (66:0)	ND	ND	0.75 ±0.14
CL (70:0)	0.77 ±0.12	ND	1.71 ±0.31
CL (70:6)	ND	ND	0.9 ±0.16
CL (72:0)	3.81 ±0.53	<LOD	<LOD
CL (72:3)	<LOD	1.04 ±0.31	ND

Table 2.3 continued

Lipid	Concentration (μM)		
	Control	Oleic Acid	Linoleic Acid
CL (72:4)	<LOD	2.68 ±0.7	ND
CL (72:7)	ND	ND	1.46 ±0.35
CL (72:8)	ND	ND	2.69 ±0.68
LPG (32:0)	0.53 ±0.18	<LOD	<LOD
LPG (32:1)	0.53 ±0.19	0.19 ±0.03	0.04 ±0.03
LPG (34:0)	0.46 ±0.2	0.05 ±0.01	<LOD
LPG (34:1)	2.97 ±0.69	0.57 ±0.11	0.08 ±0.12
LPG (34:2)	0.22 ±0.04	0.38 ±0.04	0.67 ±1.16
LPG (36:0)	<LOD	0.05 ±0.01	ND
LPG (36:1)	0.17 ±0.02	1.57 ±0.2	<LOD
LPG (36:2)	0.39 ±0.08	12.8 ±1.46	0.13 ±0.19
LPG (36:3)	<LOD	0.07 ±0.01	0.49 ±0.92
LPG (36:4)	0.05 ±0.03	<LOD	2.46 ±4.48

phospholipids, free fatty acids, and lysine-based lipids, but there is reason to believe that many more lipid classes could be detected using this analysis. By adjusting the pH of the mobile phase, it was possible to confidently detect cardiolipins, which are notoriously difficult to measure. With the implementation of representative standards (internal and external) and parallel reaction monitoring, it was possible to quantitate cardiolipin, phosphatidylglycerol, and lysyl-phosphatidylglycerol to the nanomolar range. Biological applications were shown by using a single extraction method to measure global lipid changes and quantify eight different cardiolipin species in *E.faecalis*.

2.8 Appendix

Table 2.4 Full list of compounds included in PRM.

Each lipid represents a unique m/z and formula. Only one possible tail combination is listed

***some molecular formulas may correspond to multiple tail combinations**

Lipid	*m/z*	Retention Time (min)	Tail 1	Tail 2	Tail 3	Tail 4	Formula
CL (64:0)	675.4788	0-8	16,0	16,0	16,0	16,0	C73H142O17P2
CL (64:1)	674.471	0-8	16,1	16,0	16,0	16,0	C73H140O17P2
CL (64:2)	673.4632	0-8	16,1	16,1	16,0	16,0	C73H138O17P2
CL (66:0)	689.4945	0-8	18,0	16,0	16,0	16,0	C75H146O17P2
CL (66:1)	688.4867	0-8	18,0	16,1	16,0	16,0	C75H144O17P2
CL (68:0)	703.5101	0-8	18,0	18,0	16,0	16,0	C77H150O17P2
CL (68:1)	702.5023	0-8	18,0	18,0	16,1	16,0	C77H148O17P2
CL (70:0)	717.5258	0-8	18,0	18,0	18,0	16,0	C79H154O17P2
CL (70:1)	716.518	0-8	18,0	18,0	18,0	16,1	C79H152O17P2
CL (70:3)	714.5023	0-8	18,1	18,1	18,0	16,1	C79H148O17P2
CL (70:4)	713.4945	0-8	18,1	18,1	18,1	16,1	C79H146O17P2
CL (70:5)	712.4867	0-8	18,2	18,1	18,1	16,1	C79H144O17P2
CL (70:6)	711.4788	0-8	18,2	18,2	18,1	16,1	C79H142O17P2
CL (70:7)	710.471	0-8	18,2	18,2	18,2	16,1	C79H140O17P2
CL (72:0)	731.5414	0-8	18,0	18,0	18,0	18,0	C81H158O17P2
CL (72:1)	730.5336	0-8	18,1	18,0	18,0	18,0	C81H156O17P2
CL (72:2)	729.5258	0-8	18,1	18,1	18,0	18,0	C81H154O17P2
CL (72:3)	728.518	0-8	18,1	18,1	18,1	18,0	C81H152O17P2
CL (72:4)	727.5101	0-8	18,1	18,1	18,1	18,1	C81H150O17P2
CL (72:5)	726.5023	0-8	18,2	18,1	18,1	18,1	C81H148O17P2
CL (72:6)	725.4945	0-8	18,2	18,2	18,1	18,1	C81H146O17P2
CL (72:7)	724.4867	0-8	18,2	18,2	18,2	18,1	C81H144O17P2
CL (72:8)	723.4788	0-8	18,2	18,2	18,2	18,2	C81H142O17P2
PG (32:0)	721.5025	0-4	16,0	16,0			C38H75O10P
PG (32:1)	719.4869	0-4	16,1	16,0			C38H73O10P
PG (34:0)	749.5338	0-4	16,0	18,0			C40H79O10P
PG (34:1)	747.5182	0-4	16,0	18,1			C40H77O10P
PG (34:2)	745.5025	0-4	16,0	18,2			C40H75O10P

Table 2.4 continued

Lipid	m/z	Retention Time (min)	Tail 1	Tail 2	Tail 3	Tail 4	Formula
PG (36:0)	777.5651	0-4	18,0	18,0			C42H83O10P
PG (36:1)	775.5495	0-4	18,1	18,0			C42H81O10P
PG (36:2)	773.5338	0-4	18,1	18,1			C42H79O10P
PG (36:3)	771.5182	0-4	18,2	18,1			C42H77O10P
PG (36:4)	769.5025	0-4	18,2	18,2			C42H75O10P
LPG (32:0)	849.5975	8-15	16,0	16,0			C44H87N2O11P
LPG (32:1)	847.5818	8-15	16,1	16,0			C44H85N2O11P
LPG (34:0)	877.6288	8-15	16,0	18,0			C46H91N2O11P
LPG (34:1)	875.6131	8-15	16,0	18,1			C46H89N2O11P
LPG (34:2)	873.5975	8-15	16,0	18,2			C46H87N2O11P
LPG (36:0)	905.6601	8-15	18,0	18,0			C48H95N2O11P
LPG (36:1)	903.6444	8-15	18,1	18,0			C48H93N2O11P
LPG (36:2)	901.6288	8-15	18,1	18,1			C48H91N2O11P
LPG (36:3)	899.6131	8-15	18,2	18,1			C48H89N2O11P
LPG (36:4)	897.5975	8-15	18,2	18,2			C48H87N2O11P

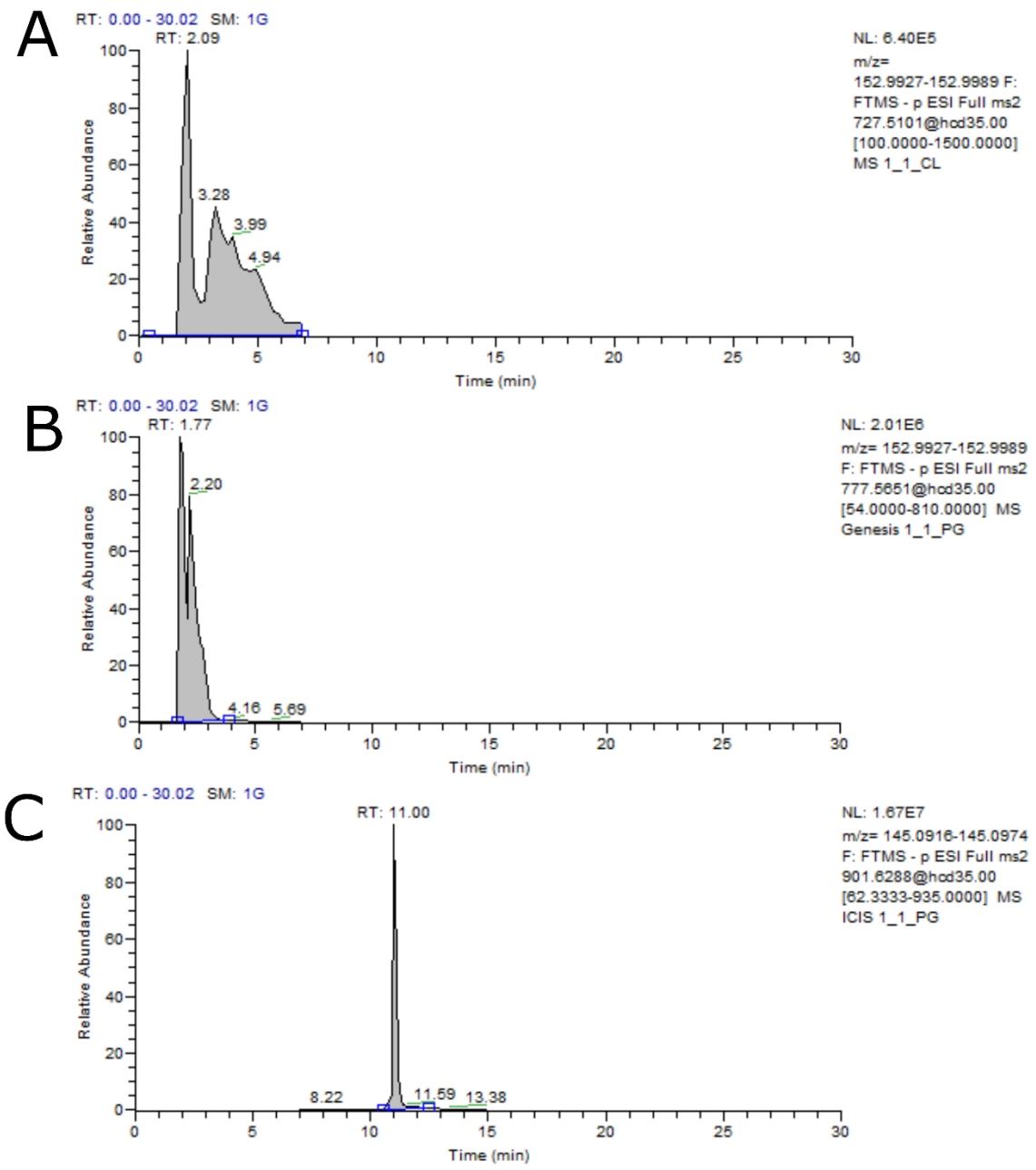

Figure 2.4 Extracted ion chromatograms of PRM data for representative compounds in targeted analysis.

A- glycerol phosphate fragment from CL 72:4 standard, B-glycerol phosphate fragment from PG 36:0 standard, C-Lysine fragment from LPG 36:2 standard.

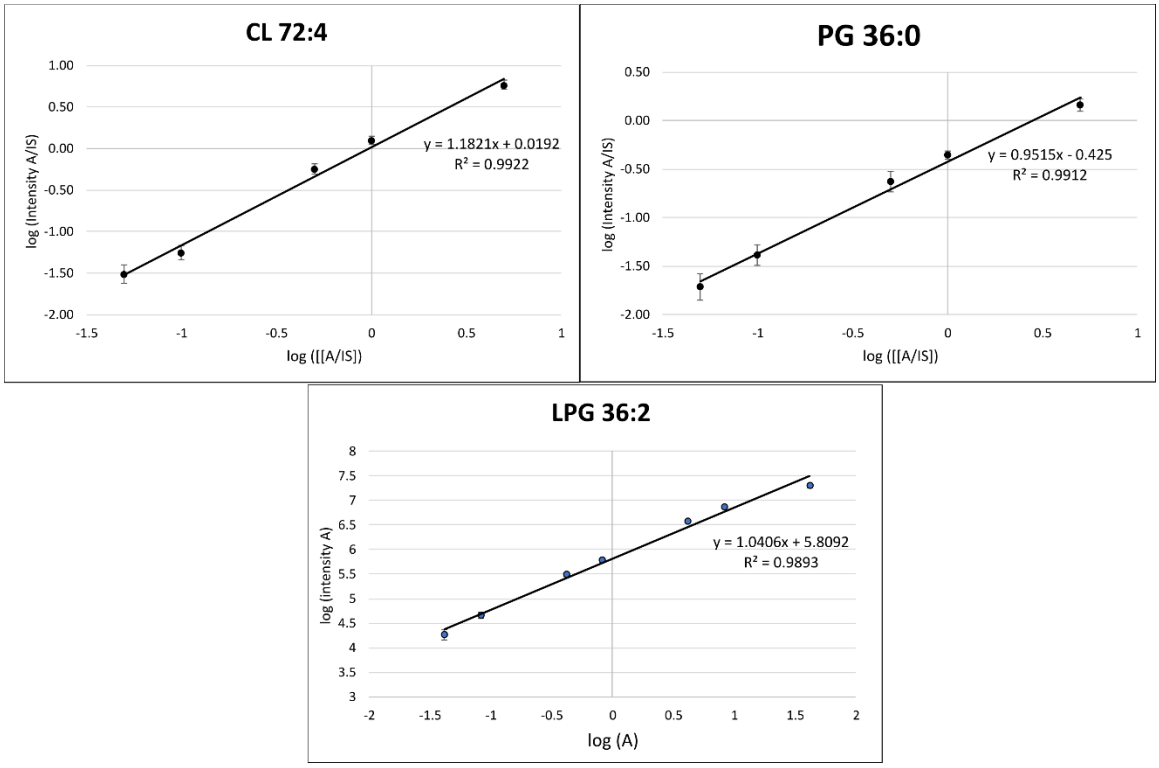

Figure 2.5 Calibration curves for the three standards used in the targeted analysis

Table 2.5 Averages for integrated areas used for calibration curves

log(Con Ratio) * for PG and CL	log (conc) * for LPG	CL 72:4	LPG 36:2	PG 36:0
-4.00	-3.08			
-4.00	-3.08			
-4.00	-3.08			
-3.30	-2.38			
-3.30	-2.38			
-3.30	-2.38			
-3.00	-2.08	-2.3868		
-3.00	-2.08		3.8532	
-3.00	-2.08			
-3.00	-2.08			-3.1543
-3.00	-2.08			-3.2586
-3.00	-2.08			
-2.30	-1.38		4.1080	-3.0072
-2.30	-1.38		4.3178	
-2.30	-1.38			
-2.30	-1.38		4.2811	-2.8156
-2.30	-1.38		4.5137	-2.6734
-2.30	-1.38		4.0632	-2.7311
-2.00	-1.08		4.5363	
-2.00	-1.08	-2.4408	4.5626	-2.7543
-2.00	-1.08		4.4596	
-2.00	-1.08		4.7190	-2.4070
-2.00	-1.08		4.8317	-2.4229
-2.00	-1.08		4.8008	-2.5099
-1.30	-0.38	-1.3098	5.3839	-2.0076
-1.30	-0.38	-1.2598	5.4223	-2.1407
-1.30	-0.38	-1.3764	5.3934	-1.8903
-1.30	-0.38	-1.7916	5.6217	-1.4476
-1.30	-0.38	-1.8053	5.5543	-1.3833
-1.30	-0.38		5.5725	-1.4174
-1.00	-0.08	-1.0549	5.6688	-1.6498
-1.00	-0.08	-1.0103	5.7153	-1.6087
-1.00	-0.08	-1.2064	5.7102	-1.6136
-1.00	-0.08	-1.3761	5.8179	-1.1210

Table 2.5 continued

log(Con Ratio) * for PG and CL	log (conc) * for LPG	CL 72:4	LPG 36:2	PG 36:0
-1.00	-0.08	-1.3489	5.8936	-1.1925
-1.00	-0.08	-1.5358	5.8941	-1.1548
-0.30	0.62	-0.1344	6.4722	-0.9013
-0.30	0.62	-0.1266	6.5331	-0.8143
-0.30	0.62	-0.0718	6.5720	-0.8535
-0.30	0.62	-0.3952	6.6557	-0.3178
-0.30	0.62	-0.3895	6.5777	-0.4373
-0.30	0.62	-0.3833	6.6061	-0.4362
0.00	0.92	0.2361	6.8547	-0.4687
0.00	0.92	0.1882	6.7911	-0.3391
0.00	0.92	0.1754	6.8171	-0.5109
0.00	0.92	-0.0491	6.8482	-0.3174
0.00	0.92	0.0333	6.8958	-0.2783
0.00	0.92	-0.0038	6.9196	-0.2540
0.70	1.62	0.8821	7.1921	0.1290
0.70	1.62	0.8950	7.2271	-0.0776
0.70	1.62	0.9121	7.1744	0.0460
0.70	1.62	0.6953	7.3607	0.2809
0.70	1.62	0.6589	7.3820	0.2845
0.70	1.62	0.5621	7.4663	0.2967

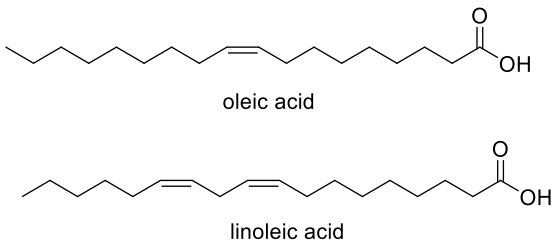

Figure 2.6 Structure of exogenous fats added to biological samples

cis-9-octadecanoic acid (oleic acid), and cis-9,12 octadecadienoic acid (linoleic acid)

Table 2.6 Ratios and p-values used to create heat map for untargeted data

Group	Ratios		p-values	
	Oleic acid/ EtOH	Linoleic acid/ EtOH	Oleic acid /EtOH	Linoleic acid /EtOH
PG(28:1)	0.03581	0.11944	0.01471	0.01775
PG(28:0)	0.07747	0.18728	0.02324	0.03091
PG(30:2)	0.03283	0.14695	0.02264	0.02664
PG(30:1)	0.08938	0.20557	0.02011	0.02715
PG(30:0)	0.06653	0.16347	0.02008	0.02570
PG(32:2)	0.06431	0.23426	0.02700	0.04005
PG(32:1)	0.09773	0.15317	0.01987	0.02351
PG(32:0)	0.15862	0.33890	0.01135	0.02538
PG(34:2)	0.09845	0.32987	0.01951	0.03617
PG(34:1)	0.09909	0.13150	0.01896	0.02150
PG(36:2)	0.17041	0.11875	0.01917	0.02003
PG(36:1)	0.08640	0.10994	0.00499	0.00470
PG(34:0)	2.11512	6.91868	0.18827	0.00950
LPG (36:4)	2.18853	5.44162	0.03862	0.00020
LPG (36:3)	0.90305	81.05640	0.83167	0.00044
LPG (36:2)	2.65211	0.68710	0.00126	0.06461
LPG (36:1)	0.88182	0.43156	0.31713	0.00700
LPG (34:2)	1.50144	1.79755	0.03007	0.01173
LPG (34:1)	1.19384	0.62900	0.26489	0.06188
LPG (34:0)	1.76964	1.82762	0.37784	0.03974
LPG (32:1)	1.32663	0.69432	0.09888	0.05592
LPG (32:0)	1.40897	1.09997	0.09222	0.18917
Oleic Acid	113.03278	0.69938	0.01543	0.30020
Linoleic Acid	27.35683	20735.98000	0.42265	0.00186

Table 2.7 Concentrations for lipids measured in each sample for the targeted method

Sample number	21	22	23	24	61	62	63	64	65	101	102	103	104	105
Group	Control	Control	Control	Control	Oleic Acid	Oleic Acid	Oleic Acid	Oleic Acid	Oleic Acid	Linoleic Acid	Linoleic Acid	Linoleic Acid	Linoleic Acid	Linoleic Acid
PG (32:0)	2.480	1.519	1.662	1.510	0.009	0.000	0.009	0.000	0.000	0.018	0.000	0.000	0.000	0.009
PG (32:1)	7.628	4.914	3.837	3.575	0.147	0.031	0.088	0.071	0.057	0.068	0.088	0.000	0.271	0.060
PG (34:0)	1.044	1.633	1.203	1.245	0.009	0.000	0.000	0.006	0.000	0.009	0.010	0.000	0.165	0.016
PG (34:1)	6.660	15.268	11.225	11.689	0.353	0.021	0.236	0.328	0.182	0.167	0.240	0.064	0.000	0.156
PG (34:2)	0.634	1.237	0.954	1.055	0.135	0.025	0.138	0.126	0.075	1.359	1.545	1.605	0.556	1.187
PG (36:1)	0.118	0.556	0.501	0.576	1.238	1.079	2.113	1.054	0.583	0.013	0.011	0.000	0.000	0.006
PG (36:2)	0.870	3.003	1.951	1.658	17.390	24.377	22.451	14.434	13.075	0.064	0.212	0.315	0.000	0.125
PG (36:3)	0.000	0.000	0.000	0.000	0.086	0.000	0.060	0.062	0.014	0.687	1.026	1.286	0.423	0.539
PG (36:4)	0.000	0.085	0.025	0.010	0.000	0.000	0.008	0.000	0.000	4.781	8.998	10.733	12.043	4.153
CL (66:0)	0.000	0.180	0.000	0.164	0.000	0.000	0.000	0.000	0.000	0.332	1.080	0.848	1.001	0.502
CL (70:0)	0.973	0.895	0.418	0.824	0.262	0.160	0.129	0.298	0.000	1.292	2.914	1.696	1.413	1.244
CL (70:6)	0.000	0.000	0.000	0.000	0.000	0.000	0.000	0.000	0.000	0.592	1.492	1.025	0.761	0.639
CL (72:0)	4.838	3.413	4.517	2.506	0.048	0.193	0.191	0.066	0.076	0.077	0.000	0.297	0.185	0.081
CL (72:3)	0.076	0.000	0.000	0.104	2.004	0.659	1.524	0.773	0.260	0.000	0.000	0.000	0.000	0.000
CL (72:4)	0.000	0.000	0.073	0.000	4.818	2.117	3.638	2.185	0.686	0.000	0.000	0.000	0.000	0.000

Table 2.7 continued

Sample number	21	22	23	24	61	62	63	64	65	101	102	103	104	105
Group	Control	Control	Control	Control	Oleic Acid	Oleic Acid	Oleic Acid	Oleic Acid	Oleic Acid	Linoleic Acid	Linoleic Acid	Linoleic Acid	Linoleic Acid	Linoleic Acid
CL (72:7)	0.000	0.000	0.000	0.000	0.000	0.000	0.000	0.000	0.000	0.657	2.721	1.503	1.458	0.969
CL (72:8)	0.000	0.000	0.000	0.000	0.000	0.000	0.000	0.000	0.000	1.345	5.269	2.739	2.383	1.737
LPG (32:0)	0.217	1.007	0.630	0.274	0.000	0.000	0.000	0.044	0.000	0.009	0.012	0.000	0.000	0.000
LPG (32:1)	0.269	1.095	0.470	0.304	0.208	0.099	0.173	0.302	0.211	0.040	0.065	0.021	0.000	0.062
LPG (34:0)	0.243	0.945	0.637	0.044	0.070	0.020	0.044	0.099	0.048	0.000	0.007	0.000	0.000	0.014
LPG (34:1)	1.791	4.974	2.394	2.746	0.628	0.254	0.548	0.956	0.506	0.114	0.093	0.067	0.007	0.164
LPG (34:2)	0.222	0.208	0.144	0.343	0.435	0.225	0.367	0.435	0.448	0.909	0.991	0.256	0.058	1.160
LPG (36:0)	0.018	0.014	0.000	0.000	0.067	0.011	0.048	0.074	0.060	0.000	0.000	0.000	0.000	0.000
LPG (36:1)	0.191	0.177	0.103	0.213	1.998	0.879	1.383	1.842	1.797	0.000	0.007	0.000	0.000	0.014
LPG (36:2)	0.471	0.285	0.227	0.587	16.290	7.966	12.288	15.357	12.116	0.211	0.150	0.028	0.000	0.157
LPG (36:3)	0.000	0.000	0.000	0.012	0.084	0.021	0.060	0.076	0.123	0.579	0.905	0.186	0.054	0.747
LPG (36:4)	0.000	0.000	0.013	0.090	0.010	0.000	0.000	0.000	0.000	2.996	4.565	0.935	0.178	3.649

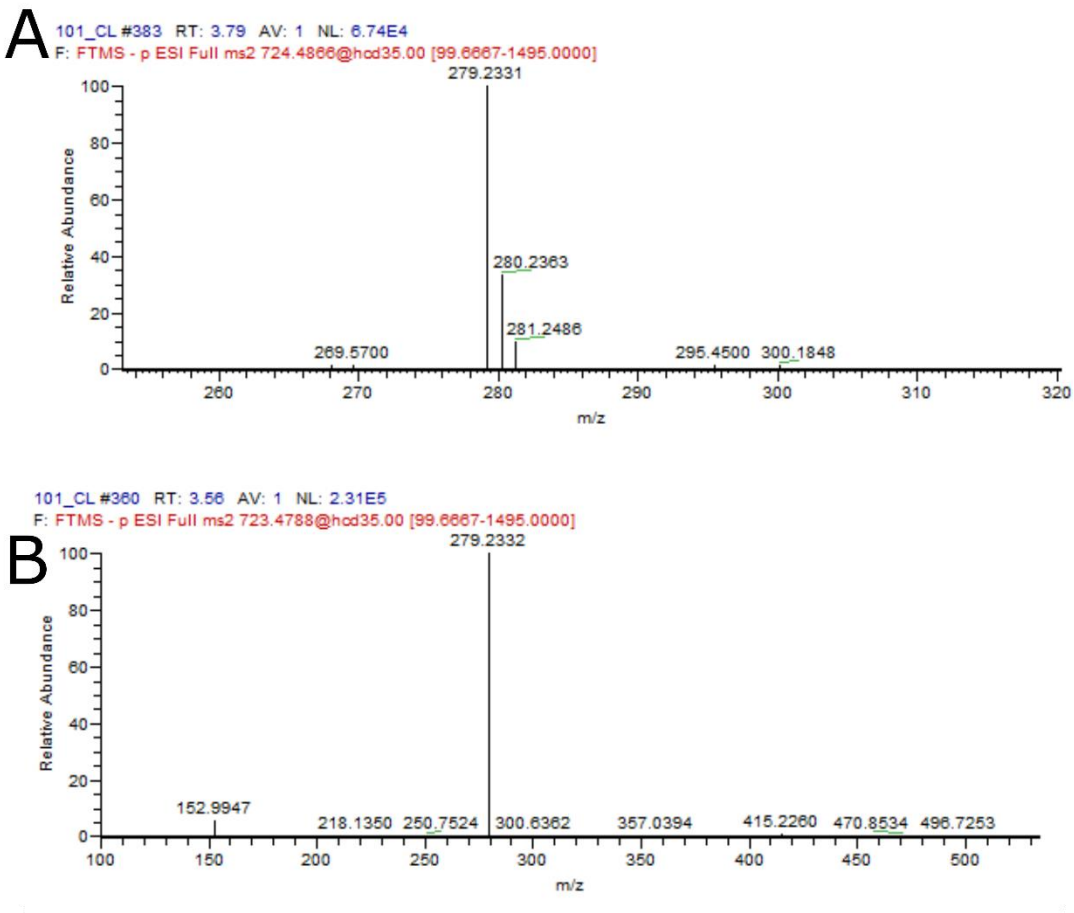

Figure 2.7 Fragmentation spectra of cardiolipin compounds detected in biological samples supplemented with linoleic acid

A- CL72:7 B-CL72:8

CHAPTER 3 MIDGUT METABOLOMIC PROFILING OF FALL ARMYWORM (*SPODOPTERA FRUGIPERDA*) WITH FIELD-EVOLVED RESISTANCE TO CRY1F CORN

Preface

This chapter focuses on understanding how an insect that was once susceptible to a toxin produced by a plant has now become resistant. This works builds on established data showing a mutation to a specific gene and subsequently altered protein expression. The use of untargeted metabolomics allows for the small molecule profiles to be collected and assessed for changes between the two groups of insects. Evaluating metabolites which show an increase in abundance provides an opportunity to identify small molecule markers present in the resistant phenotype.

The project stems from a collaboration with Dr. Juan Fuentes and Dr. Heba Abdelgaffar from the Entomology and Plant Pathology Department. They were working with a species of fall armyworm (*Spodoptera frugiperda*) that typically was not able to feed on genetically modified crops like corn. This corn plant has been modified to produce a Cry1F protein that was originally discovered in *Bacillus thuringiensis* and is toxic to many insects. This genetically modified crop has been commercialized and used extensively by the agricultural industry to combat pests and increase crop yield.

The mode of action for Cry1F toxins are well known and work as an effective insecticide but populations of *S. frugiperda* that showed resistant started showing up in Puerto Rico in 2010. Since this mutation provides a competitive advantage, crops in the southeast United States soon were threatened by this resistant insect. Previous research has shown the mutation was in the ATP binding cassette subfamily C2 (SfABCC2) gene and reduces the binding of the Cry1F toxin. The family of proteins affected also control the transport of compounds in and out of the cell and have been seen in other organisms. Armed with this information, it was hypothesized that if the fall armyworm harbored this mutation, it would be resistant, as well as produce a buildup of a unique subset of metabolites that could be used an indirect indicator of resistance.

By analyzing four different genotypes of insects and feeding them two different diets, it would be possible to monitor metabolite changes among the groups. An untargeted metabolomics analysis was performed using liquid chromatography and an Orbitrap mass spectrometer. From the 126 metabolites identified, comparative and multivariate analyses showed that metabolite profiles were unique among the resistant, susceptible, and the hybrid offspring. The diet of the insects also dictated unique metabolite profiles. Investigation of the individual metabolites produced a list of six compounds that will be used to further aid the classification of the resistant phenotype.

This research has already been published and is a great example of the versatility of the metabolomics platform in guiding researchers to explain the complicated process of environmentally evolved resistance. Hopefully, data produced from this set of experiments will lead agricultural research to a new route to combat this challenge.

A version of this chapter was originally published by in *Insect Biochemistry and Molecular Biology* and was reproduced with permission of the journal containing the following citation.

Citation:
Abdelgaffar, H.; Tague, E. D.; Castro Gonzalez, H. F.; Campagna, S. R.; Jurat-Fuentes, J. L., Midgut metabolomic profiling of fall armyworm (Spodoptera frugiperda) with field-evolved resistance to Cry1F corn. *Insect Biochemistry and Molecular Biology* **2019**

Contributions:
JF, HA, designed the experiment, performed the bioassay and wrote the manuscript. HFC and SRC, designed the metabolomics experiments, wrote the manuscript. EDT designed the experiment, extracted the samples, performed and analyzed the metabolomics data, and wrote the manuscript.

3.1 Abstract

Populations of the fall armyworm (*Spodoptera frugiperda*) have developed resistance to transgenic corn producing the Cry1F insecticidal protein from the bacterium *Bacillus thuringiensis* (Bt). Resistance in *S. frugiperda* from Puerto Rico is genetically linked to a mutation in an ATP Binding Cassette subfamily C2 gene (*SfABCC2*) that results in a truncated, non-functional Cry1F toxin receptor protein. Since ABCC2 proteins are involved in active export of xenobiotics and other metabolites from the cell, we hypothesized that Cry1F-resistant fall armyworm with a non-functional SfABCC2 protein would display altered gut metabolome composition when compared to susceptible insects. Mass spectrometry and multivariate statistical analyses identified 126 unique metabolites from larval guts, of which 7 were found to display statistically significant altered levels between midguts from susceptible and Cry1F-resistant *S. frugiperda* larvae when feeding on meridic diet. Among these 7 differentially present metabolites, 6 were found to significantly accumulate (1.3 to 3.5-fold) in midguts from Cry1F-resistant larvae, including nucleosides, asparagine, and carbohydrates such as trehalose 6-phosphate and sedoheptulose 1/7-phosphate. In contrast, metabolomic comparisons of larvae fed on non-transgenic corn identified 5 metabolites with statistically significant altered levels and only 2 of them, 2-isopropylmalate and 3-phosphoserine, that significantly accumulated (2.3- and 3.5-fold, respectively) in midguts from Cry1F-resistant compared to susceptible larvae. These results identify a short list of candidate metabolites that may be transported by SfABCC2 and that may have the potential to be used as resistance markers.

3.2 Introduction

The fall armyworm (*Spodoptera frugiperda*) is an important polyphagous pest native to tropical regions in the Americas with a long migratory range [94].

Larvae of this insect have also been reported as a devastating invasive pest of corn in Africa[95, 96]. Options for effective control of *S. frugiperda* larvae were greatly improved in 2003 by commercialization of transgenic corn producing the Cry1F insecticidal protein from the bacterium *Bacillus thuringiensis* (Bt)[97]. As other Cry toxins, the Cry1F protein recognizes receptors in the midgut of *S. frugiperda* larvae as a critical step to kill enterocytes and ultimately disrupt the midgut epithelium and facilitate deadly septicemia[98]. Field-evolved resistance to Cry1F corn has been reported in *S. frugiperda* populations from Puerto Rico[99], Florida and North Carolina[100], Brazil[101, 102], and Argentina[103].

In a strain of *S. frugiperda* from Puerto Rico, resistance to Cry1F was linked to a mutation in an ATP Binding Cassette subfamily C2 (*SfABCC2*) gene that resulted in a truncated protein and reduced Cry1F toxin binding[104]. This observation mirrored similar cases of resistance to Cry toxins linked to mutations in ABCC2 genes in *Heliothis virescens*[105], *Plutella xylostella*[106], *Helicoverpa armigera*[107], *Bombyx mori*[108] and *Spodoptera exigua*[109]. Members of the ABCC2 protein family play a critical role in detoxification and chemoprotection by controlling the efflux of both exogenous and endogenous compounds across the cell membrane[110]. These proteins have broad specificity and act upon many different compounds, including representatives of most classes of insecticides[111] However, ABC transporters are not always involved in resistance to insecticides [112], and functional interactions need to be tested experimentally. Despite diversity in susbtrate specificity and binding, ABC proteins commonly perform active export of xenobiotics from cells to reduce their intracellular concentration and thus reducing noxious effects[113]. Consequently, we hypothesized that altered ABCC2 in Cry1-resistant insects would lead to accumulation of certain metabolites in gut cells when compared to susceptible larvae. In this work, we test this hypothesis by performing the first metabolomic analysis of the midgut epithelium from an insect and quantitatively comparing metabolite patterns between susceptible and Cry1F-resistant *S. frugiperda* larvae. Identification of metabolome alterations in the midgut of resistant larvae suggests candidate metabolites that may be transported

by SfABCC2 as potential targets in the development of novel technologies to monitor for resistance to Cry toxins and Bt crops linked to alterations in ABCC2 genes. However, further studies are necessary to demonstrate the link between the significantly differentially expressed metabolites and the mutated ABCC2 gene.

3.3 Materials and Methods

3.3.1 Insect strains

Eggs of a Cry1F-susceptible strain of *S. frugiperda* (Ben) were purchased from Benzon Research (Carlisle, PA). The Cry1F-resistant *S. frugiperda* strain 456LS3 was originated from field collections in Puerto Rico and its resistance phenotype is described elsewhere[114]. The 465LS3 strain was crossed with Ben and re-selected at the F2 generation on corn event TC1507 (producing Cry1F toxin) for 7 days, and this process repeated thrice to generate a similar genomic background between the strains, except for the resistance allele present in 456LS3[104]. For the purpose of this work, heterozygous strains were generated by mating 25 female/male moths from the Ben and 456LS3 strains to generate strains 456F or 456M according to the sex of the resistant adult in the parental cross (F for female and M for male). All insect rearing and treatments were performed in incubators at 26 ± 2°C, 44% relative humidity, and an 18-h light/6-h dark photoperiod.

3.3.2 Protoxin preparation

The Cry1F protoxin was produced in a recombinant *Bacillus thuringiensis* (Bt) HD-73 strain generously provided by Dr. Jie Zhang (Institute of Plant Protection, Chinese Academy of Agricultural Sciences, Beijing, China) and described elsewhere[115]. The bacteria were grown on 1/3 tryptic soy broth (TSB) agar containing erythromycin (5 µg/ml) for three days, and then a single colony was suspended in 1 mL of autoclaved water and heated for 45 min at 70°C to kill

vegetative cells. An aliquot (500 µL) of the suspension was used to inoculate 500 mL of 1/3 TSB medium containing erythromycin. The culture was incubated for 4 days at 28 °C with agitation (160 rpm) until sporulation was confirmed by microscopic observation. Cultures were then collected by centrifugation (14,981 *g*, 4 °C for 10 min) and pellets washed three times with 1 M NaCl containing 0.1% Triton X-100 with brief (5 min) sonication before centrifugation. Washes were repeated for another 2 cycles as before using distilled water. The final pellet was re-suspended in 50 ml of solubilizing solution (50 mM Na_2CO_3, 0.1% β-mercaptoethanol, 0.1 M NaCl, pH 10.5), sonicated as above and then incubated overnight at 30°C with agitation (180 rpm). After centrifugation at 27,167 *g* for 30 min, the supernatant containing solubilized Cry1F protoxin was purified using anion exchange chromatography as described elsewhere[116]. One major absorbance peak containing Cry1F protoxin (based on band size in SDS-10%PAGE) was detected during the elution, and fractions in that peak were pooled, aliquoted and keep at -80ºC until used.

3.3.3 Bioassays

Eggs of susceptible, resistant and heterozygous strains were collected, and diet contamination bioassays were carried out under standard laboratory-controlled environmental conditions (26 ± 2°C temperature, 44% RH, 16L: 8D photoperiod) using meridic diet (Beet Armyworm diet, product #F9219B, Frontier Scientific Services, Newark, DE). Diet was poured on individual wells of 128-cell polystyrene bioassay trays (Bio-BA-128) and after setting a solution of Cry1F protoxin was applied on the surface. A range of 11 different toxin concentrations (0.0035, 0.007, 0.014, 0.028, 0.056, 0.112, 0.224, 0.445, 0.896, 1.792 and 3.585 µg/cm^2) prepared in sterile MilliQ water and a water control were tested with Ben and heterozygous neonates. Four different Cry1F protoxin concentrations (4.75, 14.4, 28.8 and 36.1 µg/cm^2) were tested for 456LS3 neonates. Sixteen neonates per concentration were tested and bioassays were replicated twice. Mortality was determined after 7 days of incubation and used to determine the Cry1F protoxin

concentration killing 50% of the larvae (LC_{50}) for each strain by Probit analysis using the PoloPlus software[117]. Differences between LC50s were considered significant if there was no overlap between the corresponding 95% confidence intervals.

3.3.4 Larval treatments

Neonates from the Ben, 456LS3, 456M, and 456F populations described above were placed either on meridic diet or V3-V4 stage leaves from corn event TC1507 producing Cry1F toxin or the non-transgenic isoline (2T777). Leaf sections (2.5 x 1.5 cm) were placed in individual plastic cups containing 1% agar to prevent desiccation. A single *S. frugiperda* neonate was placed in each cup, with 60 larvae used per strain. Leaf sections were replaced after the first 6 days of larval growth, and then every day as needed. Larvae were kept on corn leaves or meridic diet until they reached 4^{th} instar (11-14 days), and then weighed. Weight measurements were rank transferred before statistical analysis using two-way analysis of variance (ANOVA) testing for the effect of the different insect strains/ treatments on the average weight measurements with $p < 0.01$.

3.3.5 Tissue sample preparation and metabolite extraction

Polar metabolites were extracted from pools of five dissected 4^{th} instar guts to create a single biological replicate of approximately 100 mg, and a total of four biological replicates were prepared for each strain/treatment. Pooled guts were homogenized to fine pieces on ice using disposable micro tissue homogenizers (Kimble™), snap frozen in liquid nitrogen and stored at -80^0 C until further use. Sample preparation and extraction was done at 4°C unless otherwise specified. Extraction and detection methods were modified from procedures published elsewhere [118, 119]. Briefly, each biological replicate was extracted with 1.3 mL of extraction solvent (40:40:20 HPLC grade methanol: acetonitrile: water with formic acid at a final concentration of 0.1 M) pre-chilled to 4˚C, and allowed to proceed for 20 minutes at -20°C. The supernatant was collected after 5 minutes of centrifugation at 13,300 x *g* and the pellets were re-extracted with 200 µL of fresh

extraction solvent and allowed to sit for 20 minutes at -20°C before being centrifuged at the same conditions as mentioned earlier. Both supernatant fractions were combined, and a stream of dry nitrogen was used to evaporate the solvent. Sterile water (300 µL) was used to for suspend the metabolites prior to being placed in the instrument's autosampler.

3.3.6 Ultra performance liquid chromatography- high resolution mass spectrometry metabolomic analysis

Samples extracted above were separated on a Dionex Ultimate 3000 UPLC (Thermo scientific, Waltham, MA) by injecting a 10 µL sample on to a Synergi 2.5 µm reverse phase Hydro-RP 100 Å, 100 mm x 2.00 mm LC column (Phenomenex, Torrance, CA) kept at 25˚C. All solvents used for mobile phases were HPLC grade and purchased from Fisher Scientific. Solvent A consisted of 97:3 water: methanol, 10 mM tributylamine, and 15 mM acetic acid and solvent B was 100% methanol. The gradient steps included from 0 to 5 minutes 0% B, from 5 to 13 minutes 20% B, from 13 to 15.5 minutes 55% B, from 15.5 to 19 minutes 95% B, and from 19 to 25 minutes 0% B, with a flow rate of 200 µl/min. The eluent was introduced into the mass spectrometer via an electrospray ionization source conjoined to an Exactive™ Plus Orbitrap Mass Spectrometer (Thermo Scientific, Waltham, MA) [120]. Data was collected in negative mode from 85-1000 *m/z* with a resolution of 140,000 and an automatic gain control of $3x10^6$ ions.

Raw data was analyzed using MAVEN[121, 122] to align and annotate peaks within a 5-ppm window. Area under the chromatographic curve was integrated based upon an in-house verified list of metabolites using exact *m/z* and known retention times. All metabolite values were normalized based on the exact mass of the sample extracted prior to all statistical calculations. Heat maps were made by Cluster 3.0 [123] and Javatreeview 1.1[124], using $\log_2$ transformed data. P-values were calculated using Student's T-test. Partial Least Squares Discriminant Analysis (PLSDA) and Variable Importance in Projection (VIP) scores were constructed using the statistical package DiscriMiner in R version 3.1.1[125]. These

VIP scores provide a metric for determining how much influence a metabolite has on the group separation seen in the PLSDA plots. A value >1 indicates that the metabolite contributes to the group differentiation, and this was considered as a significant VIP score [126-128]. Global pathway maps were created by imputing KEGG IDs for each metabolite detected into iPath 2.0[129].

3.4 Results

3.4.1 Cry1F protoxin bioassay

As expected from resistance in 456LS3 being recessive and autosomal[114], bioassays with purified Cry1F protoxin showed no significant difference (based on overlapping 95% confidence intervals) in toxicity against Ben, 456F, and 456M larvae (**Table 3.1**). In contrast, only low mortality (12.5%) was observed when larvae from the 456LS3 strain were exposed to the highest Cry1F protoxin concentration tested (36.1 µg/cm^2). Based on this observation, we estimated that larvae from 456LS3 were >75 fold resistant to Cry1F compared to larvae from the Ben, 456F or 456M strains. In agreement with these observations, exposure of neonates from the Ben, 456M or 456F strains to Cry1F corn leaf tissue resulted in 100% mortality after seven days, while no mortality was observed for larvae of the 456LS3 strain (data not shown).

No significant difference was detected when comparing weights of 4th instar larvae from all strains fed on control diet (p = 1). When comparing artificial diet to corn leaf tissue, the mean larval weights from all the strains was significantly higher (Tukey- Kramer, $p < 0.05$) on meridic diet compared to non-Bt corn leaves (**Figure 3.1**). No significant differences were detected when comparing all four strains fed on meridic diet (p = 1), yet a significant difference in mean larval weight was detected between parental (456LS3 and Ben) strains compared to heterozygous (456F and 456M) strains when feeding on non-Bt corn leaf tissue ($p < 0.05$). Weights of larvae from the 456LS3 strain were not significantly different when fed on non-Bt or Cry1F corn leaves (p = 0.9994).

Table 3.1 Susceptibility of *S. frugiperda* lines to Cry1F protoxin in diet incorporation bioassays

Strain	LC50 (µg/cm^2)	95% CI* (lower- upper)	Slope ± Standard Error
Ben	0.52	0.39- 0.71	1.90 ± 0.20
456LS3**	NA	NA	0.02 ± 0.00
456M	0.46	0.38- 0.56	2.20 ± 0.30
456F	0.62	0.52- 0.75	1.64 ± 0.18

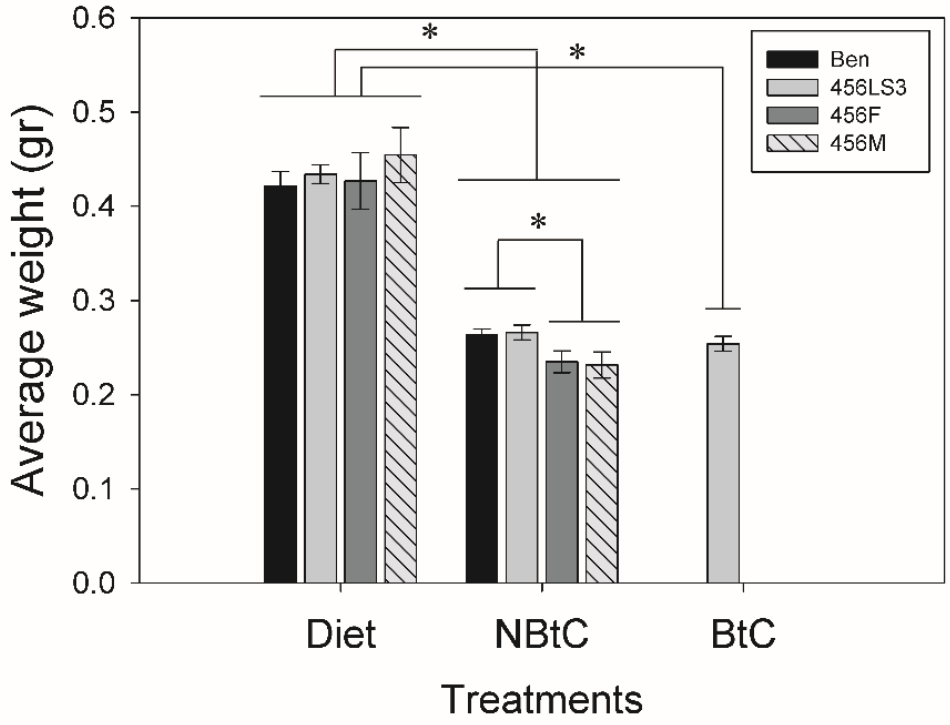

Figure 3.1 Average weight of *Spodoptera frugiperda* neonates fed on diet (Diet), corn event TC1507 producing Cry1F (BtC) or the non-transgenic isoline 2T777 (NBtC) until reaching 4th instar.

Shown are the average larval weight and the corresponding standard error from 4 biological replicates with 5 larvae each per treatment (n=20). Data was analyzed using ANOVA, significant differences in comparisons connected with lines ($p < 0.05$) are denoted with an asterisk

3.4.2 Metabolomics and multivariate data analysis

Untargeted metabolomic profiling analyses identified a large number of endogenous metabolites in larval guts, but only 126 were selected for further analysis based on annotation via known exact *m/z* and retention time. These identified metabolites were classified into different categories including amino acids, carbohydrates, organic acids, nucleotides, nucleosides, fatty acids, vitamins and other metabolites. The cellular pathways related to these metabolites are represented in **Appendix Figure 3.5.** As expected from an analysis that was focused on polar metabolites and that preferentially annotates small hydrophilic compounds, pathways with metabolites detected included metabolism of nucleotides, energy, carbohydrates, cofactors and vitamins as well as biosynthesis of secondary metabolites and degradation of xenobiotics. No metabolites related to lipid, glycan or terpenoid metabolism were identified, due to their hydrophobic nature.

In general, the majority of detected metabolite levels were higher in 456LS3 compared to the other strains (data not shown). The metabolite profiles of all *S. frugiperda* strains fed on either meridic diet (shorten as diet) or non-Bt corn (shorten as NBtC) were evaluated using multivariate analysis (**Figure 3.2**). For each strain, the metabolite profiles were represented using a Partial Least Squares Discriminate Analysis (PLSDA) scores plot (**Figures 3.2A and 3.2B**). In these PLSDA plots, the 456LS3 and Ben strains clearly displayed unique metabolite profiles from one another, while the heterozygous strains (456F and 456M) did not separate in the PLSDA and formed a third group distinct from Ben and 456LS3. These differences appeared clearer in metabolites from insects fed on meridic diet (**Figure. 3.2A**) than when fed on non-transgenic corn (**Figure 3.2B**).

In order to determine which metabolites drove the separation among the groups, the metabolites with Variable Importance in Projection (VIP) scores >1 were further examined as this VIP score indicates that the metabolite contributes

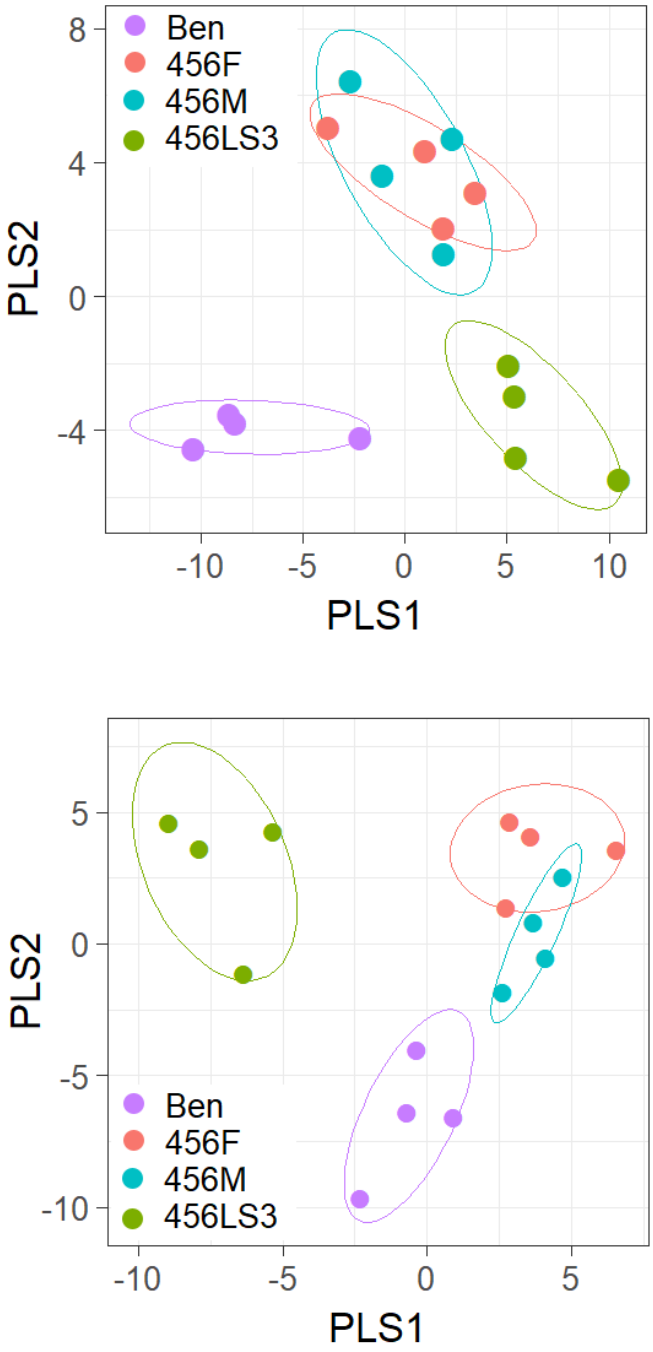

Figure 3.2 Partial Least Squares Discriminate Analysis (PLSDA) scores plots displaying different clusters when comparing metabolite profiles of midguts from *S. frugiperda* larvae from different strains fed on meridic diet (Top) or non-Bt corn leaf tissue (Bottom).

to the group differentiation. When fed the meridic diet, 51 metabolites had significant VIP scores and resulted in a clear separation of the three unique group 456LS3, 456F/456M, and Ben (**Appendix Table 3.6**). The same grouping of strains was observed using metabolites detected when larvae were fed on the non-Bt corn leaf tissue, with 63 metabolites with significant VIP scores (**Appendix Table 3.7**). Twenty of the metabolites with significant VIP scores were common to the meridic diet and non-Bt corn (**Table 3.2**), although the VIP scores varied for the same metabolite depending on treatment. Considering the total number of metabolites with significant VIP scores for each treatment, 43% of the important metabolites for the strain separation on artificial diet were shared with the non-Bt leaf treatment, while 35% of the significant metabolites for the non-Bt leaf treatment were shared with the artificial diet.

3.4.3 Comparative metabolite profiling

Comparison of the relative levels for all detected metabolites in the Ben, 456M, and 456F compared to the 456LS3 gut metabolome for larvae fed on meridic diet (**Figure 3.3 Appendix Table 3.8**) or non-Bt corn leaf tissue (**Figure 3.4, Appendix Table 3.9**) identified metabolites with increased and reduced levels associated to the 456LS3 sample. Given that metabolome differences may result from differential metabolic states in larvae, and that we detected small but significant weight differences between parental and F1 lines when feeding on corn leaf tissue (**Figure 3.1**), we focused metabolite profiling on all four strains fed on meridic diet, on Ben and 456LS3 fed on non-Bt corn, and on 456LS3 when fed on Cry1F corn compared to non-Bt corn.

Out of the total 126 metabolites identified, only 7 metabolites were found to display statistically significant ($p < 0.05$) altered levels **(Table 3.3**) when comparing metabolite patterns between susceptible (Ben, 456M and 456F) and Cry1F-resistant (456LS3) larvae fed on meridic diet. Altered metabolites included organic acids (hydroxyphenylacetate), amino acids (asparagine), nucleosides (dCMP, dTMP, and dAMP), and carbohydrates (trehalose 6-phosphate and sedoheptulose

Table 3.2 Metabolites with VIP* score >1 that support differentiation of Ben, 456M/456F and 456LS3 samples in the PLSDA multivariate space regardless of the food source.

Shown are VIP scores for samples from larvae fed on diet (Diet) and non-Bt corn leaf (NBtC).

Metabolite	Diet	NBtC
Aconitate	1.13	1.27
Allantoate	1.16	1.11
Cysteine	1.43	1.01
D.Gluconate	1.69	1.06
dAMP	1.21	1.09
dCMP	1.24	1.18
dTMP	1.15	1.10
Gluconolactone	1.20	1.00
Hydroxyisocaproic.acid	1.01	1.34
Hydroxyphenylacetate	1.43	1.30
Inosine	1.21	1.28
N-Acetylglutamine	1.39	1.23
Pantothenate	1.31	1.13
S-Ribosyl L-homocysteine	1.19	1.28
Sedoheptulose1/7-phosphate	1.38	1.07
Trehalose.6.phosphate	1.34	1.26
UDP N-acetylglucosamine	1.02	1.02
Uracil	1.30	1.03
Uric acid	1.18	1.23
Uridine	1.01	1.02

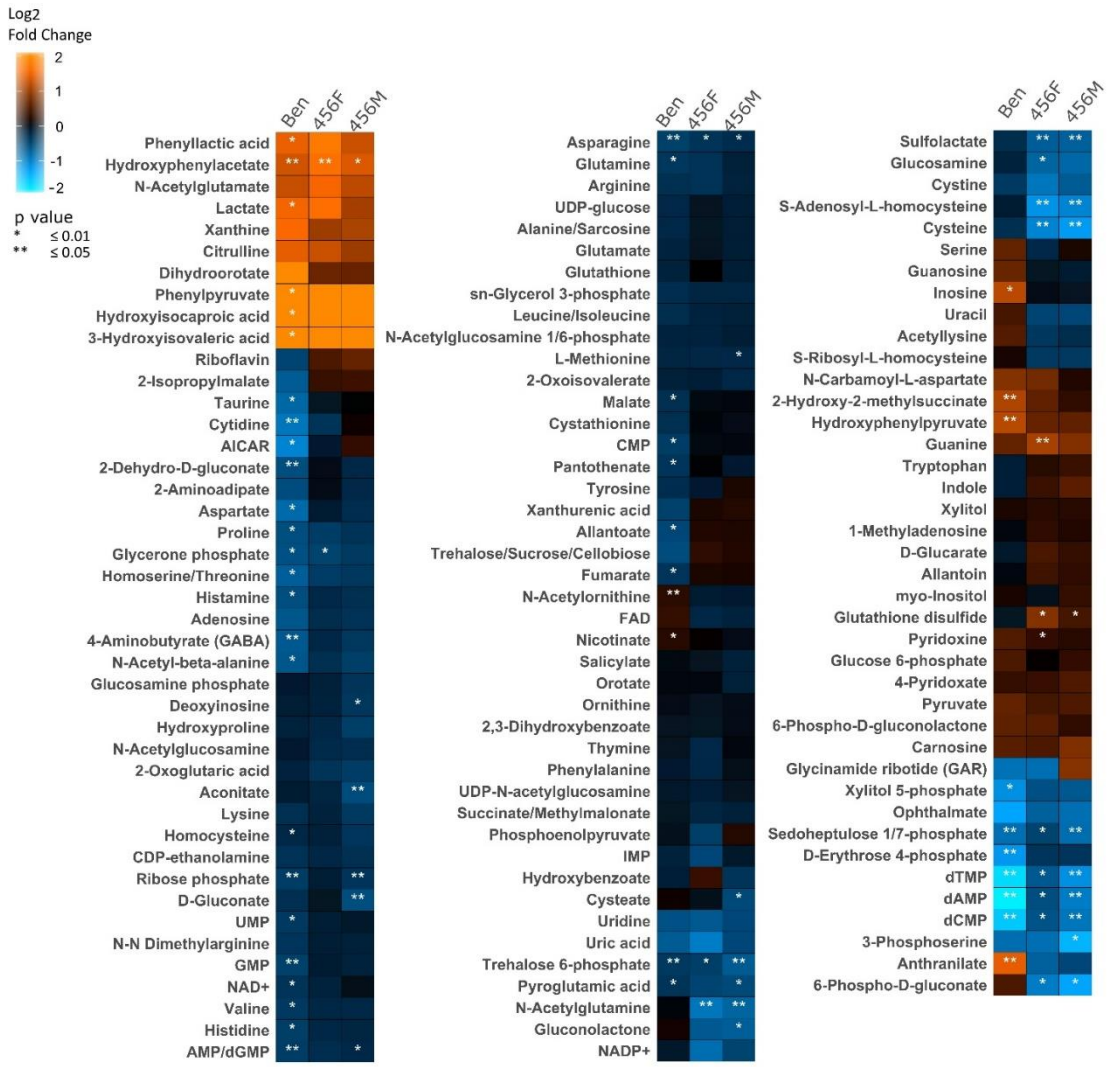

Figure 3.3 Heat maps of relative levels of metabolites detected in guts of *S. frugiperda* larvae fed on meridic diet.

The specific larvae compared in each column are shown at the top. Data are log_2 ratios of metabolites identified when comparing metabolomes from Ben, 456F, or 456M to metabolomes in guts of larvae from the 456LS3 strain. The relative fold levels for each metabolite in each comparison are shown by the key, orange indicates induction > 0, blue indicates repression < 0, with maximums at >2 and <−2. Asterisks represent level of significance (*p < 0.05, **p < 0.01), as noted in the key

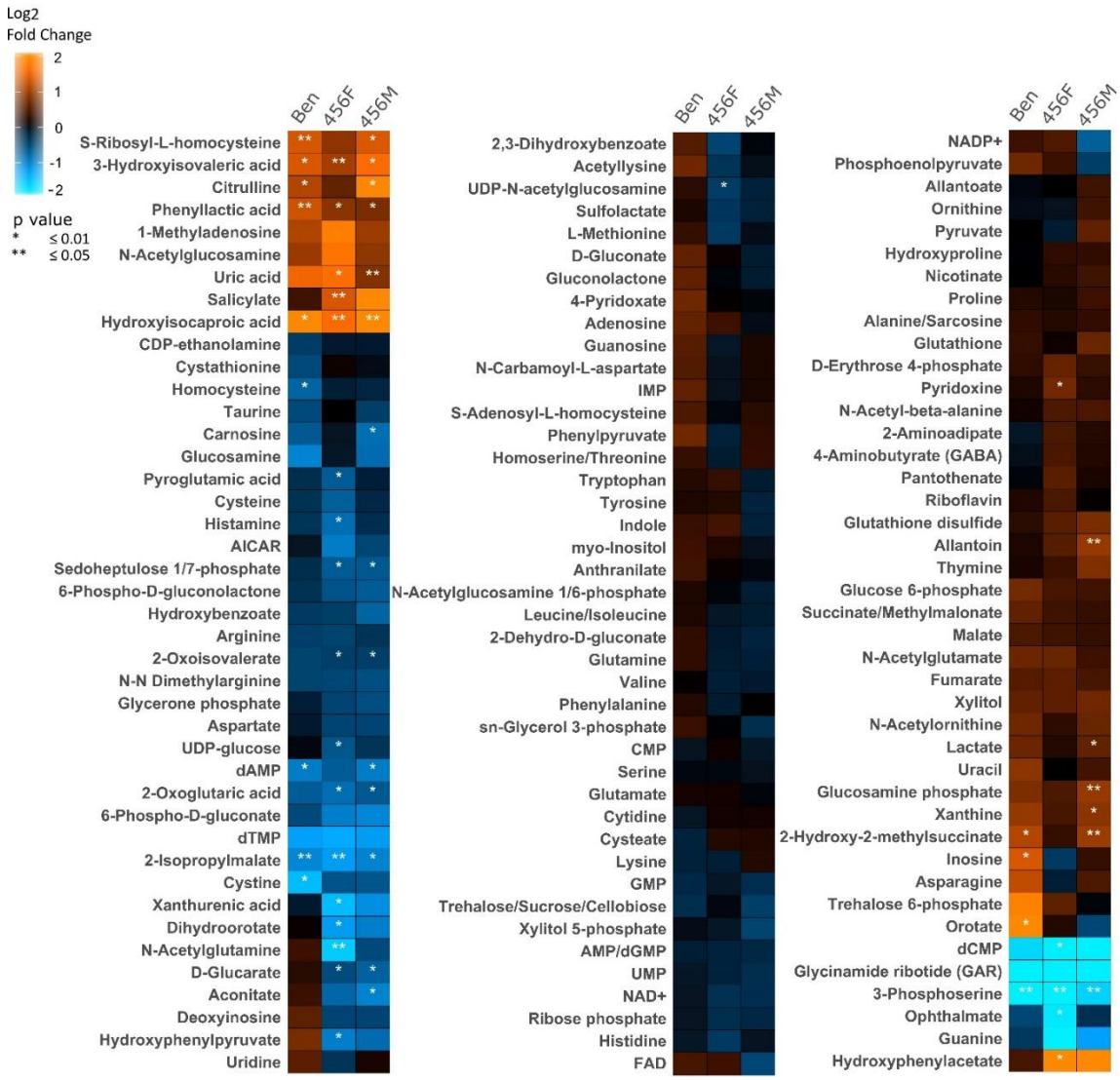

Figure 3.4 Heat maps of relative levels of metabolites detected in guts of *S. frugiperda* larvae fed on non-Bt corn leaf tissue.

The specific larvae compared in each column are shown at the top. Data are $\log_2$ ratios of metabolites identified when comparing metabolomes from Ben, 456F, or 456M to metabolomes in guts of larvae from the 456LS3 strain. The relative fold levels for each metabolite in each comparison are shown by the key, orange indicates induction > 0, blue indicates repression < 0, with maximums at >2 and <−2. Asterisks represent level of significance (*p < 0.05, **p < 0.01), as noted in the key

Table 3.3 Metabolites with significantly altered levels ($p < 0.05$) in Ben, 456M and 456F lines compared to larvae from the 456LS3 strain fed on meridic diet.

Shown are the fold change (FC) and corresponding p-value and VIP scores. Row shaded in black with white font represents lower metabolite levels in guts of larvae from the 456LS3 compared to other strains. All the other metabolites accumulated in guts from larvae of the 456LS3 compared to other strains tested.

Metabolite	Ben/456LS3		456F/456LS3		456M/456LS3	
	FC* (p-value)	VIP	FC (p-value)	VIP	FC (p-value)	VIP
Organic acids						
Hydroxyphenylacetate	2.51 (0.007)	1.40	3.23 (0.002)	1.82	2.62 (0.044)	1.45
Amino acids						
Asparagine	0.73 (0.002)	1.31	0.79 (0.029)	1.43	0.82 (0.015)	1.35
Nucleosides						
dCMP	0.34 (0.001)	1.43	0.65 (0.016)	1.48	0.53 (0.002)	1.60
dTMP	0.31 (0.004)	1.36	0.63 (0.047)	1.31	0.46 (0.009)	1.50
dAMP	0.28 (0.001)	1.40	0.67 (0.027)	1.42	0.51 (0.006)	1.55
Carbohydrates / conjugates						
Trehalose 6-phosphate	0.76 (0.005)	1.26	0.74 (0.007)	1.42	0.62 (0.0003)	1.61
Sedoheptulose 1/7 phosphate	0.55 (0.0002)	1.45	0.72 (0.023)	1.50	0.56 (0.0001)	1.66

1/7-phosphate). When comparing abundance, only hydroxyphenylacetate appeared to be at lower levels in the guts of 456LS3 larvae, while the other 6 metabolites significantly accumulated in 456LS3 compared to the other strains.

In the case of the Ben and 456LS3 gut metabolome samples fed on non-Bt corn leaf tissue (**Figure 3.4 and Table 3.4**), we observed four metabolites with significantly different levels ($p < 0.05$). Two of these metabolites, a vitamin B (orotate) and a purine nucleoside (inosine) were found at significant lower levels in the 456LS3 larval guts, while amino acids and derivatives homocysteine and cystine accumulated in the guts of resistant compared to larvae of the Ben strain (**Table 3.4**).

Metabolomic profiling of larval guts from the 456LS3 strain fed on Cry1F-producing corn and non-Bt corn leaf tissue identified 7 metabolites with distinct abundance between the two treatments. All these metabolites significantly accumulated in the guts when the larvae fed on the non-Bt isoline and included metabolites from diverse metabolic pathways (**Table 3.5).**

3.5 Discussion

Members of the ABC transporter gene family are involved in cellular defense against xenobiotics, including insecticides[112]. Despite their functional diversity [113], generally ABC proteins actively export xenobiotics from cells to reduce their intracellular concentration. Selected ABC transporter genes have been reported as functional receptors for Cry toxins in insects[104, 130-132], and mutations in these genes or alterations in their expression are linked to resistance against diverse Cry toxins[104, 106, 107, 133]. Given their ATP-driven transport activity, our hypothesis was that mutations affecting functionality of ABC transporter genes would result in alterations in the intracellular metabolome. In support of this hypothesis, previous reports demonstrated that a truncated ABCC2 protein in Cry1Ac-resistant *Helicoverpa armigera* larvae resulted in accumulation and altered

Table 3.4 Metabolites with significantly altered levels ($p < 0.05$) in Ben, 456F and 456M when compared to 456LS3 larvae fed non-Bt corn leaf tissue.

Shown are the fold change (FC) and corresponding p-value and VIP scores. Rows shaded in black with white font represents lower metabolite levels in guts of larvae from the 456LS3 compared to other strains. All the other metabolites accumulated in guts from larvae of the 456LS3 compared to other strains tested

Metabolite	Ben/456LS3		456F/456LS3		456M/456LS3	
	FC (p-value)	VIP	FC (p-value)	VIP	FC (p-value)	VIP
Fats and fatty acids						
3-Hydroxyisovaleric acid	2.54 (0.020)	1.67	2.03 (0.009)	1.60	3.05 (0.014)	1.67
Hydroxyisocaproic acid	6.75 (0.026)	1.76	6.06 (0.000)	1.76	6.20 (0.004)	1.79
Organic acids and derivatives						
Phenyllactic acid	2.43 (0.003)	1.75	1.80 (0.014)	1.54	1.69 (0.044)	1.37
2-Isopropylmalate	0.44 (0.008)	1.72	0.39 (0.007)	1.60	0.45 (0.039)	1.33
Amino acids and derivatives						
3-Phosphoserine	0.24 (0.007)	1.79	0.11 (0.006)	1.80	0.29 (0.006)	1.59

Table 3.5 Metabolites with significantly altered levels ($p < 0.05$) in guts from 456LS3 larvae fed leaf tissue from Cry1F-producing or the non-Bt corn isoline.

Shown are the fold change (FC) and corresponding p-value and VIP scores *Fold changes (FC) were calculated by dividing the value of metabolites of 456LS3 larvae receiving Bt-corn by 456LS3 line fed on non-Bt corn.

Metabolite	FC (p-value)	VIP
Amino acid metabolism		
3-Phosphoserine	0.30 (0.007)	1.69
Cystine	0.41 (0.026)	1.68
Purine metabolism		
AICA ribonucleotide	0.63 (0.041)	1.39
TCA cycle		
2-Oxoglutaric acid	0.50 (0.009)	1.66
Glutathione metabolism		
Pyroglutamic acid	0.61 (0.018)	1.61
N-Acetyl-beta-alanine metabolism		
N-Acetyl-beta-alanine	0.61 (0.031)	1.51
Valine biosynthesis		
2-Oxoisovalerate	0.68 (0.047)	1.39

susceptibility to selected synthetic pesticides[107]. In testing our hypothesis, we performed a comparative metabolite analysis between the midgut epithelium from a Cry1F-resistant strain of *S. frugiperda* homozygous for a mutation in an ABC subfamily C2 gene (*SfABCC2mut*) predicted to result in a truncated non-functional ABCC2 protein[104], and larvae with the wild type (*SfABCC2*) genotype or heterozygous for the *SfABCC2mut* allele.

Results from bioassays with Cry1F protoxin were in agreement with previous reports[114] and supported high levels of resistance in the 456LS3 strain, and that resistance is transmitted as a recessive trait. Reduced larval weights in larvae fed corn versus meridic diet, independently of the *S. frugiperda* strain, are in agreement with optimized nutritional value and adaptation of the strains to meridic diet. Lack of significant effects of Cry1F-corn compared to non-transgenic corn on 456LS3 larvae support no fitness costs associated with the *SfABCC2mut* allele, as previously reported [134]. Given the significant differences between meridic diet and non-transgenic corn treatments, we considered metabolome comparisons between the strains for both diets independently. Moreover, since parental and F1 strains displayed significantly different weight when grown on non-Bt corn tissue, we focus metabolic profiling to Ben-456LS3 comparisons for that treatment. It's interesting to note that we found a clear separation of the Ben, 456F/M and 456LS3 groups in the multivariate analysis (PLSDA), but there were only seven metabolites categorized as significant in the comparative analysis. This could point to multiple small changes in a suite of metabolites being related to the resistant phenotype; indicating that a measurement of a set of metabolites would be necessary to differentiate between the phenotypes.

While there is a lack of information on substrate specificity for ABCC2 proteins in insects, much is known in similar proteins in mammals. In BLASTp searches of the mammalian subset of proteins in NCBI, the most similar proteins to SfABCC2 are members of the multidrug resistance-associated protein 4 (MRP4) group (maximum 41% identity, 0.0 Evalue), which are unidirectional transporters localized in diverse tissues and involved in resistance to xenobiotics[135]. Substrates

of MRP4 include nucleotide analogues, glucuronide and sulphate conjugates, prostaglandins, methotrexate, and bile acids[136]. There is also evidence for specificity towards anionic conjugates, including N-acetyl-(2,4-dinitrophenyl)-cysteine[137]. In agreement with these observations, half of the metabolites accumulating in 456LS3 compared to Ben or F1 larvae when fed meridic diet were nucleosides (dCMP, dTMP, dAMP). Also, in comparisons of Ben and 456LS3 larvae fed on non-Bt corn leaf tissue, homocysteine and cysteine accumulated in 456LS3 guts. Although preliminary, these observations support that lack of a functional SfABCC2 may result in accumulation of metabolites (nucleosides and cysteine derivatives) that may be otherwise transported out of the cell by this protein. In mammals transport of nucleosides is a major feature of MRP4 proteins [136], and this may also be the case for the orthologous SfABCC2. Other metabolites accumulated in 456LS3 larvae lacking a functional SfABCC2 were carbohydrates (trehalose 6-phosphate and sedoheptulose 1/7-phosphate) and an amino acid (asparagine), which have not been described as substrates for MRP4. Interestingly, different metabolites were found to accumulate in 456LS3 compared to wild type larvae fed meridic diet and non-Bt corn leaf tissue. This observation suggests important nutritional and metabolite differences based on diet, which is reflected in the significant differences detected in larval weight between the diet treatments. Differences in metabolite composition between meridic diet and corn leaf tissue may have prevented detection of common significant differences between susceptible and resistant larvae when fed on these two diverse diets.

Interestingly, we detected 7 metabolites that were at lower levels in guts of larvae from the 456LS3 strain when they fed on Cry1F-producing corn compared to the non-Bt isoline. In this case, metabolic alterations detected would reflect interactions between Cry1F and the midgut epithelium that in 456LS3 are not conducive to toxicity. In fact, while Cry1F binding to the SfABCC2mut protein from 456LS3 larvae is not detected[104], the toxin still displays (albeit reduced) binding to midgut brush border membrane vesicles (BBMV) from 456LS3 compared to Ben[114], suggesting the potential for Cry1F interacting with midgut proteins. While

it is complex to discern the physiological relevance of the detected metabolome changes in that case, it is interesting to note the reduced levels of components of the TCA cycle (2-oxoglutaric acid) and glutathione metabolism (cystine and pyroglutamic acid), which may suggest alterations on pathways related to energy conservation and reduced oxidative stress when feeding on Cry1F corn. Although speculative, reduced levels of AICA ribonucleotide, which in hepatocytes has been shown to participate in activation of AMP-activated protein kinase and inhibition of autophagy [138], may suggest increased autophagy in 456LS3 when feeding on Cry1F-corn compared to the non-transgenic isoline. Further work to identify the pathways involved in these metabolome differences would be needed to identify physiological effects of feeding on Bt versus non-transgenic corn by Bt-resistant larvae.

In summary, we used comparative metabolomics on the midgut epithelium of susceptible and Cry1F-resistant *S. frugiperda* larvae in an attempt to identify candidate metabolites transported by SfABCC2, a transporter putatively involved in xenobiotic transport outside of the cell. Importantly, as far as we know this work represents the first metabolomics analysis of an insect midgut epithelium and provides a list of candidate metabolites that accumulate in Cry1F-resistant *S. frugiperda* lacking a functional SfABCC2 protein. Further work is needed to determine if any of these metabolites is a substrate for SfABCC2 transport. Specifically, nucleosides are good candidates as they accumulate in Cry1F-resistant larvae and are metabolites selectively and uniquely transported by homologous proteins to SfABCC2 in mammals. It is important to note that we found diverse metabolomic results depending on the diet used (meridic versus corn leaf) to rear the larvae, which suggests that diet has an important impact on the gut metabolome. Further functional assays are needed to confirm substrate specificity for SfABCC2 and to identify metabolites that may serve as markers for resistance to Cry toxins when linked to mutations altering ABC transporter function.

3.6 Appendix

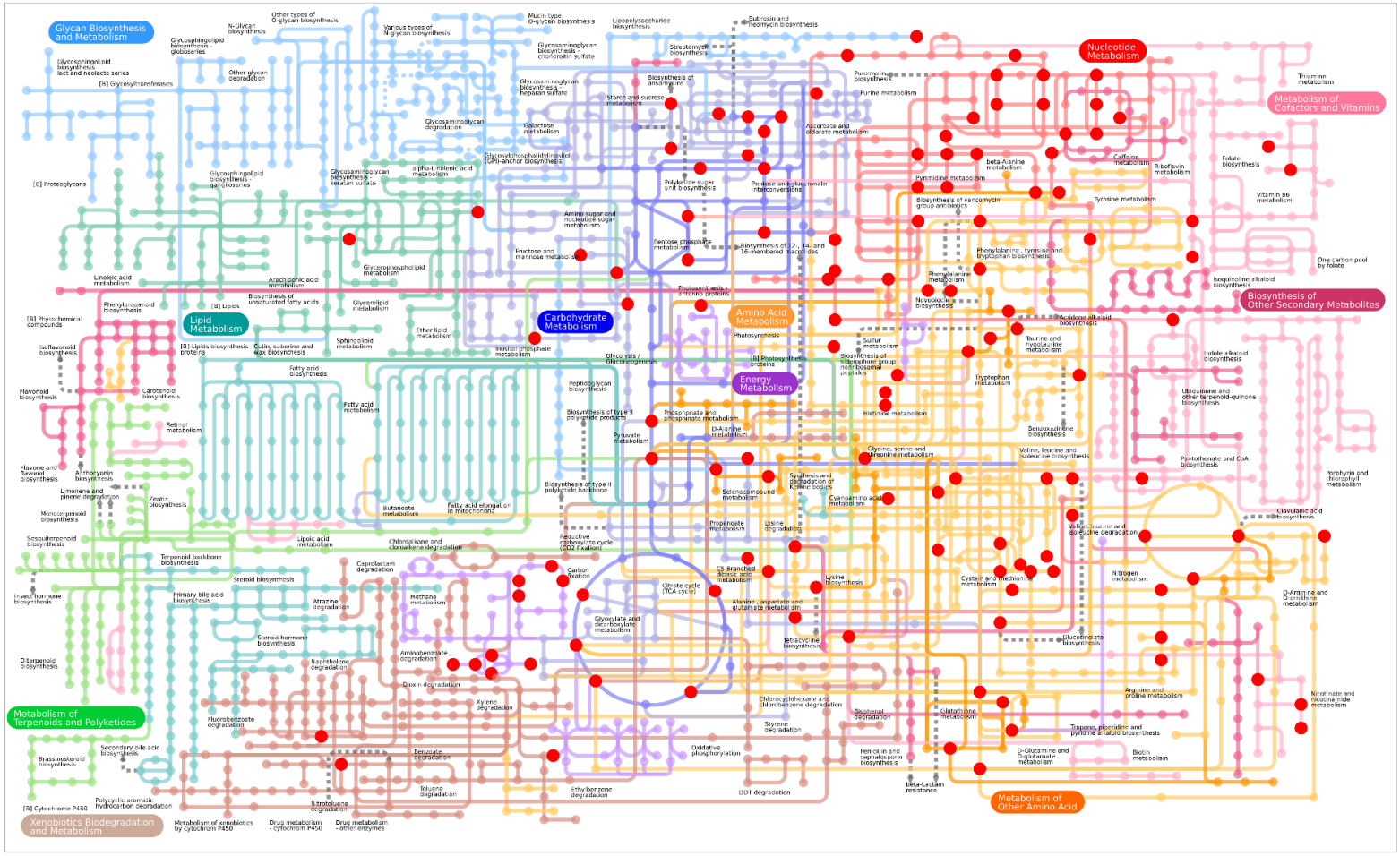

Figure 3.5 Pathway map of all the detected metabolites (red circles).

Table 3.6 Metabolites with Variable Importance in Projections (VIP) scores.

Values >1 support differentiation of Ben, 456M/456F and 456LS3 samples in the PLSDA multivariate space for samples from larvae fed on meridic diet (Diet)

Diet	
Metabolite	**VIP**
Acetyllysine	1.012811
Aconitate	1.127046
AICAR	1.373647
Allantoate	1.160851
AMP/dGMP	1.002778
Anthranilate	1.376991
Asparagine	1.031018
CMP	1.016721
Cysteate	1.678875
Cysteine	1.433473
Cytidine	1.253469
D.Gluconate	1.686835
dAMP	1.206783
dCMP	1.239109
dTMP	1.153117
Fumarate	1.171329
Gluconolactone	1.204582
Glutamine	1.070107
Glutathione	1.428188
Glutathione disulfide	1.420421
Glycerone phosphate	1.025635
Guanine	1.055911
Guanosine	1.076372

Table 3.6 continued

Diet	
Metabolite	**VIP**
Hydroxybenzoate	1.659232
Hydroxyisocaproic acid	1.007803
Hydroxyphenylacetate	1.434163
IMP	1.352404
Inosine	1.207349
Lysine	1.112805
N.Acetylglutamine	1.391089
N-Carbamoyl L-aspartate	1.319281
NAD.	1.016628
Nicotinate	1.083111
Pantothenate	1.313394
Pyridoxine	1.042443
Pyroglutamic acid	1.042945
Ribose phosphate	1.06305
S-Adenosyl L-homocysteine	1.500882
S-Ribosyl L-homocysteine	1.192648
Sedoheptulose 1/7 phosphate	1.382373
Serine	1.078238
Sulfolactate	1.347575
Trehalose 6-phosphate	1.344063
Tryptophan	1.021307
Tyrosine	1.010975
UDP N-acetylglucosamine	1.015052
Uracil	1.304287
Uric acid	1.184786

Table 3.6 continued

Diet	
Metabolite	**VIP**
Uridine	1.007443
2-Dehydro-D-gluconate	1.166845
4-Aminobutyrate/GABA.	1.024927

Table 3.7 Metabolites with Variable Importance in Projections (VIP) scores.

Values >1 support differentiation of Ben, 456M/456F and 456LS3 samples in the PLSDA multivariate space for samples from larvae fed on non-Bt corn leaf tissue (Non-Bt corn).

Non-Bt corn	
Metabolite	**VIP**
Aconitate	1.270442
Allantoate	1.113153
Allantoin	1.229113
Arginine	1.076257
Asparagine	1.048857
Carnosine	1.141665
CDP-ethanolamine	1.074607
Citrulline	1.495999
Cysteine	1.010926
Cystine	1.170498
D-Glucarate	1.338905
D-Gluconate	1.063588
dAMP	1.087411
dCMP	1.184152
Deoxyinosine	1.193241
Dihydroorotate	1.06682
dTMP	1.097837
Gluconolactone	1.004605
Glucosamine	1.047819
Glucosamine-phosphate	1.184419
Glycinamide ribotide	1.060954
Guanine	1.141443

Table 3.7 continued

Non-Bt corn	
Metabolite	**VIP**
Histamine	1.112823
Homocysteine	1.085283
Homoserine/Threonine	1.062079
Hydroxyisocaproic acid	1.338013
Hydroxyphenylacetate	1.298028
Hydroxyphenylpyruvate	1.147521
Inosine	1.278357
L-Methionine	1.033041
Lactate	1.07915
N-Acetylglutamate	1.008494
N-Acetylglutamine	1.229924
NADP	1.019977
Ophthalmate	1.26713
Ornithine	1.089846
Orotate	1.352433
Pantothenate	1.129363
Phenyllactic acid	1.287237
Phenylpyruvate	1.04756
Pyridoxine	1.236147
Pyroglutamic acid	1.250988
Pyruvate	1.03419
S-Ribosyl L-homocysteine	1.277389
Salicylate	1.347085
Sedoheptulose 1/7-phosphate	1.066303
Thymine	1.015487

Table 3.7 continued

Non-Bt corn	
Metabolite	**VIP**
Trehalose 6-phosphate	1.261634
UDP glucose	1.098695
UDP N-acetylglucosamine	1.021573
Uracil	1.0281
Uric acid	1.227349
Uridine	1.024358
2-Hydroxy-2-methylsuccinate	1.265096
2-Isopropylmalate	1.038259
2-Oxoglutaric.acid	1.123791
2-3-Dihydroxybenzoate	1.033859
3 Hydroxyisovaleric acid	1.266799
3-Phosphoserine	1.361203
6-Phospho-D-gluconolactone	1.011822
Xanthine	1.001263
Xanthurenic acid	1.048492
Xylitol 5-phosphate	1.114975

Table 3.8 Ratios and p-values used to make heat map for samples fed meridic diet

Metabolite	Ratio			p-value		
	Ben	456F	456M	Ben	456F	456M
Pyruvate	1.57	1.35	1.43	0.0775	0.0948	0.1280
Alanine/Sarcosine	0.85	0.97	0.92	0.1046	0.7850	0.4182
Lactate	2.94	3.13	2.10	0.0222	0.2915	0.1921
4-Aminobutyrate (GABA)	0.63	0.86	0.77	0.0083	0.2272	0.0576
Alanine/Sarcosine	0.85	0.97	0.92	0.1046	0.7850	0.4182
Lactate	2.94	3.13	2.10	0.0222	0.2915	0.1921
4-Aminobutyrate (GABA)	0.63	0.86	0.77	0.0083	0.2272	0.0576
Serine	1.56	0.85	1.13	0.2225	0.2431	0.5062
Histamine	0.67	0.85	0.81	0.0446	0.2873	0.0965
Uracil	1.37	0.71	0.70	0.1169	0.1812	0.1952
Proline	0.67	0.75	0.80	0.0178	0.1250	0.0718
Fumarate	0.78	1.13	1.12	0.0397	0.1917	0.2547
2-Oxoisovalerate	0.90	0.91	0.85	0.1211	0.4985	0.1406
Indole	0.91	1.30	1.51	0.6931	0.2791	0.2242
Valine	0.76	0.86	0.85	0.0231	0.2407	0.1884

Table 3.8 continued

Metabolite	Ratio		p-value			
	Ben	456F	Ben	456F	Ben	456F
Succinate/Methylmalonate	0.97	0.87	0.90	0.8014	0.3359	0.3232
3-Hydroxyisovaleric acid	7.63	6.19	4.71	0.0188	0.2140	0.1249
Homoserine/Threonine	0.61	0.75	0.77	0.0191	0.0988	0.0738
Cysteine	0.81	0.49	0.43	0.1619	0.0045	0.0026
Nicotinate	1.18	1.07	1.01	0.0238	0.5412	0.8845
Taurine	0.58	0.97	1.05	0.0111	0.9001	0.8150
Thymine	0.98	0.85	1.03	0.8845	0.3650	0.9077
Pyroglutamic acid	0.79	0.71	0.69	0.0290	0.0636	0.0197
N-Acetyl-beta-alanine	0.64	0.81	0.74	0.0426	0.1998	0.1270
Hydroxyproline	0.89	0.86	0.74	0.4975	0.3463	0.1903
Leucine/Isoleucine	0.83	0.88	0.90	0.0874	0.3097	0.2915
Asparagine	0.73	0.79	0.82	0.0020	0.0300	0.0153
Hydroxyisocaproic acid	10.12	8.95	5.01	0.0175	0.2395	0.1111
Ornithine	1.01	0.98		0.9107	0.8757	0.9152
Aspartate	0.57	0.93	0.82	0.0375	0.5978	0.1601
Malate	0.81	1.02	1.03	0.0428	0.8475	0.7458

Table 3.8 continued

Metabolite	Ratio		p-value			
	Ben	456F	Ben	456F	Ben	456F
Homocysteine	0.85	0.90	0.78	0.0248	0.5150	0.1914
Anthranilate	2.75	0.60	0.70	0.0029	0.0597	0.1904
Salicylate	1.02	0.98	0.90	0.9346	0.9225	0.2594
Hydroxybenzoate	0.91	1.27	0.79	0.6875	0.3417	0.3766
2-Oxoglutaric acid	0.88	0.79	0.75	0.5437	0.3483	0.0778
Glutamine	0.77	0.80	0.90	0.0420	0.1038	0.3263
Lysine	0.81	0.89	0.76	0.1523	0.3940	0.1007
Glutamate	0.88	0.98	0.92	0.2601	0.8676	0.4567
2-Hydroxy-2-methylsuccinate	2.18	1.54	1.23	0.0036	0.4428	0.5739
L-Methionine	0.87	0.86	0.85	0.2437	0.1391	0.0418
Guanine	1.56	2.12	1.79	0.3943	0.0048	0.1527
Xanthine	3.05	2.02	2.15	0.1190	0.1547	0.1604
Hydroxyphenylacetate	2.51	3.23	2.62	0.0070	0.0024	0.0445
Xylitol	1.13	1.18	1.18	0.3618	0.3202	0.3351
2_3-Dihydroxybenzoate	0.98	0.97	1.01	0.8806	0.8439	0.9491

Table 3.8 continued

Metabolite	Ratio		p-value			
	Ben	456F	Ben	456F	Ben	456F
Histidine	0.74	0.86	0.87	0.0215	0.1981	0.1757
Orotate	1.03	1.03	0.90	0.9221	0.9165	0.7181
Dihydroorotate	3.95	1.62	1.60	0.2400	0.1691	0.4404
Allantoin	1.03	1.33	1.23	0.8556	0.1725	0.1659
2-Aminoadipate	0.68	1.01	0.85	0.1364	0.9475	0.4154
Phenylpyruvate	11.59	6.40	5.07	0.0412	0.2545	0.1017
Phenylalanine	0.94	0.86	1.00	0.5047	0.2911	0.9885
Phenyllactic acid	2.81	3.50	2.43	0.0343	0.2679	0.0843
Phosphoenolpyruvate	0.99	0.74	1.16	0.9837	0.6711	0.8350
Uric acid	0.62	0.51	0.70	0.0735	0.1611	0.1778
Cysteate	1.09	0.99	0.69	0.3941	0.9484	0.0347
Pyridoxine	1.44	1.24	1.18	0.0686	0.0495	0.1149
Sulfolactate	0.83	0.61	0.60	0.0744	0.0071	0.0027
Glycerone phosphate	0.66	0.72	0.76	0.0251	0.0475	0.0711
sn-Glycerol 3-phosphate	0.82	0.87	0.87	0.2319	0.4211	0.4942
Aconitate	0.93	0.87	0.68	0.6470	0.4229	0.0023

Table 3.8 continued

Metabolite	Ratio		p-value			
	Ben	456F	Ben	456F	Ben	456F
N-Acetylornithine	1.20	0.93	0.94	0.0038	0.3985	0.7472
Arginine	0.81	0.80	0.89	0.1312	0.0584	0.2586
Citrulline	2.73	2.42	2.01	0.0733	0.2422	0.1075
N-Carbamoyl-L-aspartate	1.81	1.68	1.15	0.0657	0.0908	0.5871
Allantoate	0.70	1.15	1.14	0.0198	0.2700	0.2691
2-Isopropylmalate	0.62	1.28	1.31	0.0737	0.3340	0.3914
Gluconolactone	1.10	0.63	0.61	0.4120	0.0518	0.0323
Glucosamine	0.89	0.59	0.58	0.4752	0.0476	0.1054
Hydroxyphenylpyruvate	2.26	1.58	1.55	0.0090	0.1755	0.0592
myo-Inositol	1.12	0.99	1.26	0.3648	0.9372	0.4772
Tyrosine	0.82	0.94	1.13	0.1191	0.6700	0.5717
4-Pyridoxate	1.26	1.27	1.43	0.1927	0.3647	0.2110
3-Phosphoserine	0.56	0.55	0.38	0.0920	0.1181	0.0285
N-Acetylglutamine	1.04	0.53	0.59	0.7851	0.0028	0.0088
Acetyllysine	1.46	0.77	0.83	0.2072	0.1631	0.5093
N-Acetylglutamate	2.38	2.97	2.29	0.1365	0.2406	0.2470

Table 3.8 continued

Metabolite	Ratio		p-value			
	Ben	456F	Ben	456F	Ben	456F
2-Dehydro-D-gluconate	0.67	1.01	0.85	0.0097	0.9105	0.1717
D-Gluconate	0.81	0.97	0.67	0.0616	0.8352	0.0034
D-Erythrose 4-phosphate	0.44	0.78	0.78	0.0049	0.1009	0.3436
N-N Dimethylarginine	0.78	0.92	0.90	0.2855	0.7165	0.6215
Tryptophan	0.91	1.19	1.30	0.3256	0.2917	0.2196
Xanthurenic acid	0.73	1.13	1.16	0.1185	0.6654	0.3240
D-Glucarate	0.95	1.38	1.25	0.6531	0.2557	0.4385
Pantothenate	0.78	1.05	0.94	0.0130	0.4581	0.3634
N-Acetylglucosamine	0.94	0.84	0.82	0.7359	0.4260	0.3699
Cystathionine	0.81	1.04	1.01	0.3195	0.8123	0.9433
Carnosine	1.49	1.40	1.77	0.0833	0.3519	0.2041
Ribose phosphate	0.75	0.92	0.78	0.0076	0.5605	0.0098
Xylitol 5-phosphate	0.46	0.66	0.63	0.0107	0.0642	0.0569
Cystine	0.76	0.53	0.62	0.4356	0.1022	0.1906
Cytidine	0.53	0.79	1.09	0.0022	0.3419	0.6528
Uridine	0.66	0.63	0.70	0.1079	0.0907	0.1443

Table 3.8 continued

Metabolite	Ratio		p-value			
	Ben	456F	Ben	456F	Ben	456F
Deoxyinosine	0.92	0.89	0.77	0.6567	0.3643	0.0141
6-Phospho-D-gluconolactone	1.53	1.48	1.22	0.4029	0.2858	0.4819
Glucosamine phosphate	0.94	0.90	0.79	0.7055	0.4559	0.2023
Glucose 6-phosphate	1.40	1.07	1.24	0.3684	0.6342	0.2473
S-Ribosyl-L-homocysteine	1.11	0.76	0.76	0.3107	0.0778	0.1239
Adenosine	0.64	0.83	0.80	0.0547	0.3198	0.2341
Inosine	2.28	1.01	0.98	0.0249	0.9730	0.9225
6-Phospho-D-gluconate	1.40	0.51	0.41	0.6506	0.0209	0.0119
1-Methyladenosine	1.03	1.23	1.15	0.7965	0.3930	0.3437
Guanosine	1.61	0.97	0.93	0.0845	0.9057	0.7083
Glycinamide ribotide (GAR)	0.54	0.55	1.84	0.2717	0.1957	0.5969
Ophthalmate	0.41	0.60	0.55	0.0947	0.2174	0.1764
Sedoheptulose 1/7-phosphate	0.55	0.72	0.56	0.0002	0.0230	0.0001

Table 3.8 continued

Metabolite	Ratio		p-value			
	Ben	456F	Ben	456F	Ben	456F
N-Acetylglucosamine1/6-phosphate	0.88	0.88	0.92	0.2164	0.3120	0.4544
dCMP	0.34	0.65	0.53	0.0007	0.0165	0.0022
Glutathione	0.89	1.06	0.92	0.1784	0.3646	0.2829
dTMP	0.31	0.63	0.46	0.0037	0.0466	0.0093
CMP	0.75	1.02	1.03	0.0210	0.8175	0.7826
UMP	0.76	0.92	0.95	0.0221	0.3654	0.5922
dAMP	0.28	0.67	0.51	0.0011	0.0270	0.0058
AICAR	0.49	0.94	1.24	0.0237	0.7219	0.2680
Trehalose/Sucrose/ Cellobiose	0.68	1.21	1.15	0.1624	0.4500	0.4930
AMP/dGMP	0.75	0.82	0.85	0.0035	0.0710	0.0440
IMP	0.89	0.70	0.95	0.4300	0.1000	0.7965
GMP	0.73	0.93	0.89	0.0098	0.4703	0.1478
Riboflavin	0.71	1.41	1.59	0.2250	0.3287	0.5285

Table 3.8 continued

Metabolite	Ratio		p-value			
	Ben	456F	Ben	456F	Ben	456F
S-Adenosyl-L-homocysteine	0.93	0.45	0.49	0.5893	0.0068	0.0083
Trehalose 6-phosphate	0.76	0.74	0.62	0.0048	0.0449	0.0003
CDP-ethanolamine	0.80	0.86	0.81	0.2387	0.4075	0.3003
UDP-glucose	0.85	0.98	0.91	0.0631	0.8048	0.2041
UDP-N-acetylglucosamine	0.95	0.91	0.98	0.4746	0.4185	0.7811
Glutathione disulfide	0.97	1.81	1.36	0.8872	0.0375	0.0207
NAD+	0.79	0.89	1.00	0.0175	0.4182	0.9832
NADP+	0.95	0.56	0.72	0.8960	0.3236	0.5341
FAD	1.25	0.86	0.89	0.6160	0.8003	0.8073

Table 3.9 Ratios and p-values used to make heat map for samples fed non-Bt corn

Metabolite	Ratio		p-value			
	Ben	456F	Ben	456F	Ben	456F
Pyruvate	1.00	0.88	1.48	0.9940	0.5910	0.2677
Alanine/Sarcosine	1.16	1.10	1.18	0.5336	0.6927	0.4629
Lactate	1.57	1.11	1.51	0.1067	0.5861	0.0290
4-Aminobutyrate (GABA)	0.94	1.32	1.09	0.8029	0.2818	0.7453
Serine	0.97	0.97	0.93	0.9154	0.9031	0.7662
Histamine	0.74	0.51	0.77	0.2605	0.0455	0.2977
Uracil	1.82	1.00	1.28	0.0608	0.9961	0.3571
Proline	1.10	1.07	1.25	0.6906	0.6835	0.2153
Fumarate	1.40	1.45	1.31	0.3033	0.1039	0.2237
2-Oxoisovalerate	0.67	0.69	0.69	0.0826	0.0455	0.0369
Indole	1.21	1.28	0.85	0.6587	0.5741	0.6910
Valine	1.01	0.87	0.89	0.9743	0.5563	0.6240
Succinate/Methylmalonate	1.49	1.27	1.19	0.1797	0.3914	0.5299
3-Hydroxyisovaleric acid	2.54	2.03	3.05	0.0205	0.0089	0.0141
Homoserine/Threonine	1.19	0.88	1.18	0.3743	0.5077	0.3501

Table 3.9 continued

Metabolite	Ratio		p-value			
	Ben	456F	Ben	456F	Ben	456F
Cysteine	0.75	0.56	0.81	0.0806	0.1063	0.3156
Nicotinate	1.00	1.12	1.26	0.9943	0.5585	0.2053
Taurine	0.64	1.00	0.69	0.3849	0.9920	0.4408
Thymine	1.06	1.23	1.72	0.8342	0.5033	0.1316
Pyroglutamic acid	0.78	0.57	0.86	0.1779	0.0121	0.3873
N-Acetyl-beta-alanine	1.04	1.34	1.32	0.8736	0.0591	0.1383
Hydroxyproline	0.99	1.17	1.16	0.9777	0.5437	0.5450
Leucine/Isoleucine	1.08	0.91	0.88	0.7168	0.6838	0.5811
Asparagine	2.30	0.87	1.34	0.0942	0.4707	0.3344
Hydroxyisocaproic acid	6.75	3.06	6.20	0.0265	0.0005	0.0039
Ornithine	0.95	0.93	1.26	0.8099	0.7309	0.3054
Aspartate	0.89	0.66	0.66	0.6553	0.2030	0.2129
Malate	1.33	1.27	1.20	0.3380	0.2118	0.3306
Homocysteine	0.54	0.87	0.82	0.0449	0.4549	0.3467
Anthranilate	1.26	1.02	0.97	0.4852	0.9648	0.9476
Salicylate	1.26	2.53	5.37	0.4204	0.0040	0.0794

Table 3.9 continued

Metabolite	Ratio		p-value			
	Ben	456F	Ben	456F	Ben	456F
Hydroxybenzoate	0.71	0.69	0.54	0.4029	0.3930	0.2144
2-Oxoglutaric acid	0.57	0.51	0.58	0.0893	0.0104	0.0187
Glutamine	1.17	0.88	0.86	0.5814	0.3957	0.5042
Lysine	0.85	0.87	1.11	0.5117	0.4541	0.5887
Glutamate	1.05	1.04	0.98	0.8318	0.7597	0.8850
2-Hydroxy-2-methylsuccinate	2.15	1.20	1.96	0.0395	0.3954	0.0007
L-Methionine	1.20	0.71	0.95	0.4285	0.1869	0.8055
Guanine	0.72	0.19	0.38	0.4301	0.0548	0.0998
Xanthine	1.89	1.31	1.81	0.1003	0.2743	0.0388
Hydroxyphenylacetate	1.31	13.26	6.81	0.2486	0.0497	0.1554
Xylitol	1.48	1.45	1.60	0.1916	0.1883	0.1533
2_3-Dihydroxybenzoate	1.40	0.66	0.98	0.0790	0.1192	0.9529
Histidine	0.91	0.71	0.92	0.7047	0.1452	0.6588
Orotate	4.24	1.11	0.65	0.0481	0.8335	0.2073
Dihydroorotate	1.02	0.39	0.46	0.9678	0.0433	0.0653

Table 3.9 continued

Metabolite	Ratio		p-value			
	Ben	456F	Ben	456F	Ben	456F
Allantoin	1.08	1.42	1.90	0.6644	0.2853	0.0023
2-Aminoadipate	0.91	1.33	1.10	0.7361	0.4305	0.7514
Phenylpyruvate	1.59	0.85	1.16	0.0927	0.4200	0.6071
Phenylalanine	1.11	0.88	1.00	0.6520	0.5610	0.9865
Phenyllactic acid	2.43	1.80	1.69	0.0034	0.0145	0.0443
Phosphoenolpyruvate	1.59	1.23	0.69	0.4702	0.7799	0.6359
Uric acid	2.86	3.12	1.76	0.1893	0.0214	0.0056
Cysteate	0.84	1.10	1.09	0.4289	0.6560	0.7245
Pyridoxine	1.08	1.61	1.14	0.7476	0.0456	0.6334
Sulfolactate	1.07	0.73	0.85	0.6722	0.0939	0.4888
Glycerone phosphate	0.86	0.66	0.62	0.5225	0.1057	0.0649
sn-Glycerol 3-phosphate	1.21	0.99	0.78	0.5281	0.9807	0.3504
Aconitate	1.23	0.53	0.45	0.3290	0.0674	0.0426
N-Acetylornithine	1.59	1.15	1.54	0.1309	0.5123	0.0721
Arginine	0.68	0.67	0.74	0.1092	0.1081	0.1802
Citrulline	2.15	1.51	3.88	0.0169	0.1928	0.0212

Table 3.9 continued

Metabolite	Ratio		p-value			
	Ben	456F	Ben	456F	Ben	456F
N-Carbamoyl-L-aspartate	1.38	0.93	1.07	0.0872	0.7818	0.8379
Allantoate	0.97	1.00	1.26	0.8300	0.9850	0.1354
2-Isopropylmalate	0.44	0.39	0.45	0.0085	0.0069	0.0387
Gluconolactone	1.49	0.98	0.88	0.1977	0.9330	0.6078
Glucosamine	0.45	0.91	0.52	0.1936	0.8069	0.2529
Hydroxyphenylpyruvate	1.66	0.46	0.52	0.1655	0.0444	0.0750
myo-Inositol	1.24	1.09	0.93	0.4709	0.6504	0.5893
Tyrosine	1.08	1.10	0.84	0.8034	0.6812	0.4640
4-Pyridoxate	1.58	1.01	0.98	0.1528	0.9681	0.9541
3-Phosphoserine	0.24	0.11	0.29	0.0067	0.0064	0.0064
N-Acetylglutamine	1.24	0.30	0.64	0.4442	0.0002	0.1117
Acetyllysine	1.60	0.74	0.94	0.4071	0.2177	0.7337
N-Acetylglutamate	1.56	1.55	1.25	0.0784	0.1584	0.2524
2-Dehydro-D-gluconate	1.16	0.89	0.84	0.4794	0.4719	0.2915
D-Gluconate	1.48	1.02	0.88	0.1518	0.9283	0.4951
D-Erythrose 4-phosphate	1.17	1.53	1.22	0.6347	0.2965	0.4706

Table 3.9 continued

Metabolite	Ratio		p-value			
	Ben	456F	Ben	456F	Ben	456F
N-N Dimethylarginine	0.67	0.65	0.62	0.1355	0.1291	0.1031
Tryptophan	1.10	1.20	0.88	0.7581	0.5066	0.6398
Xanthurenic acid	0.89	0.33	0.42	0.7211	0.0417	0.0641
D-Glucarate	1.13	0.63	0.55	0.3620	0.0359	0.0143
Pantothenate	0.98	1.44	1.06	0.9582	0.0722	0.7715
N-Acetylglucosamine	1.94	3.26	1.85	0.3710	0.3247	0.3718
Cystathionine	0.64	1.03	0.95	0.1622	0.9075	0.8684
Carnosine	0.58	0.92	0.51	0.0902	0.7689	0.0396
Ribose phosphate	0.92	0.78	0.81	0.5439	0.0904	0.1388
Xylitol 5-phosphate	0.95	0.91	0.67	0.8135	0.6455	0.1278
Cystine	0.33	0.60	0.59	0.0147	0.0790	0.0787
Cytidine	0.91	1.04	1.04	0.6160	0.8253	0.7168
Uridine	1.45	0.74	1.06	0.2570	0.2494	0.7548
Deoxyinosine	1.46	0.66	0.66	0.1009	0.1527	0.1578
6-Phospho-D-gluconolactone	0.75	0.60	0.57	0.2695	0.1029	0.0893

Table 3.9 continued

Metabolite	Ratio		p-value			
	Ben	456F	Ben	456F	Ben	456F
Glucosamine phosphate	1.69	1.33	1.90	0.0872	0.2633	0.0072
Glucose 6-phosphate	1.62	1.31	1.26	0.1913	0.1041	0.1770
S-Ribosyl-L-homocysteine	2.51	1.84	2.56	0.0059	0.0831	0.0449
Adenosine	1.50	1.25	0.95	0.2341	0.4838	0.9083
Tyrosine	1.08	1.10	0.84	0.8034	0.6812	0.4640
4-Pyridoxate	1.58	1.01	0.98	0.1528	0.9681	0.9541
3-Phosphoserine	0.24	0.11	0.29	0.0067	0.0064	0.0064
N-Acetylglutamine	1.24	0.30	0.64	0.4442	0.0002	0.1117
Acetyllysine	1.60	0.74	0.94	0.4071	0.2177	0.7337
N-Acetylglutamate	1.56	1.55	1.25	0.0784	0.1584	0.2524
2-Dehydro-D-gluconate	1.16	0.89	0.84	0.4794	0.4719	0.2915
D-Gluconate	1.48	1.02	0.88	0.1518	0.9283	0.4951
D-Erythrose 4-phosphate	1.17	1.53	1.22	0.6347	0.2965	0.4706
N-N Dimethylarginine	0.67	0.65	0.62	0.1355	0.1291	0.1031
Tryptophan	1.10	1.20	0.88	0.7581	0.5066	0.6398
Xanthurenic acid	0.89	0.33	0.42	0.7211	0.0417	0.0641

Table 3.9 continued

Metabolite	Ratio		p-value			
	Ben	456F	Ben	456F	Ben	456F
D-Glucarate	1.13	0.63	0.55	0.3620	0.0359	0.0143
Pantothenate	0.98	1.44	1.06	0.9582	0.0722	0.7715
N-Acetylglucosamine	1.94	3.26	1.85	0.3710	0.3247	0.3718
Cystathionine	0.64	1.03	0.95	0.1622	0.9075	0.8684
Carnosine	0.58	0.92	0.51	0.0902	0.7689	0.0396
Ribose phosphate	0.92	0.78	0.81	0.5439	0.0904	0.1388
Xylitol 5-phosphate	0.95	0.91	0.67	0.8135	0.6455	0.1278
Cystine	0.33	0.60	0.59	0.0147	0.0790	0.0787
Cytidine	0.91	1.04	1.04	0.6160	0.8253	0.7168
Uridine	1.45	0.74	1.06	0.2570	0.2494	0.7548
Deoxyinosine	1.46	0.66	0.66	0.1009	0.1527	0.1578
6-Phospho-D-gluconolactone	0.75	0.60	0.57	0.2695	0.1029	0.0893
Glucosamine phosphate	1.69	1.33	1.90	0.0872	0.2633	0.0072
Glucose 6-phosphate	1.62	1.31	1.26	0.1913	0.1041	0.1770
S-Ribosyl-L-homocysteine	2.51	1.84	2.56	0.0059	0.0831	0.0449

Table 3.9 continued

	Ratio			p-value		
	Ben	456F	Ben	456F	Ben	456F
Adenosine	1.50	1.25	0.95	0.2341	0.4838	0.9083
Inosine	2.52	0.71	1.19	0.0147	0.1845	0.4339
6-Phospho-D-gluconate	0.64	0.46	0.44	0.3314	0.1617	0.1542
1-Methyladenosine	2.13	3.63	1.95	0.3329	0.3005	0.3602
Guanosine	1.42	0.90	1.07	0.2081	0.6313	0.7290
Glycinamide ribotide (GAR)	0.25	0.25	0.21	0.1342	0.1321	0.1209
Ophthalmate	0.65	0.26	0.76	0.3455	0.0495	0.4542
Sedoheptulose 1/7phosphate	0.78	0.57	0.58	0.2351	0.0475	0.0496
N-Acetylglucosamine 1/6-phosphate	1.08	0.98	0.87	0.7469	0.9045	0.3904
dCMP	0.28	0.23	0.25	0.0563	0.0448	0.0528
Glutathione	1.19	1.03	1.55	0.4646	0.9310	0.2428
dTMP	0.38	0.36	0.39	0.0657	0.0615	0.0685
CMP	0.92	1.03	0.90	0.7492	0.8693	0.5591
UMP	0.91	0.84	0.78	0.7115	0.3894	0.2398

Table 3.9 continued

Metabolite	Ratio		p-value			
	Ben	456F	Ben	456F	Ben	456F
dAMP	0.47	0.57	0.47	0.0476	0.0860	0.0495
AICAR	0.92	0.47	0.65	0.8410	0.0504	0.2252
Trehalose/Sucrose /Cellobiose	0.78	0.97	0.69	0.4786	0.9335	0.3365
AMP/dGMP	0.87	0.84	0.81	0.5128	0.3719	0.2974
IMP	1.48	0.93	1.07	0.2506	0.8385	0.8420
GMP	0.81	0.91	0.77	0.3051	0.5696	0.1853
Riboflavin	1.09	1.33	1.01	0.8576	0.4401	0.9778
S-Adenosyl-L-homocysteine	1.34	0.97	1.13	0.1014	0.8139	0.5253
Trehalose 6-phosphate	3.72	1.46	0.98	0.0810	0.2847	0.9454
CDP-ethanolamine	0.70	0.89	0.89	0.0510	0.3471	0.4215
UDP-glucose	0.97	0.59	0.74	0.8389	0.0303	0.1089
UDP-N-acetylglucosamine	1.14	0.70	0.85	0.4585	0.0443	0.2062
Glutathione disulfide	1.14	1.43	1.68	0.6086	0.1809	0.1554
NAD+	0.92	0.76	0.77	0.7297	0.2782	0.2935

Table 3.9 continued

Metabolite	Ratio		p-value			
	Ben	456F	Ben	456F	Ben	456F
NADP+	1.24	1.37	0.56	0.6605	0.4779	0.2754
FAD	1.31	1.24	0.65	0.6349	0.5540	0.3473

CONCLUSION

This dissertation has showcased three different systems each with a different goal, but all benefiting greatly from the use of metabolomics. Even though there will never be a single universal method for the detection of all metabolites, metabolomics is now being used as a screening tool that helps guide researchers into asking the right questions, and less of an approach to verify hypotheses. Metabolomics is a very powerful tool and the technique is becoming requested more by researchers outside of chemistry. As protocols and techniques become more standardized, publicly accessible libraries and databases will begin to flourish, fostering interdisciplinary work, and reducing the knowledge gap between the metabolite level and the phenotype observed. Those without specialized training can now start comprehending the data and what it means in the context of their system. No longer will there be chemists producing gigabytes of data, passing that off to the biologist, and neither knowing what the data really means.

As shown by the first chapter of this dissertation, metabolomics provides a great framework for hypothesis generating experiments. It was shown that if a bacterial cell loses the ability to produce a single enzyme, it is possible to keep growing without drastic morphological effects, but the small molecules that are present provide a unique pattern. Over 2,000 metabolite-like features indicated there is a global shift in metabolite intensities due to a single genetic mutation. Not all mutations are created equal either. Even if there are two effected enzymes in the same cycle, they will both produce a unique metabolic signature. In addition to monitoring metabolites from a global perspective, individual metabolites and the associated turnover rates were monitored. This analysis pushed the barriers of science by collecting information about metabolites that have not yet been identified. By beginning to identify these metabolites and their roles, scientists can continue to complete the understanding of metabolism.

In a completely different avenue of metabolomics I was able to develop a targeted method using a hybrid Orbitrap. Instead of using the data to make theories

about a physical phenomenon, the goal was to connect specific lipids and their changes to the bacteria's tolerance to antibiotics. Tolerance was only observed when the organism comes into contact with unsaturated fats produced by mammals. By using parallel reaction monitoring, it was possible to not only quantify specific lipids, but also learn about how these exogenous fats were restructuring the bacterial membrane. Since this method had detection limits on the order of 50 nM, it was possible to quantify even the smallest lipid change from relatively few cells. Currently, this method is being used to asses genetically modified bacteria and correlate the relationship between lipid levels and antibiotic tolerance.

The third chapter of this dissertation exemplifies the diversity of metabolomic analyses on complex systems, and its ability to answer very specific questions. The goal of this experiment was to determine what metabolites were directly connected to the resistance of a toxin in the fall armyworm. The insect investigated developed a genetic mutation that allowed it to feed on a once toxic food source. This toxin resistance was previously examined from a genomic and proteomic standpoint, but this was first time a small molecule analysis was performed. By combining several omics approaches together, it becomes possible to start understanding how metabolism works as a whole to produce an organism that is resistant. By identifying specific metabolites that significantly accumulate in the resistant strains, researches can learn what substrates are being used by the protein of interest and create new, targeted technologies to block this mode of action. This research had culminated in providing a finite list of metabolites that show promise as candidates for further investigations.

Taken together, metabolomic analyses are capable to providing insight into many of the most complex and challenging biological processes. What is presented here are only the highlights of the many types of samples and techniques I have been a part of for the last four and a half years. I feel my contributions to the field of metabolomics will strengthen and further the knowledge

for not only those chemists who work in the laboratory but also for those scientists in other disciplines who seek insight into understanding life's complex actions.

REFERENCES

1. Bodner, G. M., Metabolism Part II: The tricarboxylic acid (TCA), citric acid, or Krebs cycle. *Journal of Chemical Education* **1986,** *63* (8), 673.

2. Papagianni, M., Recent advances in engineering the central carbon metabolism of industrially important bacteria. *Microbial Cell Factories* **2012,** *11* (1), 50.

3. Lind, P. A.; Berg, O. G.; Andersson, D. I., Mutational Robustness of Ribosomal Protein Genes. *Science* **2010,** *330* (6005), 825-827.

4. Bazurto, J. V.; Dearth, S. P.; Tague, E. D.; Campagna, S. R.; Downs, D. M., Untargeted metabolomics confirms and extends the understanding of the impact of aminoimidazole carboxamide ribotide (AICAR) in the metabolic network of Salmonella enterica. *Microbial cell (Graz, Austria)* **2017,** *5* (2), 74-87.

5. Dearth, S. P.; Castro, H. F.; Venice, F.; Tague, E. D.; Novero, M.; Bonfante, P.; Campagna, S. R., Metabolome changes are induced in the arbuscular mycorrhizal fungus Gigaspora margarita by germination and by its bacterial endosymbiont. *Mycorrhiza* **2018,** *28* (5), 421-433.

6. Winter, G.; Krömer, J. O., Fluxomics – connecting 'omics analysis and phenotypes. *Environmental Microbiology* **2013,** *15* (7), 1901-1916.

7. Blattner, F. R.; Plunkett, G.; Bloch, C. A.; Perna, N. T.; Burland, V.; Riley, M.; Collado-Vides, J.; Glasner, J. D.; Rode, C. K.; Mayhew, G. F.; Gregor, J.; Davis, N. W.; Kirkpatrick, H. A.; Goeden, M. A.; Rose, D. J.; Mau, B.; Shao, Y., The Complete Genome Sequence of Escherichia coli K-12. *Science* **1997,** *277* (5331), 1453-1462.

8. Gonidakis, S.; Finkel, S. E.; Longo, V. D., Genome-wide screen identifies Escherichia coli TCA-cycle-related mutants with extended chronological lifespan dependent on acetate metabolism and the hypoxia-inducible transcription factor ArcA. *Aging cell* **2010,** *9* (5), 868-81.

9. Matsuoka, Y.; Shimizu, K., Metabolic regulation of Escherichia coli cultivated under anaerobic and aerobic conditions in response to the specific pathway gene knockouts. *Advances in Bioscience and Biotechnology* **2013,** *4* (3A), 455.

10. Steinsiek, S.; Stagge, S.; Bettenbrock, K., Analysis of Escherichia coli mutants with a linear respiratory chain. *PloS one* **2014,** *9* (1), e87307.

11. Ishii, N.; Nakahigashi, K.; Baba, T.; Robert, M.; Soga, T.; Kanai, A.; Hirasawa, T.; Naba, M.; Hirai, K.; Hoque, A.; Ho, P. Y.; Kakazu, Y.; Sugawara, K.; Igarashi, S.; Harada, S.; Masuda, T.; Sugiyama, N.; Togashi, T.; Hasegawa, M.; Takai, Y.; Yugi, K.; Arakawa, K.; Iwata, N.; Toya, Y.; Nakayama, Y.; Nishioka, T.;

Shimizu, K.; Mori, H.; Tomita, M., Multiple High-Throughput Analyses Monitor the Response of E. coli to Perturbations. *Science* **2007,** *316* (5824), 593-597.

12. Bennett, B. D.; Kimball, E. H.; Gao, M.; Osterhout, R.; Van Dien, S. J.; Rabinowitz, J. D., Absolute metabolite concentrations and implied enzyme active site occupancy in Escherichia coli. *Nat Chem Biol* **2009,** *5* (8), 593-599.

13. Datsenko, K. A.; Wanner, B. L., One-step inactivation of chromosomal genes in Escherichia coli K-12 using PCR products. *Proceedings of the National Academy of Sciences* **2000,** *97* (12), 6640-6645.

14. Yu, D.; Ellis, H. M.; Lee, E.-C.; Jenkins, N. A.; Copeland, N. G.; Court, D. L., An efficient recombination system for chromosome engineering in Escherichia coli. *Proceedings of the National Academy of Sciences* **2000,** *97* (11), 5978-5983.

15. Court, D. L.; Swaminathan, S.; Yu, D.; Wilson, H.; Baker, T.; Bubunenko, M.; Sawitzke, J.; Sharan, S. K., Mini-λ: a tractable system for chromosome and BAC engineering. *Gene* **2003,** *315*, 63-69.

16. Fozo, E. M.; Kawano, M.; Fontaine, F.; Kaya, Y.; Mendieta, K. S.; Jones, K. L.; Ocampo, A.; Rudd, K. E.; Storz, G., Repression of small toxic protein synthesis by the Sib and OhsC small RNAs. *Molecular Microbiology* **2008,** *70* (5), 1076-1093.

17. Yuan, J.; Bennett, B. D.; Rabinowitz, J. D., Kinetic flux profiling for quantitation of cellular metabolic fluxes. *Nat. Protocols* **2008,** *3* (8), 1328-1340.

18. Rabinowitz, J. D.; Kimball, E., Acidic Acetonitrile for Cellular Metabolome Extraction from Escherichia coli. *Analytical Chemistry* **2007,** *79* (16), 6167-6173.

19. Lu, W.; Clasquin, M. F.; Melamud, E.; Amador-Noguez, D.; Caudy, A. A.; Rabinowitz, J. D., Metabolomic analysis via reversed-phase ion-pairing liquid chromatography coupled to a stand alone orbitrap mass spectrometer. *Analytical Chemistry* **2010,** *82* (8), 3212-3221.

20. Guan, X. L.; Riezman, I.; Wenk, M. R.; Riezman, H., Chapter 15 - Yeast Lipid Analysis and Quantification by Mass Spectrometry. In *Methods in Enzymology*, Academic Press: 2010; Vol. Volume 470, pp 369-391.

21. Cassilly, C. D.; Farmer, A. T.; Montedonico, A. E.; Smith, T. K.; Campagna, S. R.; Reynolds, T. B., Role of phosphatidylserine synthase in shaping the phospholipidome of Candida albicans. *FEMS Yeast Research* **2017,** *17* (2), fox007-fox007.

22. Chambers, M. C.; Maclean, B.; Burke, R.; Amodei, D.; Ruderman, D. L.; Neumann, S.; Gatto, L.; Fischer, B.; Pratt, B.; Egertson, J.; Hoff, K.; Kessner, D.; Tasman, N.; Shulman, N.; Frewen, B.; Baker, T. A.; Brusniak, M.-Y.; Paulse, C.; Creasy, D.; Flashner, L.; Kani, K.; Moulding, C.; Seymour, S. L.; Nuwaysir, L. M.; Lefebvre, B.; Kuhlmann, F.; Roark, J.; Rainer, P.; Detlev, S.; Hemenway, T.; Huhmer, A.; Langridge, J.; Connolly, B.; Chadick, T.; Holly, K.; Eckels, J.; Deutsch, E. W.; Moritz, R. L.; Katz, J. E.; Agus, D. B.; MacCoss, M.; Tabb, D. L.; Mallick, P., A cross-platform toolkit for mass spectrometry and proteomics. *Nat Biotech* **2012,** *30* (10), 918-920.

23. Holman, J. D.; Tabb, D. L.; Mallick, P., Employing ProteoWizard to Convert Raw Mass Spectrometry Data. In *Current Protocols in Bioinformatics*, John Wiley & Sons, Inc.: 2002.

24. Clasquin, M. F.; Melamud, E.; Rabinowitz, J. D., LC-MS data processing with MAVEN: a metabolomic analysis and visualization engine. In *Current Protocols in Bioinformatics*, John Wiley & Sons, Inc.: 2002.

25. Sanchez, G. *DiscriMiner: Tools of the Trade for Discriminant Analysis*, 2013.

26. Smith, C. A.; Want, E. J.; O'Maille, G.; Abagyan, R.; Siuzdak, G., XCMS: Processing Mass Spectrometry Data for Metabolite Profiling Using Nonlinear Peak Alignment, Matching, and Identification. *Analytical Chemistry* **2006,** *78* (3), 779-787.

27. Kuhl, C.; Tautenhahn, R.; Böttcher, C.; Larson, T. R.; Neumann, S., CAMERA: An Integrated Strategy for Compound Spectra Extraction and Annotation of Liquid Chromatography/Mass Spectrometry Data Sets. *Analytical Chemistry* **2012,** *84* (1), 283-289.

28. Kind, T.; Fiehn, O., Seven Golden Rules for heuristic filtering of molecular formulas obtained by accurate mass spectrometry. *BMC Bioinformatics* **2007,** *8* (1), 105.

29. Gunasekera, T. S.; Paliy, O., Growth of E. coli BL21 in minimal media with different gluconeogenic carbon sources and salt contents. *Applied Microbiology and Biotechnology* **2006,** *73* (4), 968-968.

30. Thakur, C. S.; Brown, M. E.; Sama, J. N.; Jackson, M. E.; Dayie, T. K., Growth of wildtype and mutant E. coli strains in minimal media for optimal production of nucleic acids for preparing labeled nucleotides. *Applied Microbiology and Biotechnology* **2010,** *88* (3), 771-779.

31. Cunningham, L.; Gruer, M. J.; Guest, J. R., Transcriptional regulation of the aconitase genes (acnA and acnB) of Escherichia coli. *Microbiology* **1997,** *143* (12), 3795-3805.

32. Caldara, M.; Dupont, G.; Leroy, F.; Goldbeter, A.; De Vuyst, L.; Cunin, R., Arginine Biosynthesis in Escherichia coli: EXPERIMENTAL PERTURBATION AND MATHEMATICAL MODELING. *Journal of Biological Chemistry* **2008,** *283* (10), 6347-6358.

33. Cunin, R.; Glansdorff, N.; Piérard, A.; Stalon, V., Biosynthesis and metabolism of arginine in bacteria. *Microbiological Reviews* **1986,** *50* (3), 314-352.

34. Worley, B.; Powers, R., Multivariate Analysis in Metabolomics. *Current Metabolomics* **2013,** *1* (1), 92-107.

35. Worley, B.; Halouska, S.; Powers, R., Utilities for quantifying separation in PCA/PLS-DA scores plots. *Analytical Biochemistry* **2013,** *433* (2), 102-104.

36. Farrés, M.; Platikanov, S.; Tsakovski, S.; Tauler, R., Comparison of the variable importance in projection (VIP) and of the selectivity ratio (SR) methods for variable selection and interpretation. *Journal of Chemometrics* **2015,** *29* (10), 528-536.

37. Bryan, K.; Brennan, L.; Cunningham, P., MetaFIND: A feature analysis tool for metabolomics data. *BMC Bioinformatics* **2008,** *9*, 470-470.

38. Chong, I.-G.; Jun, C.-H., Performance of some variable selection methods when multicollinearity is present. *Chemometrics and Intelligent Laboratory Systems* **2005,** *78* (1), 103-112.

39. De Siervo, A. J., Alterations in the Phospholipid Composition of Escherichia coli B During Growth at Different Temperatures. *Journal of Bacteriology* **1969,** *100* (3), 1342-1349.

40. Furse, S.; Wienk, H.; Boelens, R.; de Kroon, A. I. P. M.; Killian, J. A., E. coli MG1655 modulates its phospholipid composition through the cell cycle. *FEBS Letters* **2015,** *589* (19, Part B), 2726-2730.

41. Kanfer, J.; Kennedy, E. P., Metabolism and Function of Bacterial Lipids: II. BIOSYNTHESIS OF PHOSPHOLIPIDS IN ESCHERICHIA COLI. *Journal of Biological Chemistry* **1964,** *239* (6), 1720-1726.

42. Rietveld, A. G.; Killian, J. A.; Dowhan, W.; de Kruijff, B., Polymorphic regulation of membrane phospholipid composition in Escherichia coli. *Journal of Biological Chemistry* **1993,** *268* (17), 12427-33.

43. Cronan, J. E.; Rock, C. O., Biosynthesis of Membrane Lipids. *EcoSal Plus* **2008,** *3* (1).

44. Matsumoto, K., Phosphatidylserine synthase from bacteria. *Biochimica et Biophysica Acta (BBA) - Lipids and Lipid Metabolism* **1997,** *1348* (1), 214-227.

45. Gibellini, F.; Smith, T. K., The Kennedy pathway—De novo synthesis of phosphatidylethanolamine and phosphatidylcholine. *IUBMB Life* **2010,** *62* (6), 414-428.

46. Mileykovskaya, E.; Dowhan, W., Role of membrane lipids in bacterial division-site selection. *Current Opinion in Microbiology* **2005,** *8* (2), 135-142.

47. Ankrah, N. Y. D.; May, A. L.; Middleton, J. L.; Jones, D. R.; Hadden, M. K.; Gooding, J. R.; LeCleir, G. R.; Wilhelm, S. W.; Campagna, S. R.; Buchan, A., Phage infection of an environmentally relevant marine bacterium alters host metabolism and lysate composition. *The Isme Journal* **2013,** *8*, 1089.

48. Zitka, O.; Skalickova, S.; Gumulec, J.; Masarik, M.; Adam, V.; Hubalek, J.; Trnkova, L.; Kruseova, J.; Eckschlager, T.; Kizek, R., Redox status expressed as GSH:GSSG ratio as a marker for oxidative stress in paediatric tumour patients. *Oncology letters* **2012,** *4* (6), 1247-1253.

49. Anderson, M. E., Glutathione: an overview of biosynthesis and modulation. *Chemico-Biological Interactions* **1998,** *111-112*, 1-14.

50. Dowhan, W., Molecular Basis for Membrane Phospholipid Diversity: Why Are There So Many Lipids? *Annual Review of Biochemistry* **1997,** *66* (1), 199-232.

51. Cronan, J. E., Bacterial Membrane Lipids: Where Do We Stand? *Annual Review of Microbiology* **2003,** *57* (1), 203-224.

52. Furse, S.; Scott, D. J., Three-Dimensional Distribution of Phospholipids in Gram Negative Bacteria. *Biochemistry* **2016,** *55* (34), 4742-4747.

53. Oliver, P. M.; Crooks, J. A.; Leidl, M.; Yoon, E. J.; Saghatelian, A.; Weibel, D. B., Localization of Anionic Phospholipids in Escherichia coli Cells. *Journal of Bacteriology* **2014,** *196* (19), 3386-3398.

54. Sohlenkamp, C.; Geiger, O., Bacterial membrane lipids: diversity in structures and pathways. *FEMS Microbiology Reviews* **2016,** *40* (1), 133-159.

55. Beney, L.; Gervais, P., Influence of the fluidity of the membrane on the response of microorganisms to environmental stresses. *Applied Microbiology and Biotechnology* **2001,** *57* (1), 34-42.

56. Saito, H. E.; Harp, J. R.; Fozo, E. M., Incorporation of Exogenous Fatty Acids Protects Enterococcus faecalis from Membrane-Damaging Agents. *Applied and Environmental Microbiology* **2014,** *80* (20), 6527-6538.

57. Fozo, E. M.; Rucks, E. A., Chapter Two - The Making and Taking of Lipids: The Role of Bacterial Lipid Synthesis and the Harnessing of Host Lipids in Bacterial Pathogenesis. In *Advances in Microbial Physiology*, Poole, R. K., Ed. Academic Press: 2016; Vol. 69, pp 51-155.

58. Renner, L. D.; Weibel, D. B., Cardiolipin microdomains localize to negatively curved regions of Escherichia coli membranes. *Proceedings of the National Academy of Sciences* **2011,** *108* (15), 6264-6269.

59. Romantsov, T.; Guan, Z.; Wood, J. M., Cardiolipin and the osmotic stress responses of bacteria. *Biochimica et Biophysica Acta (BBA) - Biomembranes* **2009,** *1788* (10), 2092-2100.

60. Beate, F.; Jürgen, S., Application of MALDI-TOF mass spectrometry in lipidomics. *European Journal of Lipid Science and Technology* **2009,** *111* (1), 83-98.

61. Xianlin, H.; W., G. R., Shotgun lipidomics: Electrospray ionization mass spectrometric analysis and quantitation of cellular lipidomes directly from crude extracts of biological samples. *Mass Spectrometry Reviews* **2005,** *24* (3), 367-412.

62. Watson, A. D., Thematic review series: Systems Biology Approaches to Metabolic and Cardiovascular Disorders. Lipidomics: a global approach to lipid analysis in biological systems. *Journal of Lipid Research* **2006,** *47* (10), 2101-2111.

63. Triebl, A.; Trötzmüller, M.; Hartler, J.; Stojakovic, T.; Köfeler, H. C., Lipidomics by ultrahigh performance liquid chromatography-high resolution mass spectrometry and its application to complex biological samples. *Journal of Chromatography B* **2017,** *1053*, 72-80.

64. Schwalbe-Herrmann, M.; Willmann, J.; Leibfritz, D., Separation of phospholipid classes by hydrophilic interaction chromatography detected by electrospray ionization mass spectrometry. *Journal of Chromatography A* **2010,** *1217* (32), 5179-5183.

65. Cífková, E.; Holčapek, M.; Lísa, M.; Ovčačíková, M.; Lyčka, A.; Lynen, F.; Sandra, P., Nontargeted Quantitation of Lipid Classes Using Hydrophilic Interaction Liquid Chromatography–Electrospray Ionization Mass Spectrometry with Single Internal Standard and Response Factor Approach. *Analytical Chemistry* **2012,** *84* (22), 10064-10070.

66. Ivanisevic, J.; Zhu, Z.-J.; Plate, L.; Tautenhahn, R.; Chen, S.; O'Brien, P. J.; Johnson, C. H.; Marletta, M. A.; Patti, G. J.; Siuzdak, G., Toward 'Omic Scale Metabolite Profiling: A Dual Separation–Mass Spectrometry Approach for Coverage of Lipid and Central Carbon Metabolism. *Analytical Chemistry* **2013,** *85* (14), 6876-6884.

67. Minkler, P. E.; Hoppel, C. L., Separation and characterization of cardiolipin molecular species by reverse-phase ion pair high-performance liquid chromatography-mass spectrometry. *Journal of Lipid Research* **2010,** *51* (4), 856-865.

68. Rashid, R.; Cazenave-Gassiot, A.; Gao, I. H.; Nair, Z. J.; Kumar, J. K.; Gao, L.; Kline, K. A.; Wenk, M. R., Comprehensive analysis of phospholipids and glycolipids in the opportunistic pathogen Enterococcus faecalis. *PLOS ONE* **2017,** *12* (4), e0175886.

69. Bird, S. S.; Marur, V. R.; Sniatynski, M. J.; Greenberg, H. K.; Kristal, B. S., Lipidomics Profiling by High-Resolution LC−MS and High-Energy Collisional Dissociation Fragmentation: Focus on Characterization of Mitochondrial Cardiolipins and Monolysocardiolipins. *Analytical Chemistry* **2011,** *83* (3), 940-949.

70. Valianpour, F.; Wanders, R. J. A.; Barth, P. G.; Overmars, H.; van Gennip, A. H., Quantitative and Compositional Study of Cardiolipin in Platelets by Electrospray Ionization Mass Spectrometry: Application for the Identification of Barth Syndrome Patients. *Clinical Chemistry* **2002,** *48* (9), 1390-1397.

71. Scherer, M.; Schmitz, G.; Liebisch, G., Simultaneous Quantification of Cardiolipin, Bis(monoacylglycero)phosphate and their Precursors by Hydrophilic Interaction LC−MS/MS Including Correction of Isotopic Overlap. *Analytical Chemistry* **2010,** *82* (21), 8794-8799.

72. Saito, H. E.; Harp, J. R.; Fozo, E. M., Enterococcus faecalis Responds to Individual Exogenous Fatty Acids Independently of Their Degree of Saturation or Chain Length. *Applied and Environmental Microbiology* **2018,** *84* (1).

73. Harp, J. R.; Saito, H. E.; Bourdon, A. K.; Reyes, J.; Arias, C. A.; Campagna, S. R.; Fozo, E. M., Exogenous Fatty Acids Protect Enterococcus faecalis from Daptomycin-Induced Membrane Stress Independently of the Response Regulator LiaR. *Applied and Environmental Microbiology* **2016,** *82* (14), 4410-4420.

74. Bligh, E. G.; Dyer, W. J., A RAPID METHOD OF TOTAL LIPID EXTRACTION AND PURIFICATION. *Canadian Journal of Biochemistry and Physiology* **1959,** *37* (8), 911-917.

75. J., I. S.; C., L. S. L.; H., C. M., Comparison of the bligh and dyer and folch methods for total lipid determination in a broad range of marine tissue. *Lipids* **2001,** *36* (11), 1283-1287.

76. D., H. J.; L., T. D.; Parag, M., Employing ProteoWizard to Convert Raw Mass Spectrometry Data. *Current Protocols in Bioinformatics* **2014,** *46* (1), 13.24.1-13.24.9.

77. Kessner, D.; Chambers, M.; Burke, R.; Agus, D.; Mallick, P., ProteoWizard: open source software for rapid proteomics tools development. *Bioinformatics* **2008,** *24* (21), 2534-2536.

78. F., C. M.; Eugene, M.; D., R. J., LC-MS Data Processing with MAVEN: A Metabolomic Analysis and Visualization Engine. *Current Protocols in Bioinformatics* **2012,** *37* (1), 14.11.1-14.11.23.

79. Kilelee, E.; Pokorny, A.; Yeaman, M. R.; Bayer, A. S., Lysyl-Phosphatidylglycerol Attenuates Membrane Perturbation Rather than Surface Association of the Cationic Antimicrobial Peptide 6W-RP-1 in a Model Membrane System: Implications for Daptomycin Resistance. *Antimicrobial Agents and Chemotherapy* **2010,** *54* (10), 4476-4479.

80. Nishi, H.; Komatsuzawa, H.; Fujiwara, T.; McCallum, N.; Sugai, M., Reduced Content of Lysyl-Phosphatidylglycerol in the Cytoplasmic Membrane Affects Susceptibility to Moenomycin, as Well as Vancomycin, Gentamicin, and Antimicrobial Peptides, in Staphylococcus aureus. *Antimicrobial Agents and Chemotherapy* **2004,** *48* (12), 4800-4807.

81. Joo, H.-S.; Otto, M., Mechanisms of resistance to antimicrobial peptides in staphylococci. *Biochimica et Biophysica Acta (BBA) - Biomembranes* **2015,** *1848* (11, Part B), 3055-3061.

82. Hamilton, J. A.; Kamp, F., How are free fatty acids transported in membranes? Is it by proteins or by free diffusion through the lipids? *Diabetes* **1999,** *48* (12), 2255-2269.

83. Klausner, R. D.; Kleinfeld, A. M.; Hoover, R. L.; Karnovsky, M. J., Lipid domains in membranes. Evidence derived from structural perturbations induced by free fatty acids and lifetime heterogeneity analysis. *Journal of Biological Chemistry* **1980,** *255* (4), 1286-95.

84. Van Mooy, B. A. S.; Fredricks, H. F.; Pedler, B. E.; Dyhrman, S. T.; Karl, D. M.; Koblížek, M.; Lomas, M. W.; Mincer, T. J.; Moore, L. R.; Moutin, T.; Rappé, M. S.; Webb, E. A., Phytoplankton in the ocean use non-phosphorus lipids in response to phosphorus scarcity. *Nature* **2009,** *458*, 69.

85. Sprott, G. D.; Larocque, S.; Cadotte, N.; Dicaire, C. J.; McGee, M.; Brisson, J. R., Novel polar lipids of halophilic eubacterium Planococcus H8 and archaeon Haloferax volcanii. *Biochimica et Biophysica Acta (BBA) - Molecular and Cell Biology of Lipids* **2003,** *1633* (3), 179-188.

86. Chapman, D. J.; De-Felice, J.; Barber, J., Characteristics of chloroplast thylakoid lipid composition associated with resistance to triazine herbicides. *Planta* **1985,** *166* (2), 280-285.

87. Dörmann, P.; Benning, C., Galactolipids rule in seed plants. *Trends in Plant Science* **2002,** *7* (3), 112-118.

88. Fahy, E.; Subramaniam, S.; Murphy, R. C.; Nishijima, M.; Raetz, C. R. H.; Shimizu, T.; Spener, F.; van Meer, G.; Wakelam, M. J. O.; Dennis, E. A., Update of the LIPID MAPS comprehensive classification system for lipids. *Journal of Lipid Research* **2009,** *50* (Supplement), S9-S14.

89. Fahy, E.; Sud, M.; Cotter, D.; Subramaniam, S., LIPID MAPS online tools for lipid research. *Nucleic Acids Research* **2007,** *35* (suppl_2), W606-W612.

90. Tran, T. T.; Panesso, D.; Mishra, N. N.; Mileykovskaya, E.; Guan, Z.; Munita, J. M.; Reyes, J.; Diaz, L.; Weinstock, G. M.; Murray, B. E.; Shamoo, Y.; Dowhan, W.; Bayer, A. S.; Arias, C. A., Daptomycin-Resistant Enterococcus faecalis Diverts the Antibiotic Molecule from the Division Septum and Remodels Cell Membrane Phospholipids. *mBio* **2013,** *4* (4).

91. Olofsson, G.; Sparr, E., Ionization Constants pKa of Cardiolipin. *PLOS ONE* **2013,** *8* (9), e73040.

92. Bao, Y.; Sakinc, T.; Laverde, D.; Wobser, D.; Benachour, A.; Theilacker, C.; Hartke, A.; Huebner, J., Role of mprF1 and mprF2 in the Pathogenicity of Enterococcus faecalis. *PLOS ONE* **2012,** *7* (6), e38458.

93. Mishra, N. N.; Bayer, A. S.; Tran, T. T.; Shamoo, Y.; Mileykovskaya, E.; Dowhan, W.; Guan, Z.; Arias, C. A., Daptomycin Resistance in Enterococci Is Associated with Distinct Alterations of Cell Membrane Phospholipid Content. *PLOS ONE* **2012,** *7* (8), e43958.

94. Nagoshi, R. N.; Fleischer, S.; Meagher, R. L.; Hay-Roe, M.; Khan, A.; Murua, M. G.; Silvie, P.; Vergara, C.; Westbrook, J., Fall armyworm migration across the Lesser Antilles and the potential for genetic exchanges between North and South American populations. *PLoS One* **2017,** *12* (2), e0171743.

95. Day, R.; Abrahams, P.; Bateman, M.; Beale, T.; Clottey, V.; Cock, M.; Colmenarez, Y.; Corniani, N.; Early, R.; Godwin, J.; Gomez, J.; Moreno, P. G.; Murphy, S. T.; Oppong-Mensah, B.; Phiri, N.; Pratt, C.; Silvestri, S.; Witt, A., Fall

armyworm: Impacts and implications for Africa. *Outlooks on Pest Management* **2017,** *28* (5), 196-201.

96. Goergen, G.; Kumar, P. L.; Sankung, S. B.; Togola, A.; Tamò, M., First report of outbreaks of the fall armyworm *Spodoptera frugiperda* (J E Smith) (Lepidoptera, Noctuidae), a new alien invasive pest in West and Central Africa. *PLoS ONE* **2016,** *11* (10).

97. Siebert, M. W.; Babock, J. M.; Nolting, S. P.; Santos, A. C.; Adamczyk, J. J.; Neese, P. A.; King, J. E.; jenkins, J. N.; McCarty, J.; Lorenz, G. M.; Fromme, D. D.; Lassiter, R. B., Efficacy of Cry1F insecticidal protein in maize and cotton for control of fall armyworm (Lepidoptera: Noctuidae). *Florida Entomologist* **2008,** *91* (4), 555-565.

98. Adang, M.; Crickmore, N.; Jurat-Fuentes, J. L., Diversity of *Bacillus thuringiensis* crystal toxins and mechanism of action. In *Advances in Insect Physiology Vol. 47: Insect Midgut and Insecticidal Proteins*, Dhadialla, T. S.; Gill, S., Eds. Academic Press: San Diego, CA, 2014; pp 39-87.

99. Storer, N. P.; Babcock, J. M.; Schlenz, M.; Meade, T.; Thompson, G. D.; Bing, J. W.; Huckaba, R. M., Discovery and characterization of field resistance to Bt maize: *Spodoptera frugiperda* (Lepidoptera: Noctuidae) in Puerto Rico. *J Econ Entomol* **2010,** *103* (4), 1031-1038.

100. Huang, F.; Qureshi, J. A.; Meagher, R. L., Jr.; Reisig, D. D.; Head, G. P.; Andow, D. A.; Ni, X.; Kerns, D.; Buntin, G. D.; Niu, Y.; Yang, F.; Dangal, V., Cry1F resistance in fall armyworm *Spodoptera frugiperda*: single gene versus pyramided Bt maize. *PLoS One* **2014,** *9* (11), e112958.

101. Farias, J. R.; Andow, D. A.; Horikoshi, R. J.; Sorgatto, R. J.; Fresia, P.; dos Santos, A. C.; Omoto, C., Field-evolved resistance to Cry1F maize by *Spodoptera frugiperda* (Lepidoptera: Noctuidae) in Brazil. *Crop Protection* **2014,** *64*, 150-158.

102. Monnerat, R.; Martins, E.; Macedo, C.; Queiroz, P.; Praça, L.; Soares, C. M.; Moreira, H.; Grisi, I.; Silva, J.; Soberon, M.; Bravo, A., Evidence of field-evolved resistance of *Spodoptera frugiperda* to Bt corn expressing Cry1F in Brazil that is still sensitive to modified Bt toxins. *PLoS One* **2015,** *10* (4), e0119544.

103. Chandrasena, D. I.; Signorini, A. M.; Abratti, G.; Storer, N. P.; Olaciregui, M. L.; Alves, A. P.; Pilcher, C. D., Characterization of field-evolved resistance to *Bacillus thuringiensis*-derived Cry1F delta-endotoxin in *Spodoptera frugiperda* populations from Argentina. *Pest Manag Sci* **2017**.

104. Banerjee, R.; Hasler, J.; Meagher, R.; Nagoshi, R.; Hietala, L.; Huang, F.; Narva, K.; Jurat-Fuentes, J. L., Mechanism and DNA-based detection of field-

evolved resistance to transgenic Bt corn in fall armyworm (*Spodoptera frugiperda*). *Scientific Reports* **2017,** *7* (1), 10877.

105. Gahan, L. J.; Pauchet, Y.; Vogel, H.; Heckel, D. G., An ABC transporter mutation is correlated with insect resistance to *Bacillus thuringiensis* Cry1Ac toxin. *PLoS Genetics* **2010,** *6* (12), e1001248.

106. Baxter, S. W.; Badenes-Perez, F. R.; Morrison, A.; Vogel, H.; Crickmore, N.; Kain, W.; Wang, P.; Heckel, D. G.; Jiggins, C. D., Parallel evolution of *Bacillus thuringiensis* toxin resistance in Lepidoptera. *Genetics* **2011,** *189* (2), 675-9.

107. Xiao, Y.; Zhang, T.; Liu, C.; Heckel, D. G.; Li, X.; Tabashnik, B. E.; Wu, K., Mis-splicing of the ABCC2 gene linked with Bt toxin resistance in *Helicoverpa armigera*. *Sci Rep* **2014,** *4*, 6184.

108. Atsumi, S.; Miyamoto, K.; Yamamoto, K.; Narukawa, J.; Kawai, S.; Sezutsu, H.; Kobayashi, I.; Uchino, K.; Tamura, T.; Mita, K.; Kadono-Okuda, K.; Wada, S.; Kanda, K.; Goldsmith, M. R.; Noda, H., Single amino acid mutation in an ATP-binding cassette transporter gene causes resistance to Bt toxin Cry1Ab in the silkworm, *Bombyx mori*. *Proceedings of the National Academy of Sciences of the United States of America* **2012,** *109* (25), E1591-E1598.

109. Park, Y.; Gonzalez-Martinez, R. M.; Navarro-Cerrillo, G.; Chakroun, M.; Kim, Y.; Ziarsolo, P.; Blanca, J.; Canizares, J.; Ferre, J.; Herrero, S., ABCC transporters mediate insect resistance to multiple Bt toxins revealed by bulk segregant analysis. *BMC Biology* **2014,** *12*, 46.

110. Jemnitz, K.; Heredi-Szabo, K.; Janossy, J.; Ioja, E.; Vereczkey, L.; Krajcsi, P., ABCC2/Abcc2: a multispecific transporter with dominant excretory functions. *Drug Metabolism Reviews* **2010,** *42* (3), 402-436.

111. Dermauw, W.; Van Leeuwen, T., The ABC gene family in arthropods: Comparative genomics and role in insecticide transport and resistance. *Insect Biochemistry and Molecular Biology* **2014,** *45* (0), 89-110.

112. Porretta, D.; Epis, S.; Mastrantonio, V.; Ferrari, M.; Bellini, R.; Favia, G.; Urbanelli, S., How heterogeneous is the involvement of ABC transporters against insecticides? *Acta Trop* **2016,** *157*, 131-5.

113. Locher, K. P., Mechanistic diversity in ATP-binding cassette (ABC) transporters. *Nat Struct Mol Biol* **2016,** *23* (6), 487-93.

114. Jakka, S. R.; Gong, L.; Hasler, J.; Banerjee, R.; Sheets, J. J.; Narva, K.; Blanco, C. A.; Jurat-Fuentes, J. L., Field-evolved Mode 1 resistance of the fall armyworm to transgenic Cry1Fa-expressing corn associated with reduced Cry1Fa

toxin binding and midgut alkaline phosphatase expression. *Applied and Environmental Microbiology* **2015,** *82* (4), 1023-34.

115. Zhao, C.; Jurat-Fuentes, J. L.; Abdelgaffar, H. M.; Pan, H.; Song, F.; Zhang, J., Identification of a new cry1I-type gene as a candidate for gene pyramiding in corn to control *Ostrinia* species larvae. *Applied and Environmental Microbiology* **2015,** *81* (11), 3699-705.

116. Gouffon, C.; Van Vliet, A.; Van Rie, J.; Jansens, S.; Jurat-Fuentes, J. L., Binding sites for *Bacillus thuringiensis* Cry2Ae toxin on heliothine brush border membrane vesicles are not shared with Cry1A, Cry1F, or Vip3A toxin. *Applied and Environmental Microbiology* **2011,** *77* (10), 3182-8.

117. LeOra, S. *Polo-Plus, POLO for Windows*, LeOra Software: Petaluma, CA, 1987.

118. Rabinowitz, J. D.; Kimball, E., Acidic acetonitrile for cellular metabolome extraction from *Escherichia coli*. *Anal. Chem. (Wash.)* **2007,** *79* (16), 6167-6173.

119. Tague, E. D.; Bourdon, A. K.; MacDonald, A.; Lookadoo, M. S.; Kim, E. D.; White, W. M.; Terry, P. D.; Campagna, S. R.; Voy, B. H.; Whelan, J., Metabolomics approach in the study of the well-defined polyherbal preparation Zyflamend. *Journal of Mediicinal Food* **2018,** *21* (3), 306-316.

120. Lu, W.; Clasquin, M. F.; Melamud, E.; Amador-Noguez, D.; Caudy, A. A.; Rabinowitz, J. D., Metabolomic analysis via reversed-phase ion-pairing liquid chromatography coupled to a stand alone orbitrap mass spectrometer. *Anal. Chem. (Wash.)* **2010,** *82* (8), 3212-21.

121. Melamud, E.; Vastag, L.; Rabinowitz, J. D., Metabolomic analysis and visualization engine for LC-MS data. *Anal Chem* **2010,** *82* (23), 9818-26.

122. Clasquin, M. F.; Melamud, E.; Rabinowitz, J. D., LC-MS data processing with MAVEN: a metabolomic analysis and visualization engine. *Curr Protoc Bioinformatics* **2012,** *Chapter 14*, Unit14 11.

123. de Hoon, M. J.; Imoto, S.; Nolan, J.; Miyano, S., Open source clustering software. *Bioinformatics (Oxford, England)* **2004,** *20* (9), 1453-4.

124. Saldanha, A. J., Java Treeview--extensible visualization of microarray data. *Bioinformatics (Oxford, England)* **2004,** *20* (17), 3246-8.

125. Sanchez, G. *Package 'DiscriMiner'*, 2013.

126. Li, X. Z.; Yang, X. Y.; Wang, Y.; Zhang, S. N.; Zou, W.; Wang, Y.; Li, X. N.; Wang, L. S.; Zhang, Z. G.; Xie, L. Z., Urine metabolic profiling for the pathogenesis research of erosive oral lichen planus. *Arch Oral Biol* **2017,** *73*, 206-213.

127. Xia, J.; Wishart, D. S., Web-based inference of biological patterns, functions and pathways from metabolomic data using MetaboAnalyst. *Nat Protoc* **2011,** *6* (6), 743-60.

128. Farrés, M.; Platikanov, S.; Tsakovski.Stefan;; Tauler, R., Comparison of the variable importance in projection (VIP) and of the selectivity ratio (SR) methods for variable selection and interpretation. *Journal of Chemometrics* **2015,** *29* (10), 528-536.

129. Yamada, T.; Letunic, I.; Okuda, S.; Kanehisa, M.; Bork, P., iPath2.0: interactive pathway explorer. *Nucleic Acids Research* **2011,** *39* (2), W412-W415.

130. Bretschneider, A.; Heckel, D. G.; Pauchet, Y., Three toxins, two receptors, one mechanism: Mode of action of Cry1A toxins from Bacillus thuringiensis in Heliothis virescens. *Insect Biochem Mol Biol* **2016,** *76*, 109-17.

131. Tanaka, S.; Miyamoto, K.; Noda, H.; Jurat-Fuentes, J. L.; Yoshizawa, Y.; Endo, H.; Sato, R., The ATP-binding cassette transporter subfamily C member 2 in *Bombyx mori* larvae is a functional receptor for Cry toxins from *Bacillus thuringiensis*. *FEBS Journal* **2013,** *280* (8), 1782-1794.

132. Endo, H.; Tanaka, S.; Imamura, K.; Adegawa, S.; Kikuta, S.; Sato, R., Cry toxin specificities of insect ABCC transporters closely related to lepidopteran ABCC2 transporters. *Peptides* **2017,** *98*, 86-92.

133. Fabrick, J. A.; Ponnuraj, J.; Singh, A.; Tanwar, R. K.; Unnithan, G. C.; Yelich, A. J.; Li, X.; Carriere, Y.; Tabashnik, B. E., Alternative splicing and highly variable cadherin transcripts associated with field-evolved resistance of pink bollworm to bt cotton in India. *PLoS One* **2014,** *9* (5), e97900.

134. Jakka, S. R.; Knight, V. R.; Jurat-Fuentes, J. L., Fitness costs associated with field-evolved resistance to Bt maize in *Spodoptera frugiperda* (Lepidoptera: Noctuidae). *J Econ Entomol* **2014,** *107* (1), 342-51.

135. Belinsky, M. G.; Guo, P.; Lee, K.; Zhou, F.; Kotova, E.; Grinberg, A.; Westphal, H.; Shchaveleva, I.; Klein-Szanto, A.; Gallo, J. M.; Kruh, G. D., Multidrug resistance protein 4 protects bone marrow, thymus, spleen, and intestine from nucleotide analogue-induced damage. *Cancer Research* **2007,** *67* (1), 262-268.

136. Saidijam, M.; Karimi Dermani, F.; Sohrabi, S.; Patching, S. G., Efflux proteins at the blood–brain barrier: review and bioinformatics analysis. *Xenobiotica* **2018,** *48* (5), 506-532.

137. van Aubel, R. A. M. H.; Smeets, P. H. E.; Peters, J. G. P.; Bindels, R. J. M.; Russel, F. G. M., The MRP4/ABCC4 gene encodes a novel apical organic anion transporter in human kidney proximal tubules: putative efflux pump for urinary cAMP and cGMP. *Journal of the American Society of Nephrology* **2002,** *13* (3), 595-603.

138. Meijer, A. J.; Codogno, P., Signalling and autophagy regulation in health, aging and disease. *Molecular Aspects of Medicine* **2006,** *27* (5), 411-425.

VITA

Eric Tague grew up in Blue Springs, Missouri and attend Missouri State University in Springfield, MO where he received his Bachelor of Science in Chemistry in 2012. As an undergraduate, Eric was very involved in the Student Affiliates of the American Chemical Society and held the following positions; president, secretary, and field trip coordinator. Eric was hired by the Chemistry Department's chemical stockroom to help prepare chemicals and set up equipment for the undergraduate labs. With mentorship from his undergraduate research advisor, Dr. Mark Richter, he completed 3 semesters of undergraduate research, and help publish a paper on the electrochemiluminescence of metal complexes. He was accepted into MSU's Accelerated Master's program in the fall of this senior year and joined Dr. Erich D. Steinle's research group and studied lanthanide-based ion selective electrodes. In August of 2013, Eric graduated with his Master's in Chemistry. Eric was then offered a one year visiting instructor position at Missouri State University where he taught 2 semesters of introductory chemistry and coordinated three teaching assistants who taught the corresponding laboratory. After deciding to pursue his doctorate degree, he moved to Knoxville, Tennessee to attend the University of Tennessee. Eric joined Dr. Shawn R. Campagna's biological mass spectrometry group and began studying changes in metabolite composition of microbial systems. Following the completion of his Ph.D. program in May of 2018, Eric will join the Field Applications team at Thermo Fisher Scientific.